INSTITUTO
UNIVERSITÁRIO
DE LISBOA

Smart Sensors and Virtual Environments

João Pedro Duarte Barros Monge

PhD in Information Science and Technology

Supervisor:
Doctor Octavian Adrian Postolache, Full Professor,
ISCTE - Instituto Universitário de Lisboa

December, 2025

TECNOLOGIAS
E ARQUITETURA

Department of Information Science and Technology

Smart Sensors and Virtual Environments

João Pedro Duarte Barros Monge

Phd in Information Science and Technology

Jury:
Doctor Dr. Américo, Full Professor,
ISCTE – Instituto Universitário de Lisboa (President)
Doctor Franciso Martín, Full Professor,
Universidad de Oviedo
Doctor Rui Madeira, Assistant Professor,
Instituto Politécnico de Setúbal
Doctor Nuno Souto, Associate Professor with Aggregation,
ISCTE - Instituto Universitário de Lisboa
Doctor Octavian Adrian Postolache, Full Professor,
ISCTE - Instituto Universitário de Lisboa

December, 2025

I dedicate my work to my wife and daughter, your support is something I can never truly repay. Your love and encouragement have been my greatest strength throughout this journey.

To Mom and Dad, your unwavering belief in me and the countless sacrifices you have made are the foundation of my achievements. Thank you for shaping my path with love, wisdom, and endless opportunities.

Finally, I express my sincere thanks to all those passionately working toward better healthcare through technology.

Acknowledgment

The author extends his deepest gratitude to his supervisor, Professor Octavian Postolache, whose expertise, patience, and guidance have profoundly shaped my doctoral journey. His mentorship has been invaluable in aligning my research with my long-term aspirations.

To my beloved wife, for your encouragement, love and belief in me have been my foundation. Your patience and sacrifices made this achievement possible and I am forever grateful.

I also thank my parents for their unconditional love and support, which have motivated me to pursue this PhD. Their trust in my abilities has been a constant source of motivation.

A special thanks goes out to my friend and colleague, António Raimundo, for his unwavering support and dedication throughout this academic path. The challenges we tackled together made this journey even more meaningful. The authors acknowledge Ana Charas and José Gouveia for their valuable contributions and support, which were instrumental in the completion of this work.

I thank ISCTE - University Institute of Lisbon, and IT - Instituto de Telecomunicações, for fostering an inspiring environment that contributed to my growth as a researcher.

Finally, thanks to everyone who participated in the completion of this thesis, your support made this endeavor both rewarding and fulfilling.

Resumo

A crescente procura de uma monitorização personalizada e não invasiva da saúde no desporto e na reabilitação física acelerou a integração da inteligência artificial (IA) em tecnologias de deteção vestíveis e ambientais. Esta tese explora o desenvolvimento e a aplicação de sistemas suportados por IA que visam realizar otimizações na área da reabilitação motora.

Uma das principais contribuições desta investigação é a conceção de plataformas de biossensores portáteis capazes de avaliar desequilíbrios electrolíticos, especificamente concentrações de sódio e potássio no suor, combinadas com a frequência cardíaca para apoiar a gestão da hidratação em atletas de resistência. Estas plataformas incorporam sensores electroquímicos e são acopladas a algoritmos de IA que inferem as necessidades de hidratação, permitindo recomendações personalizadas para prevenir a desidratação e melhorar o desempenho.

Para além disso, a tese apresenta um sistema desenvolvido para a análise da marcha e da postura. Utilizando técnicas de reconhecimento de padrões baseadas em IA, o sistema fornece feedback em tempo real num ambiente virtual, apoiando a reabilitação motora e a avaliação do desempenho tanto em contextos desportivos como clínicos.

Os sistemas propostos foram validados em ambientes experimentais e cenários do mundo real, demonstrando elevada robustez, facilidade de utilização e capacidade de resposta. Esta abordagem interdisciplinar, que combina biossensorização, análise eletroquímica e inteligência artificial, realça o potencial transformador dos sistemas inteligentes de monitorização da saúde nas ciências do desporto e na reabilitação. O trabalho futuro explorará a expansão destas tecnologias para a gestão de doenças crónicas e aplicações mais amplas de telessaúde.

Palavras-chave - Inteligência Artificial (IA), Biossensores Vestíveis, Sensores Eletroquímicos, Monitorização Fisiológica, Reabilitação Motora, Aprendizagem Automática, Sistemas Inteligentes de Saúde, TeleSaúde

Abstract

The growing demand for personalized and non-invasive health monitoring in sports and physical rehabilitation has accelerated the integration of artificial intelligence (AI) into wearable and ambient sensing technologies. This thesis explores the development and application of AI-supported systems designed to achieve optimizations in the field of motor rehabilitation. One of the main contributions of this research is the design of portable biosensing platforms capable of assessing electrolyte imbalances—specifically sodium and potassium concentrations in sweat combined with heart rate, to support hydration management in endurance athletes. These platforms incorporate electrochemical sensors and are coupled with AI algorithms that infer hydration needs, enabling personalized recommendations to prevent dehydration and improve performance. In addition, the thesis presents a system developed for gait and posture analysis. Using AI-based pattern recognition techniques, the system provides real-time feedback within a virtual environment, supporting motor rehabilitation and performance assessment in both sports and clinical contexts. The proposed systems were validated in experimental settings and real-world scenarios, demonstrating high robustness, ease of use, and responsiveness. This interdisciplinary approach, combining biosensing, electrochemical analysis, and artificial intelligence, highlights the transformative potential of intelligent health-monitoring systems in sports science and rehabilitation. Future work will explore the expansion of these technologies to chronic disease management and broader telehealth applications.

Keywords - Artificial Intelligence (AI), Wearable Biosensors, Electrochemical Sensors, Physiological Monitoring, Motor Rehabilitation, Machine Learning, Smart Health Systems, Telehealth

Contents

Acknowledgment iii

Resumo v

Abstract vii

List of Figures xi

List of Tables xvii

List of Acronyms xix

Chapter 1. Introduction 1

1.1. Background 3

1.2. Motivation and Framework 4

1.3. Problem Statement and Objectives 6

1.4. Thesis Overview 10

1.5. Research contributions 10

Chapter 2. Literature Review 15

2.1. Technology in Healthcare 15

2.2. Smart Sensors in healthcare 18

2.3. Virtual Environments in Healthcare 37

2.4. Applied AI in Healthcare 45

Chapter 3. Smart Sensors for Healthcare 51

3.1. Biosensors 51

3.2. Potentiostat 56

3.3. PotLink: Development of a Portable Single-Channel Potentiostat for In-Situ Analysis 59

3.4. NanoPotLink: Design of a Miniaturized Wearable Potentiostat for Continuous Electrochemical Monitoring 80

3.5. MultiPot: Implementation and Evaluation of a Four-Channel Potentiostat System for Multi-Analyte Detection 97
3.6. AIDrated: Integration of AI Algorithms with Biosensing Platforms for Hydration Assessment 117
3.7. System Architecture 117

Chapter 4. Extended Reality applications for physical rehabilitation 143
4.1. Overview 143
4.2. Mixed Reality and Augmented Reality proposed applications for Physical Rehabilitation 144
4.3. Physical Rehabilitation in AR Scenario 145

Chapter 5. Conclusions and Future Work 179
5.1. Conclusions 179
5.2. Future Work 181

Appendices 185

Appendix A. Potlink Schematic and PCB 185

Appendix B. NanoPotlink Schematic and PCB 191

Appendix C. MultiPot platform V1.0 Schematic and PCB 197

Appendix D. Multipot firmware programmer 203

Appendix E. MultiPot platform V2.0 Schematic and PCB 209

Appendix F. AIDrated platform Schematic and PCB 211

References 213

List of Figures

1.1 Primary focus areas: wearable smart sensors (left) and virtual environments for physical rehabilitation applications (right). 2

1.2 Projected increase in the elderly population and its implications. This chart shows expected population growth in various age groups until 2060. 5

1.3 Role of AI and smart technology in reducing healthcare workforce needs. This figure illustrates the numerous benefits of AI in healthcare, including training, research, end-of-life care, treatment, decision-making, diagnosis, early detection, and health maintenance. 6

1.4 Benefits and limitations of digital healthcare solutions. 7

1.5 The role of AI in healthcare. 8

1.6 Research contributions over the years. 13

2.1 Historical perspective on healthcare 1.0 to 5.0. 16

2.2 Azure Kinect skeleton tracking example. 19

2.3 Smartphone Sensors. 20

2.4 Sensors evolution. 21

2.5 Wearable sensors example application. 25

2.6 Elderly Care System Example. 26

2.7 Architecture of an ambient-assisted living system. 27

2.8 De Fazio circuit and diagram. 29

2.9 Innovative Non-invasive Glucose touch sensor. 33

2.10 Pioneering Sweat Sensing Technology by Eccrine Systems. 35

2.11 A MLP network structure. 47

2.12 nfolding example and structure of a one-unit RNN. 48

2.13 A LSTM network structure. 48

2.14 GRU network structure. 49

2.15 GNN schematic architecture. 50

3.1 Components of a biosensor. 52

3.2 Multistep amperometry method 53

3.3 Open-circuit potential measurement configuration 54

3.4 Simplified circuit for cyclic voltammetry. 55

3.5 Commercial glucometer 55

3.6 Portable drug analyzer 56

3.7 Gatorade GX Sweat Patch 56

3.8 Potentiostat schematic. 57

3.9 Block diagram of the system architecture. 60

3.10 RFduino board used in the measurement platform. 62

3.11 Internal block diagram of the LMP91000 potentiostat IC. 63

3.12 Stackable design: RFduino with potentiostat shield, programmer, and battery modules. 64

3.13 Initial testing with the modified LMP91000EVM evaluation board and RFduino. 65

3.14 Assembled PotLink prototype showing key components and connections. 66

3.15 PotLink V1.0 featuring an SPE connector for direct use with disposable sensors. 66

3.16 Flowchart of the firmware and web application integration, illustrating BLE communication, configuration, measurement, and data streaming to the cloud. 67

3.17 Registration page of PotLink for user account creation with validation. 68

3.18 Login page of PotLink with credential input and validation. 69

3.19 Home page of PotLink showing BLE connection, experiment configuration panel, and real-time electrochemical data visualization. 71

3.20 BLE connection interface. The application lists available PotLink devices and prompts the user to authorize pairing. 71

3.21 Interface after successful BLE connection. The connection button turns red, indicating an active link to the PotLink device and enabling controlled disconnection. 72

3.22 Data Visualization Screen of PotLink for reviewing and comparing saved measurements. 73

3.23 Database diagram. 74

3.24 Reference potentiostat including the following electrodes platinum WE and CE, and Ag/AgCl RE. 75

3.25 Comparative cyclic voltammograms for ferrocene obtained with the Solartron 1285 and the developed LMP91000-based system as part of the experimental validation. 76

3.26 Cyclic voltammograms of 0.01 M AA in 0.5 M H_2SO_4 at different pH values. 77

3.27 Wearable sensor nodes in the system: Xiaomi Mi Band 3 for heart rate and motion (left), and NanoPotLink sweat-sensing potentiostat (right). 82

3.28 Overall system architecture illustrating the multimodal wearable sensor network and data flow. 82

3.29 NanoPotLink system 83

3.30 Mobile app user interface: (a) Login screen allowing user authentication, and (b) Register screen enabling new user account creation. 87

3.31 Mobile app user interface: (a) Configuration screen for selecting and setting potentiostat parameters, and (b) Measurement screen displaying real-time electrochemical data visualization. 88

3.32 Mobile app user interface: (a) Concentration page displaying glucose concentration readings, and (b) Data page providing historical data access through a calendar-based interface. 90

3.33 Calibration and testing procedures for node 1. 91

3.34 The IoT potentiostat glucose measurement results for beverages with different sugar concentration 93

3.35 Indoor cycling training plan showing progression from Level 1 to Level 5 and return to Level 2. 94

3.36 Biosensor current output for a sweat glucose sample, with a stable region visible around the 5-second mark. 94

3.37 Mi Fit application output showing heart rate during the indoor cycling session. 95

3.38 Prototype PCB for the multiplexed configuration, illustrating sequential sensor addressing. 98

3.39 Different perspectives of the final four-channel PCB design. 100

3.40 External pogo-pin programming interface for firmware deployment. 102

3.41 Firmware and software integration block diagram. The system architecture links the MultiPot hardware with a PHP–MySQL backend and a React Native mobile application. Configuration parameters for each potentiostat are stored on the server and transmitted via BLE to the MultiPot device. The device executes configuration commands, performs signal acquisition, and streams pre-processed data to the app for visualization and storage. 103

3.42 Firmware flowchart of the MultiPot platform, illustrating system initialization, configuration loading from flash memory, BLE connection management, sequential configuration and sampling of the LMP91000 potentiostat front-ends, buffered data transmission via BLE, and runtime configuration updates with persistent storage. 105

3.43 User authentication workflow of the MultiPot mobile application, including (a) login and (b) registration screens. 107

3.44 Device configuration workflow showing (a) channel setup options and (b) MultiPot selection for BLE communication. 108

3.45 MultiPot real-time data monitoring. Panel (a) allows channel selection, and panel (b) demonstrates multi-analyte data visualization. 109

3.46 Post-processing and data management features of the MultiPot mobile application: (a) concentration estimation and (b) historical data retrieval. 110

3.47 Top view of the fully assembled MultiPot hardware, showing the four-channel potentiostat architecture with integrated motion sensor, power management circuitry, BLE antenna layout and SPE connectors highlighted in yellow where the printed electrodes could be connected. 111

3.48 Perspective view of the assembled MultiPot system interfaced with the external pogo-pin programmer for in-circuit firmware flashing and debugging. 112

3.49 Standalone external programmer used for firmware flashing of the Artemis microcontroller. The design employs spring-loaded pogo contacts for rapid, connector-free interfacing with the main board. 112

3.50 DummyCell. 113

3.51 Comparison between MultiPot and reference potentiostat output for CV sweep using dummy cell. 115

3.52 Block diagram of the AIDrated system architecture, highlighting the integration of electrochemical sensing, physiological monitoring, and embedded AI processing. 118

3.53 Screen-Printed Electrodes (SPE) for sodium and potassium detection. 122

3.54 Apple Watch app interface: (a) main screen displaying hydration status, (b) real-time sensor data visualization, and (c) hydration alert notification when fluid intake is required. 124

3.55 Assembled biosensing platform highlighting the main components: (green) SPE connectors and Na^+, K^+ sensors; (red) lithium battery; (yellow) Artemis microcontroller on SparkFun Thing Plus; (blue) MAX4461 dual amplifier enabling simultaneous OCP measurements. 126

3.56 Sensor calibration procedure. 127

3.57 Measured system response of the sodium sensor during calibration with varying sodium concentrations, where the x-axis represents time (seconds) and the y-axis represents the ADC output value. 128

3.58 Inverse characteristic of the ion measurement system when using Na^+ sensor. 129

3.59 Measured system response of the potassium sensor during calibration with varying potassium concentrations,where the x-axis represents time (seconds) and the y-axis represents the ADC output value. 129

3.60 Inverse characteristic of the ion measurement system when using K^+ sensor. 130

3.61 Placement of the sterile sweat collection pad on the forearm. 131

3.62 Electrolyte concentration variations during an outdoor running session. (a) Potassium concentration and (b) Sodium concentration trends, highlighting electrolyte depletion over time. 132

3.63 (a) Measured potassium concentrations and (b) measured sodium concentrations during endurance cycling exercise. 133

3.64 Comparison between Convolutional Neural Networks (CNN) and GNNs. CNNs apply convolutions over a structured grid, while GNNs generalize this operation

to arbitrary graph structures, making them more suitable for physiological data with complex interdependencies. 137

3.65 3D latent space representation of K-means clustering, highlighting patterns emerging from unsupervised analysis of the data. 139

3.66 AIDrated integrated watch band concept. 141

4.1 Overview of the system's architecture for physical rehabilitation. 146

4.2 Example of a Sensfloor use case. To provide additional protection, flooring is positioned above a sensory layer. 147

4.3 Example of a Sensfloor detecting a person fall and users' position. 148

4.4 Raspberry Pi 3 equipped with a SensFloor hat. 148

4.5 Experimental setup with laminated wood flooring installed above the SensFloor layer. Black tape marks the active sensing area. A TV screen displays a detected cell corresponding to a person standing on the floor which was taken the photo. 150

4.6 Sensfloor module. 151

4.7 Wearable Motion Measurement Unit. 152

4.8 Wearable Motion Device. (a) Device with velcro tape to facilitate the use. (b) User example using the wearable device. 153

4.9 Motion Device Operation. 153

4.10 Physiotherapist application homepage dashboards. 157

4.11 User application flow. 158

4.12 Application data flow. 159

4.13 Users' side application. 161

4.14 Edge Impulse Software 162

4.15 Confusion matrix of MLP, LSTM and GRU, respectively. 172

4.16 Training parameters over time of accuracy and loss values. 174

List of Tables

2.1 Summary of Related Works on Smart Sensors for Health and Physiological Monitoring 37

3.1 Comparison of main characteristics of MCU platforms considered 62

3.2 Comparison of potentiostat ICs 63

3.3 Summary of principal components and alternatives 64

3.4 Oxidation and reduction peak currents obtained from ferrocene cyclic voltammetry. 77

3.5 Peak and valley currents (μA) for different pH levels 78

3.6 Comparison of Multiplexer-Based and Independent LMP91000 Configurations 99

3.7 Engineering comparison of candidate microcontrollers for the MultiPot platform 100

3.8 Experimental Results of MultiPot Compared to Reference Potentiostat 115

3.9 Comparison of BLE-enabled Microcontrollers for Wearable Applications 120

3.10 Key Hardware and Sensing Features of the Apple Watch Ultra 123

3.11 Performance Metrics of the GNN Autoencoder 139

4.1 Summarised features extracted according to sensing element. 162

4.2 Volunteers Specific Biometric Information. 167

4.3 Network hyperparameters. 169

4.4 Models Performance evaluation. 175

List of Acronyms

AAL	Active and Assisted Living
AC	Alternating Current
AI	Artificial Intelligence
ANN	Artificial Neural Network
API	Application Programming Interface
AR	Augmented Reality
BLE	Bluetooth Low Energy
BT	Bluetooth
CE	Counter Electrode
CGM	Continuous Glucose Monitoring
CNN	Convolutional Neural Network
CV	Cyclic Voltammetry
EC	Electrochemical
ECG	Electrocardiogram
EIS	Electrochemical Impedance Spectroscopy
FD	Fatigue Detection
FNA	Fingernail Actuator
FSAS	Finger Side Actuators
FTDI	Future Technology Devices International
GAT	Graph Attention Network
GCN	Graph Convolutional Network
GNN	Graph Neural Network
GRU	Gated Recurrent Units

H_2O	Water
H_2O_2	Hydrogen Peroxide
HIS	Health Information Systems
HR	Heart Rate
HRV	Heart Rate Variability
IC	Integrated Circuit
IDE	Integrated Development Environment
IMU	Inertial Measurement Unit
IoT	Internet of Things
ISE	Ion-Selective Electrode
LSTM	Long Short-Term Memory
MA	Moving Average
MAE	Mean Absolute Error
MCU	Microcontroller Unit
ML	Machine Learning
MLP	Multilayer Perceptron
MSE	Mean Squared Error
MR	Mixed Reality
NLP	Natural Language Processing
OCP	Open Circuit Potential
OTA	Over-The-Air Programming
PCB	Printed Circuit Board
PPG	Photoplethysmography
REFCN	Reference Connection
ReLU	Rectified Linear Unit

RNN	Recurrent Neural Network
SPE	Screen-Printed Electrode
SWAS	Sweat Analysis System
SWV	Square Wave Voltammetry
VE	Virtual Environment
VR	Virtual Reality
WE	Working Electrode
Wi-Fi	Wireless Fidelity
WLAN	Wireless Local Area Network
WSN	Wireless Sensor Network

CHAPTER 1

Introduction

Biological monitoring is a fundamental aspect of modern healthcare and plays a vital role in disease prevention, diagnosis, and treatment. The growing demand for non-invasive, real-time monitoring solutions has driven the advancement of wearable sensor technologies capable of performing sophisticated biological analyses. These innovations address key limitations of traditional monitoring methods, which are often invasive, costly, and inaccessible to broader populations.

This thesis explores the development and application of wearable sensors for non-intrusive biological analysis, with applications in sweat analysis, hydration monitoring, and drug-intake tracking. Sweat, as a biofluid, offers a valuable non-invasive means of assessing key analytes such as electrolytes, metabolites, and drugs, providing real-time insights into an individual's physiological state. By integrating advanced materials with state-of-the-art sensing technologies, these wearable devices enable the continuous monitoring of biochemical and physiological parameters, enhancing healthcare accessibility and efficiency.

Beyond healthcare, these sensors have applications in optimizing athletic performance and preventive health strategies. For example, hydration analysis provides critical data for endurance athletes, helping to prevent dehydration and electrolyte imbalances. Likewise, drug-intake monitoring facilitates personalized medication management, improving adherence and therapeutic outcomes in patients with chronic diseases.

This research investigates the design, development, and evaluation of wearable sensors, with a particular focus on their applications in sweat analysis, hydration monitoring, and drug-intake tracking. By explicitly re-examining these domains, the thesis demonstrates the potential of non-invasive sensing platforms to improve physiological assessment, enhance therapeutic management, and support performance optimization.

The two main research areas explored in this study are wearable sensors for real-time physiological monitoring and virtual environments for physical rehabilitation. Wearable sensing technologies enable the continuous and non-invasive assessment of key biomarkers such as glucose, electrolytes, and metabolites, providing valuable insights into hydration

status and metabolic function while overcoming the limitations of traditional intermittent measurements. Complementarily, virtual environments support motor rehabilitation by delivering augmented feedback and interactive simulations that enhance therapeutic engagement and recovery outcomes. Figure 1.1 illustrates these two domains: the left panel depicts representative wearable sensors, while the right panel shows the integration of virtual environments into rehabilitation workflows.

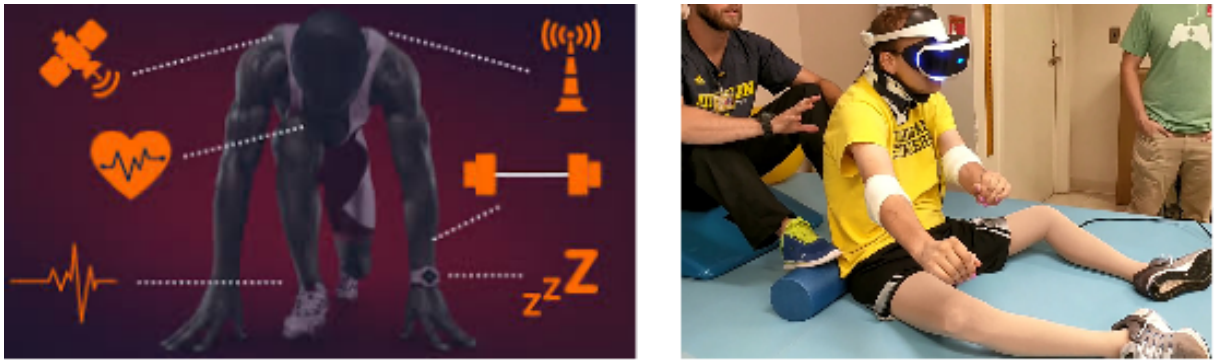


FIGURE 1.1. Primary focus areas: wearable smart sensors (left) and virtual environments for physical rehabilitation applications (right).

The two pillars of this work—wearable sensing and virtual rehabilitation—converge in an adaptive feedback cycle in which physiological information continuously informs the rehabilitation process. Wearable devices collect bio-signals such as sweat biomarkers, heart rate, and temperature, which are processed locally or at the edge to extract meaningful indicators of the user physiological state. These indicators, including hydration level estimation, electrolyte balance, and physical exertion, are then used to adjust the behavior of a virtual or extended-reality rehabilitation environment, shaping task difficulty, feedback modalities, and progression in real-time. The user motor performance and movement data generated within the virtual environment subsequently return to the AI layer, refining the system recommendations and adaptive strategies. This bidirectional exchange allows interventions to evolve dynamically, without the need for continuous clinical oversight.

By combining real-time physiological monitoring with immersive rehabilitation tools, the study highlights the potential of wearable sensors and virtual environments to support more personalized and responsive interventions in health and sports contexts. Important challenges, nevertheless, persist. Wearable technologies must operate reliably across varied real-world conditions—from high-intensity athletic scenarios to clinical rehabilitation—while maintaining measurement accuracy and user comfort. In addition, sweat

chemistry is inherently complex, and accurately distinguishing specific analytes remains technically demanding. The research presented here seeks to address these issues through advances in sensing technologies and adaptive virtual environments, contributing to more effective and individualized monitoring solutions.

1.1. Background

The healthcare industry has undergone a profound transformation with the integration of Information Systems (IS). Health Information Systems (HIS) have played a pivotal role in this shift, revolutionizing the collection, storage, management, and dissemination of patient data.

The significance of HIS comes from the critical nature of medical data. In this sector, information is more than just records—it can be the difference between life and death. Accurate, timely, and accessible patient data significantly impacts healthcare outcomes.

Recent advances in HIS have improved efficiency and patient care by streamlining workflows, reducing errors, and improving communication among healthcare professionals. These systems have also promoted a patient-centered approach, allowing individuals to access their health records easily and take an active role in their care.

With rapid technological progress, IS has evolved beyond data management. The integration of intelligent sensors and machine learning (ML) algorithms has further expanded their capabilities, enabling real-time monitoring and advanced analytics in healthcare.

Despite these advances, major challenges remain. The World Health Organization (WHO) reported in 2020 that the global health workforce reached 65 million, marking a 29% increase since the adoption of the Global Strategy on Human Resources for Health: Workforce 2030 in 2016 [**1**]. However, projections indicate a shortage of 15 million healthcare professionals by 2022, with a potential deficit of 10 million by 2030 [**1**], highlighting the urgent need for solutions in this field.

This thesis addresses these challenges, regarding the data privacy and the shortage of healthcare professionals. By integrating intelligent sensors and virtual environments, the objective is not only to enhance patient care but also to mitigate the impact of workforce shortages. The research expands on the role of these technologies in healthcare, exploring their optimization for improved patient outcomes, particularly in the accuracy and efficiency of data acquisition. In addition, this study examines the opportunities these innovations present and their contribution to the development of more efficient, effective, and accessible healthcare systems.

1.2. Motivation and Framework

Advancements in technology and medicine have significantly increased human life expectancy. However, improving quality of life is equally important as prolonging its duration. Chronic health conditions, metabolic imbalances, and inadequate monitoring of vital physiological parameters continue to impact well-being, emphasizing the need for timely and efficient healthcare interventions [**2**]. Despite progress in various fields, many healthcare monitoring systems still rely on traditional, often invasive methods, lacking widespread technological integration.

This work focuses on bridging these gaps by leveraging modern technologies to revolutionize nonintrusive health monitoring. By addressing the limitations of conventional approaches, this research integrates advanced hardware and software components to develop innovative solutions. Key technologies include smart sensors and artificial intelligence (AI), designed to monitor vital signs and biochemical markers, providing actionable real-time insights to improve individual health outcomes. Applications such as sweat analysis for hydration and electrolyte balance, metabolic monitoring, and drug-intake tracking are explored as transformative solutions to current healthcare inefficiencies.

The aging of the global population further reinforces the need for scalable and efficient healthcare solutions. In 2019, the number of individuals aged 65 and older reached 54.1 million, compared with 39.6 million in 2009, and projections estimate that this figure will rise to 94.7 million by 2060. Such demographic changes place increasing pressure on healthcare systems already affected by a shortage of professionals [**3**]. The projected growth of the elderly population is depicted in Figure 1.2, emphasizing the urgency of developing robust and accessible monitoring technologies.

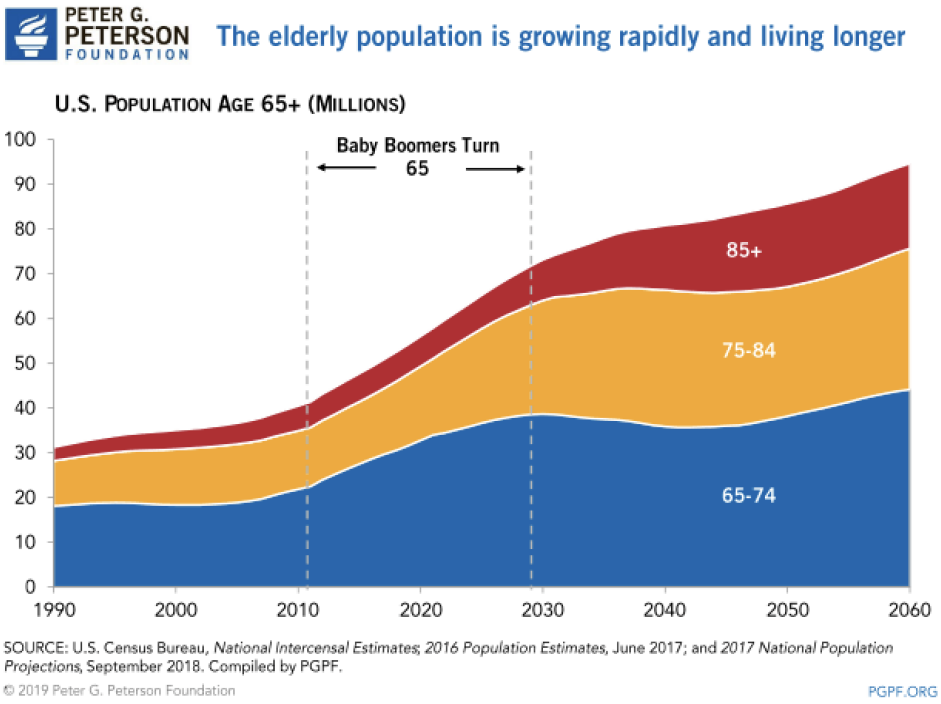


FIGURE 1.2. Projected increase in the elderly population and its implications. This chart shows expected population growth in various age groups until 2060 [**4**].

Addressing this growing demand requires a two-step strategy: reduce the reliance on manual healthcare interventions and develop innovative technologies to mitigate workforce shortages. AI plays a pivotal role in achieving these goals by enabling early diagnosis, facilitating clinical decision-making, and reducing hospital congestion through efficient treatment recommendations. The emergence of affordable wearable sensors capable of monitoring vital signs and biochemical markers has already begun to transform healthcare delivery [**5**].

The integration of AI and smart technologies is transforming healthcare across a wide range of domains, from clinical training and medical research to treatment optimization and early disease detection [**6**]. These expanding applications are illustrated in Figure 1.3. By reducing the workload of healthcare professionals, AI systems facilitate more efficient and timely clinical interventions. Complementing these advances, wearable sensors enhance healthcare quality by enabling real-time monitoring of insulin levels in diabetic patients, hydration and electrolyte balance in athletes, and cardiac function in individuals with heart conditions [**7**]. Far from being supplementary tools, these technologies are becoming essential elements of contemporary healthcare, improving patient outcomes and overall quality of life.

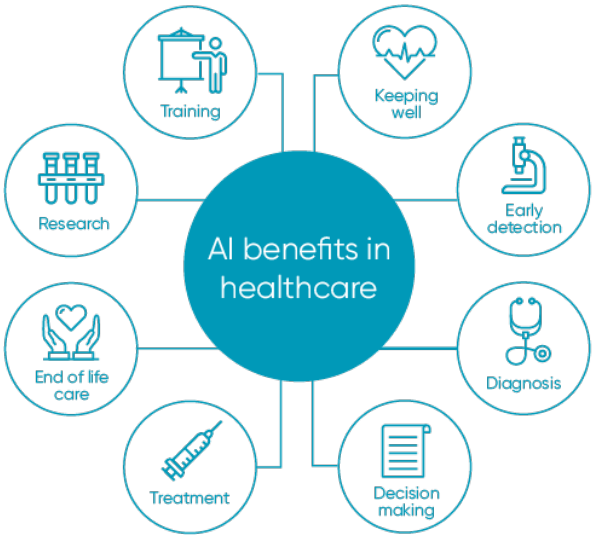


FIGURE 1.3. Role of AI and smart technology in reducing healthcare workforce needs. This figure illustrates the numerous benefits of AI in healthcare, including training, research, end-of-life care, treatment, decision-making, diagnosis, early detection, and health maintenance [**6**].

1.3. Problem Statement and Objectives

The increasing demand for efficient health monitoring systems presents substantial challenges for the healthcare industry. A growing global population and the rising incidence of chronic diseases highlight the need for real-time monitoring to prevent disease progression and improve patient outcomes. Yet, traditional healthcare systems often remain limited by inflexibility, high operational costs, and restricted accessibility.

Digital healthcare solutions offer benefits and challenges for multiple stakeholders, including patients, physicians, caregivers, healthcare systems, and the pharmaceutical sector. These advantages and limitations are summarized in Figure 1.4. Patients gain improved communication with healthcare providers, easier access to treatment information, and greater involvement in medical decision-making. Nevertheless, obstacles such as limited technical literacy, the need for training, and concerns over depersonalization remain. Healthcare professionals and caregivers similarly face challenges related to engagement, time constraints, and increased workloads. At a systemic level, digital healthcare solutions support preventive care and reduce costs, but their effective adoption requires new workflows, regulatory frameworks, and integration strategies.

Current health monitoring paradigms are heavily based on manual measurements and in-person visits, making them inefficient, error-prone, and inaccessible, particularly in

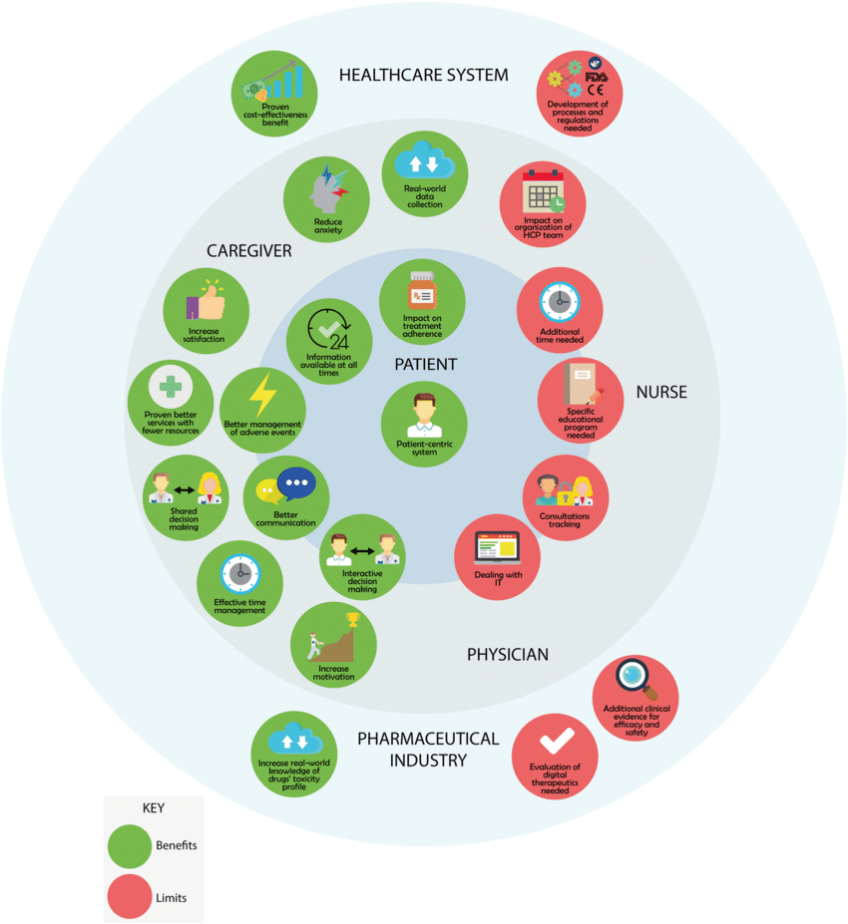


FIGURE 1.4. Benefits and limitations of digital healthcare solutions [**8**].

low-resource settings. These limitations highlight the urgent need for technological advancements that improve accessibility and reliability in health monitoring.

The advent of sophisticated sensor technology and ML presents viable solutions to these challenges. Wearable sensors and ML algorithms enable real-time health monitoring by providing continuous and accurate data collection and analysis. Figure 1.5 illustrates the transformative role of AI in healthcare.

This research focuses on designing wearable systems that integrate smart sensors and ML algorithms to advance health monitoring methodologies. The proposed systems will collect and analyze various physiological parameters, such as sweat analytes, hydration levels, heart rate, and body temperature. ML algorithms will process this data to identify patterns, detect anomalies, and provide actionable real-time insights. These systems aim to replace traditional invasive and time-consuming methods with accessible non-invasive solutions.

Specifically, the study investigates the design and implementation of a wearable biosensor analyzer for biofluid measurement. Sweat, as a readily available and non-invasive

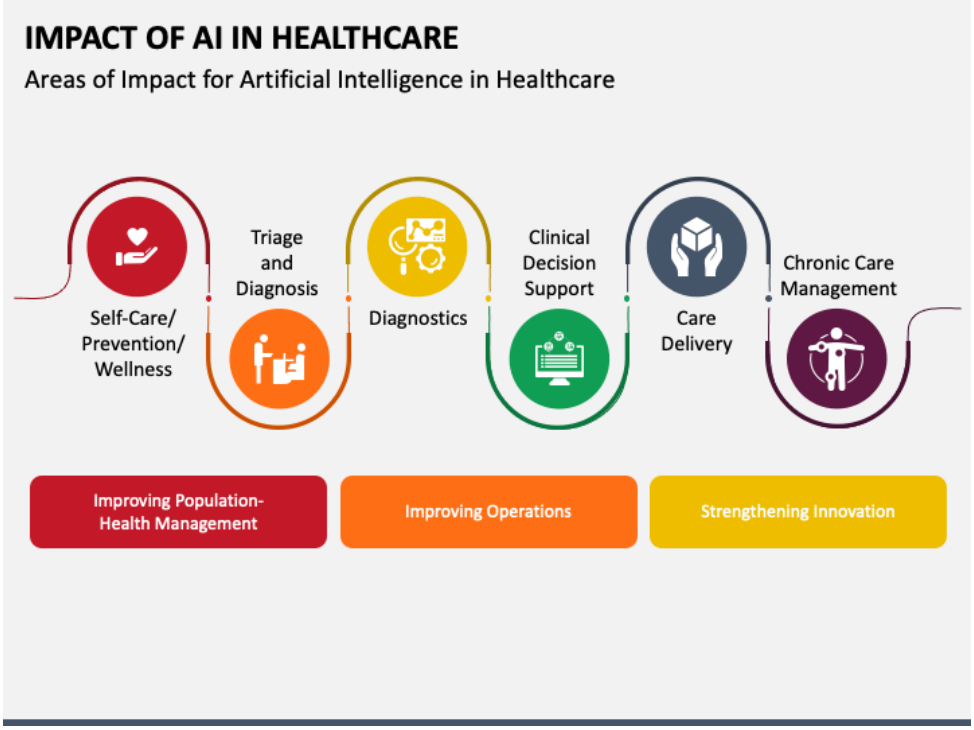


FIGURE 1.5. The role of AI in healthcare [**9**].

biofluid, is particularly valuable for monitoring analytes such as electrolytes, metabolites, and hydration levels. Wearable sensors capable of analyzing these markers provide real-time feedback, enabling personalized healthcare management. ML further improves data precision, facilitating early disease detection, improved adherence to treatment, and better health outcomes.

1.3.1. Research Questions

This research seeks to address the following key questions:

- How reliable and feasible are wearable smart sensors in acquiring meaningful biological and physiological measurements for continuous monitoring?
- How effectively can machine learning algorithms process and analyze data from these sensors to provide real-time feedback?
- What potential advantages do wearable sensors combined with ML offer in supporting personalized monitoring and management, when compared to traditional health-assessment approaches?
- Which physiological and biochemical metrics are most relevant for monitoring hydration status, electrolyte balance, and metabolic condition using wearable biosensors?

- How can the combination of wearable biosensing and real-time data analysis enhance accessibility, usability, and user engagement in physical rehabilitation and sports-performance contexts?
- What advantages and limitations do the proposed systems present relative to conventional monitoring or rehabilitation methods?

1.3.2. Objectives

Given the limitations of traditional healthcare monitoring and rehabilitation methods, the primary objectives are the following.

- Develop solutions that enable non-invasive, real-time monitoring to assess health status in relation to hydration levels.
- Enhance the accuracy, reliability, and energy efficiency of wearable smart sensors for continuous use in both clinical and athletic settings.
- Integrate AI to provide personalized health monitoring and rehabilitation.
- Design cost-effective home rehabilitation systems that reduce the need for continuous physical-therapy supervision.
- Use interactive virtual environments (VR/AR/MR) to increase patient motivation during motor recovery and improve rehabilitation outcomes.
- Reduce dependence on direct supervision from healthcare professionals by providing patients with intelligent, sensor-driven feedback.

To fulfill these objectives, the specific contributions proposed in this research include the following.

(1) Propose novel smart-sensor systems that integrate AI for real-time physiological monitoring, enabling continuous non-invasive tracking of key biomarkers such as hydration status, electrolyte balance, and metabolic health. These sensors aim to overcome the limitations of conventional health monitoring methods by providing actionable real-time data.

(2) Develop advanced virtual rehabilitation environments incorporating augmented reality and AI to enhance motor rehabilitation. These interactive systems are intended to improve patient participation, optimize therapy outcomes, and address the limitations of traditional physiotherapy methods.

(3) Identify technical challenges related to reliability, accuracy, and real-time processing of sensor data, ensuring practical implementation in both healthcare and sports.

1.4. Thesis Overview

This dissertation begins by introducing the objectives and research questions it seeks to answer, as well as providing an overview of its structure and the key contributions made. Chapter 2 provides a comprehensive review of the current state of the art in the main focus areas of this doctoral research, including intelligent sensors used to monitor various human activities, such as motor skills, vital signs, muscle movement, and neurological responses. Chapter 3 outlines the notable advancements achieved in the area of smart sensors for monitoring bioanalytes and discusses the importance of these developments. Chapter 4 examines augmented and virtual reality systems, serious games, and related case studies, surveying the current landscape of these emerging technologies and their applications. Finally, Chapter 5 offers a comprehensive discussion of the findings of this dissertation, connecting the discoveries made in this investigation with the initial objectives and research questions, and exploring the implications of this investigation in the wider academic and professional community.

1.5. Research contributions

This thesis led to the publication of several peer-reviewed works, including journal articles, book chapters, and international conference papers. These publications document the main developments and results of the research, focusing on AI-based solutions for wearable biosensing, gait analysis, and health monitoring in sports and rehabilitation. The list of scientific publications is presented below.

Scientific Journals

- JD Pereira, J Monge, O Postolache. Measurement and Applications: Electrochemical Sensors and Instruments: Main Characteristics and Applications. IEEE Instrumentation & Measurement Magazine 27 (1), 18–25
- Monge, J., Ribeiro, G., Raimundo, A., Postolache, O. and Santos, J. (2023). AI-Based Smart Sensing and AR for Gait Rehabilitation Assessment. *Information*, 14(7), 355.
- G Ribeiro, J Monge, O Postolache, JMD Pereira. A Novel AI Approach for Assessing Stress Levels in Patients with Type 2 Diabetes Mellitus Based on the Acquisition of Physiological Parameters Acquired during Daily Life. *Sensors* 24 (13), 4175 (2024).

Articles in international conferences indexed with peer review

- Monge, J. M., Postolache, O., and Pereira, J. (2025, September). Multi-channel Mobile Potentiostat for Real-Time Multi-Analyte Detection. In *2025 14th International Symposium on Advanced Topics in Electrical Engineering (ATEE).* IEEE.
- Monge, J. and Postolache, O. (2018, October). Augmented Reality and Smart Sensors for Physical Rehabilitation. In *2018 International Conference and Exposition on Electrical And Power Engineering (EPE)* (pp. 1010–1014). IEEE.
- Jin, Y., Monge, J., Postolache, O. and Niu, W. (2019, August). Augmented Reality with Application in Physical Rehabilitation. In *2019 International Conference on Sensing and Instrumentation in IoT Era (ISSI)* (pp. 1–6). IEEE.
- Paredes, T. V., Postolache, O., Monge, J. and Girão, P. S. (2021, February). Gait Rehabilitation System Based on Mixed Reality. In *2021 Telecoms Conference (ConfTELE)* (pp. 1–6). IEEE.
- Neves, J., Postolache, O., Monge, J., and Pereira, J. M. D. (2022, November). Mixed Reality and IoT for Physical Rehabilitation. In *2022 E-Health and Bioengineering Conference (EHB)* (pp. 01–06). IEEE.
- Gaspar, M., Postolache, O., Monge, J. and Mendes, J. (2023, March). Augmented Reality Serious Games for Smart Physical Rehabilitation. In *2023 13th International Symposium on Advanced Topics in Electrical Engineering (ATEE)* (pp. 1–6). IEEE.
- Monge, J., Postolache, O., Alexandre, R., de Fátima Domingues, M., Antunes, P. and Viegas, V. (2020, May). Fiber Bragg Gratings Solution for Gait Assessment. In *2020 IEEE International Instrumentation and Measurement Technology Conference (I2MTC)* (pp. 1–6). IEEE.
- Monge, J., Postolache, O., Plopa, O., Trandabat, A., Schreiner, O. and Schreiner, T. (2019, November). Glucose Detection in Sweat Using Biosensors. In *2019 E-Health and Bioengineering Conference (EHB)* (pp. 1–5). IEEE.
- Monge, J., Postolache, O., Trandabat, A., Macovei, S. and Burlacu, R. (2019, August). Mobile Potentiostat IoT Compatible. In *2019 International Conference on Sensing and Instrumentation in IoT Era (ISSI)* (pp. 1–6). IEEE.

- Monge, J., Postolache, O., Trandabat, A. and Macovei, S. (2020, October). Multi-node Potentiostat Device and Multiplatform Mobile Application for On-field Measurements. In *2020 International Conference and Exposition on Electrical And Power Engineering (EPE)* (pp. 695–698). IEEE.
- D Dias, O Postolache, J Monge. Potentiostat Network for Precision Agriculture. *2024 IEEE 22nd Mediterranean Electrotechnical Conference (MELECON)*, 885–890.

Book chapters

- Postolache, O., Monge, J., Alexandre, R., Geman, O., Jin, Y. and Postolache, G. (2021). Virtual Reality and Augmented Reality Technologies for Smart Physical Rehabilitation. *Advanced Systems for Biomedical Applications*, 155–180.

Chronogram of the research contributions

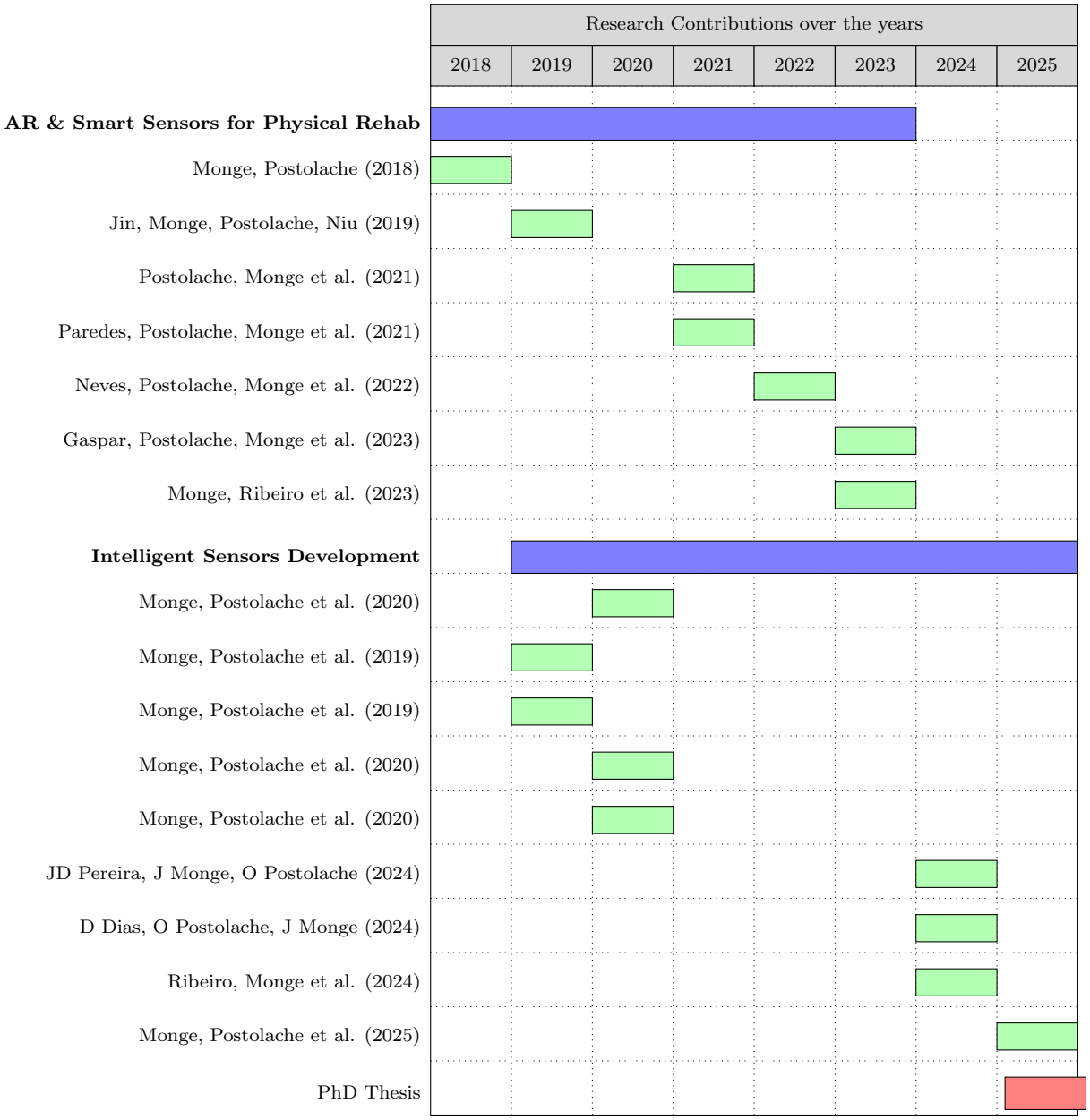


FIGURE 1.6. Research contributions over the years.

CHAPTER 2

Literature Review

The use of technology has had a major impact on the healthcare industry, particularly in physical rehabilitation and sports medicine. This chapter provides an overview of the current literature on technologies that have been applied in healthcare, such as virtual environments (VEs) and smart sensors (SSs). Examine their roles, applications, and impacts within the healthcare sector, as well as the opportunities and challenges associated with their use in physical rehabilitation and sports medicine. In addition, the chapter looks at the intersection of VE and SS and their combined influence on physical rehabilitation and sports. Finally, it identifies gaps in the existing literature and suggests avenues for future research. This review of the literature serves as a foundation for the upcoming research and provides information on how the proposed study will contribute to academic discourse and greater knowledge in this rapidly evolving field.

2.1. Technology in Healthcare

The adoption of digital technologies in the healthcare industry can improve the performance of the main healthcare business processes, particularly those that can be simplified through information technology. Implementing digital technologies can increase efficiency and improve the quality of care while reducing response times, providing benefits to a variety of stakeholders, including national health systems, clinicians, and patients. The purpose of the research by Laurenza et al. fills a gap in the existing literature by focusing on the specific implications of the adoption of digital technologies for the management of business processes by healthcare companies [**10**]. The healthcare sector is moving toward "Healthcare 5.0", a patient-centric digital wellness model that extends beyond Healthcare 4.0 by emphasizing real-time patient monitoring, ambient control and wellness, and privacy compliance using technologies such as AI, IoT, big data, and assisted networking channels. However, operational procedures, prediction model viability, resilience, and lack of ethical and regulatory frameworks are obstacles to achieving this.

Figure 2.1 provides a historical perspective on the evolution of healthcare, following its progress from Healthcare 1.0 to the envisioned Healthcare 5.0.

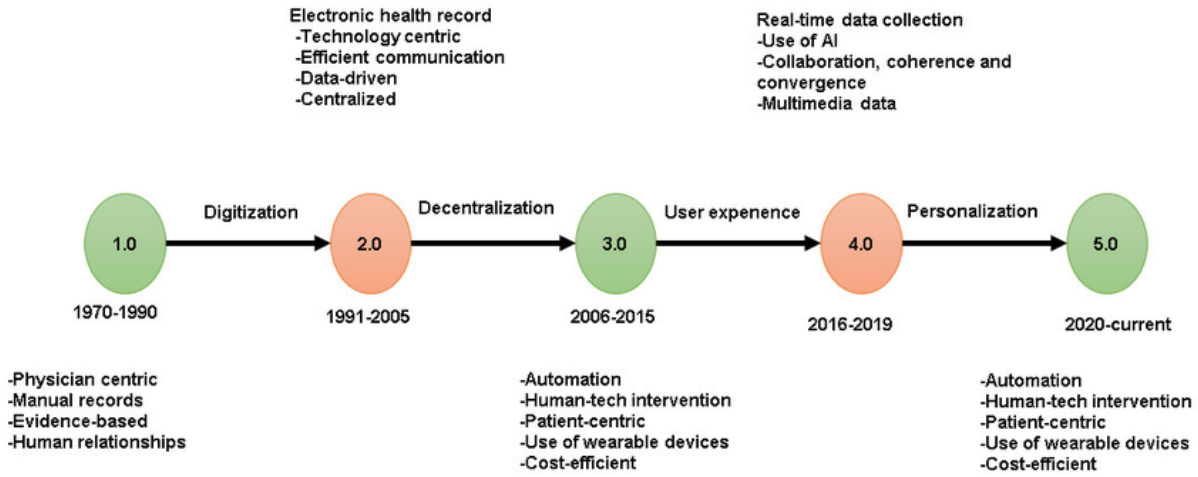


FIGURE 2.1. Historical perspective on healthcare 1.0 to 5.0 [**11**].

(1) **Healthcare 1.0:** This phase is the first stage of healthcare, characterized by traditional, individual-focused healthcare services. Physicians had complete autonomy over the care process, and technology had a minimal role. Most medical records were physical, and communication was largely face-to-face.

(2) **Healthcare 2.0:** This stage represented the incorporation of early digital technologies into the health system. Electronic health records (EHRs) started to replace physical records, and telecommunication began to facilitate remote consultations. However, these systems were still quite rudimentary and had room for improvement.

(3) **Healthcare 3.0:** Healthcare became more patient-centered at this stage. EHRs became more sophisticated and interoperable, and mobile health (mHealth) applications began to appear, allowing better patient health tracking and more personalized care. However, the potential of these technologies was not yet fully realized.

(4) **Healthcare 4.0:** Also known as Digital Health, Healthcare 4.0 is characterized by a significant increase in the use of advanced technologies such as AI (AI), Internet of Things (IoT), big data analytics and telemedicine. These technologies enable real-time monitoring, predictive analytics, and personalized healthcare, resulting in improved patient outcomes and operational efficiency.

(5) **Healthcare 5.0:** This is the envisioned future of healthcare, often referred to as "smart healthcare" or "healthcare of the future". In this stage, the healthcare

system is expected to become even more patient-centered and seamless. Healthcare 5.0 emphasizes continuous real-time patient monitoring, ambient control, and wellness. It also prioritizes privacy compliance and is expected to use explainable AI (EXAI) to make AI-based decisions more transparent and understandable.

The integration of digital technologies in healthcare, particularly smart sensors, represents an exciting frontier of innovation that has remarkable potential to transform health systems worldwide. Progress in healthcare has been noteworthy; nevertheless, certain gaps like emotive recognition, lack of personalized health applications, more precision motion capture, and AI application, deserve attention. In the evolving landscape of connected health, there is an urgent need for more research and innovative technology to unlock new opportunities, propelling healthcare towards the 5.0 era of healthcare envisioned [**12**].

This new era of healthcare offers a complex system of smart disease control, virtual care, intelligent health management, real-time surveillance, and informed decision making. This shift is supported by a variety of emerging technologies, such as nanotechnology, 5G technology, drone technology, blockchain, robotics, big data, the IoT, AI and cloud computing. Healthcare 5.0 imagines services that include remote patient monitoring, tracking, virtual clinics, emotive telemedicine, and ambient assisted living (AAL), among others [**12, 13**].

Despite its transformative potential, the journey towards resilient healthcare 5.0 is fraught with challenges. Obstacles can range from organizational issues and technological limitations to inadequate legal and regulatory frameworks. Misalignment with hospital strategies, insufficient funding, cultural and religious barriers, and individual perceptions can also pose formidable barriers. Consequently, creating resilient, technology-driven healthcare systems requires the expansion of technology infrastructure, budgetary provisions based on sustainable business models, formulation of appropriate e-health policies, standardization and synchronization of protocols, active stakeholder participation and the promotion of public-private partnerships and investments [**14**]. The following section delves into the role, capabilities, and potential of smart sensors, shedding light on their crucial contribution to shaping the future of healthcare and healthcare delivery.

2.2. Smart Sensors in healthcare

The healthcare industry is experiencing a transformation due to the use of smart sensors, which use sophisticated algorithms to collect and evaluate real-time health information. They provide personalized and proactive care, improve patient outcomes and mitigate pressure on healthcare resources. Technologies like these promise an increasingly efficient healthcare system where smart sensors filter out unnecessary data, instead focusing on key patient information. An example of this application is the calculation of the heart rate variability (HRV), a stress and emotional state indicator, from photoplethysmography (PPG) or electrocardiogram (ECG) data. Through the use of intricate algorithms on their microcontrollers, smart sensors deliver more accurate data [**15, 16**].

Wearable sensing technology, a rapidly developing branch of smart sensing, is becoming a part of our everyday lives. For example, devices such as smartwatches and bands, equipped with sensors, offer heart rate monitoring, sleep patterns monitoring, and observation of other key health indicators. The physical rehabilitation field is seeing growth in the use of smart textiles or e-textiles, with numerous studies attesting to the benefits of wearable sensors and textile-based rehabilitation systems in improving patient outcomes and efficiencies of the rehabilitation process [**17, 18, 19, 20**].

On the other hand, SensFloor, an innovative smart floor based on the embedded e-textile and capacitance principle, is a game changer in continuous patient monitoring, generates critical data for health evaluations in neurology, geriatrics, and rehabilitation, including gait speed, step count, etc., allowing early intervention by detecting asymmetric and unstable gait patterns [**21**]. In addition, it can detect falls and warn users and presents itself as a non-invasive solution for ALL.

Similarly, e-textiles find applications in improving gait analysis and indoor location monitoring. For example, Lauterbach et al. proposed a smart floor system using electronic textiles and pressure sensors for conductive measurements and to assess the plantar force distribution of the foot during gait [**22**]. In addition to this, Monge et al. introduced insoles embedded with an optical fiber sensor network using Fiber Bragg Gratings (FBG) which provided a wearable solution for plantar force distribution analysis [**23**].

The role of sensors in healthcare has expanded significantly in recent years. Equipped with Internet connectivity and sophisticated processing capabilities, many sensors now enable real-time, unobtrusive individual monitoring and broad data collection in natural environments. To fully exploit the potential of smart sensors in health research, it is

essential to understand their fundamental concepts in depth, as outlined in works like Garatva et al. [**16**].

Technologies such as Azure Kinect are capable of tracking the upper and lower limbs by creating a virtual skeleton of users with several joints as presented in Fig. 2.2, which uses elements of gamification and serious games, show promise in the rehabilitation and healthcare sectors [**24, 25**]. Their applications range from hand gesture-based elderly care [**26**] to post-stroke rehabilitation [**27**]. Users should exercise caution when using these devices. Excessive usage or improper handling of handheld controllers have been associated with injuries, particularly in systems like the Nintendo Wii [**28**]. Therefore, while technology continues to revolutionize healthcare, careful implementation and user education are key.

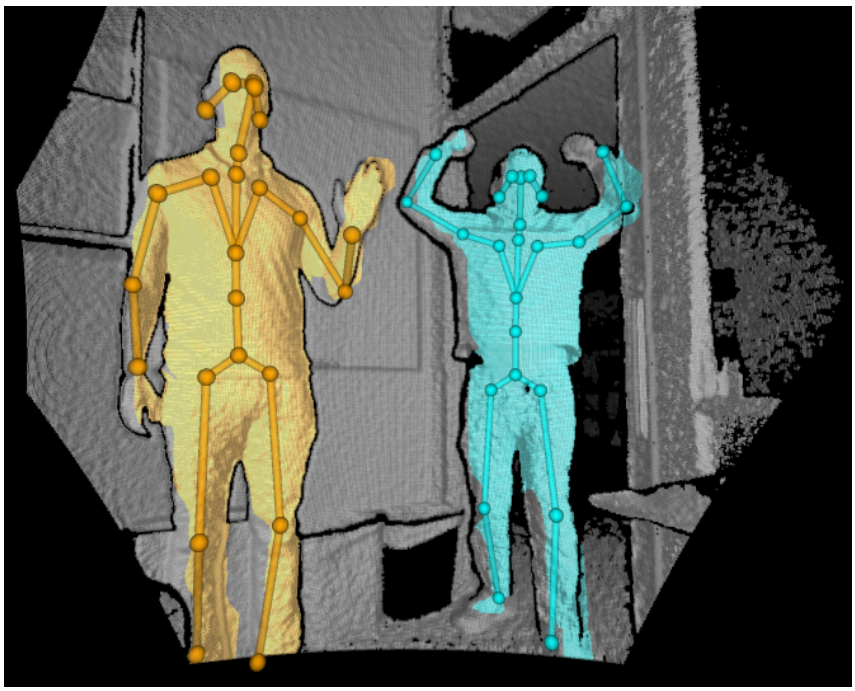


FIGURE 2.2. Azure Kinect skeleton tracking example [**29**].

The increasing use of smartphones equipped with various sensors, as illustrated in Fig. 2.3, alongside fitness bands and smartwatches, has significantly improved the accessibility of personal health monitoring. This advancement brings a new phase in personal health monitoring, providing individuals with information on heart rate, sleep patterns, physical activity, and even stress indicators [**30**].

In addition, smartphones are increasingly used for health monitoring and diagnosis. For example, their computing power, sensors, and connectivity have been used to detect diseases such as Parkinson's through tremor pattern analysis [**32, 33, 34, 35**], and to

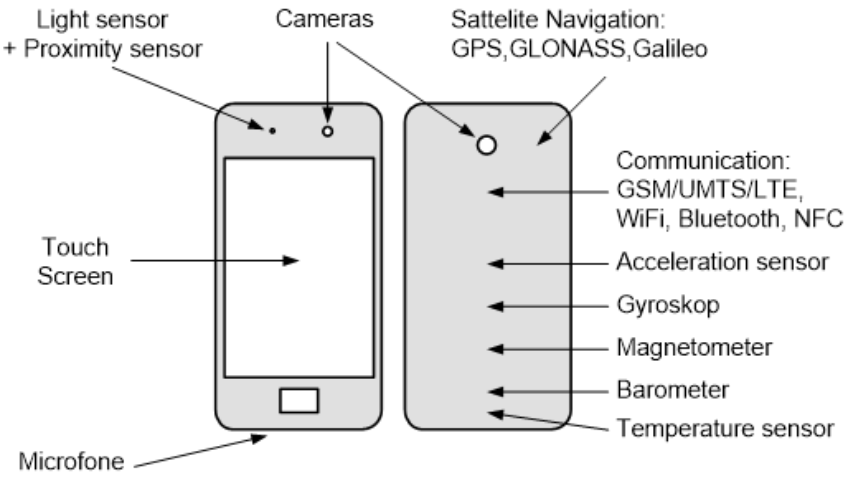


FIGURE 2.3. Smartphone Sensors [**31**].

manage diabetes through blood glucose tracking and diet recommendation apps [**36, 37, 38**].

However, fitness bands and smartwatches have quickly become critical tools for personal health management will they be capable of acquiring accurate data? They provide constant real-time health data tracking due to their ubiquitous nature, convenience, and array of integrated sensors. They have been used successfully to predict health outcomes and manage chronic cardiac conditions [**39, 40, 41, 42**].

Despite these advances, challenges remain, such as data privacy and accuracy issues and the urgent need for rigorous clinical validation of health applications and devices. Nazarian et al. presented a systematic review of the applications of these devices in the detection of cardiac irregularities [**43**], with promising results. However, these highlight the need for more comprehensive studies and the establishment of clear guidelines to fully utilize these devices to improve healthcare outcomes.

2.2.1. Overview of smart sensors and their characteristics

Understanding the realm of smart sensors involves examining their evolution over time and the innovations they have provided in the rapidly progressing domains of healthcare and sports science. To fully appreciate their role, we will unravel the nuances and essential characteristics of smart sensors, delve into their applications within healthcare and endurance sports, and shed light on how emerging ML algorithms augment the capacities of health monitoring systems. This exploration underscores the integral role that real-time analysis of the human body plays in injury prevention, personalized training, and health management. In addition, we will examine the pivotal role that edge computing plays in these fields, with an emphasis on its potential to minimize latency, improve privacy, and facilitate real-time decision making.

The evolution of sensor technology from Sensor 1.0 to Sensor 4.0 is illustrated in Figure 2.4, highlighting the progressive increase in sensor complexity and functionality and its impact on advances in healthcare and endurance sports.

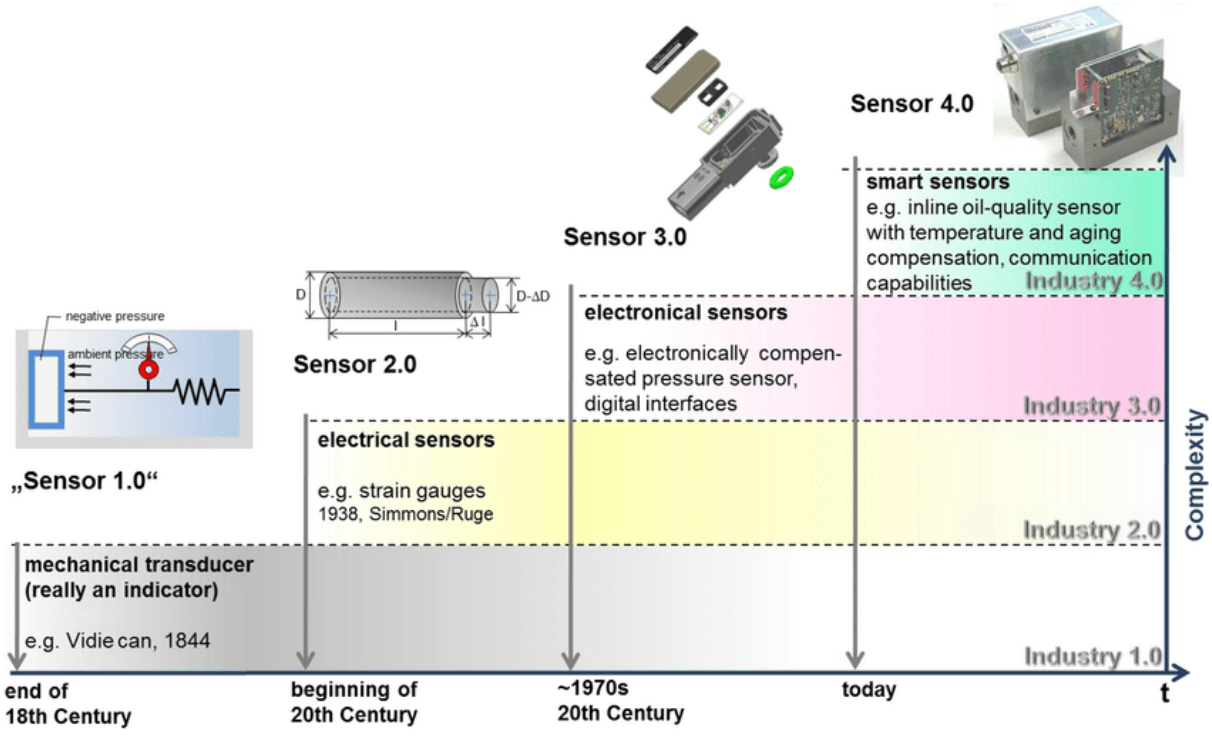


FIGURE 2.4. Evolution of sensor technology [**44**].

Sensor 1.0 (First Generation): Analog Sensors - Marking the beginning of this journey, the first-generation sensors primarily produced continuous electrical signals correlating to the measured physical parameters such as temperature, pressure, or acceleration.

Their primary limitation was their dependence on external circuits for signal conditioning and processing, which made them less adaptable and challenging to incorporate into complex systems.

Sensor 2.0 (Second Generation): Digital Sensors - Second-generation sensors, or digital sensors, facilitated the transition from analog signals to discrete digital values via analog-to-digital converters (ADC). This transformative step enabled their seamless integration with microprocessors and digital control systems, thus enhancing the performance and dependability of sensor networks.

Sensor 3.0 (Third Generation): Smart Sensors - The evolution of sensor technology ushered in the era of smart sensors. These third-generation devices amalgamated sensing elements with signal processing and communication capabilities into a single unit. Their integrated microprocessors facilitated on-board data processing, calibration, and self-diagnostics, thereby significantly increasing accuracy, reliability, and functionality. The ability to communicate with other devices and networks opened up avenues for the development of intricate and interconnected sensor systems.

Sensor 4.0 (Fourth Generation): Intelligent Sensors - The current age is dominated by "intelligent sensors". They extend the capabilities of smart sensors by incorporating advanced features such as ML algorithms, adaptive signal processing, and decision-making capabilities. These sensors can autonomously adapt to environmental changes, learn from collected data, and make informed decisions. With their improved performance, versatility, and energy efficiency, intelligent sensors have a broad spectrum of applications in healthcare and endurance sports.

The progression from Sensor 1.0 to Sensor 4.0 represents a significant technological leap. The transition from simple analog devices to intelligent sensors equipped with onboard processing and decision-making capabilities has facilitated more precise, reliable, and efficient monitoring and analysis of human body characteristics in healthcare and sports science. As sensor technology advances, we anticipate further developments in real-time human body analysis, which could improve health and performance outcomes. This comprehensive understanding of sensor technology's evolution provides a robust foundation for exploring its applications and impact in physical rehabilitation and sports medicine.

2.2.2. IEEE 1451 Standard

Continuing the trajectory of smart sensors, their development journey has seen remarkable progress from inception, with applications significantly extending into healthcare and endurance sports. An integral part of this progress was marked by the adoption of the IEEE 1451 standard. This standard, developed by the Institute of Electrical and Electronics Engineers (IEEE), responded to the pressing need for a unified and standardized approach to the interface of sensors and actuators with microprocessors, control systems, and networks [**45**].

The IEEE 1451 standard was introduced with the objective of streamlined sensor integration, improved sensor data, and support plug-and-play capabilities in sensor networks. One of its novel concepts is the Transducer Electronic Data Sheet (TEDS), a memory device that is connected to each sensor. The TEDS stores crucial sensor-specific information, such as sensor identification, calibration data, measurement range, and manufacturer details. This information allows the sensor network to automatically identify and configure connected sensors, simplifying system integration and maintenance tasks.

Further, the IEEE 1451 standard advocates the utilization of a Network Capable Application Processor (NCAP). This serves as a link between the sensors, actuators, and the network or control system. The NCAP performs multiple functions, including sensor data processing, data fusion, and communication facilitation with other network devices, thus optimizing the overall architecture of the system.

By establishing a standard framework for sensor integration and communication, the IEEE 1451 standard has been pivotal in the progression of smart sensor technology. It has encouraged greater interoperability among sensors across different manufacturers, paving the way for increasingly complex and sophisticated sensor networks in healthcare and endurance sports applications. Consequently, the IEEE 1451 standard has fueled the development of more efficient, precise, and flexible systems dedicated to monitoring and analyzing human body features. Building on this foundation, we can now go deeper into how these standardized smart sensor technologies are shaping modern healthcare and endurance sports.

2.2.3. Applications of Sensors in healthcare

In recent years, advances in sensing techniques, affordability of integrated circuits, and the progress of connectivity technologies have fueled the use of wearable equipment and sensing devices in the field of health monitoring and physical rehabilitation. Nascimento

et al. extensively reviewed these aspects of healthcare technology, focusing mainly on the implementation of sensors and their role in biomedical applications, including healthcare settings, home medical assistance, and continuous health monitoring [**46**].

Concurrent research efforts have been made to address ongoing challenges and explore future opportunities in the expanding use of wearable technologies. For example, Rogers et al. discuss the current challenges and potential future advancements in the field of rehabilitation and health monitoring, with particular emphasis on the effectiveness of wearable sensors and systems for rehabilitation [**47**].

2.2.3.1. ***Force and Pressure Sensing.*** In the realm of gait analysis and foot pressure evaluation, a wide range of sensing technologies is commonly used, including pressure sensors, inertial measurement units (IMUs), force sensors, camera-based systems, and Electromyography (EMG). These tools are widely used in the assessment of patients with neurological conditions such as multiple sclerosis (MS), Parkinson's disease, and stroke.

Although the potential of wearable sensor technology to transform physical rehabilitation has been recognized for several years, its use has largely remained within research laboratories. Lang et al. identify several barriers hindering the implementation of wearable sensor technology in routine clinical rehabilitation, involving both technological and clinical challenges. They propose a set of benchmarks to encourage widespread adoption and evaluate an existing wearable device system against these criteria, emphasizing the need for coordinated efforts to overcome the identified limitations. Progress in this direction could support more effective movement interventions across clinical, home, and community settings [**48**].

The utility of wearable sensors for fall detection and risk assessment, especially in elderly individuals, is another growing area of research interest. Ahn et al. developed preimpact fall detection algorithms using data collected by a custom-made inertial measurement unit (IMU), achieving 100% accuracy in fall detection [**49**]. Bet et al. presented a systematic review of the use of wearable sensors for the detection of fall-related events in older individuals. The review highlighted the need for consensus on aspects such as sample size, population under study and data acquisition for each application, despite the promising potential of wearable sensors for fall detection [**50**].

In recent years, there has been a growing interest in the intersection of healthcare and technology, with a particular focus on the use of wearable technology and IoT devices to support the elderly and those living with chronic disabilities. As emphasized by Rahman

et al., the design of application-specific routing protocols within healthcare settings is of utmost importance. They advocate that such designs can enhance data throughput and extend the useful life of network systems, highlighting the promising potential of these technologies [**51**].

However, despite the transformative potential of wearable technologies and sensor systems, significant research and development efforts are still required to overcome existing challenges and meet proposed benchmarks. If these obstacles can be successfully navigated, we could see a substantial improvement in the effectiveness of physical rehabilitation interventions and overall patient outcomes. The journey towards these breakthroughs calls for a concerted effort to create advanced technologies and to foster their widespread adoption within clinical practice.

Angelini et al., on the other hand, explore the potential of wearable sensors in quantifying gait alterations associated with progressive MS by placing wearable motion sensors WS1, WS2 and WS3 on the user body as illustrated in Fig. 2.5 and obtaining relevant acceleration data, it was possible to analyze user gait. They assert that these sensors can accurately differentiate individuals flagged for MS from healthy ones, and that the extent of gait changes corresponds to the severity of disability [**52**].

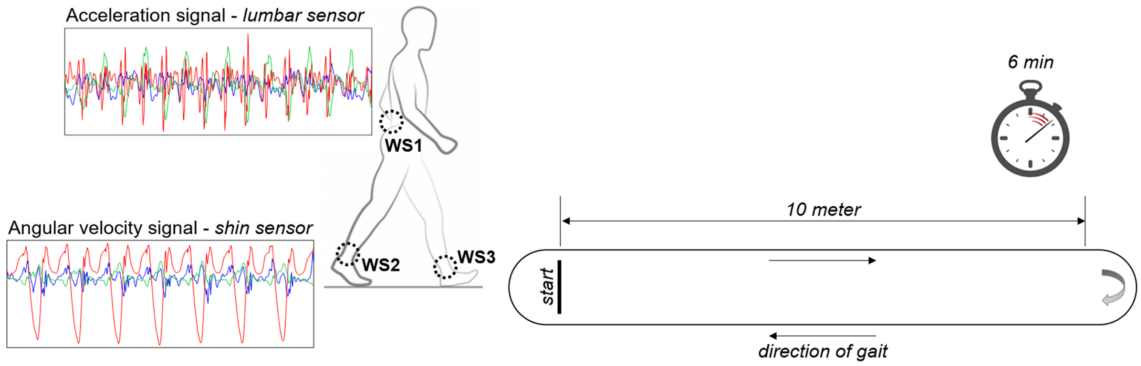


FIGURE 2.5. Wearable sensors example application [**52**].

Taking a broader view, Khoshmanesh et al. discuss the latest advancements in wearable sensors and their potential applications in personalized health monitoring, smart prosthetics, and assistive technologies. They outline areas that require further research to fully realize the potential of wearable sensors [**53**].

In a study that aims to assist visually impaired individuals, Bauer et al. introduce a system that uses deep learning techniques and low-cost wearable sensors. This system

provides critical information on potential obstacles to the user, enhancing the mobility of visually impaired people in outdoor environments [**54**].

Lastly, a comprehensive literature review conducted by Stavropoulos et al. presents an overview of IoT wearables and interconnected sensing technology in elderly care. The review draws an in-depth picture of the current state of the art, trends, and effective practices in the application of technology to elderly care [**55**]. Figure 2.6 illustrates an example of an elderly care system, highlighting the integration of IoT devices and smart sensors to enhance monitoring, safety, and quality of life.

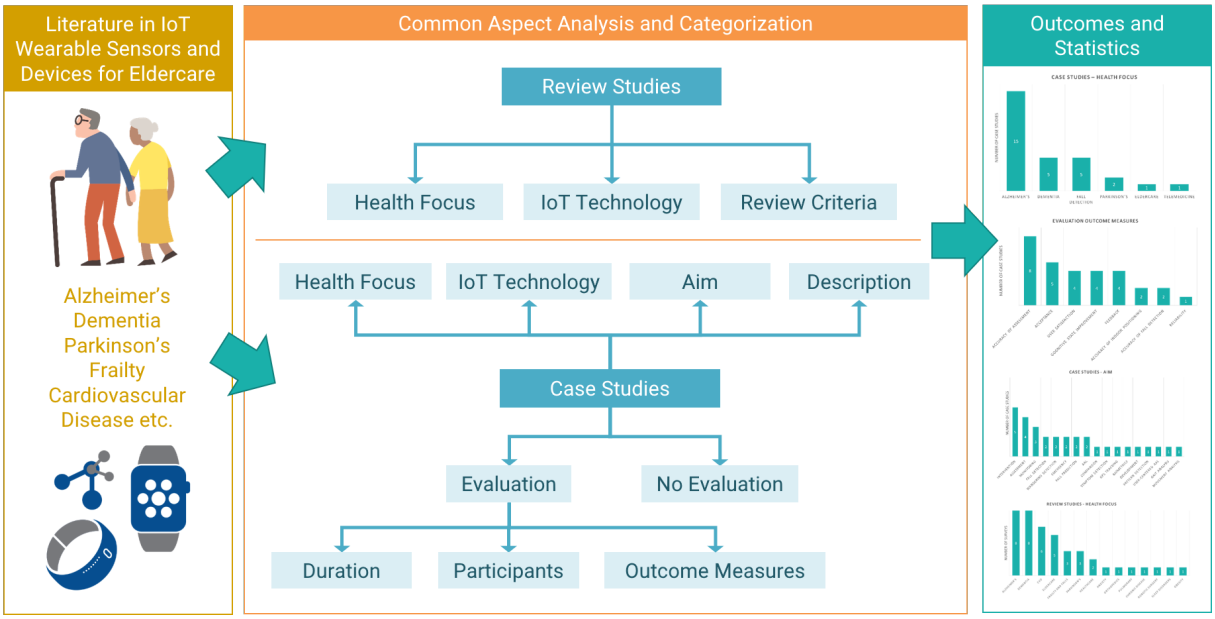


FIGURE 2.6. Elderly Care System Example [**55**].

2.2.3.2. ***Ambient Sensors.*** The transition from wearable sensors to ambient sensor technology, integrated within the environment, brings another dimension of health monitoring and support for elderly and chronically ill patients. These systems are installed in living spaces and provide unobtrusive monitoring, a feature that is particularly favorable for people uncomfortable with wearable devices. They capture changes in the environment or routine and signal any anomalies that might indicate a health problem. Recent advances in this domain are promising. Technologies that automatically adjust to a user's needs and AI-powered systems that interpret ambient sensor data are being developed, providing a richer understanding of an individual's health and well-being. However, while these strides are impactful, ongoing research is still necessary to address challenges such as privacy, security, and system integration.

Although the adoption of wearable sensors in health monitoring and rehabilitation has been rapid, the use of ambient sensors embedded within living spaces has also seen significant progress. Marques outlines the relevance of systems and architectures for AAL, given the aging of the global population [**56**]. Technologies designed to meet the needs of an aging population offer the prospect of maintaining independence for longer periods. The section discusses how advances in sensors, embedded devices, and the IoT make it possible to monitor and assist people in their homes.

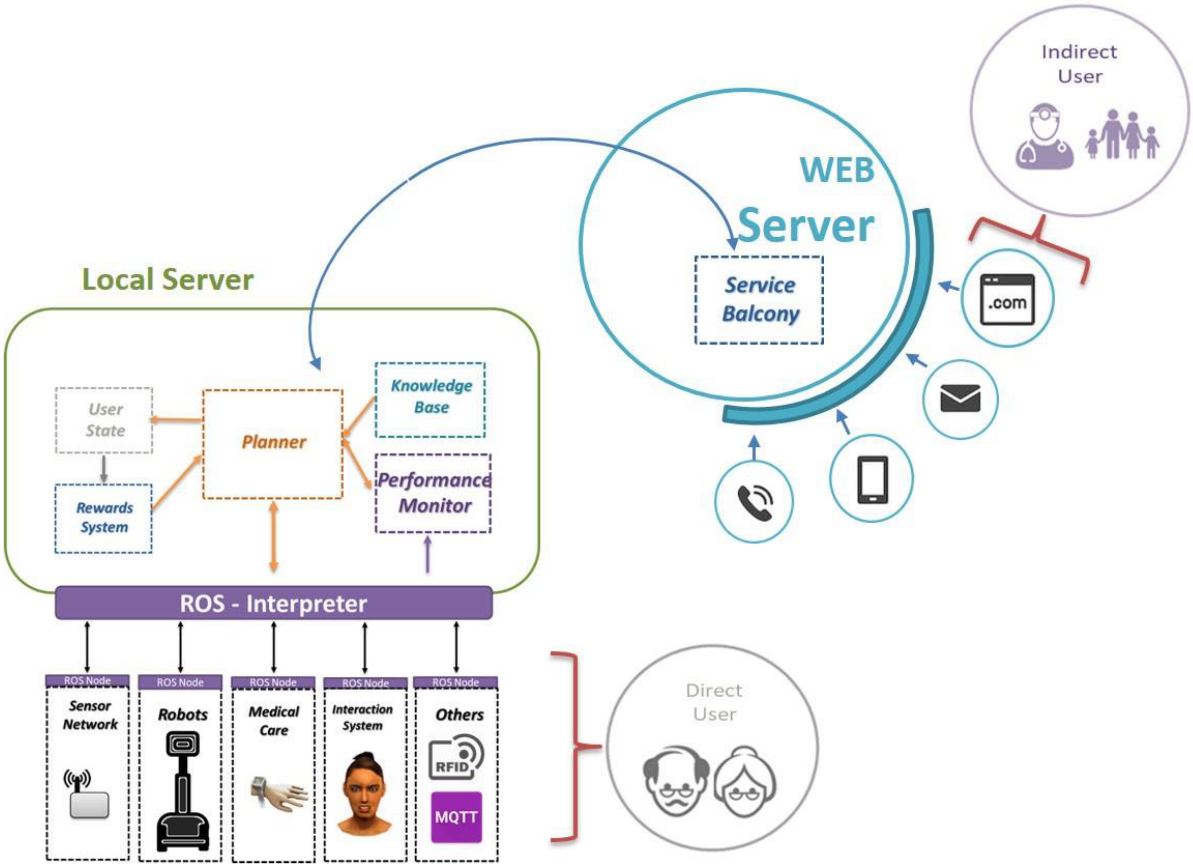


FIGURE 2.7. Architecture of an ambient-assisted living system integrating robots with a network of ambient sensors and actuators [**57**].

Integration of these ambient sensors with other forms of technology, such as robotics, can create a comprehensive assistance system for the elderly. Loza-Matovelle et al. describe the development of such a system that combines robots with a network of sensors and actuators [**57**]. Figure 2.7 illustrates the architecture of this system, showing how it adapts to user-specific needs by interacting with direct users while providing external users with remote access.

AAL technologies can provide significant support for older adults who may have cognitive and physical impairments. Genesan et al. discuss the potential of these technologies

in helping elderly people live safely and independently [**58**]. Such technologies can help maintain physical and mental health and improve quality of life, making them an essential tool in the management of age-related problems.

Cicirelli et al. present a comprehensive review of active and assisted living (AAL) systems, addressing the main trends in their development from technological and methodological perspectives [**59**]. The article highlights critical areas for future research, recognizing the potential of these systems to improve quality of life and support independent living.

2.2.3.3. ***Breath Sensing Devices.*** Breathing, a vital sign of life, has received significant attention in the realm of health monitoring. The integration of technology into this fundamental aspect of life offers a promising research path, especially in the development of novel breath-sensing devices. This section delves into various novel methodologies and advances in the field, emphasizing their applications and potential for future improvements.

Kandil et al. have presented a pioneering approach to developing an IoT context-aware system tailored specifically for the blind, visually impaired, and elderly populations. This system integrates functionalities such as improved indoor navigation, communication, and security, paving the way for an enriched assisted living environment [**60**].

Sabil et al. used the latest sensor technology to refine the detection of apneas, life-threatening pauses in breathing during sleep. They proposed tracheal sound sensors positioned at the suprasternal notch as a viable alternative to traditional thermistors, highlighting the value of these sensors in discerning patient breathing patterns [**61**].

Elevating the scope of non-invasive methods, Jagadev et al. leveraged infrared thermography to observe respiration rates without physical contact. Incorporating ML, they devised an astute "Breath Detection Algorithm" to trace nostril activities. This technique not only refined the signal-to-noise ratio, but also proficiently distinguished between regular and irregular breaths [**62**].

Li et al., on the other hand, integrated sound recognition, airflow detection, and respiratory monitoring into one unified sensor. This cotton fiber aerogel layered with polypyrrole showcased a spectrum of desirable attributes, including a broad response range, robust stability, and featherweight design. These characteristics identify the sensor as a prospective instrument for multi-faceted applications, including detection of sound signals and real-time respiratory surveillance [**63**].

Further pushing the technological frontier, He et al. debuted a wireless physiological tracking system pivoting on a pyroelectric generator. Harnessing body temperature fluctuations, this avant-garde system, when coupled with a mobile application, empowers users with the capability of tracing oral or nasal breathing patterns in real-time. Such innovations facilitate self-health assessments and generate crucial data for distant health diagnostics [**64**].

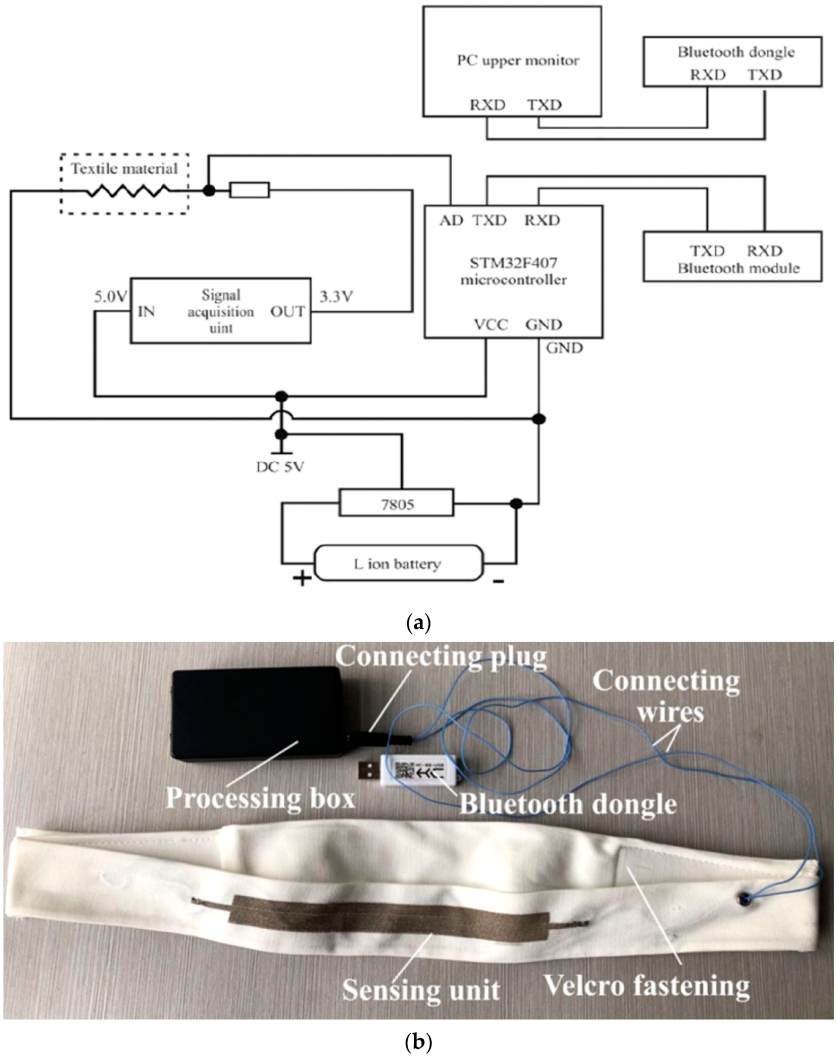


FIGURE 2.8. a) Circuit Diagram Scheme b) Non-intrusive System Prototype [**65**].

De Fazio et al. provided a holistic view of wearable sensors designed for respiratory rate monitoring. Their exploration focuses on piezoresistive and inertial sensors, prized for their unobtrusiveness, feather-like weight, and seamless integrability. Their findings resonate with the ongoing trend: transitioning towards a more user-friendly and non-intrusive health monitoring paradigm [**65**]. Figure 2.8 presents the circuit diagram and

the prototype of the non-intrusive system, highlighting its compact design and suitability for continuous respiratory monitoring.

In conclusion, the investigation by Wang et al. illuminates the future potential of respiratory monitoring through camera technology. Their analysis focuses on two significant approaches: motion-based tracking and photoplethysmography (PPG), offering an in-depth assessment of their advantages and limitations [**66**].

2.2.3.4. ***Motion Analysis Sensors.*** Motion analysis plays an important role in physical rehabilitation. This section synthesizes the ground-breaking mapping of the gait rehabilitation technology trajectory, focusing on the potential of Functional Electrical Stimulation (FES), wearable sensors, Inertial Measurment Units (IMU) and advanced rehabilitation machines.

Schifino et al. presented a paper on the use of foot drop stimulators (FDS) for stroke patients. By integrating a wearable inertial sensor, they investigated the dynamics of gait and discovered that FDS devices markedly improved the spatiotemporaloral dimensions of gait and also refined the harmonic ratio in the mediolateral sphere [**67**]. Such revelations hint at the transformative role that wearable technologies, such as FDS, can play in rehabilitating stroke survivors and streamlining their ambulatory patterns.

Another example of gait analysis is presented by Diaz et al. a wearable sensor solution for gait evaluation and rehabilitation [**68**]. Such wearables, by quantifying gait, balance, and motion range, introduce an objective flair to gait assessments. They serve as invaluable conduits for chronicling patient progress and could even hold the key to preemptively detecting movement anomalies.

Zampogna et al. emphasized the existence of a correlation between balance and neurological health. In their research, they presented a meticulous review on the role of wireless sensors in assessing balance, highlighting their monumental contribution to the management of postural volatility in patients grappling with diseases such as Alzheimer's, Parkinson's, and MS, among others [**69**].

Schmidt et al. ventured into the realm of gait rehabilitation machinery equipped with programmable footplates. Such machines are adept at offering multifaceted gait training experiences that mirror real-world scenarios, such as ascent and descent of stairs, outperforming conventional methodologies [**70**].

Ciobanu et al. echoed similar sentiments, but emphasized the overarching need to tailor training regimens to encapsulate the intricate blend of physical and psychological facets that characterize ambulation in multitasking contexts in real life [**71**].

These cohesive insights signal a paradigm shift. The motion analysis sphere is transitioning from the age-old subjective assessment modes to a more objective, individualized, and efficient system fortified by contemporary technologies.

Milosevic et al. then embarked on an investigation comparing inertial wearable sensors with the Kinect for potential deployment in domiciliary motor rehabilitation regimens [**72**]. Their exhaustive comparison revealed comparable proficiencies across both platforms, especially for broad-motion drills. However, a detailed home evaluation unraveled the distinct advantages and limitations inherent to each system.

Bavan et al., harnessing the power of a singular inertial sensor, charted patient adherence to shoulder rehabilitation drills [**73**]. Their approach, founded on supervised ML algorithms, showcased the prowess of inertial sensors in discerning specific exercises from generic movements: an innovation that could redefine treatment blueprints and increase patient participation.

In their seminal review, Picerno et al. sketched the evolution of inertial sensors, observing their metamorphosis from lab-centric gadgets to indispensable tools for prolonged movement analysis in organic environments [**74**]. As the review suggests, the future of wearables in unsupervised settings hinges on leveraging ML's capabilities to distill and interpret voluminous data churned out by these sensors.

2.2.3.5. ***Blood Monitoring Sensors.*** Technological advancements in healthcare are propelling us towards novel models, with the blood monitoring sector witnessing exceptional progress. Employing methods like PPG, infrared spectroscopy, pressure, and camera-based technology, researchers are pioneering advancements in non-invasive and precise monitoring of blood parameters.

El-Hajj et al. investigated the application of deep learning in the domain of blood pressure monitoring, especially emphasizing PPG signals [**75**]. Addressing the escalating global issue of hypertension, their study advocates for the utilization of RNN featuring bidirectional links and an intricate attention system. The findings of their research highlighted a significant association between PPG signals and blood pressure values, demonstrating notable predictive precision.

Taking into account the pressing concern about diabetes, Rachim et al. present a breakthrough in non-invasive blood glucose monitoring [**76**]. Their pioneering biosensor, marrying cost-efficiency with rapid data procurement and enhanced wearability, employs visible near-infrared spectroscopy. This innovative method discerns nuanced optical signals reflected during fluctuations in blood glucose concentrations. Their in vivo investigations yielded encouraging results, cementing a robust correlation between their estimations and reference blood glucose values.

Moving to the realm of remote blood pressure tracking, Kario et al. posit a compelling argument in favor of wearable devices [**77**]. These wearables, they argue, are poised to revolutionize hypertension management by facilitating low-stress recurrent blood pressure readings. Their research narrative extols the virtues of "anticipation medicine," a forward-looking approach that capitalizes on predictive data to prevent the onset of potential health risks.

Complementing this research thread, Djeldjli et al. explored the fascinating territory of estimating pulse wave parameters that reflect arterial stiffness and blood pressure using camera-centric methods [**78**]. Using advances in sensor technology and image processing, they put forth an ingenious non-invasive method using imaging photoplethysmography (iPPG). The results of their study are testimony to the close-knit relationship between iPPG and contact photoplethysmographic characteristics (cPPG), heralding new frontiers in remote blood pressure and arterial stiffness evaluation, along with non-contact cardiovascular diagnostics.

Collectively, these explorations underscore the exhilarating pace at which blood monitoring technologies are advancing, crafting a future where non-invasive, precise, and instantaneous health parameter tracking becomes the norm.

2.2.3.6. ***Non-Invasive Glucose Monitoring.*** In today's evolving healthcare landscape, the quest for more efficient and patient-friendly glucose monitoring is gaining momentum, particularly in light of the growing global prevalence of diabetes.

Tang et al. provide an insightful dive into the realm of non-invasive blood glucose monitoring, shedding light on its significance for those diagnosed with diabetes [**79**]. Breaking down the landscape into optics, microwave, and electrochemistry, the authors explore the potential and pitfalls of each technology. Their comprehensive overview underscores a pressing need for devices that are not only efficient but also accessible and resilient.

Battelino et al. presented the advantages of continuous glucose monitoring (CGM) in clinical trials. They claim that CGM-derived metrics, which continuously collect data, capture intricate nuances in glucose fluctuations that conventional HbA1c tests may overlook [**80**]. Stressing the necessity of streamlined CGM data collection in clinical research, they emphasize its potential in driving more precise and actionable insights.

In the context of the COVID-19 pandemic, Agarwi et al. highlight the efficacy of real-time CGM (rtCGM) for critically ill patients in intensive care settings [**80**]. Their findings illuminate the precision and feasibility of rtCGM, emphasizing its value in minimizing the need for regular point-of-care glucose checks.

Providing a fresh perspective, Sempionatto introduces an electrochemical sweat sensor at the fingertip as an innovative solution to painless glucose self-testing [**81**]. Once calibrated, the sensor promises precision in glucose readings, fostering a higher degree of patient adherence. Figure 2.9 illustrates this non-invasive glucose touch sensor, highlighting its compact design and potential for seamless integration into daily health monitoring routines.

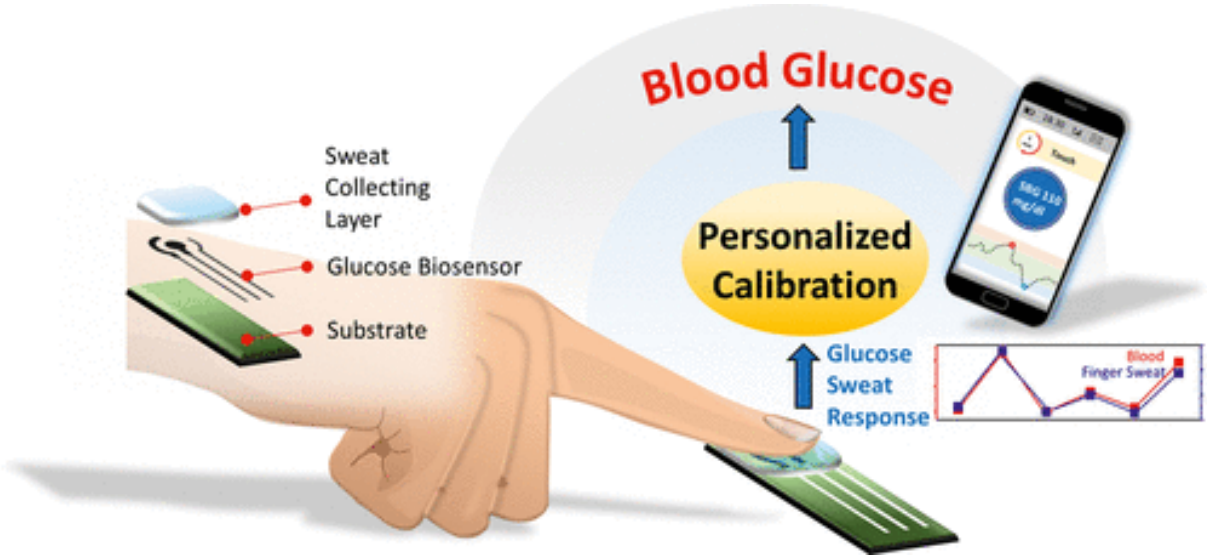


FIGURE 2.9. Innovative Non-invasive Glucose touch sensor [**81**].

Laffel conducts an in-depth analysis of the effects of CGM on glycemic control in adolescents and young adults with type 1 diabetes, a population that frequently struggles with unstable blood glucose levels [**82**]. The investigation identified a moderate, yet statistically significant, enhancement in glycemic regulation when CGM was used alongside conventional monitoring over a six-month period. Galindo et al. contribute additional insights about CGM's transformative role in healthcare environments, particularly during pandemics when reducing viral exposure is paramount [**83**].

Extending this research, Mian et al. examine the integration of CGM with insulin pumps, emphasizing their collective efficacy in transforming insulin-dependent diabetes treatment [**84**]. However, despite these clear benefits, they express concern over the inadequate prescription of this powerful technology.

In their study, Lee et al. underscore the persistent discussion around the clinical significance of state-of-the-art CGM systems, which are garnering increased attention despite being less invasive [**85**]. This notion of an unavoidable transition towards non-invasive options is echoed by Gonzales et al., who document the progression from invasive methods to those that are minimally invasive or non-invasive [**86**]. They foresee a future where these technological advancements achieve widespread adoption.

Adding to this innovative mix, Zhao et al. unveil a self-sufficient smartwatch that continuously tracks sweat glucose metrics, driven solely by solar energy, heralding a future where wearables address core safety and efficiency concerns [**87**].

In summary, the glucose monitoring domain is at the top of a transformative era, filled with innovative approaches that emphasize both patient comfort and measurement precision. However, ongoing research and investigation are essential to fully realize the potential of these advancements.

2.2.3.7. ***Sweat monitoring Sensors and Systems.*** The human body encapsulates a complex network of signals, often revealing information about its condition, capabilities, and susceptibilities. Among these signals, sweat can represent a potent source of information regarding an individual health condition. Comprising a wide array of electrolytes, metabolites, and additional biomarkers, sweat analysis represents an exciting emerging area in sports and healthcare science. In the medical field, the diagnostic capabilities of sweat are particularly valuable for conditions such as diabetes and cystic fibrosis, which notably change its composition.

Athletes, particularly those in endurance sports, have a huge benefit from sweat analysis. Monitoring elements such as sodium and potassium can relay vital information about hydration, while glucose levels in sweat offer clues about energy use. In addition, the detection of certain metabolites or stress hormones can be indicative of fatigue and recovery requirements.

A notable example of such technology is the pioneering sweat sensing system developed by Eccrine Systems (Figure 2.10). This system integrates real-time sweat analysis with wireless transmission, enabling continuous monitoring of key physiological markers. By

selectively measuring electrolytes, metabolites, and skin temperature, this wearable platform provides valuable insights into hydration, metabolic health, and overall physiological status. Such advancements bridge the gap between traditional biosensing technologies and personalized health monitoring, offering a promising tool for both medical applications and sports performance optimization.

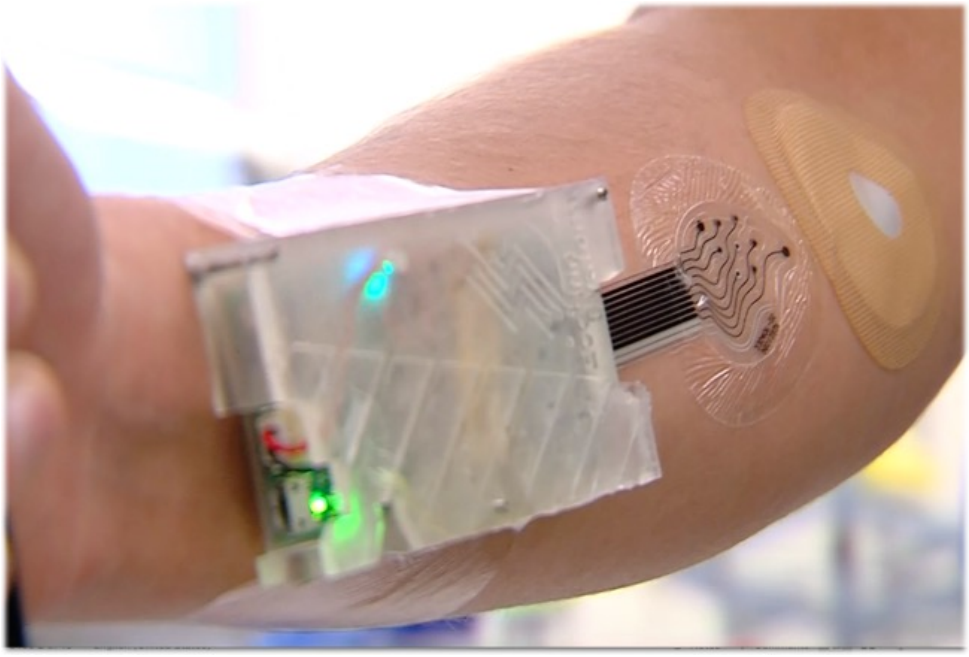


FIGURE 2.10. Pioneering Sweat Sensing Technology by Eccrine Systems [**88**].

A review by Yeung et al. encapsulates the decade-long advances in wearable devices, highlighting the proliferation of electrochemical sweat sensors in the diagnostics, healthcare and sports domains [**89**]. The authors emphasize the convenience and user-centric design of these battery-free systems.

Adopting a detailed perspective, Zafar et al. scrutinize the developing field of non-invasive CGM, with a particular focus on sweat sensor techniques [**90**]. They review the advancements made in incorporating such sensors into wearable devices and discuss the obstacles faced in bringing these technologies to market.

Lu et al., in their work, present an integrated sweat monitoring system featuring microsupercapacitors, specifically using glucose sensors rooted in NiCo2O4 / chitosan formulations [**91**]. This research underscores the real-time diagnostic potential of such devices.

Gai et al. then introduce a revolutionary wireless self-powered sweat analysis system (SWSAS) that employs selective biomarker tracking and wireless data transmission, supported by hybrid nanogenerator modules [**92**].

Further pushing the boundaries, Liu et al. showcase wearable devices powered by innovative sweat-activated biocompatible batteries [**92**]. Their stretchable battery model epitomizes the future of prolonged wireless physiological monitoring.

Transitioning from energy to drug detection, Tai et al. highlight wearable sweat sensors that aim to monitor drug intake, utilizing electrochemical differential pulse voltammetry to track caffeine levels as a prototype [**93**].

In terms of pH monitoring, both Dang et al. and Mazzara et al. present wearables tailored for this purpose [**94, 95**]. These innovations signal a future where pH assessments are both continuous and non-invasive.

In a similar vein, Yang et al. contribute with a cost-effective wearable sweat sensor, crafted through screen printing methods, to monitor real-time levels of K+ and Na+ [**96**]. Their research illuminates the intricate interaction between these ions and hydration, enriching our understanding of the health implications of sweat.

Fundamentally, the burgeoning focus on sweat-related research and technological advancements marks a pivotal shift in the field of wearable diagnostics. Extending their applications from glucose monitoring to hydration analysis, devices that detect sweat composition are set to revolutionize both personalized medicine and sports training.

Table 2.1 provides an overview of the research works focused on smart sensor technologies for different applications, detailing the main application, the sensors used, and the corresponding references.

TABLE 2.1. Summary of Related Works on Smart Sensors for Health and Physiological Monitoring

Main Application	**Sensors and References**
Ambient Sensors	**Sensors:** Motion, Light, Sound, and Air Quality Sensors. [**56, 57, 58, 59**]
Force and Pressure Sensing	**Sensors:** Pressure, Inertial, Force, EMG, FBG, Cameras. [**48, 49, 50, 51, 52, 53, 54, 55**]
Breath Sensing Devices	**Sensors:** Sound, Infrared Thermography, Pyroelectric Generator-Based, Piezoresistive, Inertial. [**60, 61, 62, 63, 64, 65, 66**]
Body Motion Analysis Sensors	**Sensors:** IMU. [**67, 68, 69, 70, 71, 72, 73, 74**]
Blood Monitoring Sensors	**Sensors:** PPG, Vis-NIR Spectroscopy, Wearables, iPPG. [**75, 76, 77, 78**]
Non-invasive Glucose Sensing	**Sensors:** Optical, Microwave, Electrochemical. [**79, 80, 81, 82, 84, 83, 85, 86, 87**]
Sweat Sensing Devices	**Sensors:** Electrochemical, Glucose Sensors ($NiCo_2O_4$ / Chitosan), Selective Biomarker Tracking, pH Monitoring. [**89, 90, 91, 92, 93, 94, 95, 96**]

2.3. Virtual Environments in Healthcare

The adoption of virtual environments in the healthcare sector is swiftly expanding, facilitating the evolution of innovative approaches to treatment, rehabilitation, and patient education. Virtual Reality (VR), Augmented Reality (AR), and Mixed Reality (MR) are generating immersive interactive experiences that are transforming healthcare practices. These cutting-edge technologies promise to enhance patient engagement, augment therapeutic outcomes, and aid in the professional development of healthcare providers. This section will examine the contemporary landscape of virtual environments within healthcare, addressing emerging trends, key applications, and potential challenges and limitations associated with their implementation.

2.3.1. Definition and types of virtual environments

Virtual environments are digital realms that replicate physical settings or create entirely novel and imaginative worlds [**97**]. These environments provide immersive experiences that allow users to interact with virtual elements through predominantly visual and auditory stimuli. With technological advancements, haptic feedback is increasingly being integrated, enabling users to "touch" or "feel" virtual objects [**98**].

These technologies fall under the broader concept of Extended Reality (XR), which encompasses Virtual Reality (VR), Augmented Reality (AR), and Mixed Reality (MR). XR represents a continuum of experiences that blend physical and digital elements with varying degrees of immersion.

(1) **XR (Extended Reality)**: XR is a collective term that includes all technologies combining real and virtual elements to different extents. It covers the full spectrum of immersion, ranging from slight digital overlays to entirely simulated environments. XR serves as the conceptual framework for VR, AR, and MR, enabling a unified understanding of immersive technologies [**99**].

(2) **VR (Virtual Reality)**: Virtual Reality provides the highest level of immersion by replacing the user's surroundings with a fully simulated environment. Using head-mounted displays with motion tracking and, frequently, handheld controllers or instrumented gloves, users can navigate and interact with three-dimensional virtual worlds [**100, 101**].

(3) **AR (Augmented Reality)**: Augmented Reality overlays digital content onto the physical world without replacing it. Through AR glasses or mobile devices, users see contextual digital elements superimposed onto their real environment, enabling interaction while maintaining awareness of the physical space [**98, 102, 103**].

(4) **MR (Mixed Reality)**: Mixed Reality blends real and virtual environments, allowing digital and physical objects to coexist and interact in real-time. Like AR, MR anchors virtual information to the real world, but it enables more immersive and dynamic interaction similar to VR [**99, 104**].

Within healthcare, the different branches of XR offer distinct advantages and limitations, making them suitable for a variety of clinical and therapeutic applications. VR has been successfully used in motor rehabilitation, pain management, and medical training [**105, 106, 107, 108, 28**]. AR has demonstrated strong potential in surgical planning

and intraoperative guidance, as well as in patient and student education [**108**]. MR, the most recent of the XR technologies, remains in early stages of adoption, yet is increasi

2.3.2. Applications of virtual environments in healthcare

Compared to traditional rehabilitation, the use of gamification and serious games has been shown to be a promising approach to motivate and engage patients during physical therapy sessions. These strategies emphasize the positive aspects of rehabilitation, leading to a more enjoyable and effective recovery process [**101**]. Games should provide clear feedback, text, and audio instructions, so that the patient can understand how to achieve their goals [**109**]. More intrusive solutions, such as VR, AR and MR systems, have been implemented with these objectives in mind and have been found to be beneficial for motor function, balance, and gait of the upper and lower extremities [**110, 111, 112, 113**]. However, highly intrusive systems, which require users to wear equipment such as goggles or multiple sensors attached to their body, may have a negative effect on user experience. These systems can potentially discourage users by causing discomfort and, in some cases, even pain.

2.3.2.1. ***Virtual Reality Applications in healthcare.*** The introduction of VR is transforming the field of healthcare by delivering immersive experiences applicable to numerous disciplines such as physical rehabilitation, psychological therapy, medical training, and patient instruction. These computer-generated environments enhance existing therapies, facilitating better patient outcomes and personalized healthcare approaches. As technological progress continues, VR's impact on healthcare is anticipated to increase significantly.

A research study by Gumaa and Youssef [**114**] found that VR technology is effective in treating chronic neck pain, shoulder impingement syndrome, rheumatoid arthritis, knee arthritis, ankle instability, and post-anterior cruciate reconstruction. However, it was not effective or inconclusive in the treatment of fibromyalgia and back pain, as well as knee arthroplasty. This suggests that VR technology can produce excellent results for a variety of medical conditions.

The utilization of VR applications in the research domain is witnessing a significant rise. Madeira et al. introduced PhysioMate, an extensive game-oriented software project tailored for physical rehabilitation. This innovative system aims to encourage physical activity and tackle both physical and cognitive deterioration, serving as a supportive tool for physical therapists, regardless of whether they are providing direct supervision. Initially

developed to aid patients in wheelchairs, it employs the Microsoft Kinect sensor to detect and follow upper-body motions, simultaneously engaging the user in a virtual setting. By integrating gaming mechanics, PhysioMate augments the rehabilitation journey through the implementation of five foundational movements essential for improving balance and motor skills. Notably, the system is accessible, as it eliminates the need for users to wear or connect any devices [**115**]. Nevertheless, the limitation of such systems lies in their lack of continuous user monitoring, potentially resulting in insufficient data when physiotherapist oversight is absent. Similar applications of VR and sensor technologies are documented in studies like [**106, 107, 116**].

There are differences between VR and AR as discussed in the introduction. AR may be more suitable for physiotherapy as it allows the user to be aware of their surroundings and visualize the real world, thus avoiding any potential accidents or falls. There are several research applications that use AR or MR for this purpose. For instance, Monge et al. developed an AR environment with smart sensors that can obtain physiological parameters from the user in real-time and also included a gamification system to encourage users to participate in exercises [**117**]. Similarly, Paredes et al. created a system for gait rehabilitation using a structure sensor, an Apple watch, and an RFduino Microcontroller-based motion sensor [**118**]. An unobtrusive system, such as the one presented in [**102**], is preferable, as it does not require the patient to physically be attached. However, the user still needs to wear googles to view and interact with the environment, so it is not yet an optimal solution.

Hu et al. [**119**] focused on the concurrent validity of using the Kinect system to evaluate knee kinematics during rehabilitation exercises. Despite the general underestimation of knee flexion and valgus by the Kinect system, it demonstrated good to excellent agreement with the VICON motion analysis system. This work implied the potential of Kinect as a clinical training device to maintain knee alignment during exercise.

Wochatz et al. [**120**] assessed the reliability and validity of Kinect V2 to capture lower limb movements during rehabilitation exercises. Their study revealed varying levels of reliability for different angles and joint positions, especially for more complex tasks. The Kinect system was found to reliably assess joint angles and positions during simpler exercises. However, it showed overestimations and underestimations for specific joints and exercises. The results suggest that the use of Kinect for early orthopedic rehabilitation might require further refinement of post-processing techniques.

These studies reveal the significant potential of motion capture systems and wearable sensors in rehabilitation exercises. While each study focuses on specific exercises and tools, a common theme is the ability of these technologies to provide accurate home monitoring. This is essential for remote configuration, control of rehabilitation programs, and encouraging patient participation. Despite its potential, it is essential to address identified limitations, such as varying reliability in complex tasks and the need for advanced data handling strategies, to enhance the effectiveness of these systems. Rehabilitation for stroke patients has seen significant improvements due to progress in VR technologies. Numerous studies have been carried out to assess the effectiveness of these technological innovations in enhancing motor capabilities and autonomy in stroke survivors.

Xavier-Rocha et al. conducted a systematic review on the use of Xbox/Kinect, a gaming technology, in rehabilitation settings after stroke [**121**]. They found that the Xbox / Kinect system was used most frequently in interventions aimed at restoring balance and motor function, although the evidence supporting its application is still limited. However, the findings encourage the inclusion of this technology in rehabilitation programs, especially those focusing on postural balance and motor skills.

On the other hand, Aguilera-Rubio et al. examined the Leap Motion Controller, a VR system designed for upper limb rehabilitation in stroke patients [**122**]. Researchers conducted a systematic review of studies and found that the Leap Motion Controller improved upper limb functionality. Nonetheless, owing to the variability among the studies, they recommended future investigations to be conducted with enhanced scientific robustness.

In a similar vein, Ogun et al. evaluated the impact of the immersive 3D VR system based on Leap Motion on upper extremity function in patients with ischemic stroke [**123**]. They found that immersive VR rehabilitation was effective in improving upper extremity function and self-care skills, although not functional independence.

Finally, Wang et al. designed and evaluated a playful VR system that uses a VR headset and force-feedback gloves for home rehabilitation [**124**]. Their virtual cat bathing simulation aimed to practice fine motor skills through various tasks, demonstrating the positive role of playfulness in the user experience of VR rehabilitation. In summary, all these studies suggest that VR technologies, such as Xbox/Kinect and Leap Motion Controller, can be beneficial in post-stroke rehabilitation, particularly in enhancing motor skills and upper limb functionality. However, more research with stringent methodology is needed to validate these findings and explore potential limitations. The role of playfulness

in VR rehabilitation, as explored by Wang et al., presents a promising avenue for further research.

2.3.2.2. *Augmented Reality Applications in healthcare.* AR has increasingly become a viable tool for rehabilitation and therapeutic purposes. The works cited below each use AR technology in unique ways to address various areas of rehabilitation and therapy.

Tokuyama et al. [**125**] developed an AR game using Microsoft Kinect that focuses on exercises in the lower extremities. Their work created a game environment where users could interact with virtual objects in real-time, providing a more engaging form of therapy for the user. This contrasts with Xavier-Rocha et al. [**121**] who used the Xbox/Kinect setup in the realm of VR primarily for post-stroke rehabilitation. Tokuyama et al. worked using technology more specifically for muscle activation of the lower extremities, suggesting the adaptability of AR to target specific areas of rehabilitation.

Chien et al. [**126**] further the usage of AR by developing a head-mounted AR game that relied solely on player gestures for controls, eliminating the need for joysticks or touch screens. The study successfully evaluated the usability of gesture-based operations and identified potential issues that could arise in the development of such interactive AR games. This gesture-controlled approach stands in contrast to the VR work of Wang et al. [**124**] that uses feedback gloves for control and interaction, demonstrating the breadth of control modalities available in AR and VR.

The work of Alnajjar et al. [**127**] integrated AR with exergaming for upper limb rehabilitation. Using a Leap Motion Controller in conjunction with Unity Game Engine, the authors developed a 3D exergame environment that demonstrated its potential in physical and neuromuscular rehabilitation of the upper limb. Their work mirrors the efforts of Aguilera-Rubio et al. [**122**], who used Leap Motion Controller® system for upper limb functionality in stroke patients but under the VR paradigm.

Boschmann et al. [**128**] utilized AR in the training of pattern classification control with a myoelectric prosthesis. They proposed a novel training framework that integrates virtual elements within a real scene from a first-person perspective. Their study showed that AR training significantly improved the performance of the subjects and provided a positive user experience. The work of Boschmann et al. shares similarities with that of Ogun et al. [**123**] who used immersive 3D VR based on Leap Motion to improve upper

extremity function in patients with ischemic stroke, both demonstrating the potential of virtual and augmented realities in improving the quality and outcomes of rehabilitation.

Lastly, Ozioko et al. [**129**] reviewed the development of smart tactile gloves for haptic interaction, communication, and rehabilitation. These gloves are used to enhance interaction with both real and virtual environments, creating an intuitive two-way haptic interface for users. The work of Ozioko et al. shares the focus on the importance of tactile feedback with that of Wang et al. [**124**] who also used force-feedback gloves, although VR setting.

In general, these studies show the potential of AR and VR technologies in creating engaging, effective and varied rehabilitation environments that can be customized to individual patient needs and the therapeutic targets of clinicians. The comparison also highlights the differences in the applications and control modalities used within AR and VR, highlighting the versatility and breadth of opportunities in the field of rehabilitation technology.

2.3.2.3. ***Mixed Reality Applications in healthcare.*** The applications of MR for the rehabilitation of patients and enhanced user experiences are evolving rapidly. Recent research investigates how MR technologies can be used for the rehabilitation of patients with upper limb dysfunctions and ataxic conditions, or to enable immersive, interactive and intuitive user experiences in MR environments.

Franzo et al. [**130**] present an exergame in MR for the rehabilitation of ataxic patients. Using Microsoft's HoloLens 2, the researchers developed a prototype that reproduces a pointing and reaching exercise for upper limb control. The study compares this with a Kinect-based prototype and an Arduino board. The MR exergame offers a better representation of patient movements due to the high sample rate of HoloLens. The findings suggest that MR has significant potential for rehabilitation, providing an immersive environment that retains a connection to the real world.

Meanwhile, Ababsa [**131**] proposes an approach to improve gesture interaction with virtual objects in MR environments by combining LMC with HoloLens. An interactive calibration procedure is described for the HoloLens-LMC device, which shows potential to enhance the user experience in MR environments. A set of preliminary experiments supports the accuracy and usability of the proposed approach.

In a broader perspective, Bailey et al. [**132**] present a range of applications of VR, MR, and virtual environment (VE) for human factor research, from accessibility design

to training and human-computer interaction studies. Research emphasizes the versatility and wide-ranging potential of these technologies in supporting various research fields and end-user applications.

Maeda et al. [**133**] propose a novel haptic device, Fingeret, which enables a wide range of haptic feedback and seamless interactions in MR environments. By combining finger-side actuators (FSAs) and a conventional fingernail actuator (FNA), the device offers haptic feedback for both physical and virtual objects without covering the fingerpad. This has potential to improve seamless interactions in MR environments.

In conclusion, MR technologies show great promise for physical rehabilitation and for improving user experiences in virtual environments. Further advances in haptic devices and gesture interaction can enhance this potential even further, opening exciting new avenues in the field of MR.

2.3.3. Limitations and challenges

Despite the great potential of virtual worlds, there are a number of obstacles that must be addressed.

(1) **Physical Discomfort and Motion Sickness**: The utilization of VR for extended periods of time can cause physical discomfort, such as eye strain, balance problems, and motion sickness, which is commonly referred to as "cybersickness." This can restrict the length of therapeutic sessions and reduce the patient's willingness to comply. [**134, 135, 136, 137, 138, 139**].

(2) **Technical Limitations**: The use of high-quality virtual environments is often limited due to the cost and availability of the necessary hardware, such as powerful computers, high-resolution displays, and precise tracking systems. Additionally, technical issues, such as latency and tracking errors, can disrupt the user experience and break the immersion. [**140**].

(3) **Adaptability and Personalization**: Creating virtual environments that can adjust to the requirements and capabilities of different patients is a challenging job. Although one-size-fits-all approaches may be suitable for some, successful rehabilitation usually necessitates tailored treatment plans. [**141**].

(4) **Lack of Standardized Metrics**: Virtual environments provide a range of techniques for tracking patient progress, however, the lack of standard metrics and protocols can make it difficult to compare results between different systems and studies.

(5) **Data Privacy and Security**: The protection and safety of patient information is of the utmost priority when it comes to any digital health technology. To comply with healthcare regulations, the transmission and storage of confidential health data must be handled with care, making the creation and utilization of virtual environment systems more intricate. [**142, 143, 144**].

2.4. Applied AI in Healthcare

In recent years, the intersection of technology and healthcare has rapidly evolved, becoming a growing field of study and development. Key among these advances is the application of AI, which has redefined the scope of healthcare delivery. AI has shown potential in diagnostics, predictive analytics, patient risk identification, drug discovery, and personalized patient care. With the advent of AI-driven technologies such as machine learning (ML) and deep learning (DL), the healthcare sector has entered an era of data-driven decision-making, allowing valuable insights to be extracted from the vast amounts of health data available today.

One of the key applications of AI in healthcare is activity recognition and monitoring, where AI-driven systems recognize and analyze individuals' daily activities without manual input. These systems employ sensors, cameras, or wearable devices to collect data and use ML algorithms to identify and interpret patterns of everyday life [**145**]. By continuously monitoring daily routines, AAL systems can detect unusual behaviors or patterns indicative of health issues, ensuring timely alerts for caregivers or medical personnel. Another critical AI application is fall detection and prevention, which addresses one of the primary concerns for the elderly. Falls can result in serious injuries, decreased independence, and overall health deterioration. AI-based detection systems utilize data from wearable devices, cameras, or floor sensors to identify falls and notify caregivers or emergency services [**146**]. Additionally, AI can predict the probability of falls through gait analysis, enabling proactive measures to mitigate risks.

AI also plays a significant role in cognitive assistance, aiding individuals with cognitive disabilities or dementia by providing reminders, guidance, and tailored interventions to support daily activities [**147**]. Leveraging natural language processing (NLP) and computer vision, these intelligent systems interpret user input and deliver appropriate responses or assistance. Furthermore, telemedicine and remote patient monitoring have been revolutionized by AI, utilizing data from sensors, wearable devices, and medical equipment to provide accurate health assessments, personalized feedback, and timely

medical advice [**148**]. This innovation allows for continuous health tracking, particularly for patients with chronic conditions, reducing the need for frequent hospital visits while improving patient outcomes.

In summary, the integration of AI into AAL has the potential to significantly enhance the quality of life, safety, and well-being of individuals, particularly the elderly and those with disabilities. AI-driven AAL solutions enable continuous monitoring, personalized assistance, and timely interventions, promoting autonomy and improving healthcare efficiency while alleviating the burden on caregivers and medical professionals.

2.4.1. Machine Learning Algorithms

2.4.1.1. ***Decision Trees and Random Forests.*** Decision Trees (DTs) are widely used in healthcare applications for their interpretability and efficiency in handling both numerical and categorical data. A DT splits the data into branches based on feature thresholds, forming a tree-like structure that leads to decisions [**149**]. However, DTs are prone to overfitting, especially with complex data.

Random Forests (RFs) address this limitation by combining multiple decision trees using an ensemble learning technique called bagging. Each tree is trained on a random subset of data, and the final prediction is obtained by aggregating the outputs of all trees [**150**]. RFs improve generalization and are effective in biosignal classification, fall detection, and physiological parameter prediction.

2.4.1.2. ***Support Vector Machines.*** Support Vector Machines (SVMs) are supervised learning models that find the optimal hyperplane separating different classes in high-dimensional space [**151**]. They are particularly effective in binary classification problems and have been applied to activity recognition and ECG signal classification in healthcare. With the use of kernel functions, SVMs can handle non-linear relationships, making them versatile in many AAL scenarios.

2.4.1.3. ***K-Nearest Neighbors.*** K-Nearest Neighbors (KNN) is a non-parametric algorithm that classifies new data points based on the majority label of their k nearest neighbors in the feature space [**152**]. Its simplicity and ease of implementation make it useful in prototype-based classification tasks, such as movement recognition or anomaly detection in sensor data.

2.4.1.4. ***Multilayer Perceptron Networks (MLPs).*** MLPs are a type of feedforward Artificial Neural Network (ANN) that were first developed in the 1980s [**153**]. MLPs

are composed of multiple layers of interconnected nodes or neurons, which transform input data into a more complex representation. They can be used for a variety of tasks, such as classification, regression, and feature extraction. The architecture of an MLP consists of an input layer, one or more hidden layers, and an output layer.

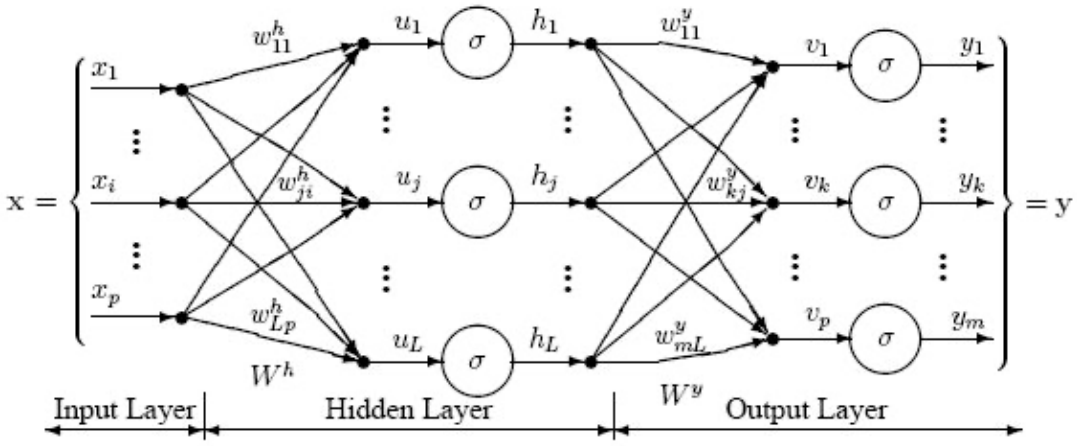


FIGURE 2.11. A MLP network structure.

An MLP can be represented as a directed graph, with the input nodes (x) representing features, hidden nodes (h) representing intermediate representations, and output nodes (y) representing predictions or target variables. Non-linearity is introduced using activation functions such as sigmoid (σ), hyperbolic tangent ($tanh$), or rectified linear unit (ReLU), enabling the learning of complex patterns. MLPs are typically trained using the backpropagation algorithm, which adjusts network weights iteratively to minimize the error between predictions and actual target values [**153**].

2.4.2. Deep Learning Algorithms

2.4.2.1. ***Recurrent Neural Networks (RNNs).*** Recurrent Neural Networks (RNNs) are a class of ANNs designed to process sequential or temporal data. Unlike traditional feedforward networks, RNNs retain a memory of previous inputs, enabling them to make predictions based on both current and past data. This makes them particularly suitable for time series analysis, where understanding temporal dependencies is critical [**154, 155, 156**].

Figure 2.12 illustrates the unfolding process of an RNN over time, highlighting how information is propagated through recurrent connections across successive time steps.

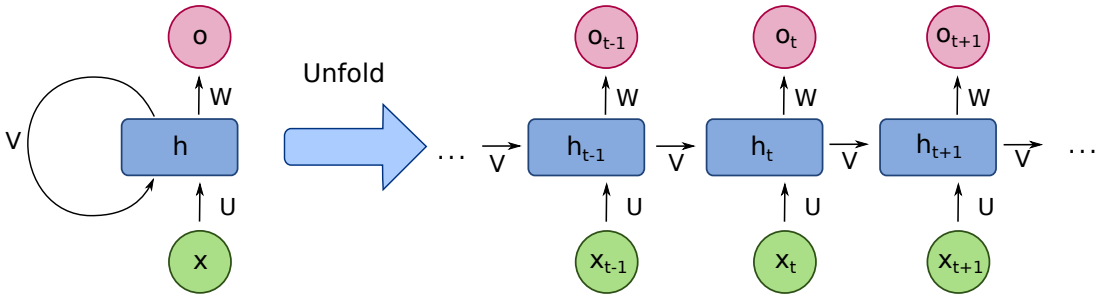


FIGURE 2.12. Unfolding example and structure of a one-unit RNN [**157**].

Training RNNs can be challenging due to the vanishing gradient problem, where gradients become too small to facilitate effective learning of long-term dependencies. To address this limitation, more advanced recurrent architectures such as Long Short-Term Memory (LSTM) networks and Gated Recurrent Units (GRUs) were proposed. RNN-based models have been widely adopted in healthcare applications for analyzing temporal health data, enabling outcome prediction and early detection of clinical events.

2.4.2.2. ***Long Short-Term Memory Networks (LSTMs).*** LSTM networks are a specialized form of RNNs designed to capture long-term dependencies in sequential data. Their internal structure, shown in Figure 2.13, is based on memory cells regulated by input, forget, and output gates that control the flow of information through the network.

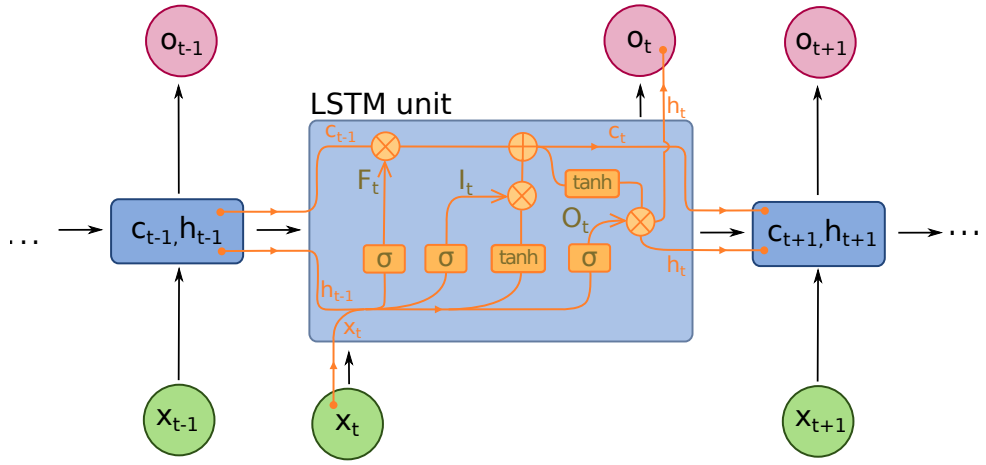


FIGURE 2.13. A LSTM network structure [**158**].

These gates process variables such as x_t, h_{t-1}, and c_{t-1} using activation functions including the sigmoid (σ) and hyperbolic tangent ($tanh$). This gated mechanism enables LSTMs to mitigate the vanishing gradient problem and retain relevant information over extended time intervals [**159**].

2.4.2.3. *Gated Recurrent Units (GRUs).* Gated Recurrent Units (GRUs), introduced by Cho et al. [**160**], simplify the LSTM architecture while maintaining strong performance in modeling temporal dependencies. As illustrated in Figure 2.14, GRUs employ only two gates—an update gate and a reset gate—resulting in a more compact recurrent structure.

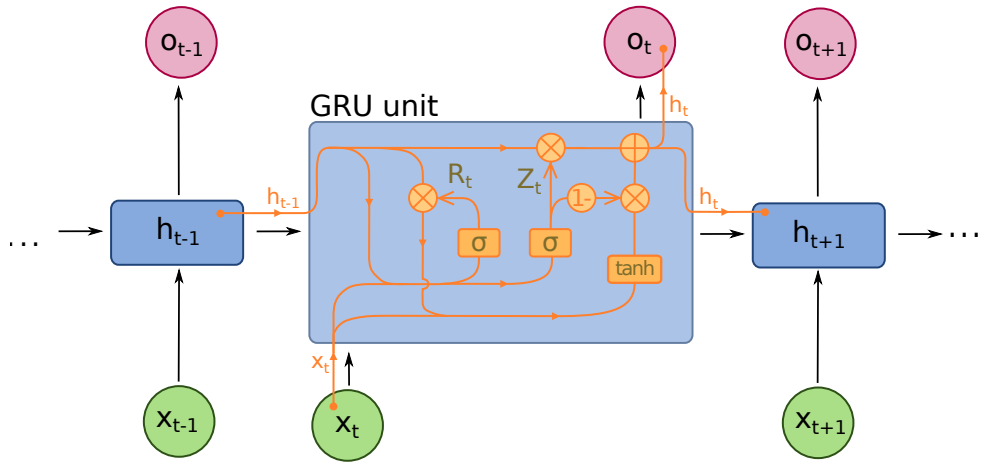


FIGURE 2.14. GRU network structure [**161**].

The reduced architectural complexity of GRUs leads to faster training and lower computational cost compared to LSTMs, while still enabling the learning of long-term dependencies. Consequently, GRUs have been successfully applied in domains such as natural language processing, speech recognition, and image captioning [**162**].

2.4.2.4. *Graph Neural Networks (GNNs).* Graph Neural Networks (GNNs) extend deep learning techniques to graph-structured data, where relationships between entities (nodes) are as important as the entities themselves [**163, 164**]. GNNs use message passing between nodes to learn embeddings that capture both local and global structure.

In AAL and wearable systems, data is often collected in structured formats—e.g., body-worn sensors at different locations, or joint positions in a skeletal model—making GNNs suitable for tasks like activity classification, gait analysis, or hydration pattern prediction. GNNs can also model temporal-spatial relationships when combined with recurrent layers or attention mechanisms, offering robust performance in complex multi-sensor scenarios.

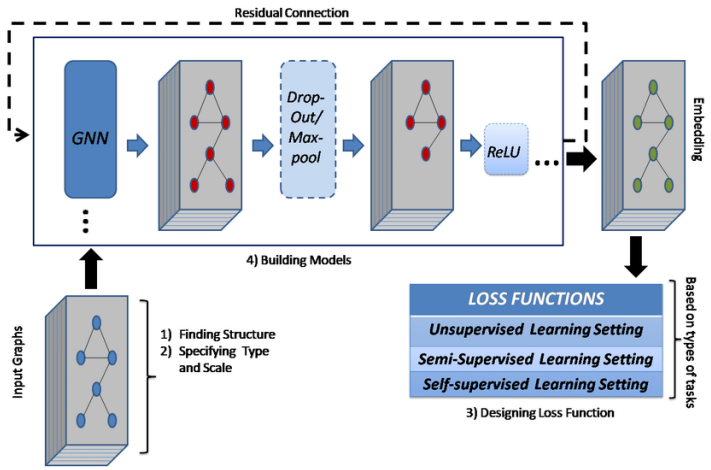


FIGURE 2.15. GNN schematic architecture [**165**].

In conclusion, while smart sensing systems and AI-driven platforms have the potential to revolutionize real-time health monitoring, several critical gaps remain in the literature. Advancements in sensor fusion, wearable AI, sweat biomarker validation - including sodium (Na^+), potassium (K^+), and glucose detection using energy-efficient hardware design are necessary to bridge these gaps and unlock the full potential of next-generation health monitoring technology. The integration of edge AI into wearable devices, particularly for hydration and electrolyte tracking, represents a significant step forward in personalized and real-time health assessment. Furthermore, as wearable sensing systems continue to evolve, addressing ethical and privacy concerns will be crucial in ensuring widespread adoption and regulatory approval. Future research should focus on refining these technologies to create seamless, non-invasive, and intelligent health monitoring solutions for both sports performance and clinical applications.

CHAPTER 3

Smart Sensors for Healthcare

The development of advanced sensor platforms plays a pivotal role in enabling non-invasive, continuous health monitoring. In this chapter, we present the research and engineering work behind the creation of an intelligent wearable sensing platform designed to integrate and enhance processing, communication, and multi-sensor measurement capabilities through iterative design.

This work focused on the development of smart potentiostats with wearable, single and multi-channel capabilities, achieved through the progressive refinement of four successive systems. Each design stage represented a step toward greater functional integration, informed by experimental validation and performance assessment. The improvements addressed signal fidelity, data-transmission robustness, and the incorporation of heterogeneous sensing elements. The resulting systems combined electrochemical modules for sodium (Na^+) and potassium (K^+) detection with additional wearable-oriented components for heart-rate (HR), peripheral-oxygen-saturation (SpO_2), and motion monitoring, forming a cohesive multi-analyte sensing platform optimized for continuous physiological assessment.

The chapter begins by outlining the objectives and design considerations that guided the development of the Potlink Platform. It then traces the platform evolution across iterations, detailing the technical challenges encountered and the solutions adopted. Special attention is given to enhancements in onboard data processing, communication protocols, and the optimization of sensor performance and integration.

The chapter concludes with an evaluation of a hydration sensing device, underscoring its potential applications in healthcare monitoring and its readiness for real-world deployment. Overall, this chapter illustrates the essential role of iterative design and validation in developing intelligent wearable platforms capable of supporting reliable, real-time health data acquisition.

3.1. Biosensors

Biosensors are analytical devices that couple a biological recognition element with a physicochemical transducer to detect specific analytes and convert their presence or

concentration into a quantifiable signal. These systems have become indispensable in fields such as healthcare, environmental monitoring, and food safety due to their inherent specificity, sensitivity, and capability for real-time analysis. In healthcare, biosensors enable non-invasive monitoring by detecting biomarkers in biofluids such as sweat, saliva, and blood.

3.1.1. Components of a Biosensor

A typical biosensor comprises three primary components, as illustrated in Fig. 3.1:

- **Bioreceptor:** The component that selectively interacts with the target analyte. Examples include enzymes, antibodies, nucleic acids, or even whole cells.
- **Transducer:** Responsible for converting the biochemical interaction into a measurable electrical signal. Common transduction mechanisms are electrochemical, optical, or piezoelectric.
- **Electrical Signal Processor:** Amplifies and processes the raw signal, yielding an interpretable output correlated to analyte concentration.

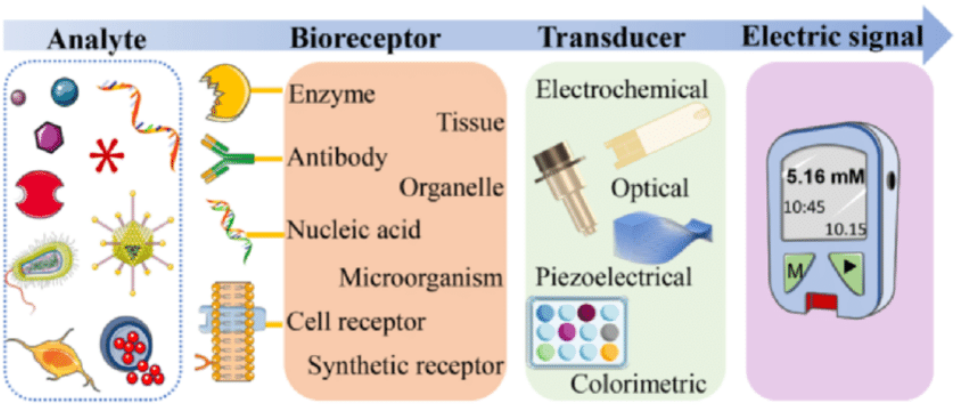


FIGURE 3.1. Components of a biosensor [**166**]

3.1.2. Types of Electrochemical Biosensors

Electrochemical biosensors are extensively employed in healthcare due to their high sensitivity, selectivity, and ability to facilitate real-time monitoring. These devices function by measuring electrical signals that arise from biochemical reactions, thereby enabling the detection of a wide range of analytes in biological fluids. This section reviews the principal types of electrochemical biosensors, namely amperometric, potentiometric, voltammetric, and impedimetric sensors.

3.1.2.1. *Amperometric Biosensors.* Amperometric biosensors measure the current generated by oxidation or reduction reactions at a working electrode under a controlled potential. A potentiostat governs this applied voltage, allowing precise monitoring of current variations linked to biochemical transformations. This approach is particularly effective in enzymatic sensors where oxidoreductase enzymes generate electroactive species—such as hydrogen peroxide (H_2O_2) that are subsequently detected electrochemically.

A widely known application is glucose monitoring, where glucose oxidase catalyzes glucose oxidation, producing H_2O_2, which is then oxidized at the electrode surface. The resulting current is directly proportional to the glucose concentration, enabling accurate blood sugar management in diabetic patients. To improve selectivity and reduce interference, such sensors often incorporate functional membranes or nanostructured layers.

Multistep amperometry extends this concept by sequentially applying different potentials, allowing the interrogation of multiple reactions within a single measurement cycle, as depicted in Fig. 3.2. This enhances versatility by enabling simultaneous detection of various analytes or intermediates, although disentangling overlapping processes can pose challenges.

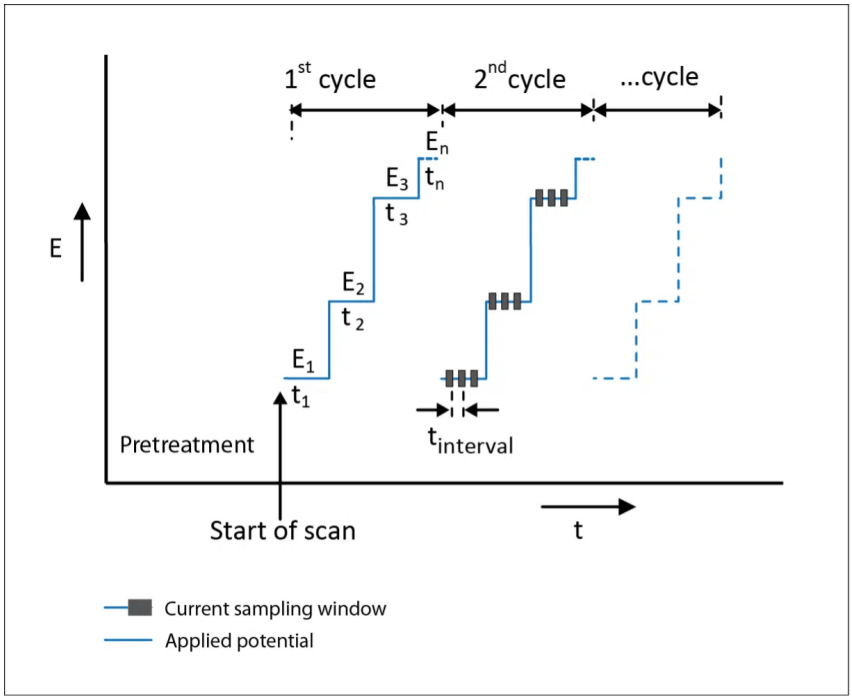


FIGURE 3.2. Multistep amperometry method

3.1.2.2. *Potentiometric Sensors.* Potentiometric sensors quantify the potential difference between two electrodes under near-zero current conditions. The measured potential reflects the electrochemical equilibrium established by the ion activity in the solution.

Ion-selective electrodes (ISEs) are the most prevalent form, capable of detecting ions such as K^+, Na^+, Ca^{2+}, and NH_4^+.

A key advantage of potentiometric sensors is their low power consumption, rendering them highly suitable for integration into wearable and portable health monitoring devices [**167**].

3.1.2.3. ***Open-Circuit Potential (OCP).*** The open-circuit potential (OCP) technique involves recording the equilibrium potential between a working electrode and a reference electrode without imposing an external current, as shown in Fig. 3.3. This high-impedance approach ensures minimal perturbation of the system, making it ideal for continuous, non-invasive ion monitoring—such as tracking Na^+ and K^+ concentrations in sweat.

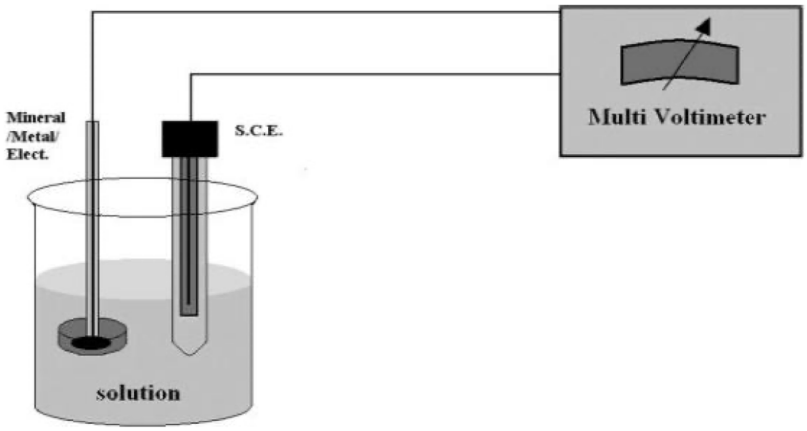


FIGURE 3.3. Open-circuit potential measurement configuration

3.1.2.4. ***Voltammetric Biosensors.*** Voltammetric biosensors measure current as a function of a dynamically varied potential, producing characteristic voltammograms that reveal redox potentials, reaction kinetics, and analyte concentrations. The most widely used technique is cyclic voltammetry (CV), illustrated in Fig. 3.4, where the applied potential is cyclically swept and reversed, capturing both oxidation and reduction processes.

Squarewave voltammetry further enhances sensitivity by overlaying a squarewave pulse on a staircase potential, facilitating alternating perturbation and relaxation of concentration gradients. This approach increases faradaic signal strength while minimizing non-faradaic background currents, making it well-suited for detecting trace analyte levels.

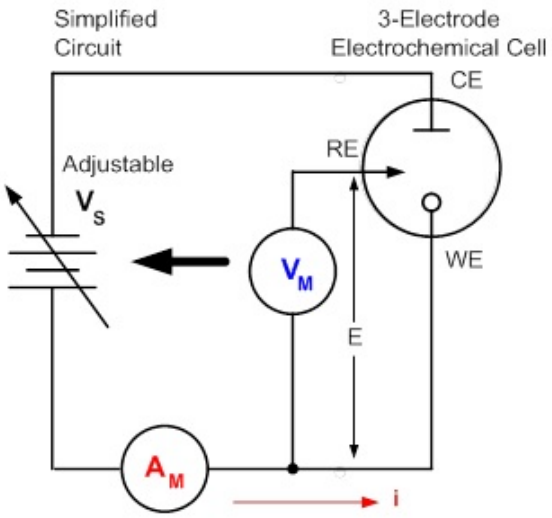


FIGURE 3.4. Simplified circuit for cyclic voltammetry [**168**]

3.1.3. Biosensing Applications in Health Monitoring

Amperometric and voltammetric biosensors have transformed healthcare by enabling precise, real-time monitoring of biochemical markers. Notable applications include:

- **Glucose Monitoring:** Amperometric biosensors form the foundation of commercial glucose monitoring systems (Fig. 3.5) used globally by diabetic patients. Continuous glucose monitoring (CGM) devices, such as those by Dexcom and Abbott (Freestyle Libre), leverage wearable amperometric sensors to provide continuous glucose data, improving glycemic control and reducing complications.



FIGURE 3.5. Commercial glucometer

- **Drug Detection:** Voltammetric biosensors enable monitoring of therapeutic drug levels and forensic detection of illicit substances. For instance, sensors have been developed to continuously track chemotherapy drug concentrations (Fig. 3.6), aiding dose optimization and minimizing toxicity. Portable voltammetric devices also allow rapid on-site screening for narcotics, supporting law enforcement activities.



FIGURE 3.6. Portable drug analyzer

- **Biofluid Analysis:** Sweat analysis using wearable electrochemical sensors offers a non-invasive window into hydration and electrolyte balance. Devices such as the Gatorade GX Sweat Patch (Fig. 3.7) quantify sodium and chloride levels, providing actionable insights for athletes. Similarly, platforms from Eccrine Systems monitor sweat glucose and cortisol, highlighting prospects in stress and metabolic monitoring.



FIGURE 3.7. Gatorade GX Sweat Patch [**169**]

3.2. Potentiostat

A potentiostat is a critical electronic instrument used in electrochemical experiments to control the voltage difference between a WE and a Reference Electrode (RE) while adjusting the current in a counter electrode (CE) to maintain the desired potential difference [**170**]. Fig. 3.8 illustrates a schematic of a traditional potentiostat circuit. This precise control is fundamental for enabling accurate measurements of key electrochemical

parameters, which makes potentiostats indispensable in research and practical applications.

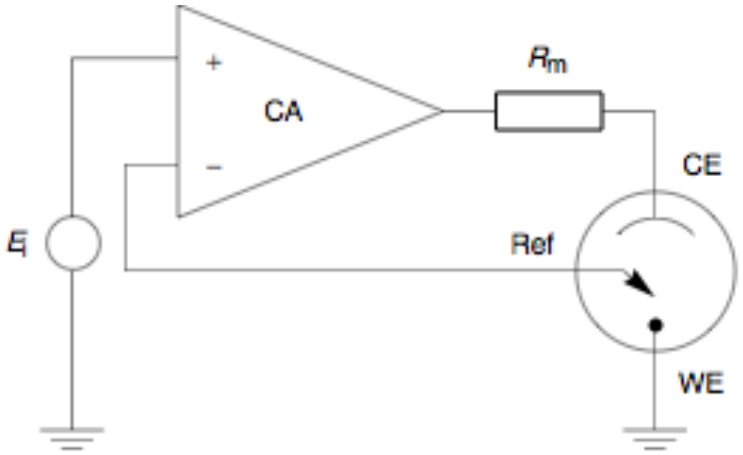


FIGURE 3.8. Potentiostat schematic [**171**].

In healthcare, potentiostats play an essential role in biosensing and diagnostics. One of the most recognized applications is in glucose sensors used for diabetes management. These sensors rely on a potentiostat to measure the current generated during the enzymatic oxidation of glucose, providing real-time blood sugar readings to aid in effective diabetes control. Beyond glucose, potentiostats are used in biosensors designed to detect a wide range of other critical biomarkers, including lactate, cholesterol, and neurotransmitters [**172**]. These applications enable early detection of diseases, personalized treatment, and continuous monitoring of chronic diseases.

The utility of potentiostats extends beyond healthcare in fields such as environmental monitoring and food safety. For example, potentiostats facilitate the detection of heavy metals in water, promoting environmental safety and public health [**173**]. In the food industry, they are used to identify harmful substances and contaminants, ensuring the safety and quality of food products. These applications highlight the versatility of potentiostats in the resolution of challenges across various domains.

Advancements in technology have significantly transformed potentiostats from bulky, expensive laboratory equipment into portable, affordable, and efficient devices. This evolution has expanded their applications to point-of-care testing and home diagnostics. For example, wearable potentiostats integrated with wireless communication and mobile devices enable real-time health monitoring and management, making them highly suitable for non-invasive diagnostics and personalized healthcare.

In the context of endurance sports, potentiostats have demonstrated potential to revolutionize athlete health monitoring. When integrated into wearable sensors for sweat analysis, they provide real-time feedback on key parameters such as electrolyte balance, hydration levels, and lactic acid concentration during prolonged physical activity. This information allows athletes to make timely adjustments, optimize their performance and minimize the health risks associated with dehydration and overexertion.

Potentiostats are transformative tools that enable precise, real-time measurements of biochemical markers, making them indispensable in a range of applications. From managing chronic diseases such as diabetes to improving athletic performance and ensuring environmental and food safety, these devices exemplify the convergence of innovation and practicality. With ongoing advances in technology, potentiostats are poised to play an even more integral role in healthcare and beyond, driving innovation and improving quality of life.

3.3. PotLink: Development of a Portable Single-Channel Potentiostat for In-Situ Analysis

3.3.1. Introduction and Objectives

This chapter presents the development of PotLink, a portable electrochemical measurement platform designed for wearable and real-time electrochemical analysis. Beyond the construction of the device itself, the overarching objective of this work is to provide an accessible, low-power, and wirelessly connected solution that enables electrochemical sensing to move beyond laboratory settings and into mobile, IoT-enabled applications. This motivation arises from the growing need for flexible electrochemical monitoring tools that can be deployed in field conditions, integrated into wearable systems, and used by non-expert operators.

The system architecture is centered on the LMP91000 potentiostat integrated circuit, selected for its ability to perform precise electrochemical signal acquisition at low power, making it suitable for continuous or periodic monitoring in portable environments. To enable wireless communication, the platform employs an RFduino microcontroller with integrated Bluetooth Low Energy (BLE) functionality. Together, these components form a compact, battery-powered hardware platform capable of transmitting data wirelessly to external devices.

A key feature of the system is its cross-platform web-based interface. This application utilizes the Web Bluetooth API to establish direct BLE communication between the RFduino and various client devices, including laptops, tablets, and smartphones. This architecture removes the need for dedicated native applications or device-specific drivers, allowing users to configure, control, and visualize electrochemical measurements directly from a standard web browser.

To ensure long-term data availability and integration into broader Internet of Things (IoT) ecosystems, a PHP-based web application and database are hosted on a remote server. This design enables data synchronization across devices and supports remote monitoring, multi-user access, and the creation of distributed sensing networks.

In summary, this chapter outlines the design objectives of PotLink, which include enabling portable electrochemical monitoring, ensuring cross-platform accessibility, reducing system complexity, and supporting IoT-compatible data acquisition. It also details the integration of hardware and software components and evaluates the performance of the platform, highlighting both its capabilities and limitations.

3.3.2. Materials and Methods

3.3.2.1. ***System Overview:*** The proposed system consists of a computation platform connected to an LMP91000 potentiostat integrated circuit and a wireless Bluetooth communication interface. The system adopts a server-based architecture: the PHP web application and database run remotely, while the user device serves solely as an interface for interaction. Data collected by the wearable potentiostats are sent to the server for processing, storage, and visualization.

The overall system architecture is illustrated in Figure 3.9. It integrates the electrochemical front-end, wireless communication module, and external user devices into a single portable measurement platform.

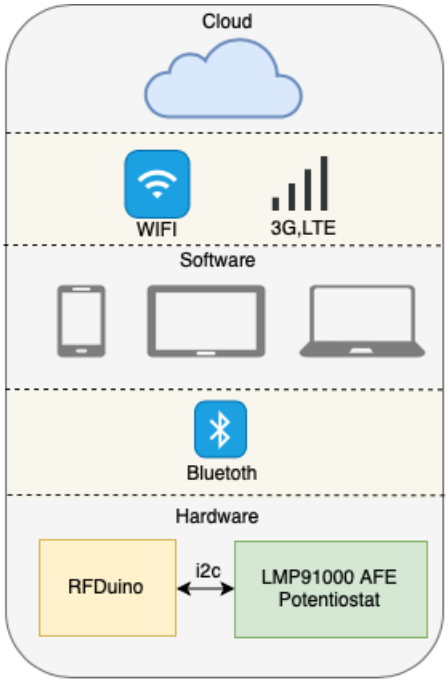


FIGURE 3.9. Block diagram of the system architecture.

A web application was developed in PHP to provide acquisition control and a graphical user interface, ensuring maximum compatibility with a range of devices including laptops, tablets, and smartphones. This design allows users to operate the potentiostat directly from their own devices, avoiding the need for dedicated hardware controllers and thereby reducing the overall system cost.

Communication between the potentiostat and the web application is established via Bluetooth Low Energy (BLE), also referred to as Bluetooth 4.0. The web application is hosted on a web server, which also provides the database infrastructure for this system. This database operates as a relational database, enabling immediate remote access and synchronization of measurement data across connected devices.

3.3.2.2. *Hardware Design:* The hardware implementation of the proposed system integrates a microcontroller unit (MCU), a potentiostat analog front-end (AFE), precision voltage reference, power regulation and battery management circuits, assembled on a compact custom PCB. This section details the main components and design considerations.

3.3.2.3. *Microcontroller:* The microcontroller chosen for this work is the RFduino, based on the Nordic Semiconductor nRF51822 SoC, which integrates a 32-bit ARM Cortex-M0 processor operating at 16 MHz. This MCU also includes an embedded Bluetooth Low Energy (BLE) transceiver, enabling low-power wireless communication with external computation units such as smartphones, laptops, or tablets. The RFduino supports I^2C and SPI interfaces, allowing straightforward integration with the LMP91000 potentiostat IC, and incorporates a 10-bit onboard ADC sufficient for the required signal acquisition.

A critical selection factor was the ease of firmware development and rapid prototyping. The RFduino is fully compatible with the Arduino IDE, unlike other BLE-enabled microcontrollers that typically require more complex toolchains such as Keil, GCC, or IAR Embedded Workbench.

Table 3.1 compares the RFduino with alternative platforms considered during the design phase. While devices like the TI CC2541 and nRF52832 offered similar low-power BLE capabilities, their development environments were more involved and often necessitated additional breakout boards or custom firmware. The RFduino provided an optimal trade-off among performance, simplicity, and hardware footprint.

In contrast to the widely used ATmega328P, which lacks built-in BLE and requires external modules such as the HC-05 or HM-10 for wireless communication, the RFduino combines BLE and analog acquisition in a single compact module. Although ESP32 platforms are highly capable and popular, they generally consume more power and have a larger footprint.

Considering compactness, low-power operation, native BLE support, and ease of prototyping, the RFduino shown in Figure 3.10 was selected as the optimal solution.

TABLE 3.1. Comparison of main characteristics of MCU platforms considered

Characteristic	**RFduino**	**TI CC2541**	**nRF52832**
Core	ARM Cortex-M0	8051	ARM Cortex-M4F
Clock Frequency	16 MHz	32 MHz	64 MHz
Flash Memory	256 KB	128 KB	512 KB
RAM	16 KB	8 KB	64 KB
BLE Version	4.0	4.0	5.0
ADC Resolution	10-bit	12-bit	12-bit
Power Consumption	Very Low	Low	Very Low
Programming Support	Arduino IDE	IAR/CCS	Segger/GCC
Module Size	20 × 20 mm	14 × 22 mm	10 × 16 mm

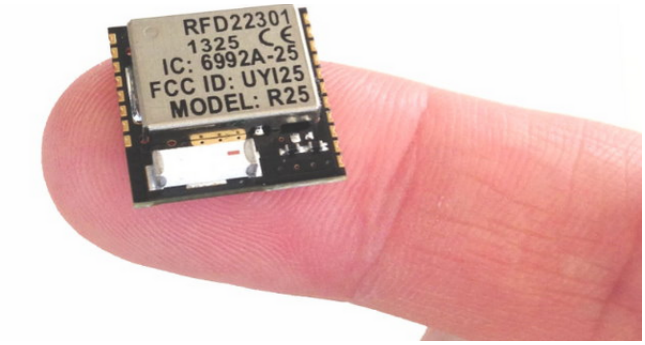


FIGURE 3.10. RFduino board used in the measurement platform.

3.3.2.4. ***Potentiostat Integrated Circuit:*** The potentiostat front-end is based on the LMP91000, a low-power, programmable analog front-end designed by Texas Instruments for electrochemical sensing. It supports both two- and three-electrode configurations and uses a transimpedance amplifier (TIA) with programmable gain from 2.75 kΩ to 350 kΩ, enabling current measurements from approximately 5 μA to 750 μA. This flexibility is suitable for amperometric and ion-selective applications where compactness and energy efficiency are critical.

The device also features programmable reference voltages and biasing, maintaining a stable potential between the working and reference electrodes over an operating range of 2.7–5.25 V with a typical quiescent current below 10 μA. Figure 3.11 shows the internal block structure of the LMP91000.

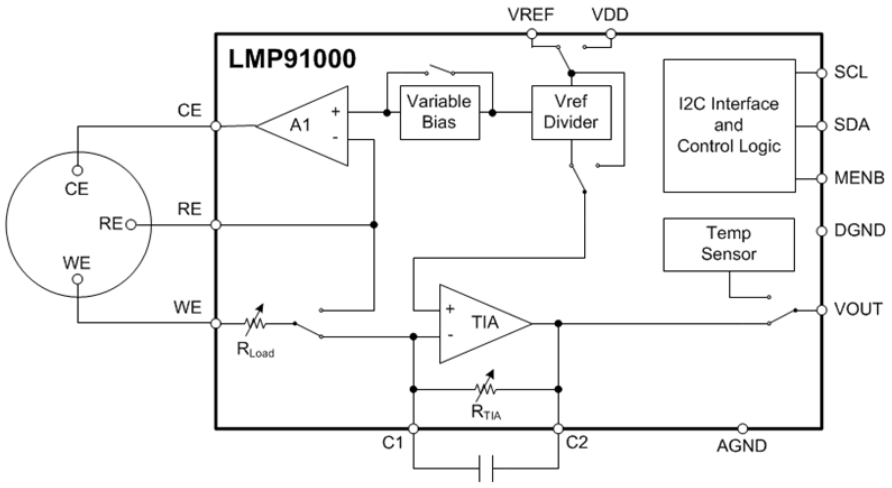


FIGURE 3.11. Internal block diagram of the LMP91000 potentiostat IC.

Alternative solutions, such as the ADuCM355 from Analog Devices, incorporate a potentiostat and an ARM Cortex-M3 processor, extending the measurable current range (10 nA to 1 mA) and providing additional electrochemical functionalities. Nonetheless, its higher power consumption and integration constraints make it less compatible with the modular and energy-efficient architecture pursued in this work. Table 3.2 summarizes the main differences.

TABLE 3.2. Comparison of potentiostat ICs

Feature	**LMP91000**	**ADuCM355**
Architecture	AFE potentiostat only	Integrated AFE + MCU + ADC
Processor	-	ARM Cortex-M3
Current Range	5–750 μA	10 nA–1 mA
Gain Control	Programmable TIA	Programmable TIA + PGA
Interface	I^2C	SPI / UART
Voltage Range	2.7–5.25 V	1.8–3.6 V
Quiescent Current	$\sim$10 μA	$\sim$50 μA (excluding MCU)
Development Tools	Arduino-compatible	IAR / Keil / GCC

3.3.2.5. ***Additional Components:*** To ensure stable and precise reference voltages essential for reliable electrochemical measurements, the MCP1501T was integrated. This precision reference generates a constant 2.048 V output with low drift and low quiescent current, maintaining measurement accuracy even under battery discharge conditions.

For battery management, the MCP73831T was selected as a compact, programmable single-cell Li-Ion/Li-Poly charger. Compared to alternatives like the TP4056 or MAX1555, the MCP73831T facilitates tighter PCB integration and flexible current configuration, improving safety and efficiency.

Table 3.3 lists the selected key components and alternatives considered during the design process.

TABLE 3.3. Summary of principal components and alternatives

Function	**Selected Component**	**Alternatives**	**Main Characteristics**
Analog Front-End	LMP91000	AD5940, LMP91200	Programmable TIA and bias for portable sensing
Voltage Reference	MCP1501T	TL431, LM4040	Stable 2.048 V, low drift, low quiescent current
Battery Charger	MCP73831T	TP4056, MAX1555	Compact Li-Ion charger with flexible current settings

3.3.2.6. ***Modular Design.*** The system leverages the stackable RFduino architecture alongside a custom potentiostat shield. This approach simplifies future expansion by allowing additional sensor modules, such as humidity or temperature sensors, to be easily stacked. Figure 3.12 shows typical stackable configurations.

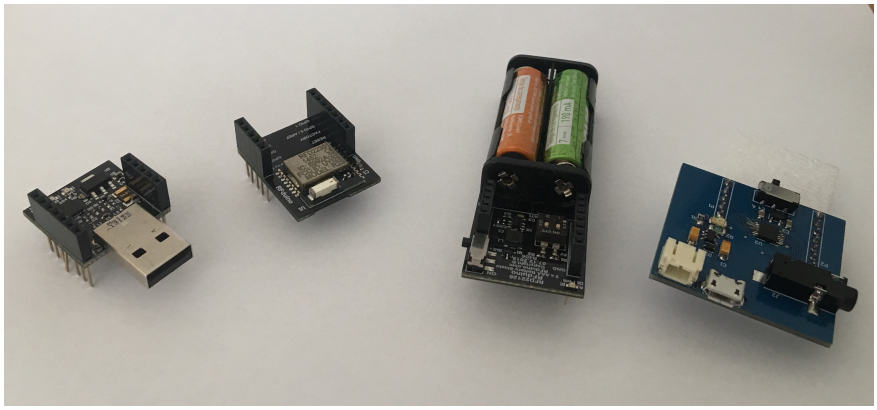


FIGURE 3.12. Stackable design: RFduino with potentiostat shield, programmer, and battery modules.

As illustrated in Figure 3.13, the initial stage of development employed the LMP91000EVM evaluation board from Texas Instruments connected to an RFduino module. This configuration was used to verify the electrical and communication compatibility between the potentiostat and the microcontroller, as well as to assess their joint performance in data acquisition and signal integrity. These preliminary tests confirmed stable operation and established the foundation for subsequent integration into custom PCB designs.

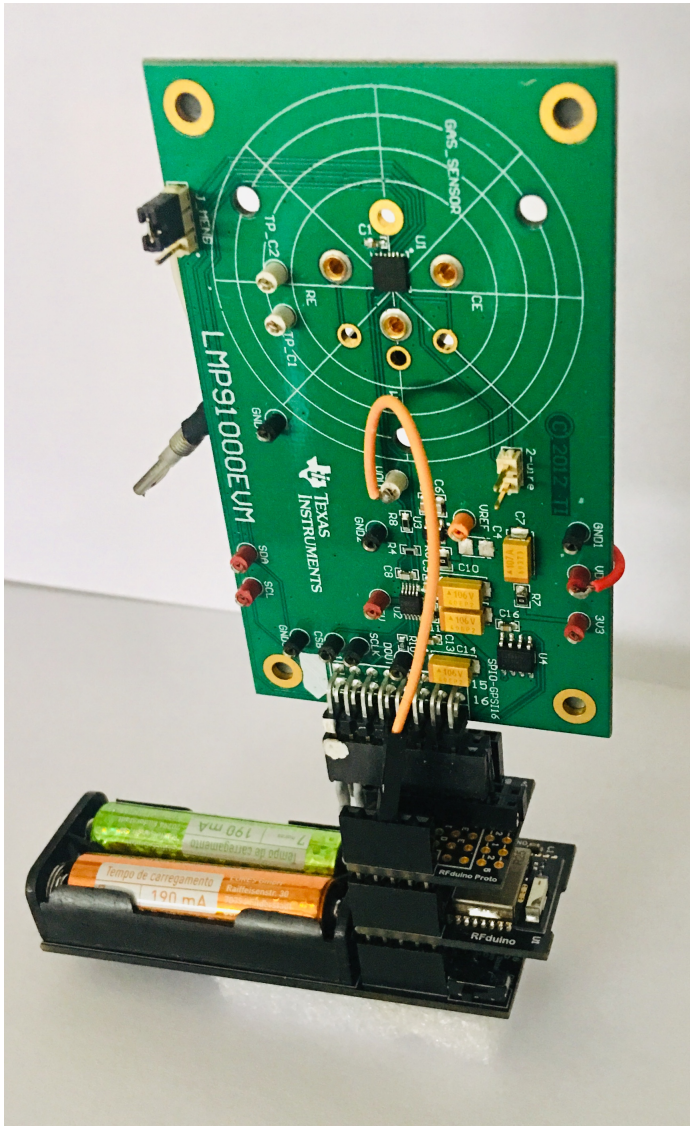


FIGURE 3.13. Initial testing with the modified LMP91000EVM evaluation board and RFduino.

Figure 3.14 illustrates the assembled prototype, highlighting the key interfaces: lithium battery JST connector (orange), micro-USB charging port (green), electrode jack (red), power switch (blue), and the RFduino module beneath the custom shield (yellow).

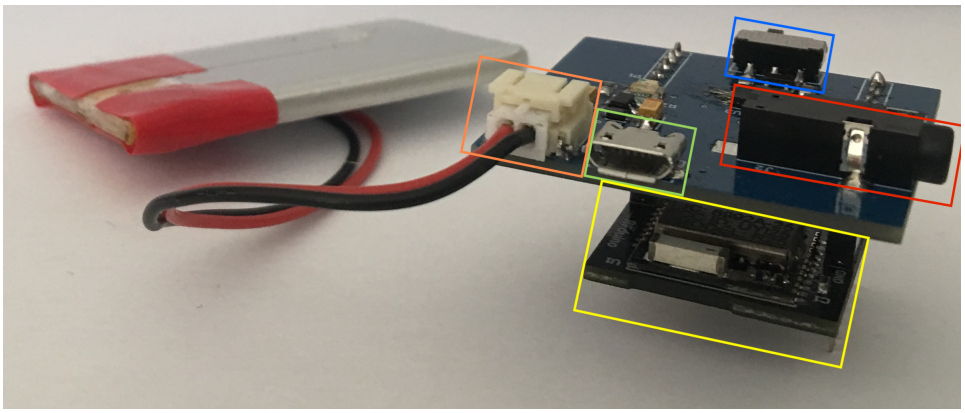


FIGURE 3.14. Assembled PotLink prototype showing key components and connections.

The final version of the platform (Figure 3.15) includes a dedicated screen-printed electrode (SPE) connector, improving stability and compatibility with commercial disposable sensors.

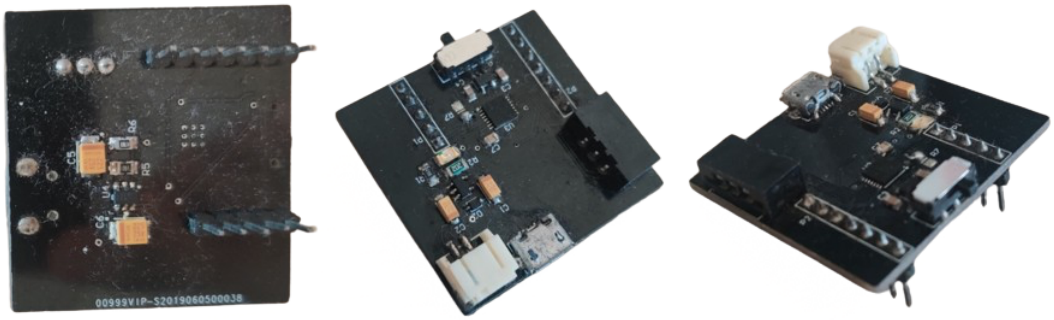


FIGURE 3.15. PotLink V1.0 featuring an SPE connector for direct use with disposable sensors.

The detailed schematics and PCB layouts for the final implementation are provided in Appendix A.

3.3.3. Software

The software architecture of the system was designed to deliver a platform-independent, user-friendly solution for controlling the potentiostat and monitoring electrochemical measurements in real-time. It comprises two main components: the firmware implemented on the microcontroller and a cross-platform web application, supported by a real-time cloud database. Together, these enable efficient in-situ electrochemical analysis with wireless operation.

3.3.3.1. ***Firmware.*** The firmware running on the RFduino microcontroller is responsible for configuring the LMP91000 potentiostat via I^2C, acquiring analog measurements,

and transmitting data to external devices over Bluetooth Low Energy (BLE). Upon initialization, the firmware advertises BLE availability, waiting for a connection from a client device, such as a laptop or smartphone.

Once connected, it receives a JSON payload from the web application containing the potentiostat configuration parameters. These parameters are used to program the LMP91000 registers. The firmware then begins continuous data acquisition, sampling the output of the potentiostat and sending the data back over BLE to the client device for real-time visualization. This process continues until the measurement is completed, after which the firmware returns to a standby state, ready for the next configuration.

Figure 3.16 summarizes this interaction, showing the BLE connection, configuration, measurement, and data storage flow.

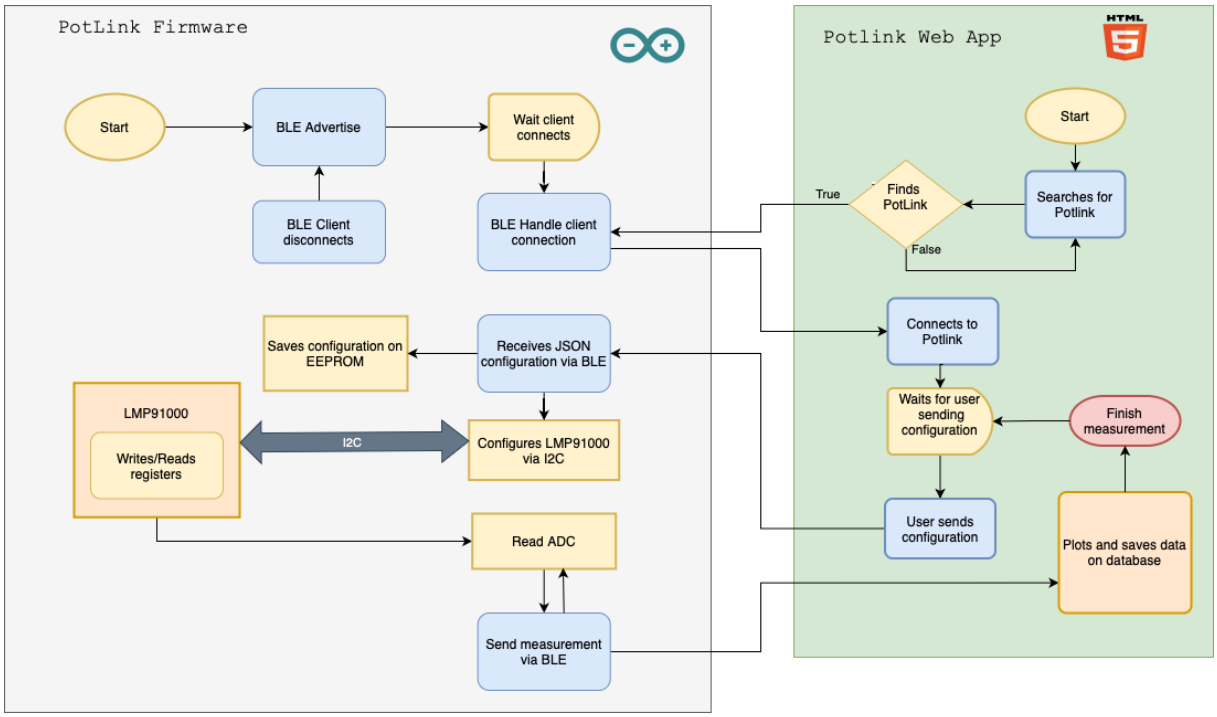


FIGURE 3.16. Flowchart of the firmware and web application integration, illustrating BLE communication, configuration, measurement, and data streaming to the cloud.

3.3.3.2. *Web Application.* The PotLink web application was developed as a responsive Progressive Web App (PWA) to ensure broad accessibility across desktops, tablets, and smartphones without the need for installing native software. Communication with the PotLink device is established directly through BLE using the Web Bluetooth API, which is supported by modern Chromium-based browsers. This eliminates the need for

intermediary drivers or applications, enabling direct communication in environments such as Android, Chrome OS, Windows (Chrome 70+), and MacOS (Chrome 56+).

Once a BLE connection is established, the application sends the configuration JSON to the device, receives the streamed measurement data, and simultaneously plots the data in real-time while storing it in the cloud database for subsequent analysis. After completing a measurement, the application returns to an idle state, ready to start a new experiment with updated parameters. This workflow offers an interactive and adaptable environment for conducting electrochemical experiments.

3.3.3.3. *Main Application Interfaces.* The primary pages of the PotLink web application are detailed below, along with figures illustrating each interface.

Registration Page: New users can register by providing a username, email, and password. The system enforces data integrity through client-side validation, and all passwords are securely encrypted before storage in the database, ensuring confidentiality and protection against unauthorized access.

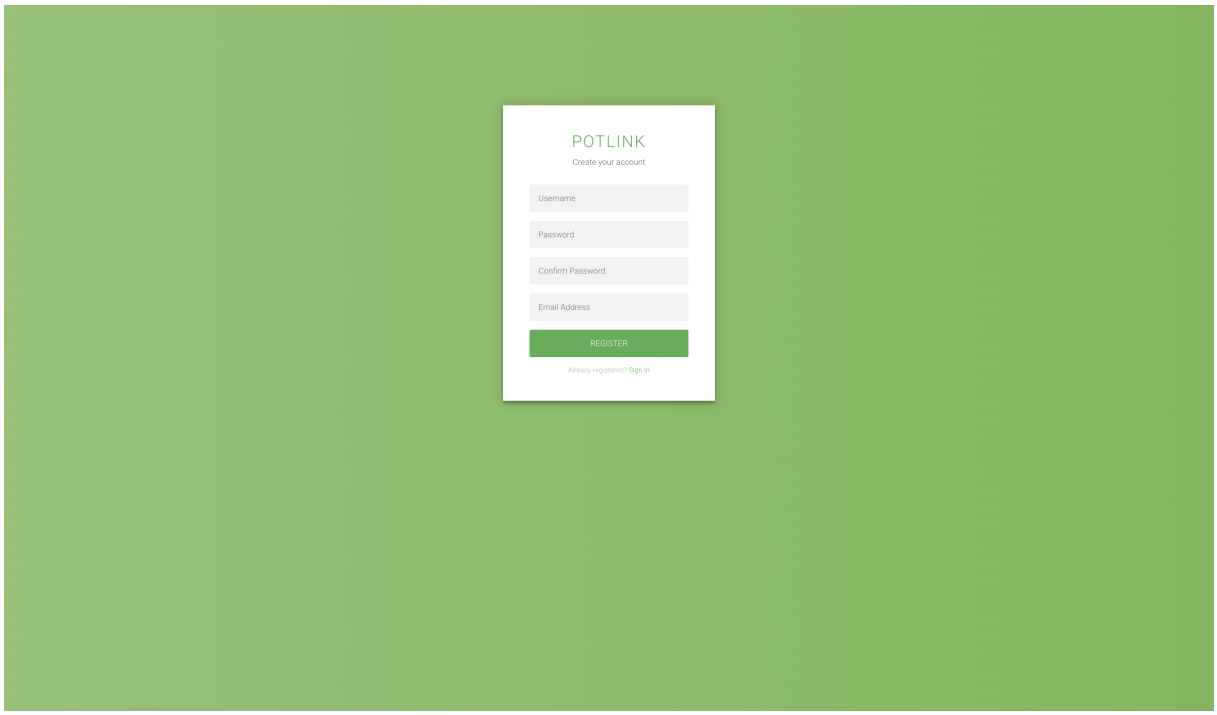


FIGURE 3.17. Registration page of PotLink for user account creation with validation.

Login Page: The login page provides secure access to the application by requiring the entry of valid credentials before any functionality becomes available. Validation feedback enhances both usability and security, ensuring that only authenticated users can access and operate the platform.

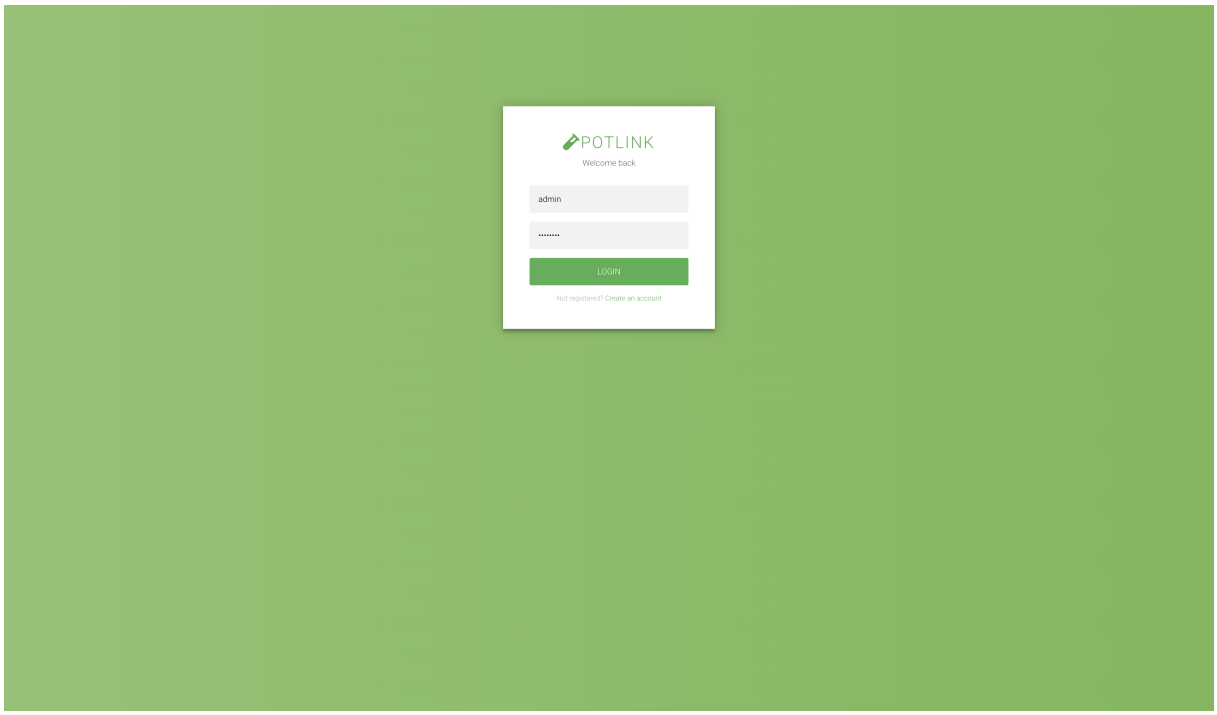


FIGURE 3.18. Login page of PotLink with credential input and validation.

Home Page: After authentication, users are directed to the home page presented in Figure 3.19, which serves as the main page of the PotLink platform. This screen integrates all essential controls for configuring, initiating, and monitoring electrochemical experiments. The home page is organized into distinct interactive regions to optimize user workflow:

- **Top navigation bar**: A top navigation bar provides quick access to core actions, including connecting to PotLink via Bluetooth LE, refreshing the current view, navigating to the stored data visualization section to review past measurements, or securely logging out of the system.
- **Panel on the left:** This panel is dedicated to the detailed setup of the electrochemical experiment. Users can precisely define all parameters required to control the potentiostat. Each configuration field plays a specific role:
  - **TIA Gain (Transimpedance Amplifier Gain)**: Sets the conversion factor from current to voltage, directly influencing the sensitivity and current measurement range of the system.
  - $\mathbf{R_{Load}}$ **(Load Resistor)**: Adjusts the load conditions of the cell circuit, affecting both the stability and the dynamic range of current detection.
  - **Reference Source**: Allows selection between internal and external reference electrodes, enabling the user to control whether the system maintains

the potential relative to a built-in reference or an external Ag/AgCl (or equivalent) electrode.

- **Internal Zero**: Defines the baseline voltage offset (typically a percentage of the supply voltage) around which the applied potential waveform is centered, ensuring proper biasing of the electrochemical cell.
- **FET Short**: A software-controlled feature that temporarily grounds the working electrode to discharge residual charge, useful for stabilizing the electrode before or after measurement cycles.
- **Operation Mode**: Specifies the voltammetric technique to be used, such as cyclic voltammetry (CV), linear sweep voltammetry (LSV), or square wave voltammetry (SWV), determining how the potential is varied during the experiment.
- **Start Potential (Ebegin), Lower Potential(EVtx1), and Upper Potential(EVtx2)**: Define the voltage scan range and direction. The *start potential* is the initial voltage applied, while the *lower* and *upper* potentials set the boundaries of the voltage sweep, collectively defining the electrochemical window explored during the test.

Once these parameters are configured, they are transmitted directly to the potentiostat via BLE, allowing seamless remote setup of the device.

- **Panel on the right:** As the experiment runs, this panel presents live graphical plots of the electrochemical measurements. Typically displayed as current versus potential (voltammograms), these plots are dynamically updated as data streams in from the potentiostat. Users can interact with the graph and monitor the evolution of the electrochemical response in real-time.

This integrated interface ensures that all critical experimental controls, parameter settings, and real-time visualization tools are cohesively presented, enabling a seamless workflow that extends from precise configuration through to data acquisition and live electrochemical analysis. Such a design minimizes cognitive load on the user, reduces procedural errors, and enhances the reproducibility of experiments by maintaining all essential functionalities within an intuitive, unified environment.

The process of establishing a Bluetooth Low Energy (BLE) connection exemplifies this streamlined approach. Initiation begins when the user interacts with the blue connection button, as depicted in Figure 3.19. Upon activation, the web application invokes the Web

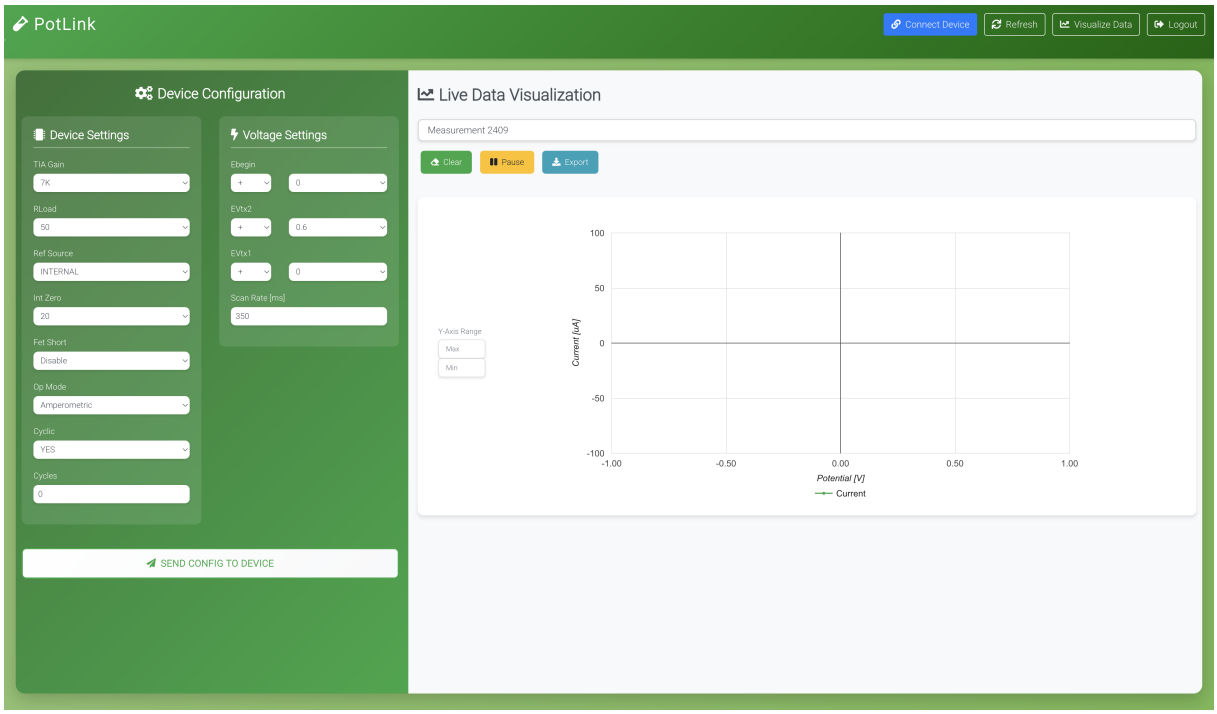


FIGURE 3.19. Home page of PotLink showing BLE connection, experiment configuration panel, and real-time electrochemical data visualization.

Bluetooth API, prompting a browser-native dialog that enumerates available PotLink devices. This pop-up window, illustrated in Figure 3.20, guides the user to authorize Bluetooth communications and to select the appropriate device from the detected list.

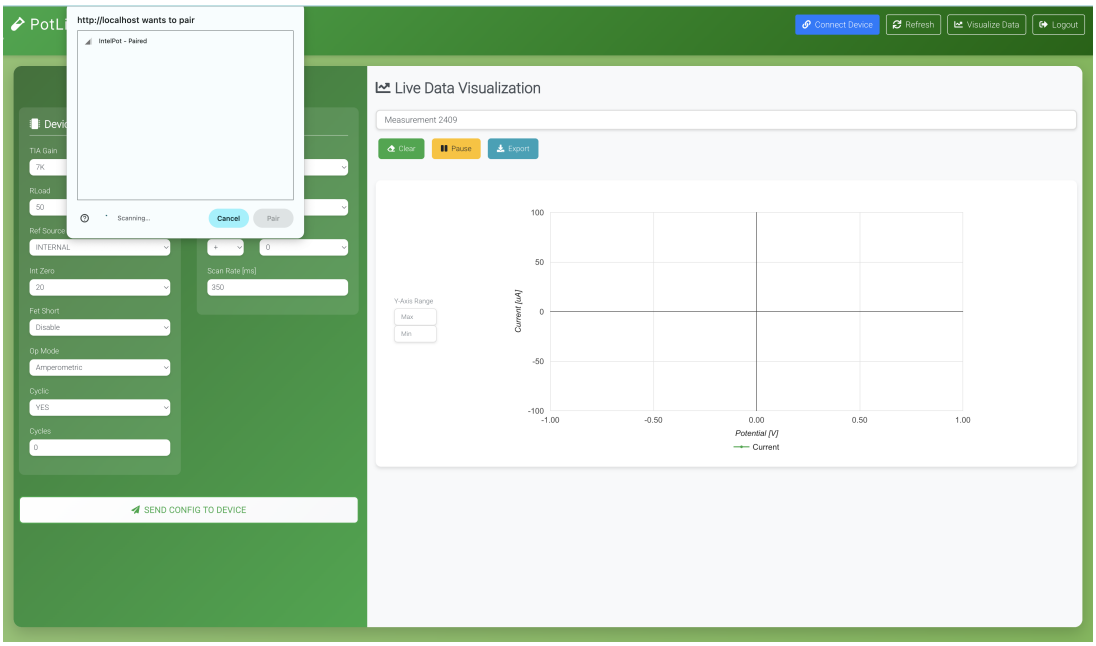


FIGURE 3.20. BLE connection interface. The application lists available PotLink devices and prompts the user to authorize pairing.

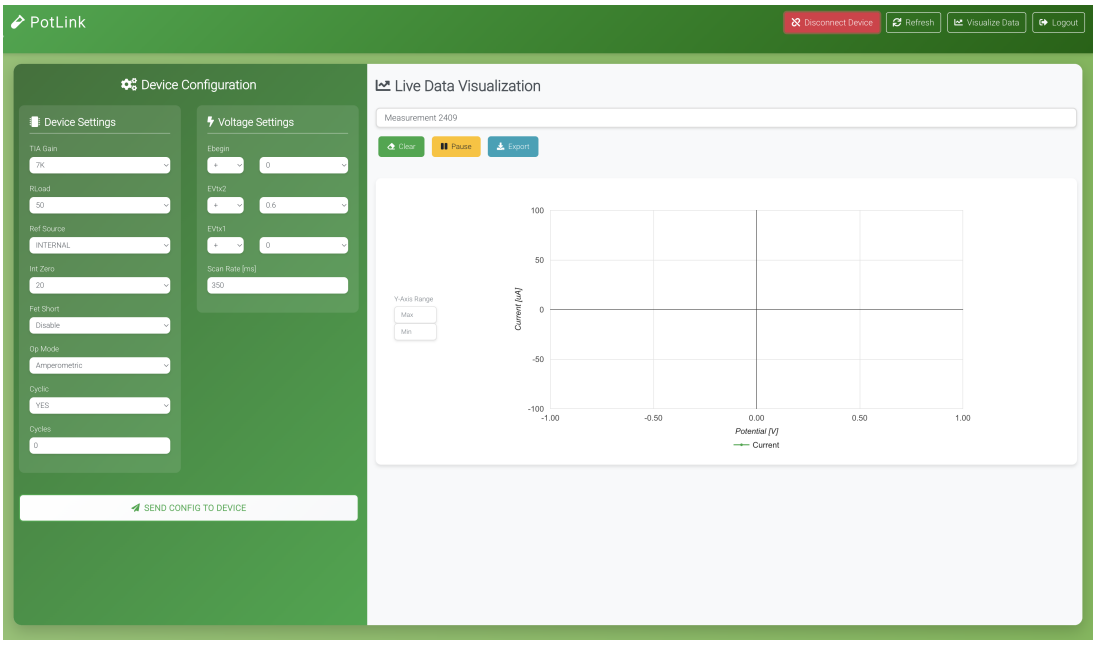


FIGURE 3.21. Interface after successful BLE connection. The connection button turns red, indicating an active link to the PotLink device and enabling controlled disconnection.

Upon successful pairing and establishment of the BLE communication channel, the interface provides immediate visual confirmation by changing the connection button from blue to red, thereby signaling an active session. In this state, the functionality of the button is reversed, allowing it to serve as a disconnect control to terminate the session when desired. Figure 3.21 illustrates the application state following a successful connection, with the device fully linked and ready to receive experimental configurations and stream measurement data.

This BLE workflow, which includes device discovery, secure pairing, and dynamic session management, demonstrates the system's focus on robustness, usability, and operational transparency. By integrating these mechanisms directly into the web interface, the platform removes the need for intermediary applications or device-specific drivers, improving cross-platform portability and enabling rapid deployment across diverse experimental environments.

Data Visualization Screen: The Data Visualization Screen provides a comprehensive interface for exploring previously acquired measurements. Users can browse, filter, and interactively analyze stored experimental data, facilitating detailed comparative studies across different sessions. This capability is essential for longitudinal assessments, validation of experimental repeatability, and in-depth electrochemical behavior analysis under varying conditions.

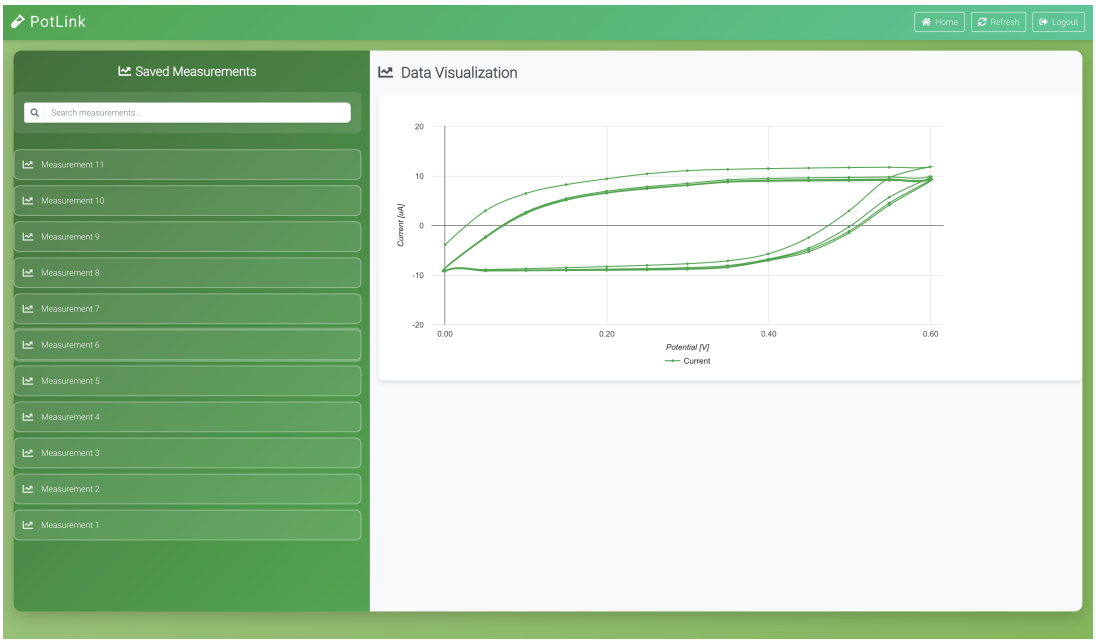


FIGURE 3.22. Data Visualization Screen of PotLink for reviewing and comparing saved measurements.

3.3.3.4. ***Navigation Overview.*** The typical navigation flow through the PotLink application can be summarized as follows:

(1) Users initiate by logging in or registering a new account (Figures 3.18 and 3.17).

(2) Following successful authentication, they are directed to the home page, which integrates experiment configuration, BLE device connection, and real-time data visualization (Figure 3.19).

(3) Stored measurements and associated analytical insights are accessible via the Data Visualization Screen (Figure 3.22), supporting retrospective evaluations and comparative analyses.

This structured navigation ensures an intuitive yet powerful user experience, seamlessly bridging live experimental control with advanced post-experimental data exploration.

3.3.3.5. ***Database System.*** This project employs a MySQL relational database to support robust, structured storage of all experimental data and user information. MySQL was selected due to its widespread adoption, maturity, and strong support for complex queries and transactions, making it well suited for managing scientific data that require consistency and integrity.

The database schema was specifically designed to accommodate the requirements of the PotLink system and is illustrated in Figure 3.23. It consists of three principal tables:

- **users table**: Stores registered user accounts, including unique identifiers, usernames, encrypted passwords, and associated metadata. This table underpins the authentication process and ensures secure access control to the system.
- **voltammetry table**: Records high-level metadata about individual measurements. It includes fields such as the measurement title, the type of electrochemical sensor used, and establishes a link to the user who performed the experiment. This association provides clear ownership of experimental sessions and allows categorization by sensor type or experimental purpose.
- **data table**: Contains the detailed electrochemical measurement results acquired during experiments, including time-stamped current and potential values. Each record is linked back to its corresponding entry in the `voltammeter` table, preserving the context of the measurement, and indirectly to the user who initiated it. This relational design enables efficient retrieval and comprehensive retrospective analysis.

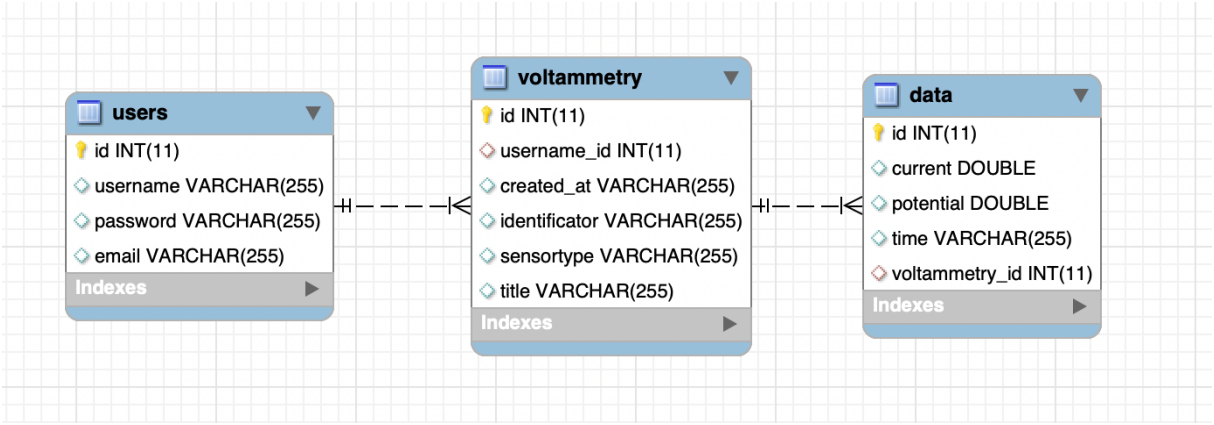


FIGURE 3.23. Database diagram.

This relational structure ensures that measurement data are rigorously organized and easily queryable for comparative studies or long-term tracking. The database enforces referential integrity through foreign keys, maintaining consistent relationships between experiments, devices, and user accounts.

Figure 3.23 presents the complete entity-relationship diagram (ERD) of this schema, highlighting primary and foreign key constraints, as well as the interdependencies among the tables.

3.3.4. Validation Results

3.3.4.1. ***Comparative Cyclic Voltammetry with a Laboratory-Grade Potentiostat.*** To validate the developed system, cyclic voltammetry (CV) experiments were performed in direct comparison with a commercial laboratory-grade potentiostat, the Solartron 1285 (Ametek), known for its high accuracy in low-current electrochemical measurements. CV was chosen for this assessment due to its sensitivity to electrode kinetics and instrumentation fidelity, serving as a robust benchmark for potentiostat evaluation [**174**].

Both systems were configured with identical parameters using a three-electrode setup: a platinum disc as the working electrode (WE), a platinum wire as the counter electrode (CE), and an Ag/AgCl reference electrode (RE), shown in Figure 3.24. The electrolyte consisted of 0.1 M tetrabutylammonium tetrafluoroborate ($TBABF_4$) in acetonitrile with 0.05 mM ferrocene, selected for its well-characterized reversible redox behavior.

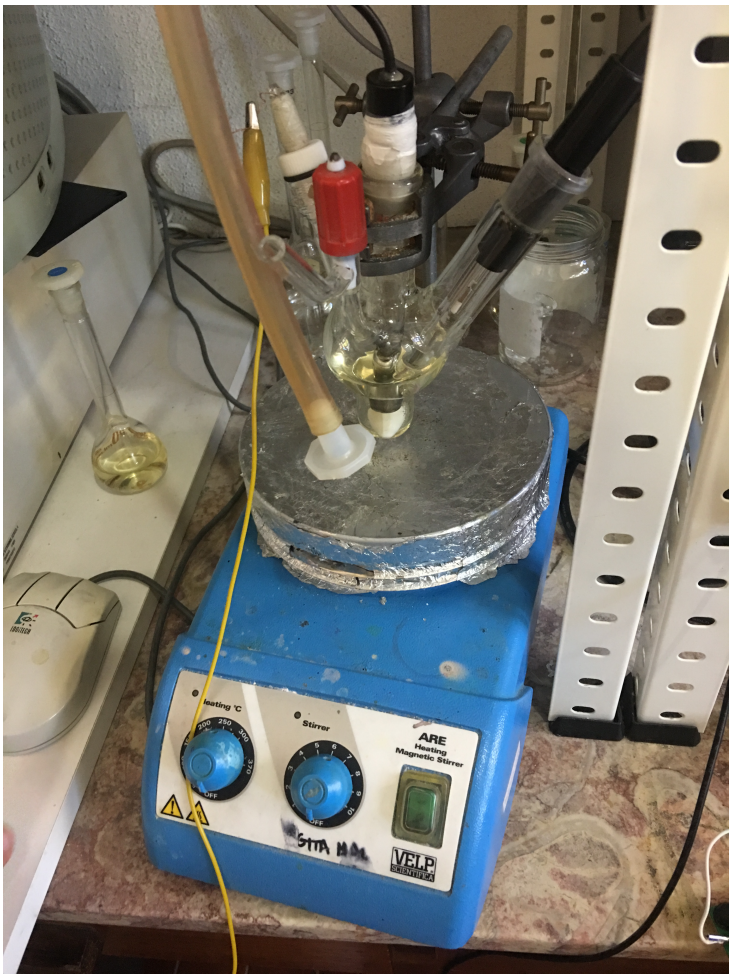


FIGURE 3.24. Reference potentiostat including the following electrodes platinum WE and CE, and Ag/AgCl RE.

The LMP91000 potentiostat was configured through the RFduino using I^2C communication, with a bias point at 20% of V_{ref}, a transimpedance amplifier resistance R_{tia} of 35 kΩ, and a load impedance of 10 Ω. The CV sweep ranged from 0 V to 0.6 V and back.

The output current was computed using:

$$I_{out} = \frac{\left(V_{out} - (V_{ref} \times 0.2)\right)}{R_{tia}} \tag{3.1}$$

where V_{ref} was 2.5 V. The resulting current data were transmitted in real-time to the web application.

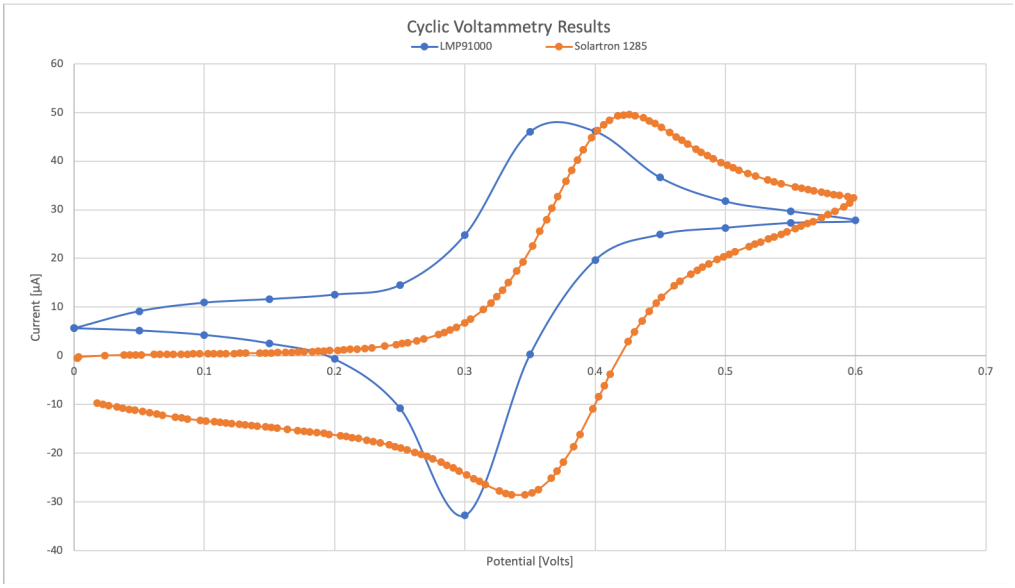


FIGURE 3.25. Comparative cyclic voltammograms for ferrocene obtained with the Solartron 1285 and the developed LMP91000-based system as part of the experimental validation.

Figure 3.25 presents the voltammograms obtained from both systems. The Solartron reference equipment, operating with a higher sampling frequency, superior analog filtering, and precise factory calibration, produced smoother and more consistent curves. In contrast, the developed potentiostat exhibited minor misalignment and increased noise in the redox peaks, mainly due to differences in sampling resolution, electrode conditioning, and uncompensated solution resistance. These factors can cause potential shifts and baseline variations, which are expected in early-stage calibration. Nevertheless, the custom platform successfully reproduced the characteristic ferrocene redox response, thereby confirming the correct electrochemical functionality and overall reliability of the system.

3.3.4.2. *Peak Analysis.* Quantitative results are summarized in Table 3.4. Both systems demonstrated comparable differences between oxidation and reduction peaks, highlighting that despite differences in resolution and sampling density, the developed device reproduces the essential electrochemical characteristics.

TABLE 3.4. Oxidation and reduction peak currents obtained from ferrocene cyclic voltammetry.

	Oxidation (μA)	**Reduction (μA)**	**Diff (μA)**
PotLink System	46.10	-32.81	78.91
Solartron 1285	49.54	-28.56	78.10

These findings confirm that the developed platform achieves results close to a high-end commercial device, at a fraction of the cost, with only minor deviations attributed to differences in ADC resolution and internal reference stability.

3.3.4.3. *Cyclic Voltammetry at Different pH.* Additional experiments assessed the capability of the system to differentiate solutions of varying pH using cyclic voltammetry (CV). Tests were performed on 0.01 M ascorbic acid (AA) in 0.5 M sulfuric acid (H_2SO_4), adjusting the pH across a range from 2 to 7. Figure 3.26 shows the voltammograms obtained.

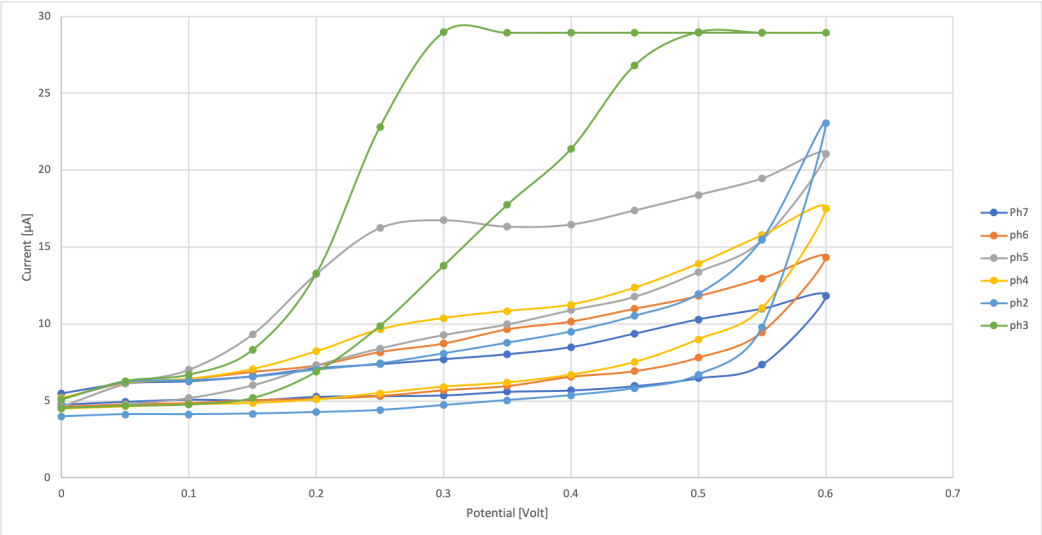


FIGURE 3.26. Cyclic voltammograms of 0.01 M AA in 0.5 M H_2SO_4 at different pH values.

As illustrated in Figure 3.26, the voltammogram corresponding to pH 3 appears truncated when compared with the other curves. This behavior results from the analog-to-digital converter (ADC) of the acquisition system reaching its input voltage limit during

the potential sweep. At this pH, the oxidation current exceeded the measurable input range of the ADC, causing signal saturation and leading to a premature cut-off of the waveform. Consequently, the recorded potential window was restricted, producing the apparent discontinuity in the curve. This limitation arises from the finite dynamic range of the ADC and the absence of automatic gain control rather than from any electrochemical anomaly in the solution. Future versions of the system will address this by expanding the measurable input range or implementing programmable attenuation to prevent signal saturation during high-current responses.

Peak and valley currents were extracted and are summarized in Table 3.5. The evolution of these values demonstrates the capability of the system to detect shifts in electrochemical behavior as a function of pH, highlighting its suitability for analytical applications.

TABLE 3.5. Peak and valley currents (μA) for different pH levels

pH	**2**	**3**	**4**	**5**	**6**	**7**
Valley	3.98	4.50	4.49	4.63	4.63	6.10
Peak	23.04	28.94	17.52	9.78	14.34	11.81

Overall, the results demonstrate that the portable system effectively captures electrochemical signatures across different experimental conditions, supporting its use in low-cost, on-site analytical applications.

3.3.5. Potlink System Strengths and Drawbacks

Potlink demonstrated the feasibility of integrating a potentiostat with a web application for real-time monitoring; however, several limitations were identified, motivating the development of the next iteration.

A key limitation of the initial design was its reliance on a separate microcontroller, with the RFDuino acting as the primary processing unit. This separation increased the system's overall size and complexity, which was not ideal for wearable applications. Additionally, the RFDuino microcontroller posed significant challenges due to its limited processing capabilities, constraining its ability to handle computationally intensive tasks. Furthermore, RFDuino has been discontinued, resulting in a lack of ongoing support and compatibility with modern software tools, which further justified the need for a redesign.

The web application, while functional, was limited by the compatibility of the Bluetooth API. The use of the Chrome Web Bluetooth API restricted the operation of the system to specific browsers and platforms, reducing its accessibility and usability for a wider range of users.

Another important consideration was the size of the system. Although functional, the prototype design did not fully optimize the form factor for wearable applications. Significant miniaturization was feasible and recommended to improve portability and integration into wearable devices.

These limitations highlight the need for a more integrated and efficient design in the next iteration. By incorporating a single unified PCB, selecting a more powerful and supported microcontroller, and addressing compatibility issues, the next prototype aims to deliver a more compact, robust, and user-friendly biosensing platform suitable for wearable applications.

3.4. NanoPotLink: Design of a Miniaturized Wearable Potentiostat for Continuous Electrochemical Monitoring

NanoPotLink represents a significant evolution in the PotLink platform, addressing limitations identified in previous designs and introducing major advances in both hardware and system architecture. Unlike the earlier standalone potentiostat implementations, this iteration was explicitly conceived as part of a wearable sensor network (WSN), combining multiple complementary sensing nodes to achieve more robust physiological monitoring.

The primary objective of NanoPotLink was to improve system integration, improve wireless communication protocols, and assess the feasibility of non-invasive glucose detection in sweat as part of a broader multimodal approach. In this architecture, the first sensing node is the custom-developed wearable potentiostat (NanoPotLink) for sweat biomarker detection, while the second node is a commercial fitness band (Xiaomi Mi Band 3) used to capture additional physiological parameters such as heart rate and body movement.

Observation of glucose alone through sweat remains a complex challenge due to several physiological and biochemical constraints. Sweat glucose concentrations are typically orders of magnitude lower than those found in blood and exhibit high variability influenced by sweat rate, skin permeability, ambient temperature, and humidity. These fluctuations, along with contamination and interindividual differences, hinder reliable quantification and correlation with blood glucose levels. Consequently, relying solely on sweat glucose measurements is insufficient for a meaningful interpretation or trend prediction.

To address these intrinsic limitations, the system was designed as a network of synchronized wearable nodes. By integrating the sweat glucose signals from NanoPotLink with heart rate and activity data from the Mi band, it becomes possible to apply data fusion techniques that take advantage of the physiological interaction between the cardiovascular response, physical activity, and metabolic demand. This multimodal strategy enhances the robustness of estimation models, filters out artifacts caused by sweat rate or motion, and ultimately supports more reliable tracking of glucose dynamics in a non-invasive manner.

A major hardware innovation in NanoPotLink is the integration of the RFDuino directly onto the printed circuit board (PCB), eliminating the need for an external microcontroller module. This reduced the device's form factor and complexity while maintaining

Bluetooth Low Energy (BLE) connectivity. In previous system versions, the external microcontroller increased both size and system overhead, limiting wearability and efficiency.

To complement hardware improvements, a dedicated mobile application was developed to replace the earlier web-based interface. This app enables direct BLE communication with the potentiostat, offers enhanced real-time data visualization, and provides a more seamless and user-centric experience. The transition away from the Chrome Web Bluetooth API addressed platform compatibility issues and contributed to improved responsiveness and usability.

Chronoamperometry was retained as the core electrochemical technique for glucose detection because of its suitability for low-concentration analyte monitoring [**175**]. However, the system architecture was explicitly designed to be modular and extensible, supporting additional biosensors for analytes such as lactate and electrolytes. This flexibility is particularly valuable in sports and performance contexts, where continuous information on hydration and metabolic function is critical.

This chapter details the design, development, and functional validation of the NanoPotLink system, emphasizing improvements in miniaturization, power management, and communication efficiency within a networked wearable framework. The results confirm the effectiveness of these enhancements and establish NanoPotLink as a robust platform for next-generation wearable biosensing applications.

3.4.1. Materials and Methods

3.4.1.1. ***System Overview.*** This section introduces the architecture of the NanoPotLink system, a low-power wearable biosensing platform designed for the real-time monitoring of sweat biomarkers during physical activity as part of a multimodal sensor network. NanoPotLink represents the third iteration in a series of electrochemical sensing systems developed throughout this work, now explicitly designed to operate alongside additional wearable nodes.

As illustrated in Figure 3.27, the system comprises two primary sensor nodes: the NanoPotLink potentiostat for sweat analysis (right) and a commercial Xiaomi Mi Band 3 fitness tracker (left) used for monitoring heart rate and motion. By combining these independent yet synchronized nodes, the system is able to correlate sweat biomarker fluctuations with cardiovascular and activity patterns, enabling a more detailed interpretation of the physiological state of the user.

The implementation of this sensor network is justified by the inherent variability and susceptibility of sweat-based measurements to external and physiological factors such as sweat rate, ambient temperature, and motion artifacts [**176**]. The inclusion of complementary data streams enables the experimental assessment of multimodal data fusion approaches aimed at mitigating these limitations. This configuration provides a framework to explore how combined physiological signals may enhance the robustness of glucose trend estimation, particularly under dynamic exercise conditions.

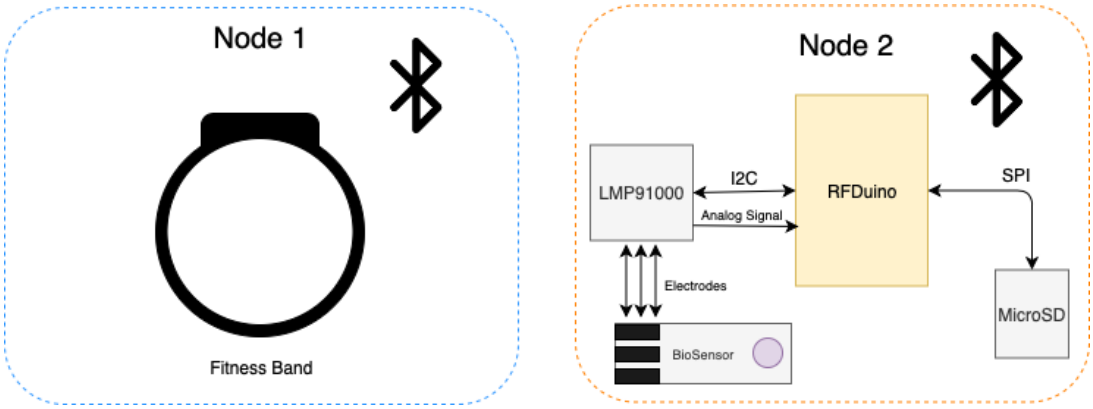


FIGURE 3.27. Wearable sensor nodes in the system: Xiaomi Mi Band 3 for heart rate and motion (left), and NanoPotLink sweat-sensing potentiostat (right).

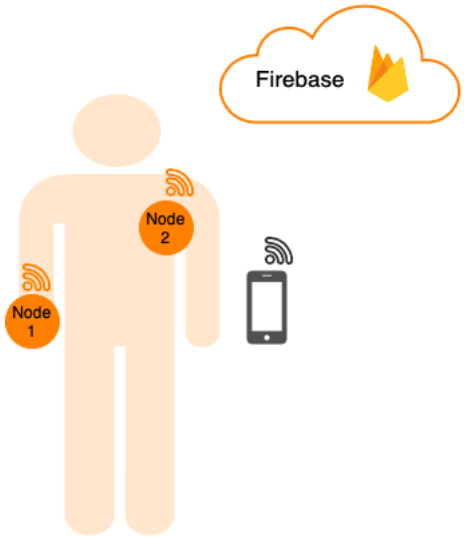


FIGURE 3.28. Overall system architecture illustrating the multimodal wearable sensor network and data flow.

The complete architecture is shown in Figure 3.28. The hardware layer consists of the NanoPotLink potentiostat node and the auxiliary fitness band node. Data from these sensors is acquired locally and transmitted via Bluetooth Low Energy (BLE) to a mobile device. BLE was selected for its low power consumption and broad compatibility.

At the software level, the dedicated mobile application manages device communication, real-time data visualization, and user interaction. For advanced processing, such as machine learning-based trend estimation and long-term tracking, the system connects to a cloud backend. This hybrid local/cloud approach enables immediate feedback as well as more sophisticated analyses over time.

Together, this architecture supports a more comprehensive assessment of physiological status, demonstrating how integrating multiple wearable sensing modalities can overcome the individual limitations of sweat-based measurements and advance non-invasive monitoring solutions.

The following sections describe the hardware implementation of the NanoPotLink node in detail, followed by an explanation of the software architecture covering the mobile app and backend components.

3.4.1.2. ***Hardware Description.*** The NanoPotLink system retained the fundamental hardware components established in earlier iterations, including the RFDuino microcontroller, the LMP91000 potentiostat IC, a lithium battery charging circuit, and an FTDI interface for programming. A major enhancement in this version was the direct integration of the RFDuino onto the PCB, eliminating the need for a separate microcontroller module. This change significantly reduced the overall footprint and improved the mechanical robustness of the system, making it more suitable for wearable applications. Bluetooth Low Energy (BLE) communication was preserved to ensure efficient wireless data transmission.

The complete schematic and PCB design files for NanoPotLink are provided in Appendix B.

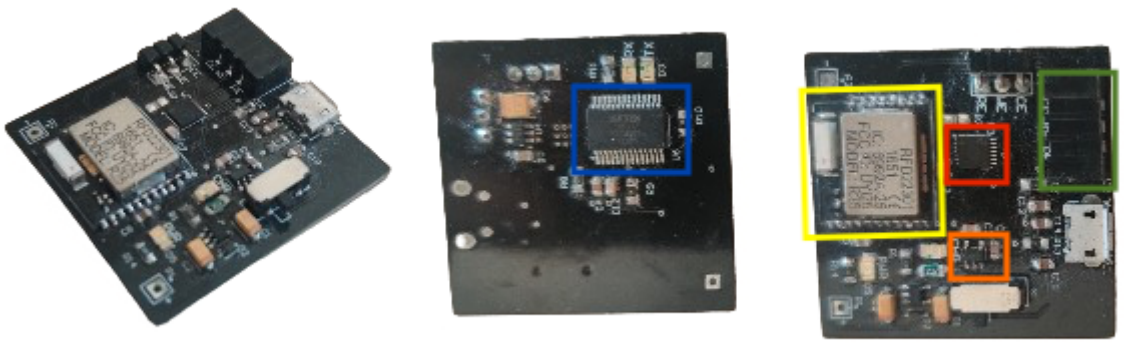


FIGURE 3.29. NanoPotLink system

As illustrated in Figure 3.29, the updated PCB layout highlights the main functional regions using color-coded outlines for improved readability and component identification:

- **Blue region**: FTDI programming interface for serial communication and firmware upload.
- **Yellow region**: RFDuino microcontroller, responsible for processing and BLE communication.
- **Red region**: LMP91000 potentiostat IC for electrochemical signal acquisition.
- **Orange region**: Lithium battery charger IC responsible for power management and safe battery operation.
- **Green region**: SPE (Screen-Printed Electrode) connector for interfacing with disposable biosensors.

The system also includes a USB connector for charging and optional data transfer, as well as a 3.3 V voltage reference and regulator to ensure analog stability and consistent performance. These refinements significantly enhanced the device's reliability, portability, and integration while maintaining its core electrochemical sensing and wireless communication capabilities.

To enhance measurement accuracy, a dedicated voltage reference chip was incorporated to provide a stable and precise potential for electrochemical sensing. This addition improves the reliability of the biosensing platform, ensuring consistent readings under different conditions. These hardware enhancements contribute to the portability, usability, and overall accuracy of the system, making it more practical for real-world deployment in wearable biosensing applications.

A Xiaomi Mi Band 3 fitness tracking device was used together with the developed system, integrated through the BLE GATT protocol. In this version, data acquisition from the fitness band was fully incorporated into the React Native application, allowing seamless real-time synchronization and storage of physiological parameters directly within the application. This enhancement removes dependence on third-party software, creating a more cohesive and efficient user experience while ensuring that all collected data are managed within a unified platform.

3.4.2. Software: Embedded and high level software

The software layer of the NanoPotLink system comprises two main components: the mobile application for user interaction and device communication, and the cloud-based infrastructure for data storage, synchronization, and remote access. Several options were considered during the development phase for both the mobile and backend components, with the final choice based on criteria such as cross-platform compatibility, low-latency communication, ease of integration, scalability, and community support.

The firmware was developed in Arduino C and deployed on an RFDuino platform, leveraging the RFduinoBLE library to establish Bluetooth Low Energy (BLE) communication with the mobile application. It manages low-level operations including BLE advertising and connection handling, parsing of configuration data received via BLE, and programming the LMP91000 analog front-end through the I2C protocol. This design enables real-time reconfiguration of potentiostat parameters and continuous acquisition of sensor data, which is then transmitted back to the mobile application for visualization and subsequent storage in the cloud infrastructure.

3.4.2.1. ***Mobile Application:*** Multiple approaches were evaluated for the development of the mobile application. Native development using Swift (iOS) and Kotlin/Java (Android) offers optimal performance and full hardware access but requires maintaining two separate codebases, increasing development time and complexity. Hybrid solutions like Ionic or Cordova were also considered but were discarded due to limitations in performance and BLE (Bluetooth Low Energy) handling.

React Native emerged as the preferred framework due to its ability to build high-performance cross-platform applications using a single codebase. Developed by Meta, React Native provides near-native performance, supports BLE communication libraries, and allows rapid iteration and deployment on both Android and iOS platforms. Its active developer community and extensive plugin ecosystem also contributed to the decision.

3.4.2.2. ***Cloud Database and Backend.*** For the cloud backend, several database platforms were evaluated, including traditional SQL-based solutions (e.g., MySQL, PostgreSQL), NoSQL options (e.g., MongoDB, CouchDB), and backend-as-a-service (BaaS) platforms such as AWS Amplify and Google Firebase.

Firebase was selected as the backend solution due to its integration with mobile platforms, built-in support for real-time databases, and simplified deployment process. Developed by Google, Firebase provides a scalable cloud-hosted NoSQL database that enables

live synchronization of biosensor data with minimal configuration. The adopted architecture follows a serverless model, in which the backend infrastructure is fully managed in the cloud, eliminating the need for dedicated server maintenance and allowing automatic scaling based on demand. This configuration supports real-time monitoring, efficient data storage, and reliable data retrieval, which are essential for time-sensitive physiological sensing applications. In addition, Firebase includes native authentication, hosting, and analytics services, further simplifying overall system integration.

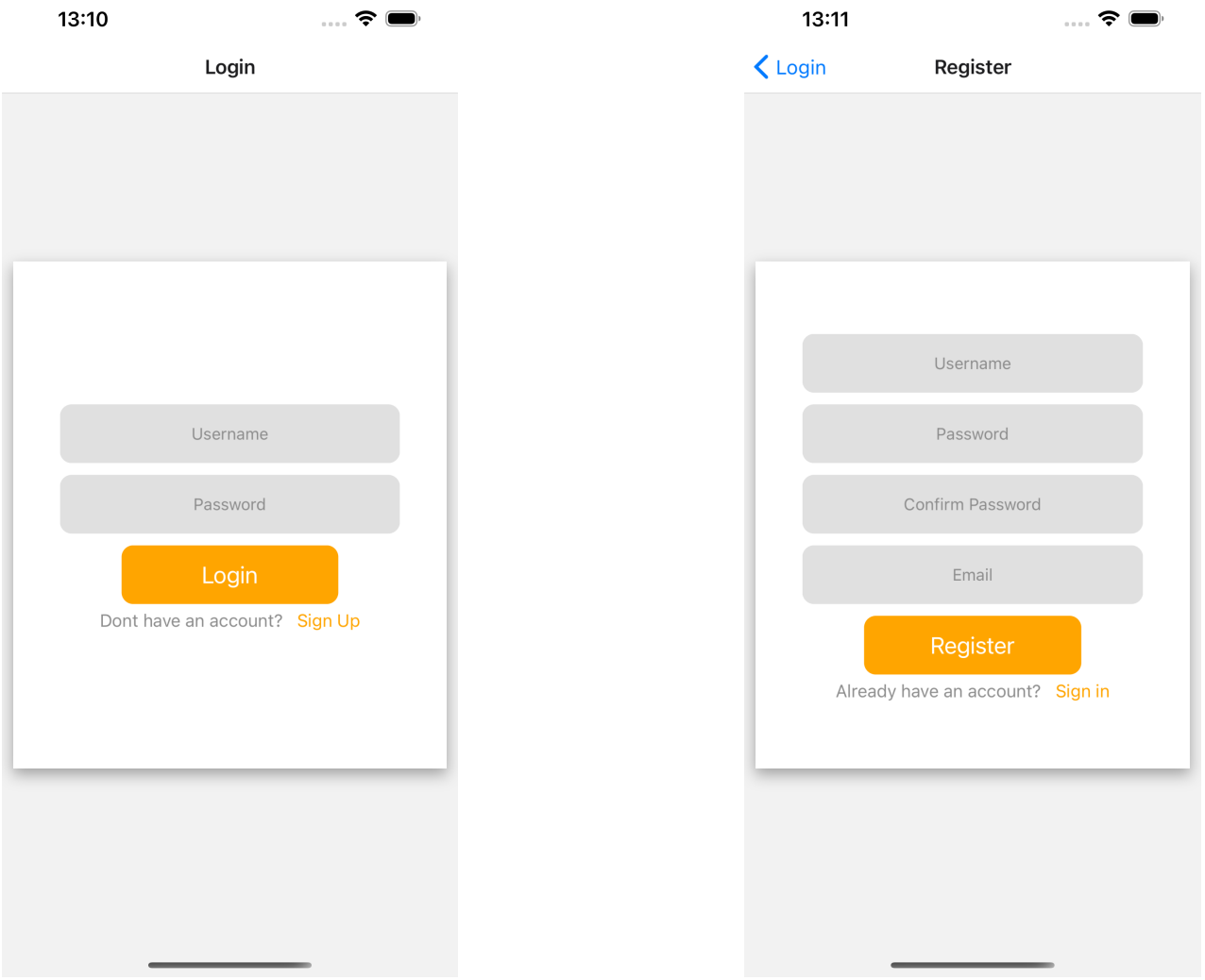
3.4.2.3. ***Software Implementation:*** The software implementation for NanoPotLink combines a React Native mobile application with Firebase as the backend service. The application handles Bluetooth communication with the NanoPotLink device and local data caching. Sensor data are transmitted to Firebase in real-time, where they are stored, synchronized, and made accessible for further analysis or visualization. This architecture provides a robust, scalable, and user-friendly platform suitable for wearable biosensing and remote health monitoring applications.

3.4.2.4. ***Login Screen:*** The login screen illustrated in Fig. 3.30a allows users to securely access the application by entering their registered email and password. Each user account stores measurement data, enabling personalized data tracking and history retrieval.

3.4.2.5. ***Register Screen:*** The registration screen demonstrated in illustrated in Fig. 3.30b enables new users to create an account, ensuring that each user has an individual profile for storing and accessing measurement data.

3.4.2.6. ***Configuration Screen:*** The configuration screen illustrated in Fig. 3.31a automatically scans for available potentiostat devices via BLE and displays detected devices for selection. This ensures seamless connectivity between the mobile application and the biosensing platform, allowing for a user-friendly and efficient setup.

Once a device is selected, users can configure the potentiostat by adjusting critical electrochemical parameters that are tailored to their specific sensing application. The ability to fine-tune these settings is essential for optimizing the measurement accuracy and adapting the system to different types of biosensors. The configurable parameters are:

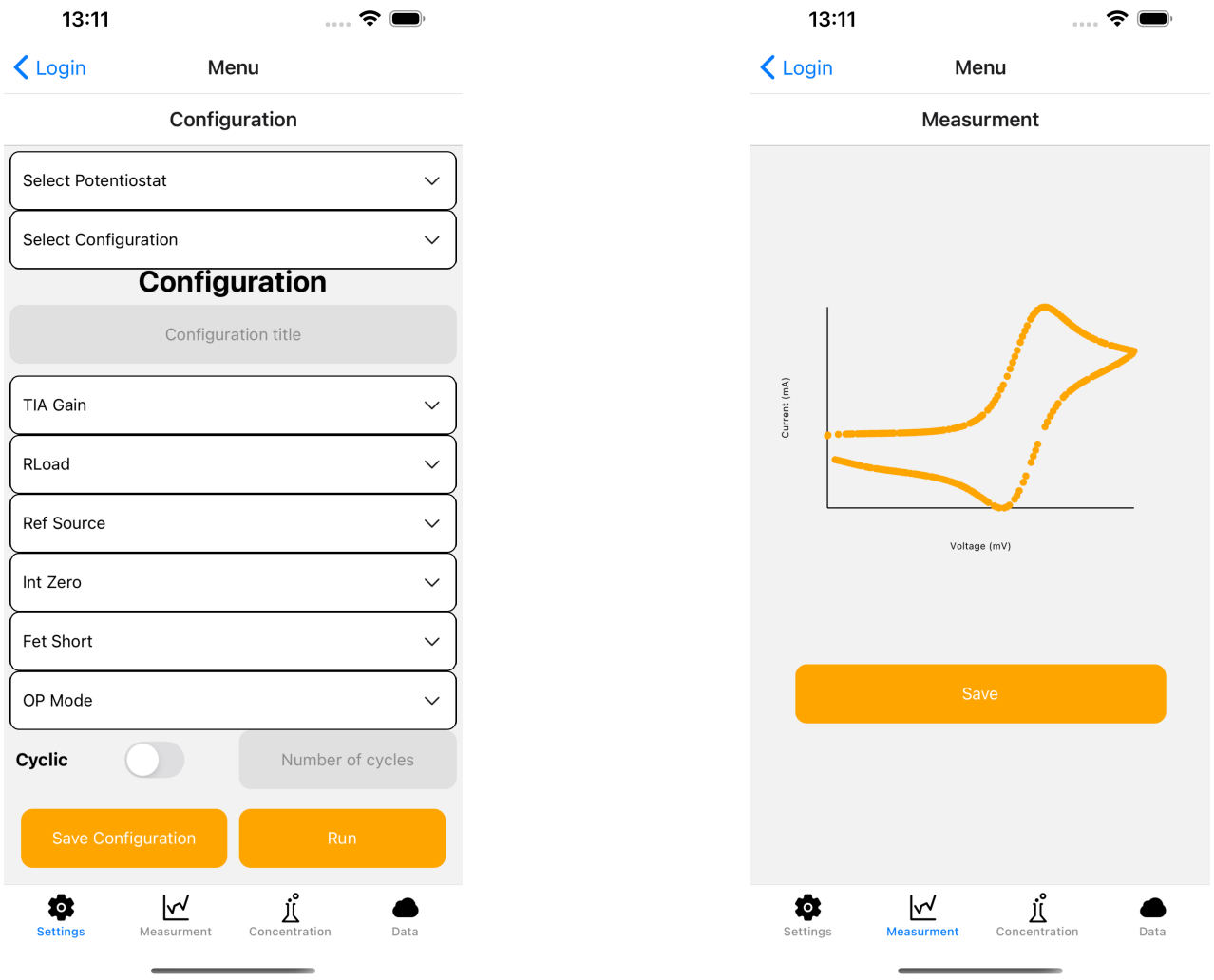


(A) (B)

FIGURE 3.30. Mobile app user interface: (a) Login screen allowing user authentication, and (b) Register screen enabling new user account creation.

- **TIA Gain:** Configures the transimpedance amplifier gain, determining the amplification of the sensor's current signal. Proper selection of gain is crucial to achieve the best signal-to-noise ratio in electrochemical detection.
- **R Load:** Sets the sensor's internal load resistance, affecting current flow and measurement sensitivity. The correct value ensures stable sensor operation and accurate readings.
- **Reference Source:** Defines whether an internal or external reference voltage is used for signal processing. This selection influences the potential stability of the WE.
- **Internal Zero:** Adjusts the internal baseline potential for electrochemical measurements, ensuring that the WE operates at an appropriate voltage.

- **FET Short:** Enables or disables FET short circuit, affecting circuit stability and measurement precision. This setting is important for conditioning the sensor before measurements.
- **Operating Mode:** Selects between different electrochemical measurement modes, such as two-electrode or three-electrode configurations. These modes define the arrangement of the reference, counter, and WEs.
- **Cyclic Mode:** Configures CV settings, including the number of cycles to be performed. This setting is critical for obtaining the oxidation-reduction profiles of the target analytes. This only takes effect when Cyclic toogle is on. Otherwise the system will perform step voltammetry.



(A) (B)

FIGURE 3.31. Mobile app user interface: (a) Configuration screen for selecting and setting potentiostat parameters, and (b) Measurement screen displaying real-time electrochemical data visualization.

Users can save configurations for future use, minimizing manual setup and ensuring consistency across measurements. Once configured, they can proceed to the measurement page, where real-time graphical data visualization provides immediate electrochemical feedback, enabling trend monitoring, anomaly detection, and sensor validation. This streamlined workflow enhances usability, making the system accessible for both researchers and athletes needing real-time electrolyte and hydration monitoring. The integration of BLE communication, real-time adjustments, and data visualization ensures adaptability across various biosensing applications.

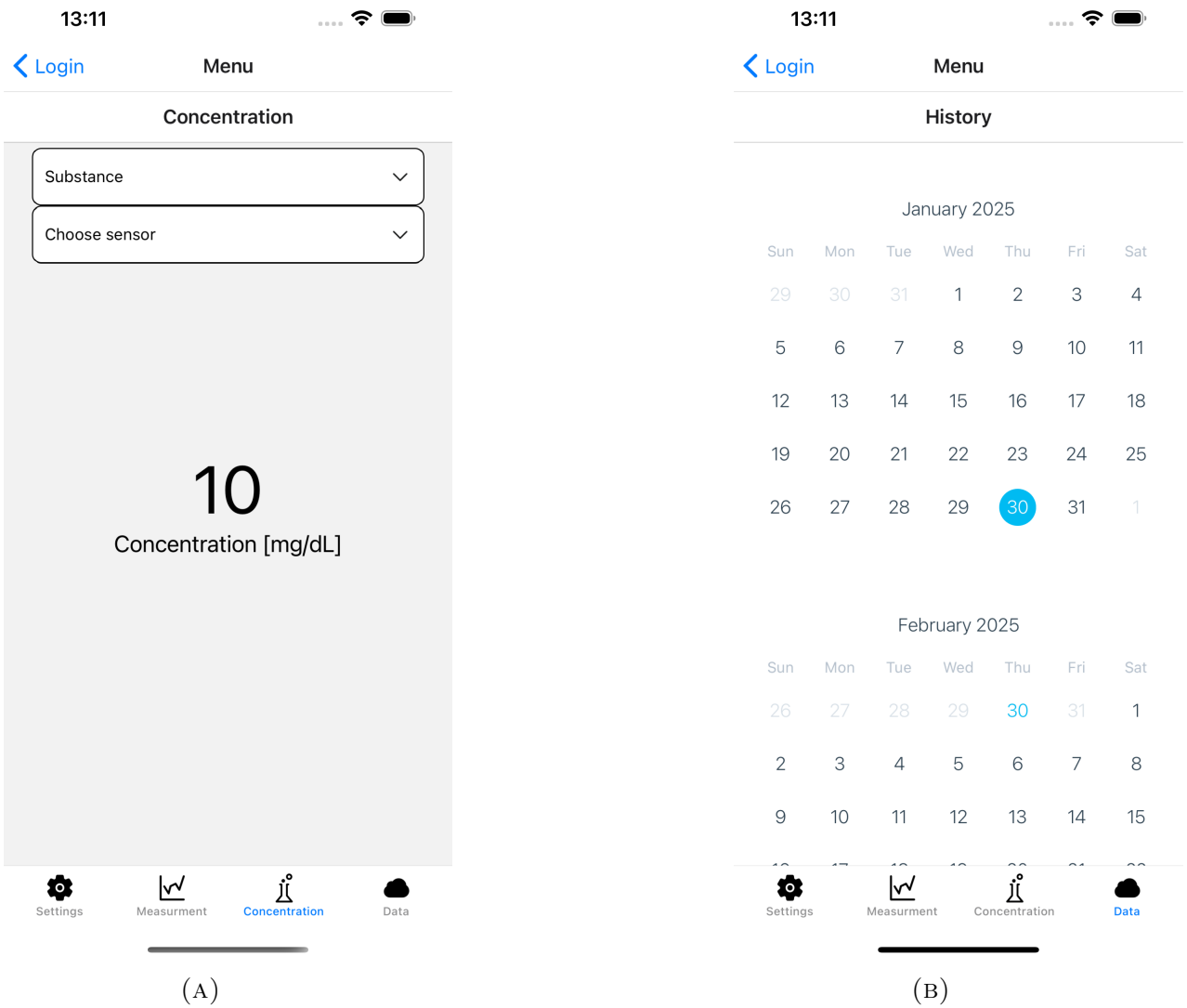
3.4.2.7. ***Measurement Page:*** The measurement page illustrated in Fig. 3.31b provides real-time visualization of data acquired from the potentiostat. The data is displayed as a plot, allowing users to monitor electrochemical signals dynamically.

3.4.2.8. ***Concentration Page:*** The concentration page represented in Fig. 3.32a displays the concentration of a specific substance based on calibrated sensor data. In this iteration, the system was calibrated exclusively for glucose measurements.

3.4.2.9. ***Data Page:*** The data page illustrated in Fig. 3.32b allows users to access previous measurement records using a calendar-based interface. This feature facilitates long-term monitoring and trend analysis of electrochemical readings.

3.4.2.10. ***Application Overview:*** The mobile application features a bottom navigation bar that allows users to seamlessly switch between different sections. Its architecture is built to provide real-time data acquisition, processing, and visualization while ensuring a user-friendly experience. The integration of BLE via *react-native-ble-plx* enables efficient communication with the potentiostat, while Firebase Cloud Firestore ensures secure data storage and real-time updates. Visualization components leverage the `react-native-svg` and D3 libraries, providing high-quality graphical representations of biosensor data. This application marks a significant improvement over the previous web-based implementation, enhancing usability, system integration, and real-time monitoring capabilities.

3.4.2.11. ***Real-Time Database:*** In this project, the Firebase Cloud Firestore was utilized as the database service. Although Cloud Firestore is a NoSQL database, it offers features such as scalability and flexibility, which enable the potentiostat to be operated remotely in real-time.



(A) (B)

FIGURE 3.32. Mobile app user interface: (a) Concentration page displaying glucose concentration readings, and (b) Data page providing historical data access through a calendar-based interface.

3.4.3. Calibration procedure

Chronoamperometry was employed for glucose analysis as a result of its high sensitivity and rapid response time. This electrochemical technique involved setting a 0V bias potential for 1 second to allow the biosensor to stabilize, followed by maintaining a 0.5V potential for 29 seconds. The resulting current was measured using the RFDuino ADC, which converted the analog signal into a current value corresponding to glucose concentration.

Figure 3.33 illustrates the diagram of the calibration and testing methods associated with node1. The experimental protocol was divided into distinct steps to ensure accurate calibration and validation of biosensor performance.

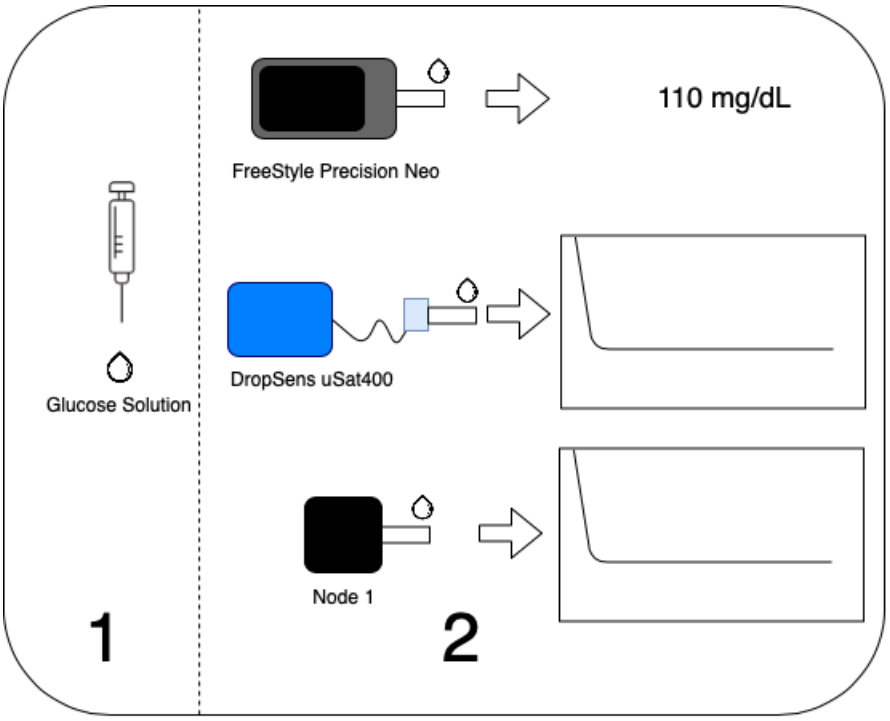


FIGURE 3.33. Calibration and testing procedures for node 1.

Box 1 of the diagram details the preparation of solutions with known glucose concentrations, where six samples with increasing glucose levels were prepared to establish a calibration curve. These solutions were carefully mixed to ensure uniform distribution of glucose molecules, minimizing measurement variability.

In Box 2, these prepared solutions were analyzed using an electrochemical sensor integrated with the potentiostat system. The sensor response was recorded for each glucose concentration, generating a current that was plotted to determine the sensitivity and linearity of the sensor. To validate the precision of the biosensor, the results were compared with a reference glucose analyzer.

The reference glucose analyzer used was the FreeStyle Neo Precision, a commercially available blood glucose meter that measures glucose concentrations in mg/dL. It is designed for blood samples and operates within a detection range of 25 to 500 mg/dL. This comparison allowed the system to be benchmarked against an industry-standard method, ensuring reliability in real-world applications.

To further refine the calibration accuracy, each sample was measured in triplicate, reducing potential errors caused by signal noise or electrode inconsistencies. The acquired data were then processed using a least-squares regression approach to derive a calibration equation, which was later applied to predict glucose levels in sweat samples.

To assess sensor stability and repeatability, measurements were performed at multiple time points, ensuring minimal signal drift during extended use. Environmental factors such as temperature and humidity were also monitored, as they could impact sensor performance. These considerations ensured that the biosensor maintained reliable performance under different experimental conditions.

By integrating chronoamperometry with a carefully controlled calibration protocol, this method provided a robust foundation for non-invasive glucose monitoring, paving the way for real-time biosensing applications in wearable healthcare devices.

3.4.4. Experimental Validation

The experimental protocol consisted of evaluating the performance of the developed system using commercially available Freestyle Precision glucose test strips, followed by validation against the Freestyle Precision Neo glucose meter. The protocol involved preparing a set of glucose solutions with different concentrations obtained by diluting a commercially available sugary drink. Each solution was measured using both the IoT Potentiostat and the Freestyle Neo device to enable comparative analysis.

The Freestyle Precision Neo meter was used as the reference instrument for glucose quantification in the prepared solutions. However, because the meter is designed specifically for blood glucose monitoring in diabetes patients, it is unable to report values below 25 mg/dL or above 500 mg/dL. As a result, solutions falling outside this measurable range were classified qualitatively as either “low” (below 25 mg/dL) or “high” (above 500 mg/dL). This limitation was taken into account during the interpretation and comparison of results between the two measurement systems.

Fig. 3.34 represents the first results. As can be observed in the figure, the first second represents a sensor stabilization period where no potential is applied, the potential is stepped to 0.5V and held constant for 29 seconds. The sensor provides a reliable result after 5 seconds.

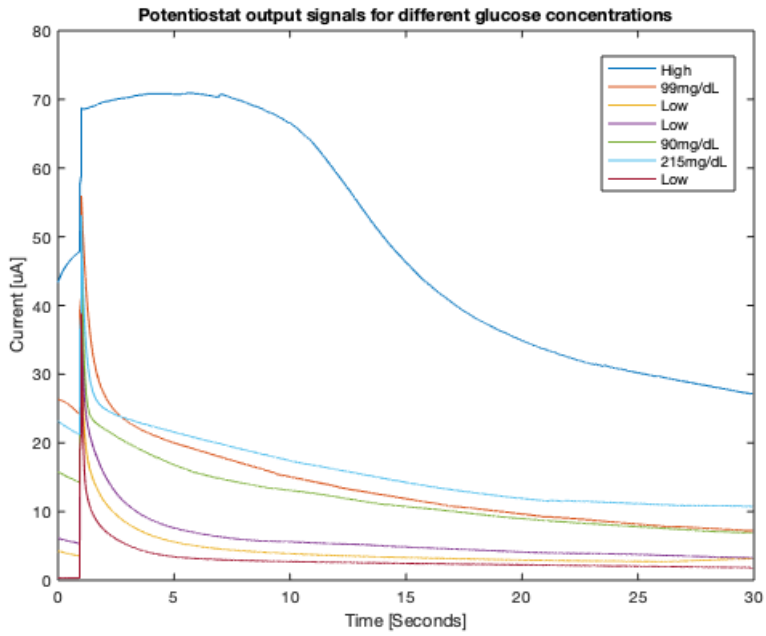


FIGURE 3.34. The IoT potentiostat glucose measurement results for beverages with different sugar concentration

3.4.4.1. ***Proof-of-Concept Sweat Monitoring During Indoor Cycling.*** To evaluate the feasibility of using the developed platform for monitoring dynamic changes in sweat composition, a preliminary proof-of-concept experiment was conducted with a single participant (24 years old). The participant performed a one-hour indoor cycling session following a structured intensity protocol, illustrated in Fig. 3.35. The exercise was carried out on an indoor bike equipped with five resistance levels. The sequence started at Level 1, increased progressively to Level 5, and then decreased back to Level 1. This controlled progression was designed to induce systematic variations in metabolic demand and perspiration rate.

During the exercise session, six sweat samples were collected at predefined intervals and analysed using the proposed device. The experiment took place in an enclosed environment to accelerate perspiration and ensure consistent sample collection conditions. Figure 3.36 shows an example of the biosensor output during one of the measurements, highlighting a zoomed-in region around the 5-second mark where the sensor response stabilised. Although the biosensors used were originally intended for higher glucose concentration ranges, this experiment aimed to assess their responsiveness at the lower levels typically found in sweat.

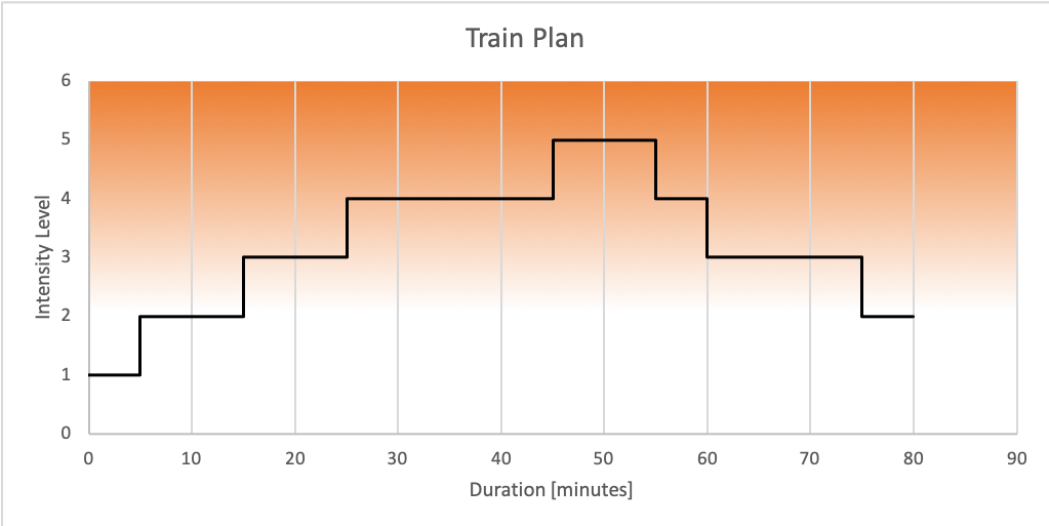


FIGURE 3.35. Indoor cycling training plan showing progression from Level 1 to Level 5 and return to Level 2.

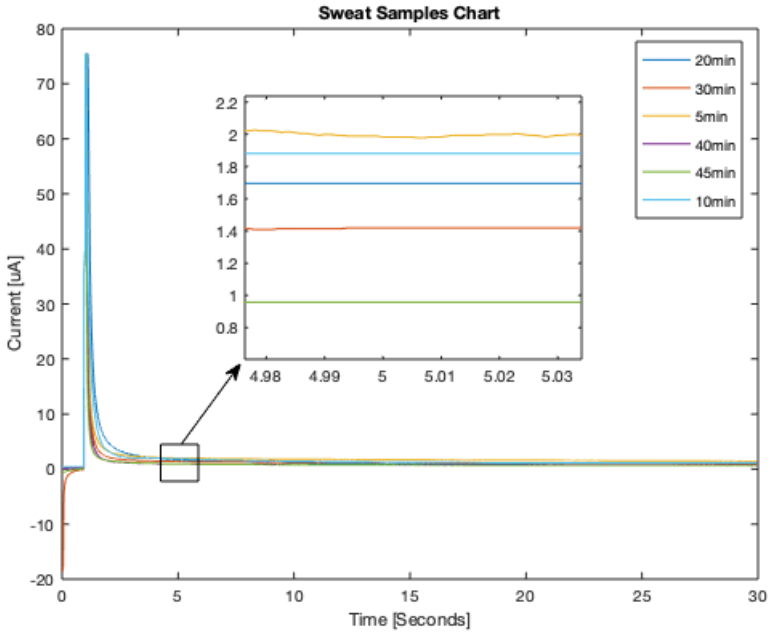


FIGURE 3.36. Biosensor current output for a sweat glucose sample, with a stable region visible around the 5-second mark.

Heart rate and exertion were simultaneously monitored using a consumer fitness band, with an example of the recorded heart rate displayed in Fig. 3.37. During the initial moderate-intensity phase (Level 1 to Level 3), the biosensor displayed a slight downward trend in glucose levels. As intensity increased toward Level 5, the signal exhibited a more pronounced decrease, consistent with increased glucose utilisation as metabolic activity intensified. Although the biosensors were not specifically optimised for the low

concentration ranges of sweat, the platform was still capable of detecting relative trends corresponding to physiological changes.



FIGURE 3.37. Mi Fit application output showing heart rate during the indoor cycling session.

This preliminary single-subject experiment primarily serves as a functional validation of the integrated system. The results show that the platform can detect relative variations in sweat glucose levels under controlled changes in exercise intensity. While further studies with a larger group of subjects are needed to establish statistical significance and to calibrate the sensors for accurate quantification at sweat-level concentrations, these initial findings demonstrate the system's potential for dynamic sweat analysis and provide a foundation for future refinements and broader validation.

3.4.5. NanoPotLink System Strengths and Drawbacks

NanoPotlink introduced significant advances over the first iteration, including the integration of the RFDuino directly onto the PCB, a dedicated mobile application for real-time data acquisition and visualization, and improved system portability. The adoption of BLE communication allowed efficient and low-power data transfer, enhancing the usability

of the biosensing platform. Although these improvements made the system more practical for wearable applications, several limitations were identified, which guided design decisions for a new system.

One of the primary challenges was the processing limitations of the RFDuino. Although its integration into the PCB reduced system complexity, its computational power remained constrained, limiting the potential for on-board signal processing and advanced data handling. To overcome this, future iterations will explore the use of a more powerful microcontroller capable of supporting real-time data processing while maintaining low power consumption.

Another limitation was the manual adjustment of electrochemical sensing parameters via the application. While the mobile app provided an intuitive interface for configuring settings such as TIA Gain, R Load, and Reference Source, future iterations will explore automated calibration procedures and adaptive measurement configurations to enhance user experience and improve measurement accuracy.

The system, while successfully calibrated for glucose detection, requires further validation for detecting additional analytes, such as lactate and electrolytes. Expanding the biosensing capabilities of the platform is a key focus for the next iteration, allowing for broader applications in health monitoring and sports performance tracking.

In terms of design, further miniaturization and power optimization will be pursued to enhance the wearability and usability of the device. The integration of a more efficient power management system, including extended battery life and optimized energy consumption, will be essential for enabling continuous monitoring applications.

These limitations highlight the need for ongoing improvements in hardware, sensor adaptability, and usability. The next iteration will focus on increasing processing power, improving system automation, expanding analyte detection capabilities, and optimizing the overall design for enhanced portability and long-term usability.

3.5. MultiPot: Implementation and Evaluation of a Four-Channel Potentiostat System for Multi-Analyte Detection

3.5.1. Overview

MultiPot is a four-channel potentiostat platform developed to address the growing need for real-time, multi-analyte electrochemical sensing in portable and wearable applications. Conventional single-channel potentiostats limit the ability to monitor several biomarkers simultaneously, which is essential in contexts where physiological, biochemical, or environmental parameters interact dynamically. Multi-analyte detection is particularly important in fields such as sports physiology, metabolic monitoring, point-of-care diagnostics, and environmental sensing, where capturing correlated biochemical trends enables more robust interpretation than isolated measurements.

To meet these requirements, MultiPot integrates a custom-designed printed circuit board (PCB) and an optimized hardware–firmware stack that ensures high signal fidelity, low noise, and scalability within a compact form factor. At its core, the Artemis microcontroller provides the computational throughput, power efficiency, and peripheral interfacing necessary for simultaneous multi-channel data acquisition and processing. The system architecture supports flexible front-end configurations, enabling either parallel or multiplexed sensor operation depending on the target application.

A mobile application complements the hardware by offering configuration control and real-time visualization of multi-channel sensor data. By supporting simultaneous measurement of several electrochemical signals, MultiPot enables richer physiological insight, improved anomaly detection, and more accurate modelling of dynamic biochemical processes. Target application domains include biochemical monitoring, sports performance analytics, and environmental diagnostics, where multi-analyte sensing provides clear advantages over traditional single-parameter approaches.

3.5.2. Comparison of Hardware Architectures

Two front-end configurations were evaluated for multi-analyte sensing performance:

(1) **Multiplexer-based architecture**: a single LMP91000 potentiostat sequentially switched across multiple sensors, as detailed in Appendix C.

(2) **Multi-chip architecture**: four independent LMP91000 potentiostat front-ends, each dedicated to a single channel, as detailed in Appendix E.

The multiplexer-based design offers reduced hardware cost and board complexity but exhibits switching delays, transient artifacts, and elevated noise levels due to shared analog paths, limiting its suitability for real-time, parallel detection. The multi-chip configuration, while more resource-intensive, ensures true simultaneous acquisition with superior signal integrity and reduced cross-talk.

In the four-chip configuration, parallel acquisition is achieved through the use of four LMP91000 potentiostat front-ends. Each device is configured via the I^2C bus while maintaining an independent analog output. Because the LMP91000 lacks programmable I^2C addressing, individual devices are selectively enabled through dedicated GPIO control lines to avoid bus conflicts. Although initialization occurs sequentially, concurrent sampling is maintained through isolated analog channels, ensuring high measurement integrity and minimizing inter-channel interference.

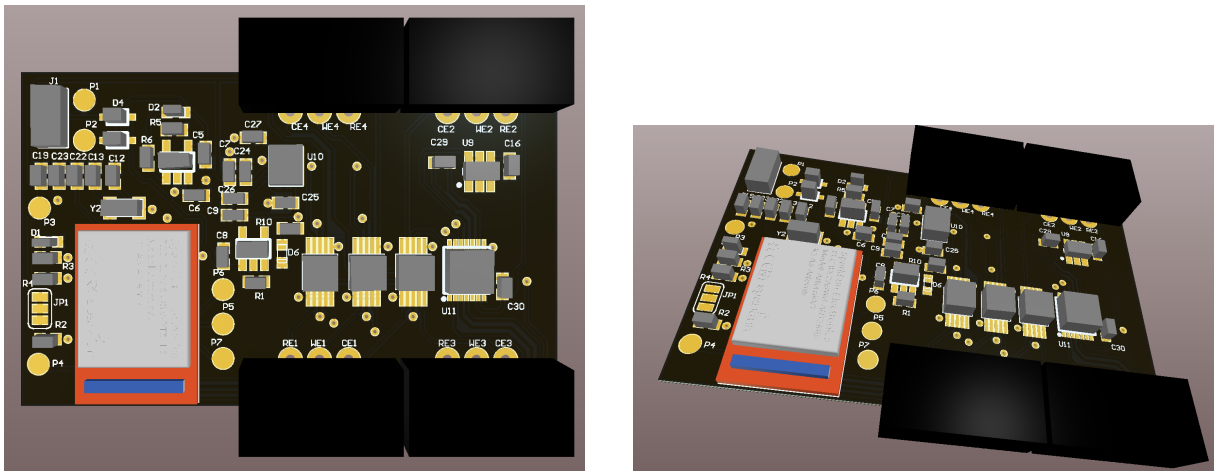


FIGURE 3.38. Prototype PCB for the multiplexed configuration, illustrating sequential sensor addressing.

A comparative summary of both front-end architectures is provided in Table 3.6. Experimental results demonstrate that the independent four-chip configuration achieves superior accuracy, lower cross-talk, and improved temporal stability, at the expense of increased PCB complexity and marginally higher power consumption. These results confirm that architectural separation of the analog front-ends provides measurable gains in performance for concurrent electrochemical sensing applications.

TABLE 3.6. Comparison of Multiplexer-Based and Independent LMP91000 Configurations

Feature	**Multiplexer-Based**	**Four Independent LMP91000**
Measurement Mode	Sequential (time-multiplexed)	Parallel (independent channels)
Signal Quality	Higher noise due to switching artifacts	High fidelity, isolated analog paths
Sampling Speed	Limited by switching latency	Unaffected by channel scaling
Cross-Talk	Observable (shared analog path)	Negligible
Channel Configuration	Uniform across sensors	Individually configurable
Real-Time Compatibility	Restricted	Fully compatible
Hardware Complexity	Low	Moderate (GPIO control required)
Power Consumption	Lower	Slightly higher

3.5.3. Hardware Architecture

The MultiPot hardware platform, presented in Fig. 3.39, was developed to achieve high-fidelity, low-noise electrochemical measurements while maintaining modularity, scalability, and compactness suitable for portable and wearable deployments. The architecture integrates four LMP91000 potentiostat front-ends, an Artemis microcontroller responsible for data acquisition and communication, an inertial measurement unit (IMU) based on the LSM9DS1 sensor, an MCP73831 Li-ion battery charger, and a CH340 USB-to-serial interface used solely for debugging and development.

The printed circuit board (PCB), designed in *Altium Designer*, adopts a dual-layer structure with spatial and electrical separation between analog and digital domains to mitigate coupling noise. The ground plane was partitioned into analog and digital sections, interconnected through a controlled impedance bridge to minimize return current interference. Sensitive analog traces, including the transimpedance amplifier outputs from each LMP91000, were routed as short, shielded differential paths to reduce parasitic capacitance and electromagnetic susceptibility. Power decoupling capacitors were strategically placed adjacent to each potentiostat front-end to stabilize the supply voltage and suppress high-frequency noise. This layout strategy ensures accurate current-to-voltage conversion and reliable signal acquisition even during concurrent multi-channel operation. A complete schematic and corresponding PCB footprints are included in Appendix E.

Microcontroller Selection: The selection of the Artemis microcontroller was driven by the specific requirements of multi-channel electrochemical sensing in portable and wearable contexts. In contrast to conventional single-channel systems, the MultiPot platform requires simultaneous acquisition from four potentiostat front-ends, precise timing

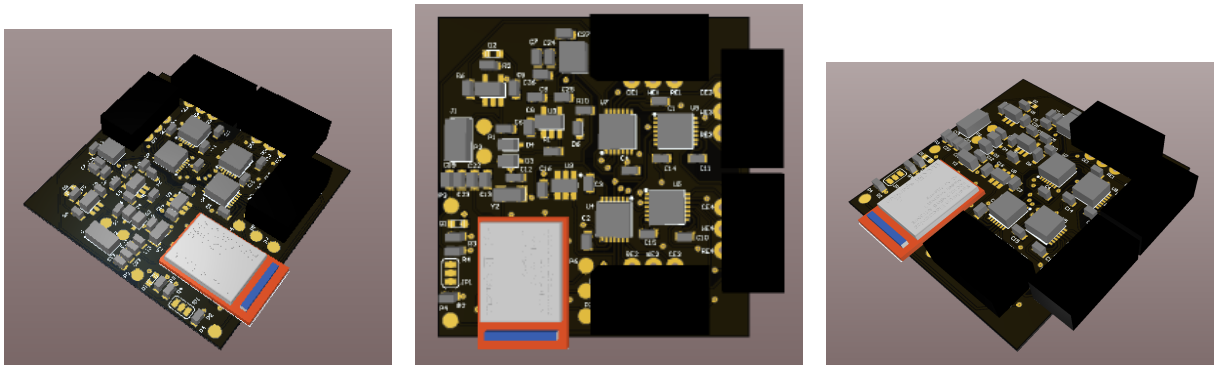


FIGURE 3.39. Different perspectives of the final four-channel PCB design.

synchronization, low-noise digital operation, and sufficient computational headroom for on-device signal conditioning and data handling. These requirements impose constraints on processing throughput, peripheral availability, and power efficiency.

The Artemis microcontroller, based on an ultra-low-power ARM Cortex-M4F core, offers an advantageous balance between computational performance and energy efficiency. Its floating-point unit (FPU) enables efficient real-time signal processing, while its high-speed SPI and I^2C interfaces support concurrent communication with multiple LMP91000 front-ends and auxiliary sensors. Furthermore, its low active and sleep power consumption makes it particularly suitable for battery-powered and wearable deployments, where thermal stability and long operational lifetime are critical.

Compared to commonly used alternatives such as ESP32-, nRF52-, or STM32-based platforms, Artemis provides superior energy efficiency at comparable computational capability, while avoiding unnecessary wireless stacks or peripheral overhead that could introduce additional noise or power consumption. A comparison of representative microcontrollers is presented in Table 3.7, highlighting the rationale behind the Artemis selection for the proposed architecture.

TABLE 3.7. Engineering comparison of candidate microcontrollers for the MultiPot platform

Microcontroller	**CPU Core**	**Max Clock**	**Active Current**	**Key Interfaces**
Artemis	ARM Cortex-M4	96 MHz	~6 mA @ 48 MHz	SPI, I^2C, UART
ESP32	Dual-core Xtensa LX6	240 MHz	~80–240 mA	SPI, I^2C, UART, Wi-Fi, BLE
nRF52	ARM Cortex-M4	64 MHz	~5.3 mA @ 64 MHz	SPI, I^2C, UART, BLE
STM32 (F4 series)	ARM Cortex-M4	168 MHz	~25 mA @ 84 MHz	SPI, I^2C, UART

Motion Sensor Integration: The inclusion of the LSM9DS1 IMU enhances the functionality of the system by enabling motion-aware electrochemical sensing. This sensor supports tri-axial acceleration, angular velocity, and magnetic field measurements,

allowing the system to quantify user movement and orientation in real-time. Such capability is critical for wearable biochemical applications, where body motion can introduce mechanical stress, variations in contact pressure, or microfluidic instability, all of which may distort electrochemical responses. By synchronizing the IMU data stream with electrochemical sampling timestamps, motion artifacts can be characterized and either compensated algorithmically or used as contextual metadata. Furthermore, motion-derived features can support the interpretation of biochemical variations in dynamic conditions, such as lactate or sweat electrolyte levels during physical exertion. The integration of the IMU establishes a hybrid biosensing architecture that merges chemical and kinematic data to enable more robust and context-aware physiological monitoring.

Power and Programming Subsystems: Power management and firmware deployment were optimized for compactness and modularity. To reduce the overall board area and mechanical thickness, the on-board USB-C programmer was omitted in favor of an external pogo-pin interface (Fig. 3.40). This interface provides temporary contact for in-circuit programming and debugging, without adding permanent bulk or connector stress to the enclosure. The pogo-pin adapter connects directly to the Artemis SWD and UART lines, ensuring full compatibility with standard flashing utilities.

Energy storage and charging are managed through a single-cell Li-ion battery controlled by the MCP73831 linear charger. The device includes thermal regulation and preconditioning for deeply discharged cells, ensuring operational safety during autonomous use. Power path routing was designed to minimize ground potential variation between analog front-ends and digital subsystems. Local low-dropout regulators (LDOs) isolate analog reference lines from the noisy digital domain, maintaining consistent biasing for the LMP91000 units and reducing baseline drift. The CH340 USB-to-UART interface remains available through test pads, allowing wired debugging when necessary without compromising the sealed or wearable form factor.

Wireless Communication and Layout Optimization: Wireless data transmission relies on the Artemis platform's integrated Bluetooth Low Energy (BLE) transceiver, which provides low-power bidirectional communication with a paired mobile device. The removal of a fixed USB interface improved mechanical robustness and reduced electromagnetic interference near the analog front-end.

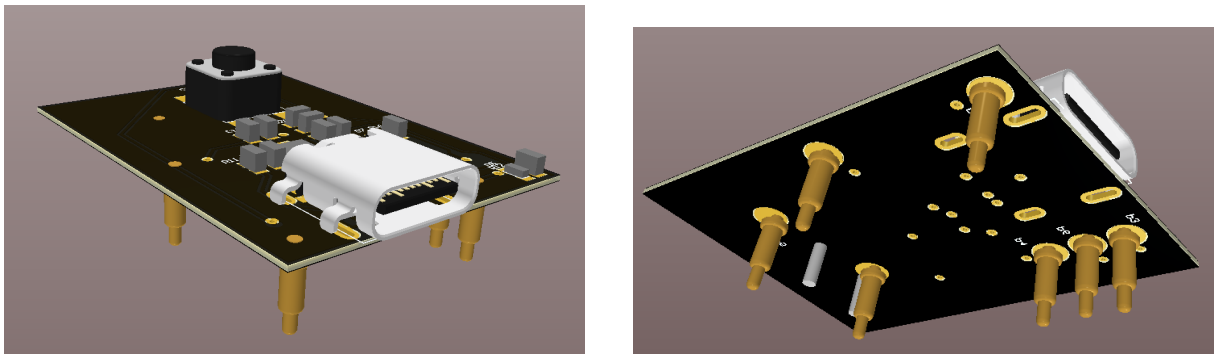


FIGURE 3.40. External pogo-pin programming interface for firmware deployment.

The PCB layout was further refined to maintain uniform ground potential across all analog channels, mitigating offset drift and inter-channel crosstalk. Mechanical considerations were incorporated into the layout to enable integration within rigid-flex or encapsulated wearable formats, ensuring both electrical stability and physical durability. Over-the-air (OTA) firmware updating was experimentally verified at the bootloader level but not deployed in the final firmware due to incomplete BLE library support for the Artemis platform, which limited the reliability of large binary transfers.

3.5.4. Firmware, Software, and Mobile Application

The MultiPot software ecosystem, illustrated in Fig. 3.41, comprises three main layers: the embedded firmware running on the Artemis microcontroller, the backend infrastructure (PHP and MySQL), and a cross-platform mobile application developed in *React Native*. Together, these layers form an integrated pipeline for configuration, data acquisition, wireless transmission, and visualization of multi-analyte electrochemical data.

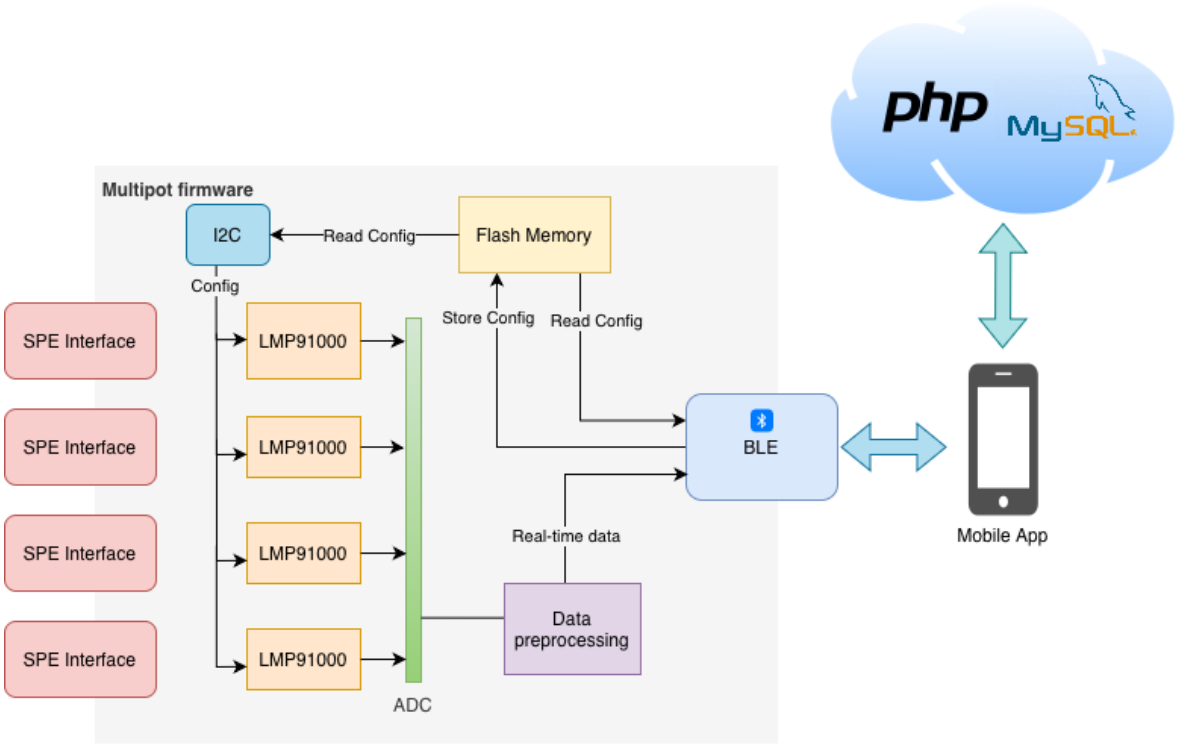


FIGURE 3.41. Firmware and software integration block diagram. The system architecture links the MultiPot hardware with a PHP–MySQL backend and a React Native mobile application. Configuration parameters for each potentiostat are stored on the server and transmitted via BLE to the MultiPot device. The device executes configuration commands, performs signal acquisition, and streams pre-processed data to the app for visualization and storage.

Firmware Architecture: The embedded firmware, developed in the Arduino environment using the ArduinoBLE library, orchestrates the operation of the MultiPot platform and manages the four LMP91000 potentiostat front-ends. Figure 3.42 illustrates the overall firmware execution flow, from system initialization to real-time data acquisition, communication, and configuration management.

Upon power-up or reset, the firmware starts Bluetooth Low Energy (BLE) advertising and checks for the presence of a previously stored configuration in flash memory. If a valid configuration is available, it is loaded to restore the last operating state, ensuring

continuity after power loss. Otherwise, the system waits for a BLE connection and incoming configuration commands from the mobile application. Once a device is connected, new configuration parameters can be received, applied, and persistently stored in flash memory for subsequent operation cycles.

After configuration, the system enters the measurement phase, where the four LMP91000 potentiostat front-ends are addressed sequentially through the I^2C bus using GPIO-controlled enable lines to prevent address conflicts. For each channel, the firmware configures the corresponding potentiostat, acquires electrochemical signals through the analog-to-digital converter (ADC), and stores the samples in an internal buffer. A lightweight pre-processing stage, including digital filtering and baseline correction, is applied to reduce noise and improve signal quality.

As shown in Fig. 3.42, buffered data are transmitted in real-time to the mobile application via BLE whenever a connection is active. The firmware continuously monitors the communication state, allowing measurement to proceed independently of connectivity while ensuring timely data transmission when possible. This architecture supports runtime reconfiguration, persistent storage of operating parameters, and robust multi-channel electrochemical acquisition suitable for portable and wearable applications.

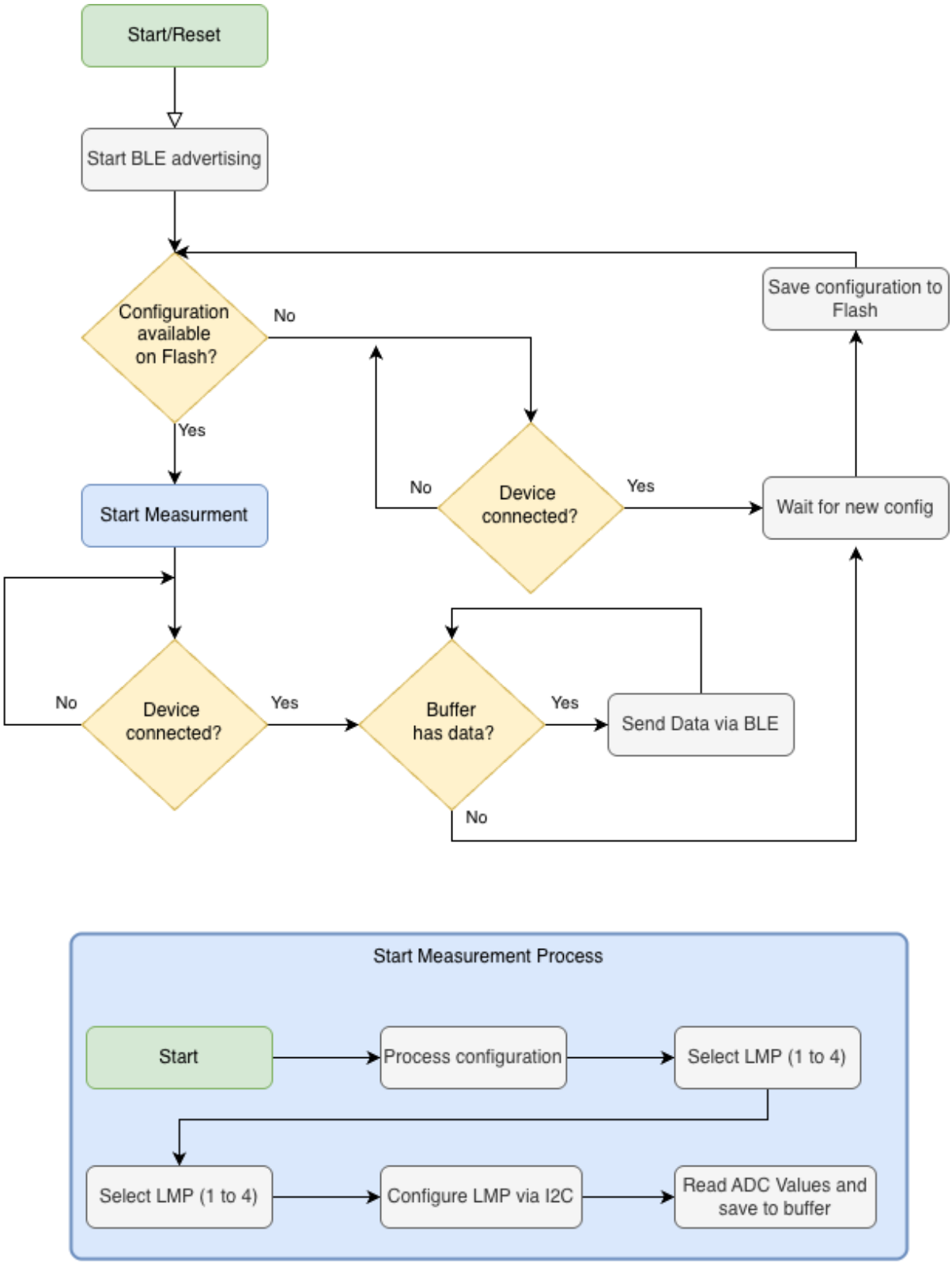


FIGURE 3.42. Firmware flowchart of the MultiPot platform, illustrating system initialization, configuration loading from flash memory, BLE connection management, sequential configuration and sampling of the LMP91000 potentiostat front-ends, buffered data transmission via BLE, and runtime configuration updates with persistent storage.

Backend API and Database: The backend layer, implemented in PHP with a MySQL relational database, stores user profiles, device configurations, and measurement datasets. The RESTful API exposes endpoints for data retrieval and potentiostat configuration management. Each MultiPot device can be individually registered, enabling user-specific calibration curves and measurement profiles. This architecture supports both local and remote data synchronization, allowing continuous monitoring and post-processing through external analytical tools.

Mobile Application Architecture: The user-facing component is a cross-platform mobile application developed in *React Native*, designed to manage user authentication, device configuration, real-time visualization, and data management. The application communicates with the MultiPot device via Bluetooth Low Energy (BLE) and interfaces with the backend PHP–MySQL server through RESTful HTTPS endpoints, enabling synchronized operation between hardware and cloud-based data storage.

The overall workflow of the mobile interface follows the user journey from authentication to data visualization, as illustrated in Figs. 3.43–3.46.

User Authentication and Registration: The initial interface (Fig. 3.43) includes two entry points: Fig. 3.43(a) shows the login screen, where users authenticate using their email and password credentials. Fig. 3.43(b) presents the registration page, which allows the creation of new user accounts before accessing the main dashboard. Both interfaces are linked to the backend through secure API calls that validate credentials and synchronize user profiles.

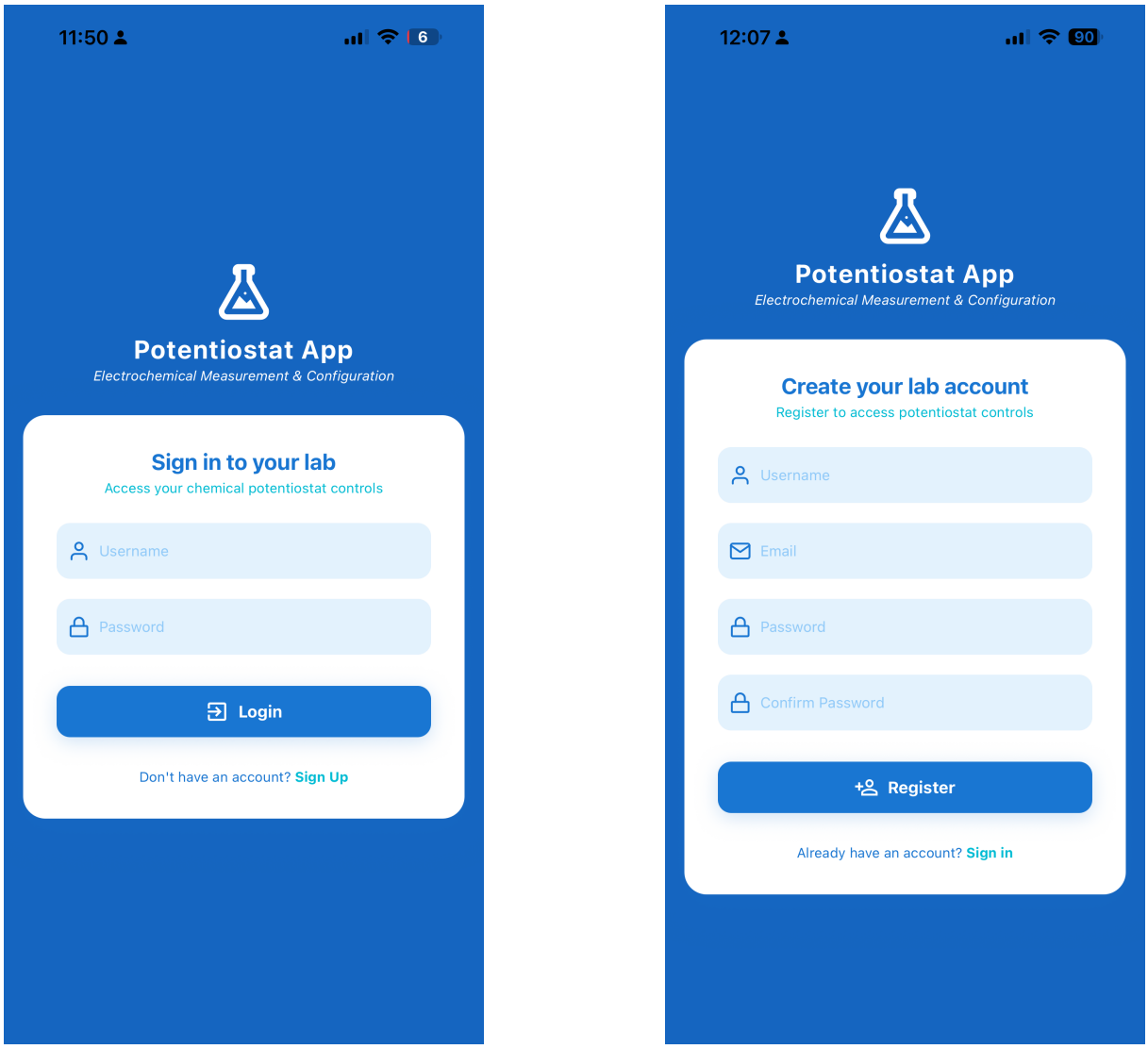


FIGURE 3.43. User authentication workflow of the MultiPot mobile application, including (a) login and (b) registration screens.

Device Selection and Configuration: Following authentication, users proceed to device setup and configuration. As shown in Fig. 3.44(a), the configuration interface enables per-channel adjustment of potentiostat parameters such as bias voltage, transimpedance gain, and sampling rate. The device selection screen, depicted in Fig. 3.44(b), allows users to connect to available MultiPot devices via BLE, displaying device identifiers and connection status.

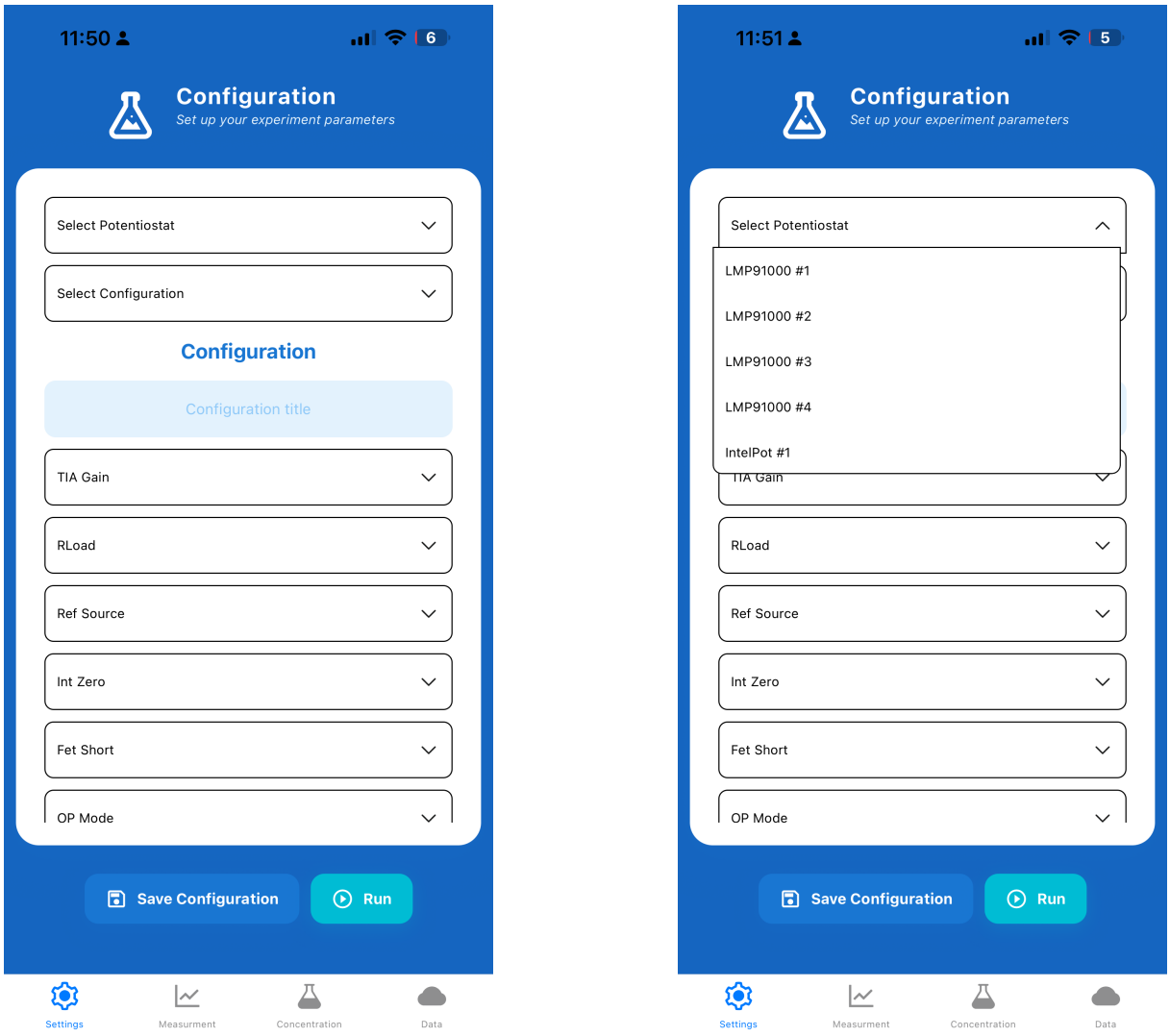


FIGURE 3.44. Device configuration workflow showing (a) channel setup options and (b) MultiPot selection for BLE communication.

Real-Time Visualization and Multi-Channel Monitoring: Once configuration is complete and the device connection established, the user can monitor electrochemical signals in real-time. Fig. 3.45(a) shows the potentiostat channel selector, which allows the user to specify which of the four channels should be actively plotted. Fig. 3.45(b) illustrates simultaneous data visualization for two selected channels, demonstrating the multi-analyte sensing capability of the system. The real-time chart updates dynamically as new data packets are received from the device through BLE, ensuring immediate feedback during experiments.



FIGURE 3.45. MultiPot real-time data monitoring. Panel (a) allows channel selection, and panel (b) demonstrates multi-analyte data visualization.

Concentration Calculation and Data Management: Beyond live monitoring, the mobile application supports the conversion of raw electrochemical readings into biochemical concentration values and offers database visualization tools (Fig. 3.46). Fig. 3.46(a) shows the concentration calculation interface, where calibration equations—defined for specific sensors and analytes—are applied to convert measured currents into concentration values. Fig. 3.46(b) presents the database view, which lists stored measurements and enables users to retrieve or export historical data for offline analysis. This dual functionality expands the usability of MultiPot for both laboratory and field-based studies.

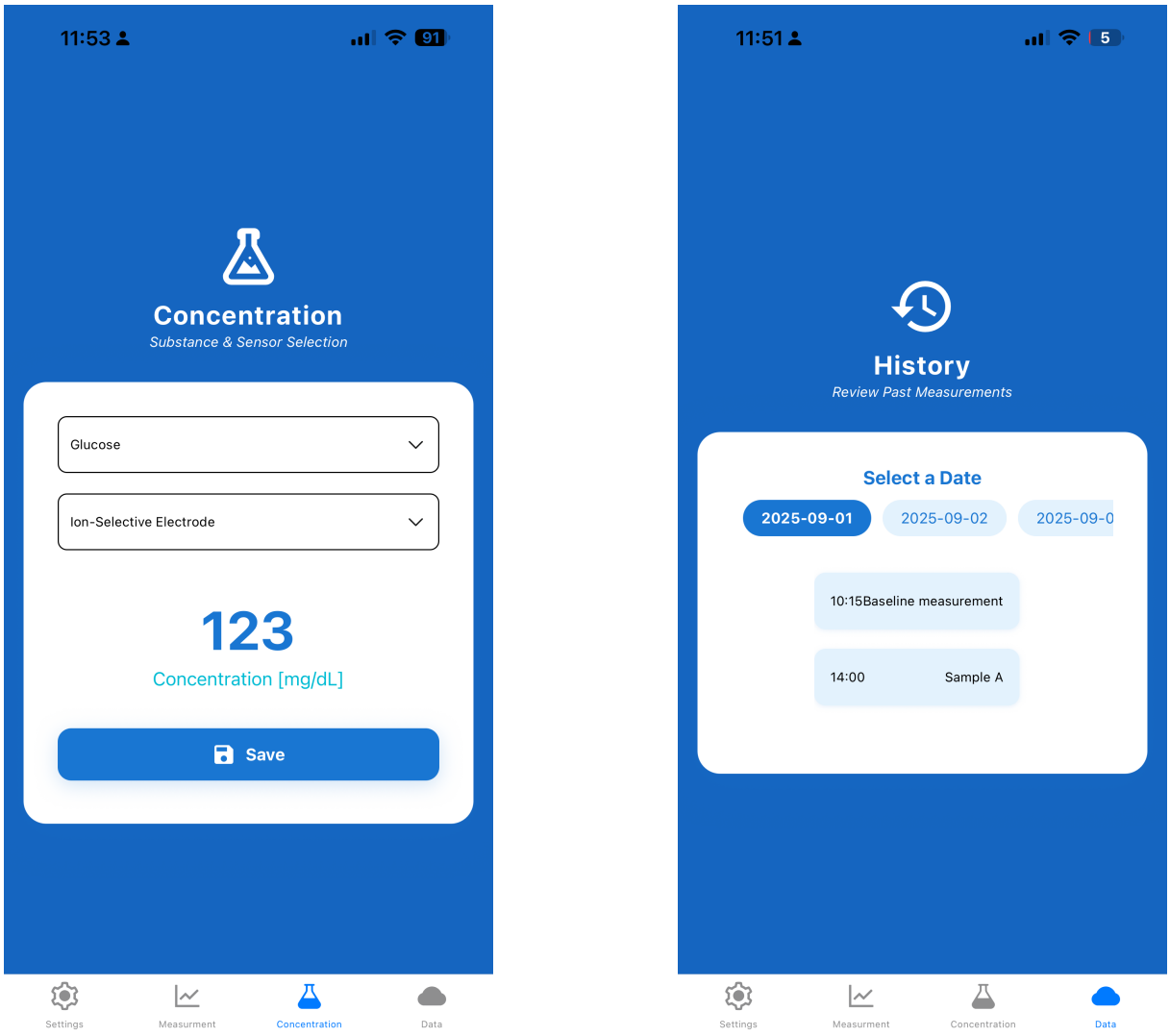


FIGURE 3.46. Post-processing and data management features of the MultiPot mobile application: (a) concentration estimation and (b) historical data retrieval.

All software layers were evaluated for communication stability and synchronization accuracy. BLE performance was validated up to a continuous data rate of 40 Hz per channel without observable packet loss. Flash memory ensures that device configuration persists between sessions, and the PHP–MySQL backend manages user profiles, calibration coefficients, and historical datasets. Together, these components form a cohesive and scalable software ecosystem that enables real-time, multi-channel electrochemical monitoring with user-friendly data visualization and management capabilities.

3.5.5. Complete System Assembly and Integration

After PCB fabrication, all surface-mount components were assembled and tested to produce the final integrated MultiPot system, illustrated in Figs. 3.47–3.49. The assembly

phase focused on achieving mechanical compactness, electrical reliability, and modular connectivity between the main sensing board and the external programming module.

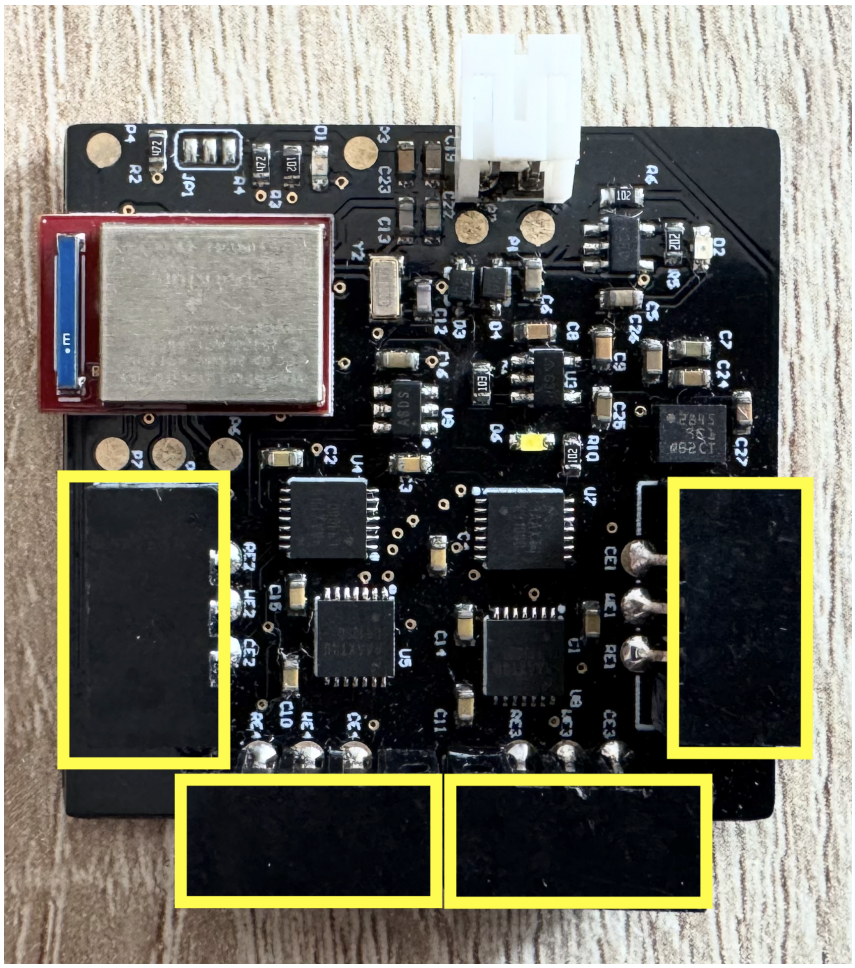


FIGURE 3.47. Top view of the fully assembled MultiPot hardware, showing the four-channel potentiostat architecture with integrated motion sensor, power management circuitry, BLE antenna layout and SPE connectors highlighted in yellow where the printed electrodes could be connected.

The completed system, shown in Fig. 3.48, integrates the core sensing board with the pogo-pin programming interface for firmware deployment. This connection enables seamless reprogramming and debugging without requiring a permanent connector, preserving the structural integrity of the enclosure. The modular approach facilitates iterative firmware updates and rapid hardware validation while maintaining a minimal footprint for wearable operation.

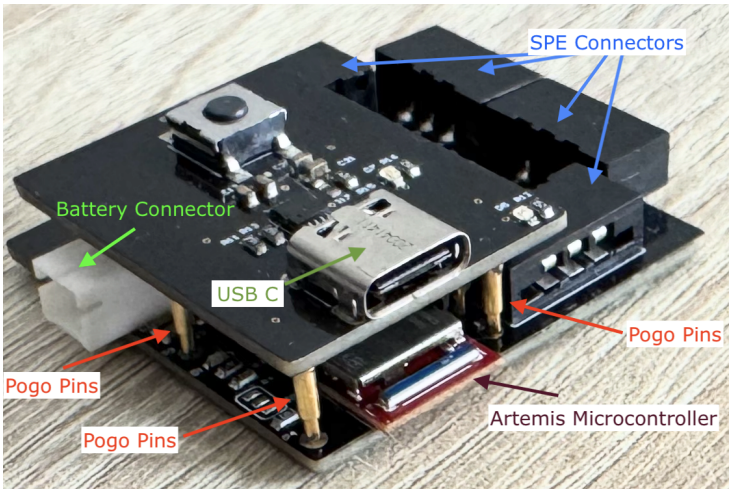


FIGURE 3.48. Perspective view of the assembled MultiPot system interfaced with the external pogo-pin programmer for in-circuit firmware flashing and debugging.

A standalone view of the external programmer module is presented in Fig. 3.49. The programmer features spring-loaded pogo contacts, USB-to-UART conversion, and voltage level translation, ensuring reliable communication with the Artemis microcontroller during firmware upload. Once programming is completed, the module can be detached, leaving the sensing unit fully autonomous for battery-powered operation.

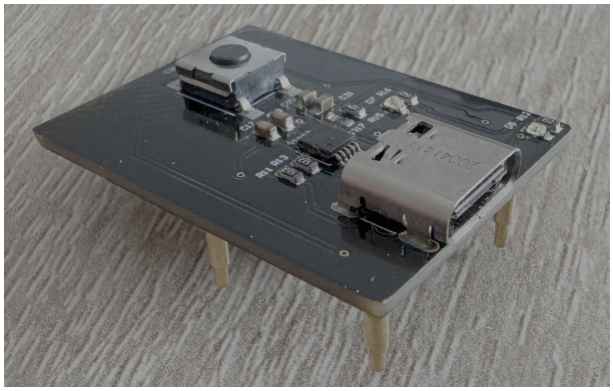


FIGURE 3.49. Standalone external programmer used for firmware flashing of the Artemis microcontroller. The design employs spring-loaded pogo contacts for rapid, connector-free interfacing with the main board.

The final assembly demonstrates a balance between compactness, serviceability, and modular scalability. The combination of low-profile components, efficient power routing, and detachable programming hardware results in a portable and mechanically robust biosensing platform suitable for both laboratory testing and wearable electrochemical monitoring scenarios.

3.5.6. Experimental Validation

To evaluate the performance of the MultiPot system, a series of controlled experiments were conducted to assess its accuracy, cross-talk, and power efficiency. The setup included:

- **MultiPot device:** four-channel prototype with Artemis MCU and LMP91000 chips.
- **Reference device:** Dropsens µStat400 potentiostat.
- **Dummy cell:** RC network composed of a 10 kΩ resistor and a 22 nF capacitor, used to emulate the electrical impedance of an electrochemical cell.

  Dummy cells are widely employed in the validation and functional testing of potentiostat systems prior to experiments with real electrochemical sensors or biological samples. Their primary purpose is to provide a stable, reproducible, and well-characterized electrical load that mimics the equivalent circuit of an electrochemical interface, typically represented by resistive and capacitive elements associated with solution resistance and double-layer capacitance.

  The use of an RC-based dummy cell allows verification of key potentiostat functionalities, including correct biasing of the working electrode, stability of the control loop, accuracy of current-to-voltage conversion, and dynamic response during transient measurements such as cyclic voltammetry or step-based excitation. Unlike real electrochemical cells, dummy cells are not affected by electrode degradation, surface chemistry variations, or environmental conditions, making them particularly suitable for debugging, calibration, and comparative validation against reference instrumentation.

  The selected RC values (10 kΩ and 22 nF) were chosen to provide a well-defined and reproducible electrical load, ensuring a measurable dynamic response within the operational bandwidth of the LMP91000-based potentiostat. Such RC configurations are commonly reported in the literature and in application notes for the functional validation of potentiostats and electrochemical front-ends, particularly during initial testing and calibration phases of portable and wearable sensing platforms [**174, 177**].

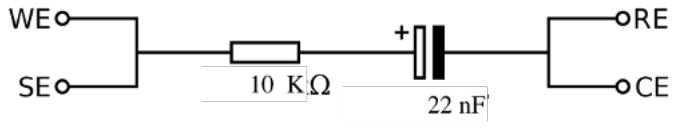


FIGURE 3.50. DummyCell.

- **Measurement software:** Dropview for reference data, MultiPot mobile app for BLE acquisition.

A cyclic voltammetry (CV) sweep from 0 V to 0.6 V was applied to compare the current–voltage characteristics obtained with both instruments. Since the sampling frequencies of the two systems were not identical, data alignment was performed using a nearest-neighbor matching method to ensure point-by-point comparability. The quantitative evaluation of agreement between the reference instrument and the developed device was carried out using two complementary error metrics: the root mean square (RMS) error and the normalized root mean square error (NRMSE).

The RMS error measures the absolute deviation between the current values recorded by both systems and is defined as

$$\mathrm{RMS} = \sqrt{\frac{1}{n}\sum_{i=1}^{n}\left(I_{\mathrm{ref},i} - I_{\mathrm{MultiPot},i}\right)^2}, \tag{3.2}$$

where $I_{\mathrm{ref},i}$ and $I_{\mathrm{MultiPot},i}$ represent the current readings of the reference system and the tested device, respectively, and n denotes the total number of aligned samples. A lower RMS value indicates a closer match between the two current profiles.

To complement this metric, the normalized root mean square error (NRMSE) expresses the deviation as a proportion of the dynamic range of the reference signal, enabling direct comparison across different measurement scales. It is defined as

$$\mathrm{NRMSE} = \frac{\sqrt{\frac{1}{n}\sum_{i=1}^{n}\left(I_{\mathrm{ref},i} - I_{\mathrm{MultiPot},i}\right)^2}}{\max(I_{\mathrm{ref}}) - \min(I_{\mathrm{ref}})}. \tag{3.3}$$

Lower NRMSE values correspond to higher agreement relative to the signal amplitude. The calculated performance metrics obtained from these comparisons are summarized in Table 3.8.

TABLE 3.8. Experimental Results of MultiPot Compared to Reference Potentiostat

Metric	**Result**
RMS Error vs Reference	83.05 %
NRMSE	45.13 %
R^2 (Coefficient of Determination)	-0.5993
Power Consumption	41.2 mW
Channel Crosstalk	0.42 %

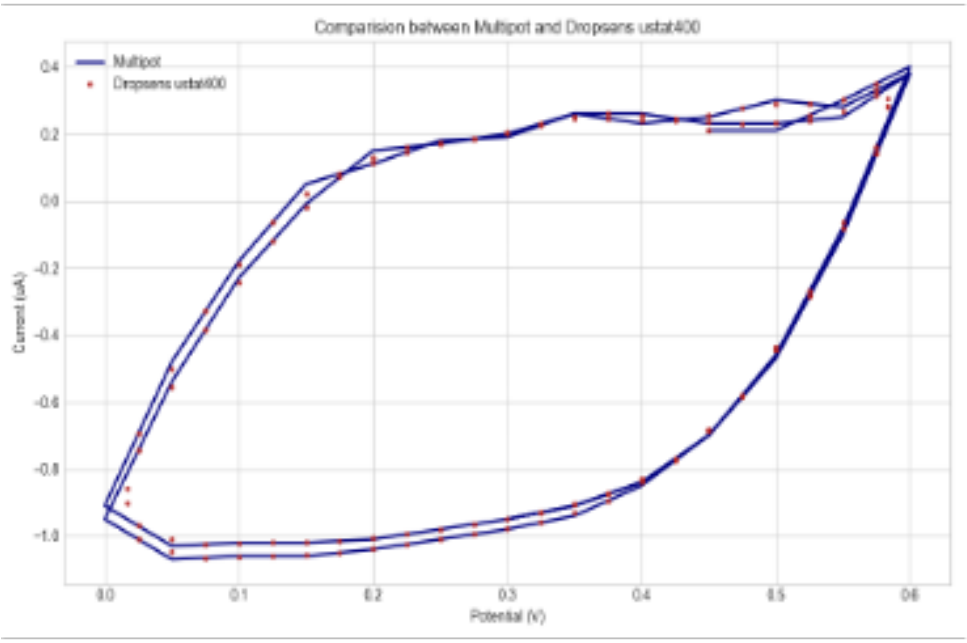


FIGURE 3.51. Comparison between MultiPot and reference potentiostat output for CV sweep using dummy cell.

Although numerical metrics indicate a systematic deviation between devices, visual inspection of the CV curves confirms similar waveform shape and amplitude. The high RMS and NRMSE values primarily result from small offset drifts and clock synchronization differences, not from random noise. Crosstalk measured below 0.5%, validating the isolation of independent channels.

The total power consumption of 41.2 mW corresponds to approximately 45 hours of continuous operation on a 500 mAh battery—suitable for wearable sensing applications.

3.5.7. Multipot Strengths and Limitations

The MultiPot system demonstrates stable and reliable multi-channel electrochemical sensing with high signal fidelity and minimal inter-channel interference. The four-channel architecture enables true parallel acquisition, ensuring consistent performance across simultaneous analyte measurements. The integrated hardware–software framework, combining on-board preprocessing, BLE communication, and mobile data visualization, establishes a comprehensive and scalable platform for real-time biosensing applications.

Measured crosstalk remained below 0.5%, confirming the electrical isolation of the analog front-ends. Power efficiency of approximately 41.2 mW allows more than 40 hours of continuous operation from a standard 500 mAh cell, validating the suitability of the system for portable and wearable scenarios. These results demonstrate that MultiPot successfully bridges the gap between benchtop-grade precision and embedded, low-power sensing.

Some design constraints persist, particularly the inherent limitation of the LMP91000 front-end, which does not natively support open-circuit potential (OCP) measurement modes. This restricts certain electrochemical methods such as impedance spectroscopy and OCP tracking. Nevertheless, the modular signal-conditioning design readily accommodates the integration of complementary amplifiers or analog front-ends to expand measurement capabilities without altering the existing digital or communication architecture.

Ongoing developments will emphasize:

- Enabling secure over-the-air (OTA) firmware updates to facilitate remote software maintenance and scalability.
- Implementing advanced calibration and digital phase-alignment algorithms to further reduce systematic drift and enhance quantitative accuracy.
- Extending supported electrochemical techniques to include OCP and impedance-based sensing for broader analytical applicability.

3.6. AIDrated: Integration of AI Algorithms with Biosensing Platforms for Hydration Assessment

3.6.1. Introduction

Electrolytes such as sodium and potassium are indispensable to maintaining physiological homeostasis, directly influencing fluid balance, nerve impulse transmission, and muscle contraction. In endurance athletes, excessive sweat losses can precipitate significant electrolyte disturbances, leading to hyponatremia, muscle cramps, reduced performance, and, in severe cases, cardiac arrhythmias. The capacity to monitor these biomarkers in real-time is therefore of substantial interest, enabling individualized hydration strategies that mitigate physiological stress and optimize endurance capacity.

The AIDrated platform advances this field by integrating ion-selective electrochemical sensing with embedded edge intelligence, facilitating continuous, non-invasive monitoring of sodium and potassium levels. Through dedicated potentiometric circuits and machine learning–based interpretation, the system transcends conventional hydration monitoring approaches, offering a multimodal framework that captures the interplay between electrolyte dynamics and cardiovascular regulation.

A key innovation lies in the implementation of real-time analytics directly on a standalone Apple Watch application, leveraging on-device neural processing to eliminate reliance on external computing infrastructure or cloud connectivity. This architecture is particularly suited to ultra-endurance events and field conditions where connectivity may be intermittent or absent. The platform synthesizes ion concentration trends with heart rate (HR) and heart rate variability (HRV) to generate personalized hydration assessments and timely dehydration warnings.

This chapter details the hardware design, signal acquisition strategies, firmware architecture, and AI integration underpinning this wearable system, collectively advancing the state of the art in physiological monitoring for sports science and personalized health.

3.6.2. Materials and Methods

3.7. System Architecture

The AIDrated platform was conceived as a comprehensive wearable system for real-time hydration assessment, integrating multimodal physiological sensing with embedded machine learning for on-device inference. Figure 3.52 illustrates the high-level architecture, comprising electrochemical sensing modules, an ultra-low-power microcontroller,

wireless communication interfaces, and external physiological data streams acquired via the Apple Watch Ultra.

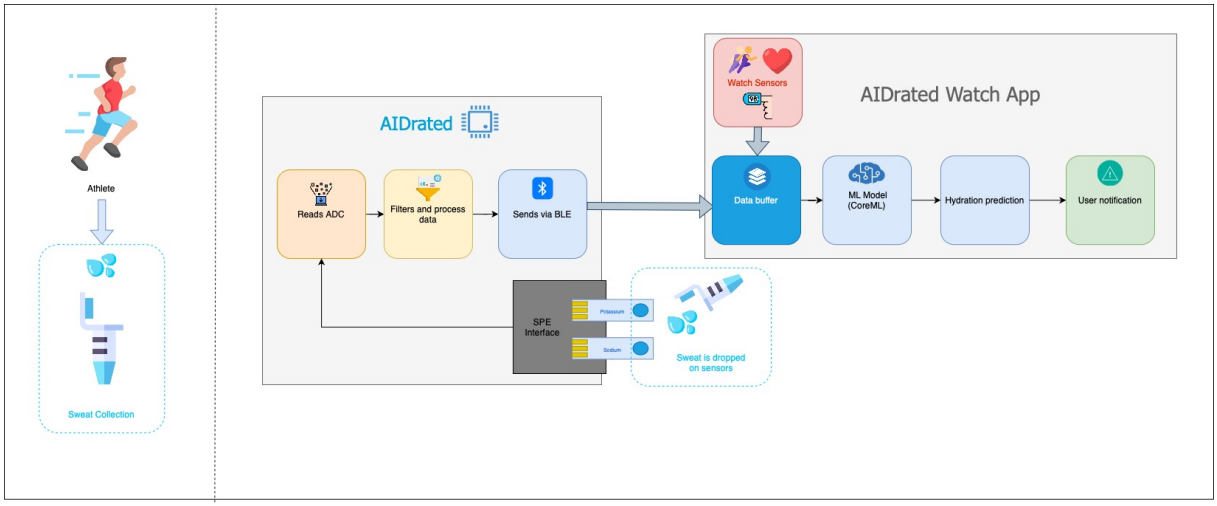


FIGURE 3.52. Block diagram of the AIDrated system architecture, highlighting the integration of electrochemical sensing, physiological monitoring, and embedded AI processing.

3.7.1. Embedded System and Sensor Interface

At the core of the hardware implementation is the Artemis microcontroller, selected for its combination of ultra-low-power consumption, integrated BLE 5.0 communication, and compatibility with rapid prototyping environments (Arduino and Ambiq SDKs). This facilitates both energy-efficient wearable operation and streamlined development of embedded inference pipelines.

The electrochemical sensing subsystem employs ion-selective electrodes (ISEs) tailored for sodium and potassium detection in sweat. Each sensor interfaces with a dedicated MAX4461 instrumentation amplifier, optimized for high-impedance potentiometric measurements. This Open Circuit Potential (OCP) configuration allows precise tracking of voltage shifts proportional to ionic activity, without imposing current draw that could perturb the electrochemical equilibrium.

The amplified signals are digitized via the Artemis ADC and timestamped, forming synchronized data streams with cardiovascular and thermal parameters acquired from the Apple Watch Ultra—namely HR and HRV. This multimodal dataset serves as the foundation for the machine learning models, enabling nuanced interpretation of hydration status that accounts for the complex interplay of electrolyte balance, autonomic regulation, and thermoregulatory responses.

The complete architecture thus supports seamless real-time acquisition, preprocessing, and wireless transmission, facilitating decentralized hydration analytics directly on edge devices. This closed-loop integration exemplifies a new paradigm in wearable biosensing: fusing electrochemical measurements with physiological telemetry and AI-based personalization in a compact, field-ready system.

3.7.2. Apple Watch Ultra and AI-Based Analysis

The Apple Watch Ultra acts as the BLE central device and computational hub of the system. A custom watchOS application initiates measurements, establishes a BLE connection with the AIDrated board, and continuously receives sensor data (sodium and potassium signals).

Simultaneously, the Apple Watch collects complementary physiological data from its built-in sensors:

- **Heart rate (HR)** – via optical/electrical sensors
- **Heart rate variability (HRV)** – derived from inter-beat intervals
- **Physical activity level** – using IMU-based motion tracking

An embedded machine learning model is deployed on the watch, leveraging its dual-core S8 SiP and on-chip Neural Engine for real-time inference. This model combines data from the electrochemical sensors (sweat sodium and potassium) with physiological data (HR, and activity) to estimate the individual's hydration requirements.

The model was trained offline and deployed in CoreML format, enabling low-latency, on-device decision-making without the need for internet connectivity. Based on its prediction, the watch app can issue hydration alerts or recommend fluid intake, personalized to the user's physiological state and activity level.

3.7.3. System Integration Summary

The AIDrated system architecture offers a seamless integration of low-power wearable sensing with edge AI computing. By combining sweat electrolyte measurements with cardiovascular and thermal data, it enables a more robust and individualized hydration assessment compared to conventional approaches based on a single parameter. The architecture supports further expansion with additional biosensors or cloud synchronization if needed, but was specifically designed to operate fully autonomously and privately in a standalone wearable configuration.

3.7.4. Hardware Implementation

The AIDrated platform was engineered as a compact single-board system that seamlessly integrates power management, processing, and electrochemical sensing into a unified design. This approach enhances mechanical robustness, simplifies assembly, and ensures future compatibility with ergonomic enclosures for wearable deployment.

3.7.4.1. *Board Architecture.*

Power Management: The board includes a dedicated power management section, featuring a 3.3 V low-dropout (LDO) regulator to guarantee stable power delivery to all components. An MCP73831 IC handles safe charging of a 3.7 V Li-Po cell, supporting USB or battery operation with automatic power source switching. This architecture enables energy-efficient operation critical for long-term wearable health monitoring.

Processing Unit: Processing is performed by the Artemis microcontroller module (SparkFun), built on the Ambiq Apollo3 Blue SoC. This ultra-low-power system combines a 32-bit ARM Cortex-M4F processor (up to 96 MHz) with integrated BLE 5.0, achieving deep sleep currents under 2 μA and active operation as low as 6 μA/MHz. Table 3.9 compares the Artemis with alternative BLE-enabled microcontrollers evaluated during development.

TABLE 3.9. Comparison of BLE-enabled Microcontrollers for Wearable Applications

MCU	**Core**	**BLE**	**Active Current**	**Deep Sleep Current**
Artemis (Apollo3)	ARM Cortex-M4F @96 MHz	BLE 5.0	6 μA/MHz	<2 μA
nRF52840	ARM Cortex-M4 @64 MHz	BLE 5.0, Thread, ZigBee	20–30 μA/MHz	~1.5 μA
ESP32	Dual-core Tensilica @240 MHz	BLE 4.2 + WiFi	80–100 μA/MHz	~5 μA

The Artemis was chosen for its balance of performance, power efficiency, and BLE integration, as well as its compatibility with the Arduino and Ambiq SDKs, which accelerates embedded ML development.

3.7.4.2. *Electrochemical Sensing Section.*

Amplification and Signal Conditioning : The platform incorporates two MAX4461 instrumentation amplifiers for Open Circuit Potential (OCP) readings, selected after extensive evaluation of precision amplifiers. The MAX4461 offers ultra-low input offset voltages (typically $<150\,\mu$V), low supply current ($<750\,\mu$A), and rail-to-rail outputs, maximizing ADC dynamic range for improved resolution. It operates from a single 3.3 V supply and its compact SOT23-5 footprint supports high-density layouts essential for wearable form factors.

Sensor Interfaces : The board features four custom-designed SPE (Screen-Printed Electrode) mounts, providing reliable connections to disposable biosensors and flexible positioning to optimize sweat sampling during physical activity.

3.7.4.3. ***Biosensors for Electrolyte Monitoring.***

Potassium Biosensor : The ZPS POT-000-00066 sensor uses a three-electrode configuration with a carbon WE, Ag/AgCl RE, and CE on a 24.45 mm × 7.05 mm alumina substrate. Designed for OCP measurements, it enables real-time potassium tracking. It requires storage at 2–8 °C, protected from UV, with an estimated shelf life of one year.

Sodium Biosensor : Similarly, the ZPS SOD-000-00068 sensor is a three-electrode device with dimensions identical to the potassium sensor. It measures sodium via OCP, providing continuous, non-invasive electrolyte assessment. It is stored between 2–15 °C and 20–50% RH to maintain performance.

Both sensors integrate seamlessly into the SPE mounts on the board, as shown in Figure 3.53.

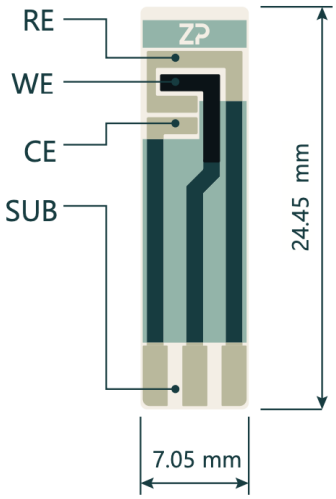


FIGURE 3.53. Screen-Printed Electrodes (SPE) for sodium and potassium detection.

3.7.4.4. ***Edge AI and Physiological Monitoring with Apple Watch Ultra.*** The Apple Watch Ultra serves as the edge AI processing unit and provides advanced physiological sensing. Its S8 SiP features a dual-core processor and dedicated Neural Engine, enabling real-time on-device machine learning inference. Integrated optical and electrical heart sensors offer continuous HR and HRV monitoring. Table 3.10 summarizes these capabilities.

TABLE 3.10. Key Hardware and Sensing Features of the Apple Watch Ultra

Component	**Description**
Processor	Apple S8 SiP (64-bit dual-core CPU)
Neural Engine	On-chip engine for ML inference
Optical HR Sensor	Continuous photoplethysmography
Electrical HR Sensor	ECG-level electrical heart monitoring
HRV Monitoring	Analysis of autonomic responses
Skin Temperature Sensor	Tracks thermoregulation changes
BLE Connectivity	Integrates with external biosensors
Battery Life	Up to 36 hours with optimized tracking

3.7.4.5. ***Circuit Schematics.*** Complete schematics for the power management, microcontroller integration, and electrochemical circuits are provided in Appendix F to support reproducibility and future modifications.

3.7.5. Software

3.7.5.1. ***AIDrated Watch App.*** The Apple Watch Ultra application was developed as a standalone platform to provide real-time hydration monitoring and sensor data visualization without requiring an external smartphone. The interface is designed to provide intuitive feedback to users, ensuring easy access to hydration status and physiological parameters during endurance activities. Figure 3.54 illustrates the primary screens of the application.

The main screen (Figure 3.54a) shows a hydration status indicator represented by a droplet icon that depletes over time based on the loss of sweat electrolytes. This visual representation provides an intuitive way for users to assess their hydration levels in one glance. As sodium and potassium depletion increases, the droplet becomes smaller, serving as a real-time hydration gauge.

The sensor data screen (Figure 3.54b) displays real-time physiological parameters, including sodium (Na^+) and potassium (K^+) concentrations, heart rate (HR), heart rate variability (HRV), and ambient temperature. This screen allows users to track electrolyte trends and correlate hydration status with cardiovascular and thermoregulatory responses. By integrating multiple physiological inputs, the app provides a comprehensive overview of hydration dynamics.

When critical levels of dehydration are detected, the hydration alert screen (Figure 3.54c) issues a notification, warning the user to take immediate action. The notification is based on a ML model running on the Apple Watch, analyzing trends in electrolyte levels and physiological stress markers. The real-time alert system ensures timely intervention, helping athletes avoid performance decline and health risks associated with dehydration.



(A) (B) (C)

FIGURE 3.54. Apple Watch app interface: (a) main screen displaying hydration status, (b) real-time sensor data visualization, and (c) hydration alert notification when fluid intake is required.

This application interface, coupled with the Edge AI processing capabilities of the Apple Watch Ultra, provides an efficient and user-friendly solution for hydration management in endurance sports. The ability to monitor hydration levels, visualize real-time physiological data, and receive proactive alerts ensures optimal performance and safety during prolonged physical exertion.

3.7.5.2. ***Firmware.*** The firmware for the Artemis microcontroller was developed using the Arduino framework and the ArduinoBLE library to enable efficient BLE communication with the Apple Watch Ultra. It is responsible for executing electrochemical OCP measurements using the MAX4461 instrumentation amplifiers, continuously monitoring sodium (Na^+) and potassium (K^+) ion levels from the biosensor. Additionally, the firmware facilitates BLE communication by implementing the GATT protocol, ensuring real-time data transmission to the Apple Watch. Whenever new Na^+ and K^+ values are available, they are instantly sent via BLE notifications, allowing seamless integration with the hydration monitoring system. This BLE-based implementation optimizes system responsiveness by maintaining low-latency communication and enabling real-time physiological tracking.

3.7.6. On-Device AI: Core ML Model for Hydration Prediction

A graph neural network (GNN) is a type of deep learning model specifically designed to process graph-structured data. Unlike traditional neural networks, which operate on fixed-size input vectors, GNNs can model complex relationships between interconnected data points. In the context of hydration prediction, physiological parameters such as heart rate (HR), heart rate variability (HRV), ambient temperature, and sodium and potassium concentrations in sweat may exhibit interdependent or correlated behaviors. By representing these features as nodes on a graph, with edges that capture correlations between them, a GNN can learn meaningful patterns and hydration trends in an unsupervised manner, even without labeled data.

To implement this model, we utilized PyTorch Geometric for efficient graph-based deep learning, leveraging graph-attention networks (GATs) to enhance feature interactions dynamically. The model was trained to detect hydration patterns through contrastive learning and then converted to Core ML using coremltools, ensuring compatibility with Apple Watch Ultra. The converted model allows real-time on-device hydration tracking, enabling personalized insights without requiring cloud-based processing. This integration ensures low-latency predictions while preserving user privacy, making it an efficient solution for wearable AI applications.

3.7.7. Validation Results

The evaluation of the final prototype was conducted in two phases: calibration of the biosensors and real-scenario experiments. The calibration phase established the relationship between the sensor output and known electrolyte concentrations, while the real-scenario experiments validated the system's performance under physiological conditions. These results also provided the dataset to train the AI model.

An assembled circuit board containing the key components of the final biosensing platform was prepared for testing and demonstration purposes. Fig. 3.55 highlights the main elements on the board, identified by colored boxes: the green box marks the SPE connectors along with the sodium and potassium screen printed electrodes (SPE sensors); the red box indicates the lithium battery that supplies power to the system; the yellow box shows the Artemis microcontroller mounted on the Thing Plus board from SparkFun, responsible for data acquisition and wireless communication; and the blue box encloses the MAX4461 dual amplifier chip, which enables simultaneous measurements of open circuit

potential (OCP) on two channels. This arrangement provided a compact and portable platform suitable for both calibration and real-scenario validation experiments.

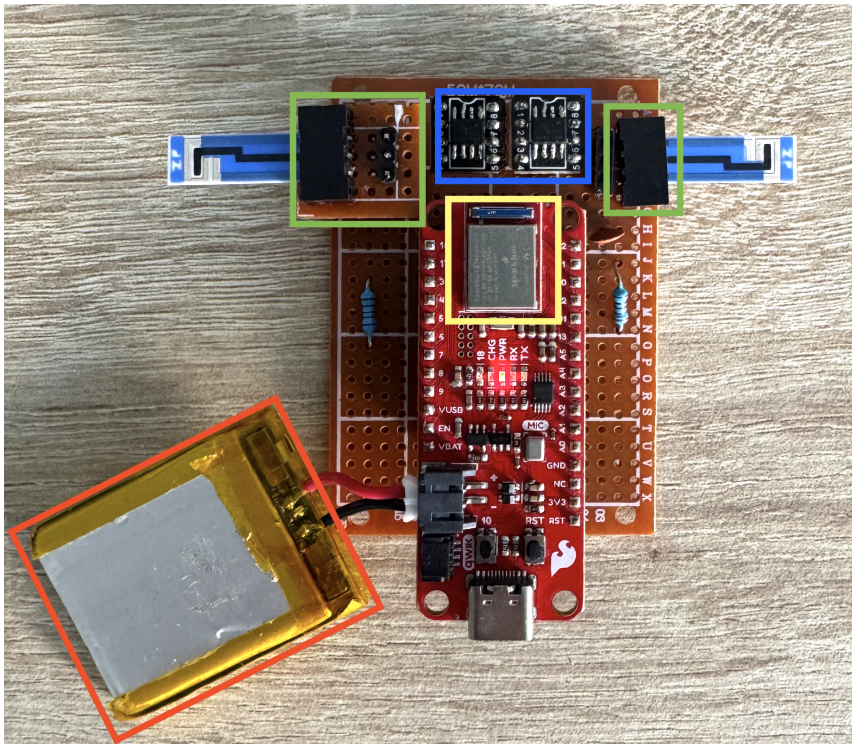


FIGURE 3.55. Assembled biosensing platform highlighting the main components: (green) SPE connectors and Na^+, K^+ sensors; (red) lithium battery; (yellow) Artemis microcontroller on SparkFun Thing Plus; (blue) MAX4461 dual amplifier enabling simultaneous OCP measurements.

3.7.8. Calibration of the Biosensors

The biosensors were calibrated using test solutions with known concentrations of sodium and potassium. For each sensor, a set of standard solutions was prepared as illustrated in Fig. 3.56, and their corresponding analog signal outputs were recorded. The data obtained were then plotted to derive a calibration equation for each sensor, allowing accurate concentration estimation in real-world conditions.

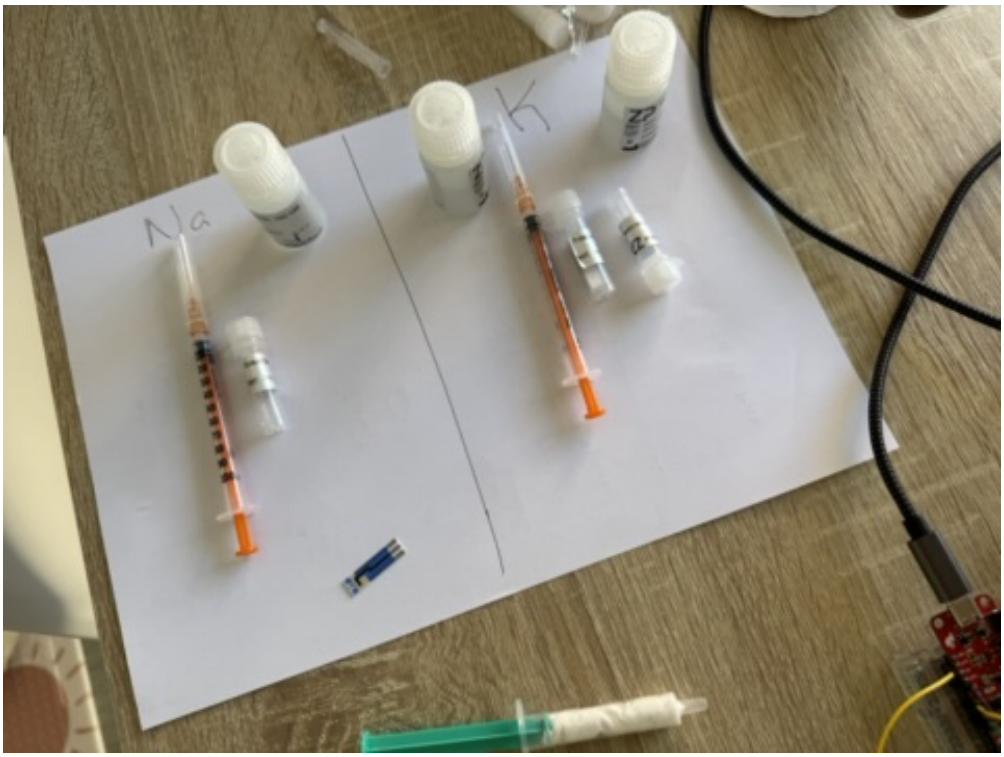


FIGURE 3.56. Sensor calibration procedure.

Sodium sensor calibration was conducted using a series of standard solutions with known concentrations, ranging from 0 mM to 320 mM. This calibration process was essential to establish a relationship between the ADC output and the actual sodium concentration in the sample. The calibration results are presented in Fig. 3.58, where the sensor response follows a characteristic increase trend corresponding to the incremental concentrations of sodium.

The calibration curve demonstrates a direct correlation between ADC values and sodium ion concentration, with higher concentrations producing higher ADC readings. However, a distinctive initial peak is observed at the beginning of each measurement. This peak represents the sensor stabilization phase, during which the electrochemical interface between the ISE and the solution reaches equilibrium. This transient response is expected in electrochemical sensors and indicates that a brief waiting period is necessary before recording a stable concentration value.

To ensure accurate and repeatable measurements, the final sensor readings were taken only after the stabilization phase, eliminating transient fluctuations. The data obtained from this calibration process allowed the derivation of an equation that maps ADC values to sodium concentrations, enabling real-time estimation of electrolyte levels in sweat samples during endurance activities.

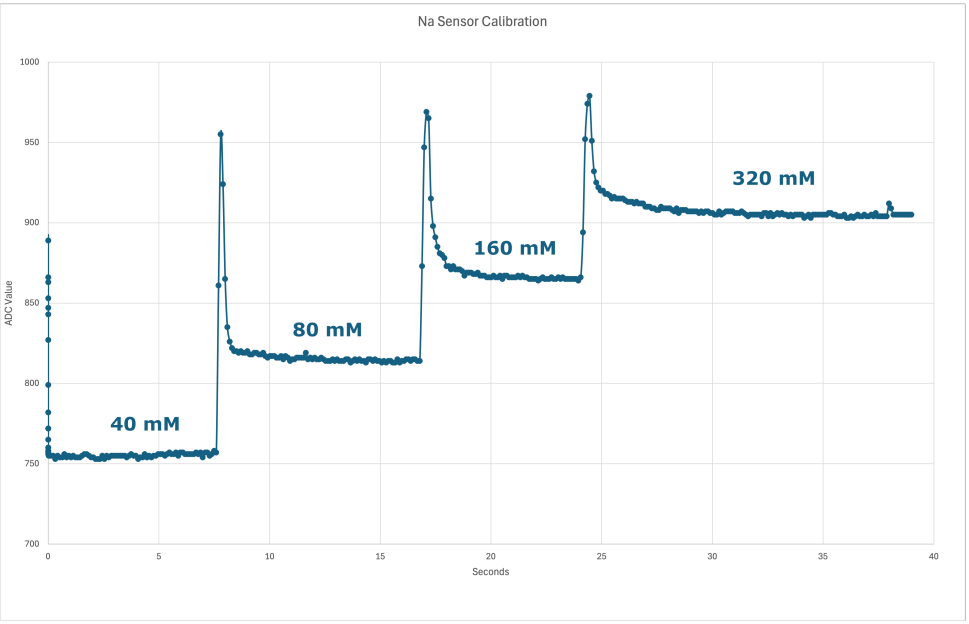


FIGURE 3.57. Measured system response of the sodium sensor during calibration with varying sodium concentrations, where the x-axis represents time (seconds) and the y-axis represents the ADC output value.

The calibration equation derived from the data in Figure 3.58 provides a mathematical model that maps the ADC output to the corresponding sodium concentration. Specifically, the calibration follows an exponential relationship given by

$$y = 0.0013\, e^{0.0136\, x}$$

where y represents the sodium concentration (in appropriate units, e.g., mmol/L), and x denotes the raw ADC output. This equation is fundamental for real-time monitoring, as it allows the system to interpolate intermediate values and estimate sodium levels dynamically. By applying this calibration function, the biosensing platform can accurately quantify sodium concentration in sweat, thereby facilitating electrolyte balance assessment during prolonged physical activity.

Potassium (K^+) sensor calibration followed a similar procedure, with standard concentrations between 0 mM and 8 mM. The results are presented in Figure 3.59. Unlike the sodium sensor, the potassium sensor exhibits a longer stabilization period at the beginning of each measurement, requiring additional time before reliable readings can be obtained. This delay is attributed to the sensor response time, which must be considered when implementing real-time monitoring.

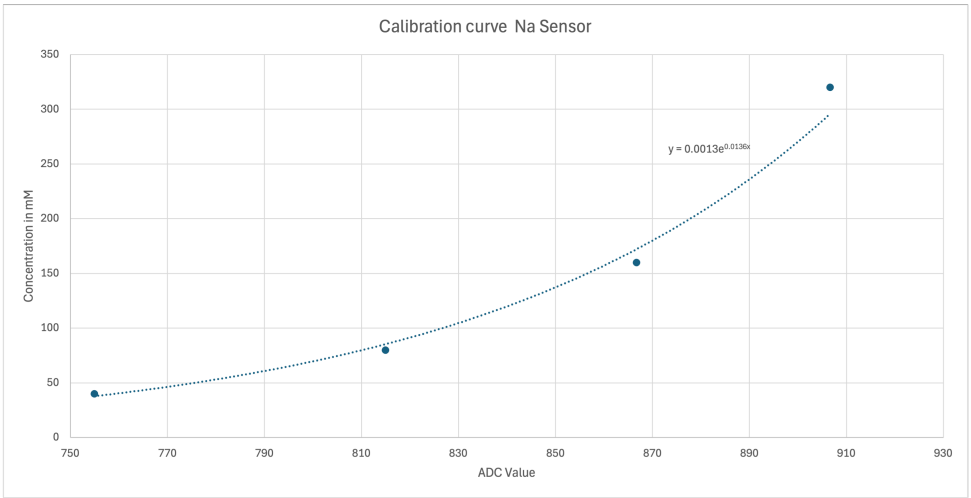


FIGURE 3.58. Inverse characteristic of the ion measurement system when using Na^+ sensor.

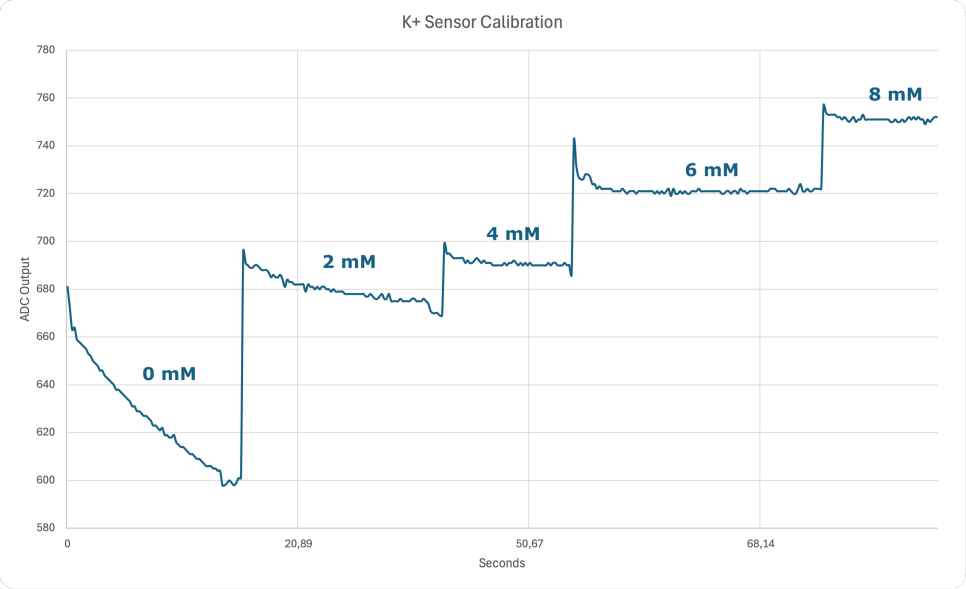


FIGURE 3.59. Measured system response of the potassium sensor during calibration with varying potassium concentrations,where the x-axis represents time (seconds) and the y-axis represents the ADC output value.

The calibration equation extracted from Figure 3.59 establishes the relationship between ADC values and potassium concentration, enabling precise estimation of electrolyte levels in sweat. Specifically, this calibration is represented by the linear equation

$$y = 0.0639\,x - 40.282$$

where y denotes the potassium concentration (e.g., in mmol/L) and x corresponds to the raw ADC output. This calibration function is essential to ensure accurate potassium monitoring, which plays a critical role in muscle function and maintaining overall electrolyte balance during prolonged physical exertion.

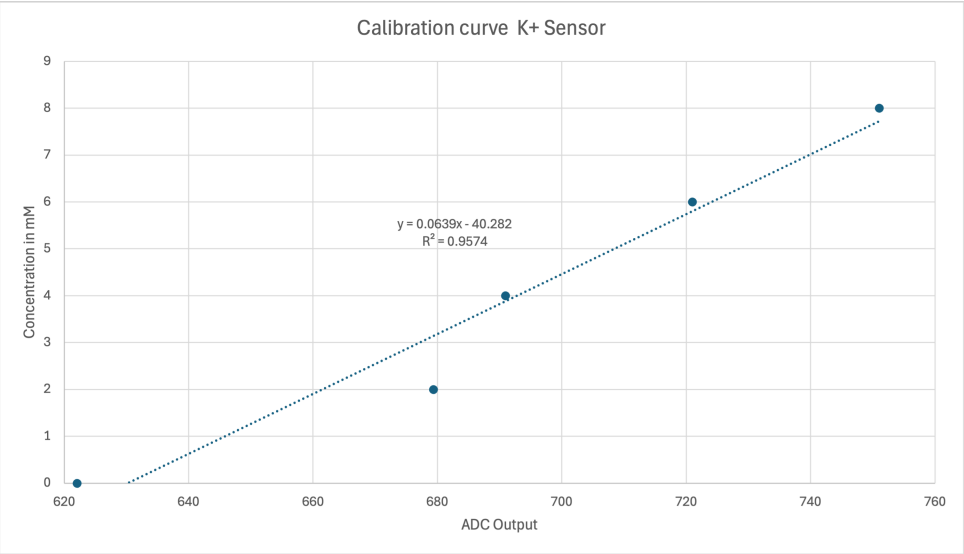


FIGURE 3.60. Inverse characteristic of the ion measurement system when using K^+ sensor.

The derived calibration equations were then integrated into the firmware, allowing real-time estimation of ion concentration based on sensor readings. The obtained calibration coefficients were validated with independent test solutions to ensure measurement accuracy.

3.7.9. Real-Scenario Experiments

To validate the AIDrated platform in real-world conditions, two experimental scenarios were conducted: outdoor running and indoor cycling. The objective was to assess the effectiveness of hydration monitoring and collect data for AI model training.

Sweat was collected using a commercially available sterile absorption pad, approximately 40 mm × 40 mm × 2 mm in size, chosen for its high wicking efficiency, biocompatibility, and convenience of placement on the skin. The pad was applied on the subjects forearm as illustrated in Figure 3.61, and sweat was collected at predefined intervals. A new pad was used for each measurement to ensure sterility and to prevent cross-contamination between sampling points. Prior to use, pads were verified to be free of electrochemically active contaminants through blank potentiostat tests under the same measurement conditions.



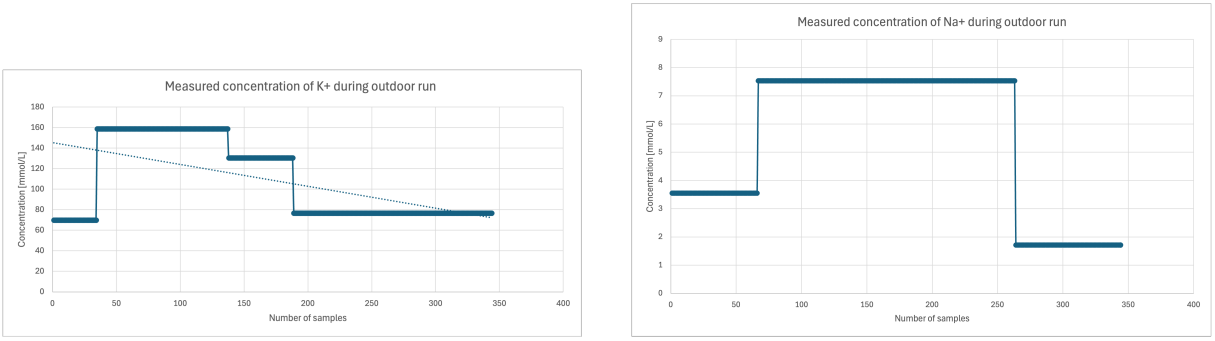
FIGURE 3.61. Placement of the sterile sweat collection pad on the forearm.

In order to obtain a larger sample of each measurement, we compressed the pad with a serynge.

3.7.9.1. ***Outdoor Running Experiment.*** Participants engage in a running session outdoors, while the biosensing platform was used to analyze sweat samples. Sweat was collected using a dedicated pad that was periodically compressed to extract the accumulated sample. At predefined intervals, such as every 15 minutes, the extracted sweat was analyzed using the developed sensor system. The concentration of Sodium and Potassium ions was recorded and plotted over time to observe electrolyte fluctuations during exercise. In addition, physiological parameters, including HR and HRV, were synchronized with biosensing data to provide a complete assessment of hydration status. This integrated approach allowed the creation of a data set that included multiple physiological parameters. This data set serves as a foundation for the development of ML models capable of providing personalized hydration recommendations for endurance athletes.

Figures 3.62a and 3.62b present the measured potassium and sodium concentrations, respectively, throughout the running session. As the athlete did not consume fluids during training, a noticeable decrease in ion concentration is observed toward the end of the session. This reduction suggests a progressive loss of electrolytes, indicating the onset of dehydration.

The observed trend highlights the importance of continuous electrolyte monitoring, as a drop in ion levels serves as a physiological marker of dehydration, signaling the need for fluid replenishment to maintain optimal performance and prevent adverse effects on endurance.

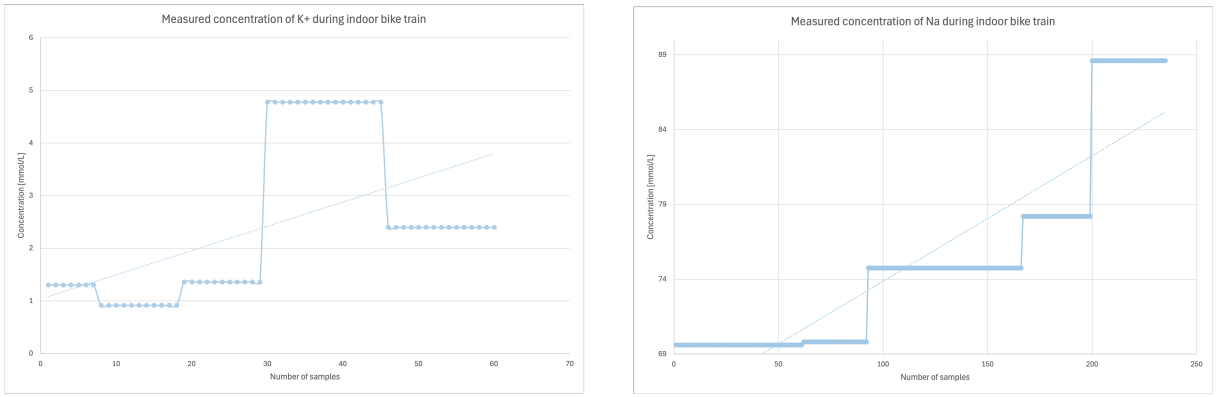


(A) (B)

FIGURE 3.62. Electrolyte concentration variations during an outdoor running session. (a) Potassium concentration and (b) Sodium concentration trends, highlighting electrolyte depletion over time.

3.7.9.2. ***Indoor Cycling Experiment.*** A second experiment was conducted in a controlled indoor environment using a cycling turbo trainer, providing stable and reproducible exercise conditions while allowing precise monitoring of physiological responses. Similarly to the running experiment, sweat was collected periodically and analyzed to assess variations in electrolyte concentration. The indoor setting allowed control over temperature and humidity, isolating environmental effects that could influence sweat rate and composition.

The results obtained from the cycling experiment, presented in Figure 3.63a and Figure 3.63b, reveal distinct trends in potassium and sodium concentrations during endurance exercise. Potassium levels exhibited a significant drop toward the final measurements, similar to the observations in the running experiment. This decline may indicate increased potassium depletion over time due to prolonged muscle activity.



(A) (B)

FIGURE 3.63. (a) Measured potassium concentrations and (b) measured sodium concentrations during endurance cycling exercise.

In contrast, sodium concentrations exhibited a continuous increase throughout the exercise session, suggesting progressive sweat sodium accumulation over time. However, since direct markers of hydration status were not evaluated in this study, no definitive conclusions can be drawn about the participant's systemic state of dehydration. This pattern may also reflect the nature of cycling, which generally involves lower overall intensity compared to running and can result in a distinct sweat composition and electrolyte loss profile. Physiological differences between participants likely contributed as well, given that the runner was female and the cyclist male, potentially influencing sweat rate and electrolyte dynamics.

Environmental conditions during the tests may have further impacted sweat rate and composition. The indoor cycling experiment was performed under controlled temperature and humidity, whereas the outdoor running session was subject to varying environmental factors that could affect thermoregulation and hydration demands. These observations underscore the importance of accounting for exercise modality, ambient conditions, and individual physiological characteristics when interpreting electrolyte loss and hydration-related measurements in endurance activities.

3.7.10. AI Model Training and Data Augmentation

Due to the challenges associated with conducting blood analysis, laboratory facilities and obtaining medical permissions, we opted for an unlabeled dataset, as it would be necessary to perform several blood analyzes in order to obtain valuable information on the hydration level of a subject. Instead of using predefined hydration labels, we collected

real-world physiological data from the AIdrated platform and the Apple Watch Ultra sensors. Sodium and Potassium concentrations in sweat were measured at regular intervals, whereas HR, HRV and ambient temperature were collected in real-time. This was due to the difficulty of adapting the test prototype to be wearable and obtaining good sweat samples.

3.7.10.1. ***Feature Selection for Hydration Monitoring:*** The selection of HR, HRV, Na^+, K^+ and ambient temperature was based on their physiological relevance to hydration status. HR is a crucial parameter as it tends to increase when a person is dehydrated due to a reduction in plasma blood volume, forcing the heart to work harder to maintain circulation. HRV which reflects the regulation of cardiac function by the autonomic nervous system, decreases under dehydration and heat stress, indicating a higher physiological stress [**178**]. The balance of electrolytes, particularly the concentrations of Na^+ and K^+ in sweat, serves as an essential hydration marker. Sodium plays a key role in fluid retention and neuromuscular function, while potassium is critical for muscle contraction and cellular function. As dehydration progresses, imbalances in these electrolytes can lead to loss of performance and health risks such as muscle cramps or more severe conditions such as heat exhaustion [**179**]. Body temperature is another critical factor, as dehydration impairs the body's ability to regulate heat through sweat evaporation, causing an increase in internal temperature. These physiological parameters are not independent; rather, they correlate with each other due to the integrated response of the body to hydration and thermal regulation [**180**]. For example, as the ambient temperature increases, sweat production increases to facilitate cooling, leading to greater loss of Na^+ and K^+, which in turn can influence HR and HRV. A decrease in sodium levels can lead to reduced blood volume, requiring an increase in HR to maintain circulatory function. Similarly, when HRV decreases due to stress induced by dehydration, it reflects increased activation of the sympathetic nervous system, which further influences HR and temperature regulation. Furthermore, as body temperature increases due to inadequate hydration, the cardiovascular system is strained, requiring higher HR to dissipate heat. This thermoregulation response is amplified by the loss of electrolytes, which affects neuromuscular function and overall performance. The strong interdependence of these factors makes it essential to consider them collectively for the assessment of hydration, as each parameter dynamically affects the others in response to environmental and physiological conditions.

An increase in body temperature is an early indicator of thermal stress related to dehydration. In addition, ambient temperature significantly influences hydration needs by affecting sweat rate. Higher external temperatures lead to increased sweat production, causing more fluid and electrolyte loss, while lower temperatures can sometimes mask dehydration symptoms as sweat evaporates more quickly.

3.7.10.2. ***Machine Learning Model Selection:*** Several unsupervised ML algorithms were tested, including K-Means Clustering, DBSCAN (Density-Based Clustering), Gaussian Mixture Models (GMM), Autoencoders, and GNNs. Among these, the GNN-based autoencoder demonstrated the best performance due to its ability to learn latent representations while preserving relationships between physiological parameters.

3.7.10.3. ***Dataset, Preprocessing, and Validation:***

Dataset size: We collected multi-session recordings using the AIDrated platform and Apple Watch Ultra sensors, comprising six sessions from two unique participants, totaling approximately three hours of physiological data. Each record included sweat electrolyte concentrations (Na^+, K^+) measured at regular intervals, and HR, HRV and ambient temperature streamed in real-time. Due to the difficulty of adapting the prototype for continuous wearable sampling and the ethical constraints of obtaining blood-based reference measurements, the available dataset was necessarily limited. To enable model training and proof-of-concept evaluation, additional synthetic samples were generated by augmenting the real data within physiologically plausible ranges derived from literature and prior studies. These augmented data were used exclusively to expand the feature space and stabilize unsupervised learning, not to claim clinical accuracy.

Preprocessing pipeline: Signals were (i) time-aligned and resampled to a common grid; (ii) per-feature normalized using z-score ($\tilde{x} = (x - \mu)/\sigma$) to avoid scale dominance; (iii) lightly smoothed with a short moving window to reduce sensor jitter without distorting trends; (iv) cleaned for outliers via a robust interquartile-range (IQR) rule with winsorization (extremes capped at the 1st/99th percentiles); and (v) gap-filled using a forward–backward fill limited to short gaps to prevent drift. Model inputs were structured as fixed-length overlapping windows to preserve temporal continuity while balancing the number of samples.

Validation protocol: Given the small sample size, the validation strategy focused on avoiding overfitting and subject leakage. A grouped split by participant ($\sim$70% train,

15% validation, 15% test) was used, with entire participants held out in each fold. Hyperparameters were tuned on the validation set with early stopping, and robustness was checked through grouped K-fold cross-validation and multiple random seeds to assess variance in reconstruction error. The objective was not to achieve clinical precision but to demonstrate that the AI model could identify consistent latent relationships among physiological variables even with limited input diversity.

Evaluation metrics: Because hydration states were inferred without ground-truth labels, model performance was assessed through reconstruction-based metrics: Mean Squared Error (MSE), Root Mean Squared Error (RMSE = $\sqrt{\text{MSE}}$), Mean Absolute Error (MAE), and the coefficient of determination R^2. For the best-performing GNN autoencoder, we obtained MSE = 0.02197, MAE = 0.1023, $R^2 = 0.9782$, yielding **RMSE** = 0.148.[1] These values indicate low reconstruction deviation and strong internal consistency, confirming the model's ability to capture meaningful physiological patterns despite limited data (see Table 3.11).

Notes on clustering validity and proof of concept: After encoding, K-means clustering was applied in the latent space to obtain four unsupervised hydration clusters. As true hydration labels were unavailable—since Na^+ and K^+ reference values would require blood analysis and medical authorization—no external validation could be performed. Instead, internal indices such as the silhouette score and visual cluster separation were used to verify structural consistency. The present experiment should therefore be interpreted strictly as a *proof of concept*: it demonstrates the technical feasibility of integrating multi-sensor data and AI-based inference for hydration monitoring, while acknowledging that accurate clinical validation will require medically supervised sampling with approved biochemical reference measurements.

3.7.10.4. ***Graph Neural Network (GNN) Model.*** GNNs were chosen for their effectiveness in modeling structured data such as physiological sensor readings over time [**163**]. Unlike traditional ML models that treat data as independent samples, GNNs leverage the relationships between features, making them particularly suitable for analyzing physiological data where different variables influence each other dynamically. The model architecture consists of graph convolutional layers (GCNConv), which propagate and aggregate information from neighboring nodes in the graph, allowing the network to learn

[1] RMSE computed as $\sqrt{0.02197}$.

meaningful feature representations. These layers help preserve the inherent structure of physiological interactions, such as the correlation between heart rate and electrolyte levels.

The representation of the latent space plays a crucial role in the model, as it captures an abstract and lower-dimensional encoding of the physiological signals. By encoding physiological parameters into this space, the model can generalize patterns that differentiate hydration states without requiring labeled data. The decoder network reconstructs the original signals from the latent embeddings, ensuring that the learned representations retain key physiological characteristics.

To further analyze hydration states, we applied K-means clustering to the learned latent space. This step enables the identification of distinct hydration clusters based on the encoded representations, allowing for meaningful separation into four hydration levels. The effectiveness of this approach lies in the combination of graph-based learning, which retains relationships between features, and clustering, which organizes data into distinct states.

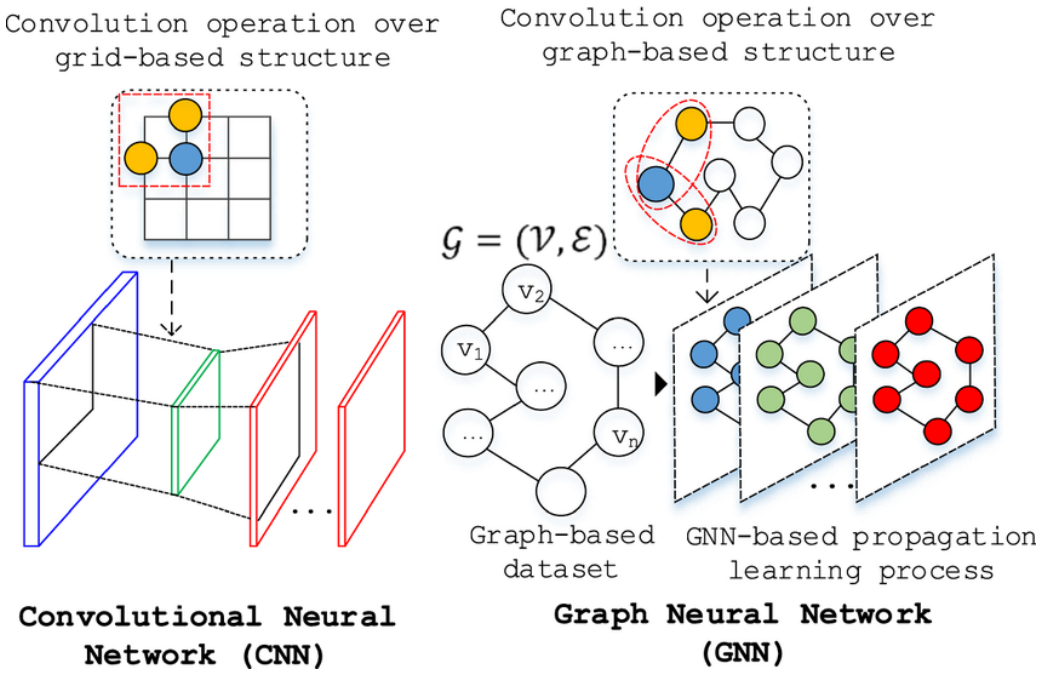


FIGURE 3.64. Comparison between Convolutional Neural Networks (CNN) and GNNs. CNNs apply convolutions over a structured grid, while GNNs generalize this operation to arbitrary graph structures, making them more suitable for physiological data with complex interdependencies [**181**].

3.7.10.5. ***Latent Space Visualization.*** Three-dimensional projection of the latent space representations learned by the Graph Neural Network (GNN) autoencoder are presented in Figure 3.65. In this context, the latent space constitutes a lower-dimensional

abstract feature space in which the original high-dimensional physiological and electrochemical data are embedded.

The GNN encoder transforms complex multimodal inputs comprising heart rate, heart rate variability, ambient temperature, and sweat electrolyte concentrations into latent embeddings that capture the essential underlying relationships and structural dependencies among these variables. Unlike traditional neural networks, GNNs exploit the inherent graph-based topology of physiological data, where nodes represent individual features, and edges model their interdependencies. This enables the encoder to preserve local and global correlations that are physiologically meaningful, such as the interactionon between electrolyte depletion and cardiovascular stress markers.

The resulting latent representations provide salient information about hydration-related physiological states in a compact form. Applying K-means clustering to these embeddings reveals distinct groups within the latent space, as evidenced by the clear separation of four groups in Figure 3.65. This separation suggests that the model has successfully organized the data into discrete patterns or regimes, which may correspond to different hydration states or physiological adaptation levels during endurance exercise.

This clustering within the latent space not only demonstrates the model's ability to extract complex multimodal signals but also highlights its potential for unsupervised categorization of hydration status without requiring explicit ground-truth labels. This capability is particularly advantageous in contexts where invasive reference measurements (e.g., plasma osmolality) are impractical or unavailable.

3.7.10.6. ***Model Evaluation.*** To assess the performance of the model, we used the mean squared error (MSE), the mean absolute error (MAE) and the R squared error (R^2) instead of precision, as this is an unsupervised learning problem where there are no ground truth labels for direct comparison. MSE measures the average squared reconstruction error and should be as low as possible, while MAE represents the absolute reconstruction error, indicating how much the reconstructed values deviate from the original inputs. The square R (R^2) measures how well the model explains the variance in physiological data, with values close to 1 indicating excellent predictive performance. Since clustering is performed unsupervised, traditional accuracy metrics cannot be computed, as there are no predefined hydration categories to validate against. Instead, reconstruction error-based metrics provide insight into how well the model captures a meaningful structure in the data.

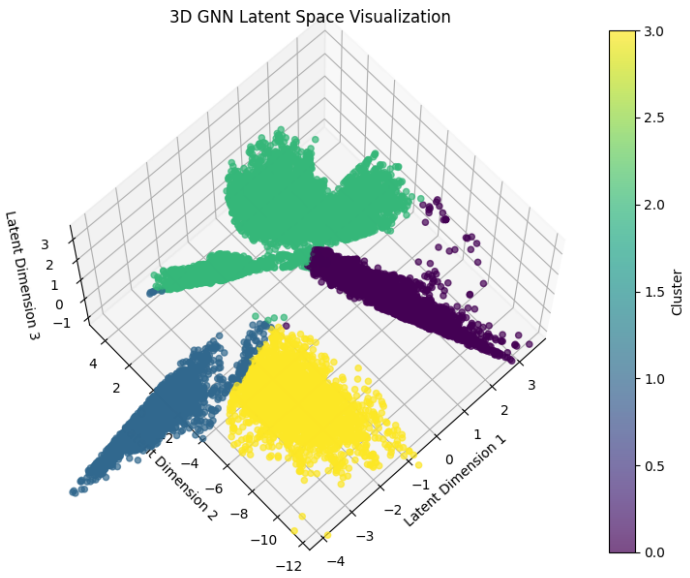


FIGURE 3.65. 3D latent space representation of K-means clustering, highlighting patterns emerging from unsupervised analysis of the data.

The results presented in Table 3.11 indicate that the GNN Autoencoder achieved high accuracy in predicting hydration levels. The low MSE of 0.02197 suggests a minimal deviation between the predicted and actual values, confirming that the model effectively captures the underlying patterns in the data. Similarly, the MAE of 0.1023 indicates that the average prediction deviation remains within an acceptable range for practical applications.

The R^2 score of 0.9782 demonstrates a strong correlation between the predicted and actual hydration levels. An R^2 value close to 1.0 suggests that the model successfully explains most of the variability in hydration status based on the input physiological parameters. These results validate the effectiveness of the GNN Autoencoder in processing real-time biosensing data, reinforcing its potential for hydration monitoring during endurance sports. The model's high predictive performance ensures reliable assessments without requiring constant recalibration, making it suitable for real-world deployment.

Metric	**Value**
Mean Squared Error (MSE)	0.02197
Mean Absolute Error (MAE)	0.1023
R-Squared (R^2)	0.9782

TABLE 3.11. Performance Metrics of the GNN Autoencoder

3.7.10.7. *Conversion to CoreML for Edge Deployment.* The trained model was converted into a CoreML package for deployment on the Apple Watch Ultra [**182**]. The conversion offers several advantages, including on-device inference, eliminating the need for cloud connectivity, low latency for real-time hydration monitoring, and optimized execution on Apple's Neural Engine, which enhances battery efficiency. However, certain challenges arise, such as the fact that graph structures are not natively supported in CoreML. Consequently, edge relationships had to be approximated using a fully connected representation, and computational constraints on embedded devices limit the complexity of the model that can be deployed.

3.7.10.8. *Conclusion and Future Work.* This work demonstrated the feasibility of the AIDrated system as an integrated solution for real-time sweat biomarker monitoring and hydration assessment, combining wearable electrochemical sensing with intelligent data processing. The proposed GNN-based hydration prediction model showed high accuracy in identifying hydration-related patterns from physiological data, enabling effective clustering of hydration states. By deploying the model locally on an Apple Watch Ultra, the system provides personalized hydration insights without requiring continuous internet connectivity, reinforcing its suitability for sports and outdoor use.

Building on these results, future developments will focus on transforming the current prototype into a fully integrated and unobtrusive wearable device. A primary objective is the further miniaturization of the hardware through a redesign based on a rigid-flex PCB architecture. This approach will enable seamless integration of the sensing electronics, power management circuitry, and electrochemical interface directly into a smartwatch band, such as that of the Apple Watch. The flexible PCB section will conform to the curvature of the wrist, while rigid sections will house critical components including the potentiostat IC, BLE transceiver, and battery management circuitry.

To improve sensor–skin interaction and ensure more consistent sampling, future iterations may incorporate screen-printed electrodes (SPEs) or microneedle-based sensors on the inner surface of the band. The Apple Watch will act as the local processing and user-interaction unit, allowing AI inference and data visualization to be offloaded from the sensing band. This design choice enables the wearable module to remain compact and energy-efficient while supporting advanced analytics.

A conceptual illustration of the envisioned smartwatch band integration is shown in Fig. 3.66, highlighting the proposed form factor and placement of the sensing elements.



FIGURE 3.66. AIDrated integrated watch band concept.

Further research will include long-term validation studies involving larger participant cohorts to assess robustness, inter-user variability, and long-term stability of sweat-based measurements. Additionally, future work may explore the adoption of Federated Learning (FL) approaches to enable privacy-preserving and personalized hydration models, allowing each user to benefit from adaptive predictions while keeping sensitive physiological data locally on the device.

Overall, the AIDrated system establishes a solid foundation for continuous, personalized, and non-invasive hydration monitoring, with potential extensions to broader physiological monitoring and real-time fitness and health applications.

CHAPTER 4

Extended Reality applications for physical rehabilitation

This chapter extends the work presented in Chapter 3 by exploring complementary technological strategies aimed at improving health and physical performance. While Chapter 3 focused on the development of wearable biosensing systems for monitoring physiological parameters, this chapter investigates the use of virtual environments to support physical rehabilitation. Together, these approaches contribute to a broader research line centered on the application of artificial intelligence and emerging technologies to healthcare and sports. In particular, the integration of physiological monitoring with immersive virtual environments opens new possibilities for personalized, adaptive rehabilitation protocols guided by AI-driven insights.

4.1. Overview

The integration of advanced technologies, such as virtual environments (VEs), AR, MR, and AI, has significantly transformed the landscape of physical rehabilitation. These innovations enable immersive, interactive, and patient-centered therapeutic approaches, enhancing engagement and improving rehabilitation outcomes. By incorporating wearable sensors and AAL technologies, rehabilitation processes can be tailored to individual needs, ensuring more precise assessments and adaptive therapy.

This chapter presents the research contributions related to the application of VEs, AR, and MR in physical rehabilitation, with a particular focus on AI-driven methodologies and sensor-based monitoring. The work explores how these technologies create intelligent rehabilitation frameworks by integrating real-time physiological and motion data from wearable sensors, facilitating adaptive interventions for improved recovery.

The initial sections will examine the role of AR and MR in rehabilitation environments, highlighting their potential to merge physical and digital interactions, thus improving motor learning and functional recovery. Furthermore, the discussion will explore how AI algorithms use data collected from wearable sensors to personalize therapy sessions, optimize rehabilitation exercises, and predict patient progress.

Finally, this chapter will provide an overview of the impact of AI-assisted VEs in rehabilitation, emphasizing their role in delivering personalized, data-driven therapeutic

interventions. The integration of these technologies paves the way for more effective, engaging, and accessible rehabilitation programs, ultimately improving patient outcomes and promoting advancements in digital healthcare solutions.

4.2. Mixed Reality and Augmented Reality proposed applications for Physical Rehabilitation

Mixed Reality (MR) and Augmented Reality (AR) are rapidly advancing technological domains whose unique capabilities enable innovative and immersive experiences. By seamlessly integrating physical and digital environments, these technologies hold significant promise for physical rehabilitation, offering novel enhancements to traditional therapeutic approaches [**104, 111, 113, 183**].

This section will delve into the practical applications of MR and AR within the realm of physical rehabilitation, providing a comprehensive exploration of various case studies. These will demonstrate how these technologies have been effectively implemented to improve the rehabilitation process, offering a more engaging, interactive, and personalized therapeutic experience. By carefully examining these cases, we can gain a deeper understanding of the transformative impact of MR and AR within the healthcare field, specifically in rehabilitation practices.

Balance is a fundamental aspect of motor control and a critical focus in physiotherapy, particularly for populations recovering from neurological injuries, musculoskeletal impairments, or age-related decline. Effective balance maintenance relies on the integration of sensory inputs from the visual, vestibular, and proprioceptive systems, alongside coordinated neuromuscular responses [**184, 185**].

Traditional balance assessment employs both clinical scales, such as the Berg Balance Scale (BBS) and the Timed Up and Go (TUG) test, and instrumented methods such as force platforms that quantify center of pressure (COP) dynamics [**186**]. While these tools provide valuable quantitative and clinical insights, they are typically performed in controlled clinical settings and may not fully reflect balance performance during daily functional activities. In addition, such assessments often provide limited patient engagement and real-time feedback during rehabilitation.

Integrating Mixed Reality (MR) and Augmented Reality (AR) technologies into balance assessment and training offers the potential to address these limitations. By creating

interactive, immersive environments, MR and AR can simultaneously challenge and evaluate postural control under more functionally relevant conditions, potentially enhancing neuroplastic adaptations and motivation during therapy [**187, 104, 111**].

This section discusses the incorporation of MR and AR into balance-focused rehabilitation, reviews conventional measurement techniques, and highlights anticipated benefits and challenges in clinical applications.

4.3. Physical Rehabilitation in AR Scenario

The developed platform implements a novel approach for categorizing user balance by leveraging data from a smart sensing floor (SensFloor) combined with IMU measurements, processed through neural network models. Based on the user's position and motion, the system attempts to classify balance into three levels. It has the potential to be used in different environments and could be combined with other systems. Thanks to these features, the system is able to track the user's balance and classify it.

The theoretical foundation of this research is based on the integration of AI and AR technologies in the field of gait rehabilitation. This framework is based on the understanding that current methods for gait analysis frequently rely on manual monitoring, which is prone to errors and does not provide comprehensive real-time data. With an AI-driven, non-intrusive method, it is possible to improve monitoring by providing continuous and accurate data collection, resulting in better patient outcomes.

This theoretical framework proposes a sequential process of data collection using smart sensing technology, data analysis and interpretation using AI algorithms, and feedback via an AR system. This novel method allows for real-time monitoring of patients' gait characteristics, which is accessible to both physical therapists and patients.

The primary goal of this framework is to enable the creation of personalized training plans based on accurate, real-time data, which has the potential to significantly improve rehabilitation outcomes. This theoretical perspective serves as the foundation of this research, providing a lens through which to comprehend its goals, methodology, and implications.

In this section, a description of the hardware and software components of the system is presented.

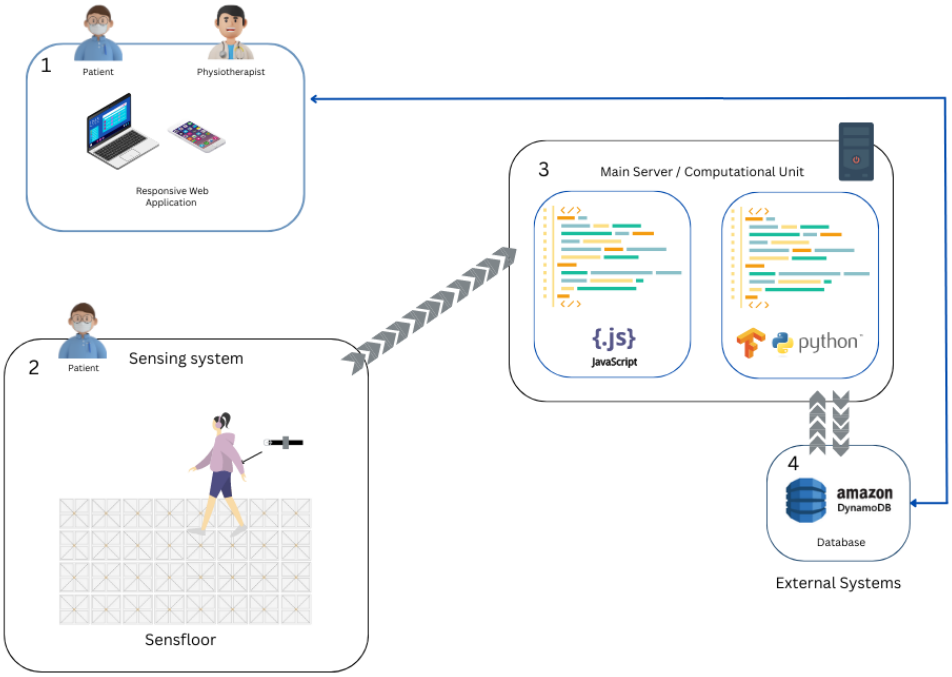


FIGURE 4.1. Overview of the system's architecture for physical rehabilitation.

4.3.1. System Architecture

The architecture of the system for physical rehabilitation, as shown in Figure 4.1, is divided into four blocks. Block 1 represents the applications in which both the user and the physiotherapist interact with the system. This interface allows for visualization of training performance and configuration of various training parameters.

Block 2 illustrates the sensing components of the system. The SensFloor system transmits data to a hat unit connected as a shield to the Raspberry Pi. A Node.js script then retrieves this data and forwards it to the database. A wearable motion sensor, equipped with an ESP32 microcontroller, also sends data directly to the database via its wireless capabilities.

Block 3 reveals the software components responsible for data handling and pre-processing. Within this block, the Node.js application plays a key role by incorporating a preprocessing mechanism specifically designed to address potential false positives that may arise during the training process. This mechanism operates by analyzing the distance between new and previous data points, automatically discarding any data points that exceed a predefined threshold. By implementing this approach, the Node.js application ensures the reliability and accuracy of the training data. Moreover, the Node.js application facilitates the seamless transfer of data to the database, streamlining the storage of pre-processed

data for further analysis. As part of the preprocessing stage, a separate Python script retrieves the data from the database to apply ML algorithms. Currently, this Python software operates on a dedicated machine. It conducts essential preprocessing tasks on the data from the IMU, such as calculating the average, minimum, maximum, root-mean-square, and standard deviation. These calculated features are crucial for the subsequent classification performed by our models, also included in this Python script.

Finally, Block 4 symbolizes the system's database, which utilizes Amazon DynamoDB for data storage. By providing a comprehensive overview of the system's architecture, we hope to enhance readers' understanding of the relationship and interaction between its various components.

4.3.2. Hardware Description

This section provides an overview of the two main hardware components used in our system: the sensor floor and the IMU. Both components play a crucial role in data acquisition and processing, enabling effective monitoring and analysis of the environment and user movements.

4.3.2.1. ***SensFloor.*** SensFloor, by FutureShape, is a large area sensor floor that can be installed beneath all kinds of flooring, making it invisible (Figure 4.2) and nonintrusive. It is made of a 3mm thick underlay with capacitive sensor arrays that can detect people and conductive materials. This system, created by Future-Shape GmbH, is based on large-area capacitive sensor technology, which provides high spatial resolution and sensitivity (Figure 4.3). It is also incredibly flexible because it is made up of separate modules that can be combined in a variety of scenarios.



FIGURE 4.2. Example of a Sensfloor use case. To provide additional protection, flooring is positioned above a sensory layer [**188**].

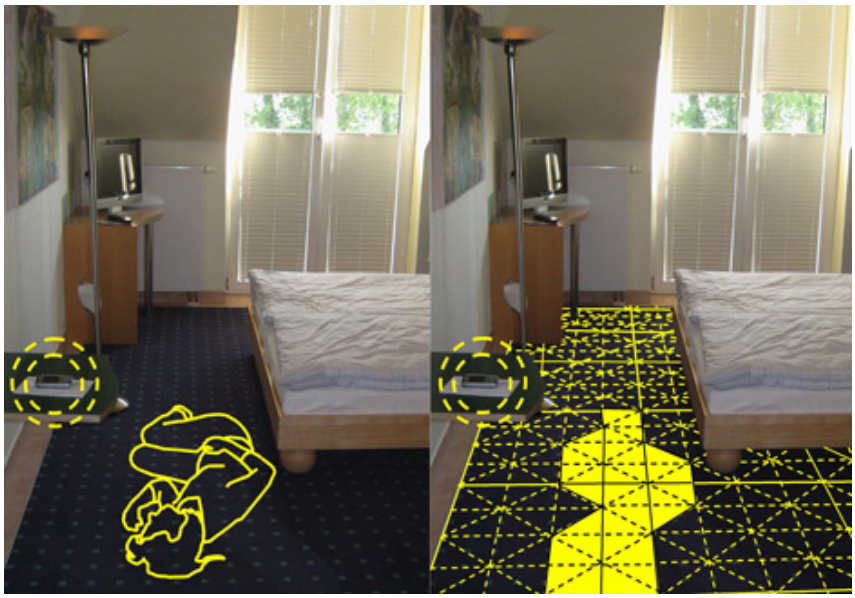


FIGURE 4.3. Example of a Sensfloor detecting a person fall and users' position [**189**].

The SensFloor system is composed several components:

(1) **Textile sensor layer:** A grid of capacitive sensors is embedded within a thin, flexible textile in this layer. The sensor grid is made up of conductive fibers that have been woven into the fabric in a specific pattern to allow for precise foot position detection. The sensor grid's size and resolution can be tailored to meet the needs of various applications.



FIGURE 4.4. Raspberry Pi 3 equipped with a SensFloor hat.

(2) **SensFloor Raspberry hat unit (Figure 4.4):** This unit collects data from the textile sensor layer and communicates with external devices. The control

unit contains ADCs that convert capacitance signals into digital data. It also includes a microcontroller for data processing and a communication interface for sending processed data to external devices like the Raspberry Pi in our setup.

(3) **Raspberry Pi 3:** The Raspberry Pi 3 is a credit card-sized single-board computer with a 1.2GHz quad-core ARM Cortex-A53 CPU, 1GB LPDDR2 RAM, and a Broadcom VideoCore IV GPU. With a dual-band 802.11n wireless LAN and Bluetooth 4.1 support, it has built-in wireless and Bluetooth connectivity. Four USB 2.0 ports, a full-size HDMI port, a 3.5mm audio jack, a microSD card slot for storage, and a 40-pin GPIO header for connecting to other hardware are included on the board. The board is powered by a micro-USB port and is compatible with a variety of operating systems, including Linux distributions and Windows 10 IoT Core. In addition to camera and display interfaces, the Raspberry Pi 3 has a CSI camera port and a DSI display port for connecting to cameras and displays. Because of its small size, low cost, and extensive feature set, it is a popular choice for hobbyist projects, educational initiatives, and commercial applications.

(4) **Power supply:** To ensure optimal performance, the SensFloor system requires a stable power source. The power supply is typically connected to the control unit and supplies the voltage and current required to run the system.



FIGURE 4.5. Experimental setup with laminated wood flooring installed above the SensFloor layer. Black tape marks the active sensing area. A TV screen displays a detected cell corresponding to a person standing on the floor which was taken the photo.

(5) **Protective flooring:** The system employs an 8 mm high-density fiberboard (HDF) laminated wood floor with an AC5 rating, indicating suitability for heavy industrial use due to its excellent durability and resistance to wear. As illustrated in Figure 4.5, this protective floor is installed directly over the SensFloor e-textile sensing layer. Black tape visibly marks the perimeter of the active sensing region. The AC5-rated HDF ensures that while users interact with the system, the underlying SensFloor remains safeguarded against mechanical damage, preserving its functionality. Moreover, the laminated surface does not interfere with the capacitive sensors' ability to detect foot positions and movements with high precision. This combination of materials allows the smart floor to reliably capture gait and posture data, supporting applications in both residential and clinical environments. In the Figure 4.5, the display screen shows a detected cell corresponding to a person located above the sensing area, demonstrating real-time position tracking.

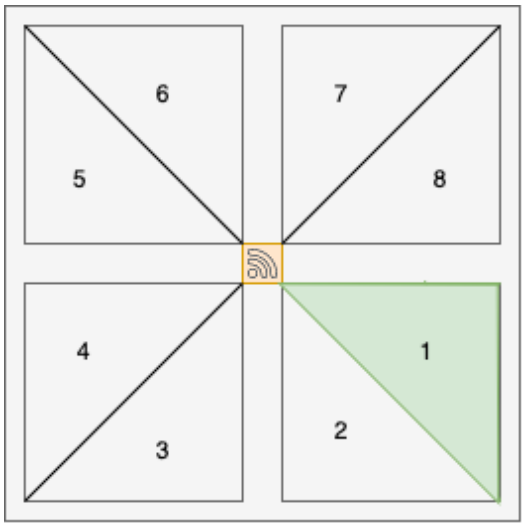


FIGURE 4.6. Sensfloor module.

The SensFloor system detects capacitance changes produced by a user's foot on the sensor grid. These capacitance variations are converted into digital data and sent to the high-performance computational unit for further analysis and implementation in ML algorithms, virtual environment rendering, and user interaction via the mobile application. Sensor events are noticed in eight triangular sensor areas (enumerated from 1 to 8 in Figure 4.6) below the feet when a person walks across the floor. In the Sensfloor underlay, eight sensor regions are linked to each radio module. Sensor events are wirelessly relayed (868 MHz) from the radio module located in the middle of the Sensfloor tile highlighted in orange in Figure 4.6 to the Sensfloor transceiver hat connected to the raspberry pi. Its purpose is to process sensor events from sensor modules, analyze time sequences, and reconstruct movement trajectories of individuals walking on the floor [**190**].

4.3.2.2. ***Motion Sensing System.*** Typically, sensors such as accelerometers and gyroscopes are used in the development of gait monitoring solutions; however, they are not ideal for obtaining precise data regarding the position of a body or object. Thus, for the purposes of this study, a wearable module containing an IMU (LSM9DS0) that combines accelerometer, gyroscope, and attitude data was developed as illustrated in Figure 4.7. The wearable module contains the following componets:

(1) **LSM9DS0 IMU Sensor**: The LSM9DS0 is a 9-axis motion sensor module that incorporates in a single package a 3-axis accelerometer, a 3-axis gyroscope, and a 3-axis magnetometer. Accelerometers measure linear acceleration, gyroscopes measure angular velocity, and magnetometers measure magnetic field strength. By combining these three kinds of measurement, the LSM9DS0 can

provide precise information regarding an object's orientation and movement in three-dimensional space. The LSM9DS0 communicates with an ESP32 microcontroller via an I2C interface, and each of its sensors has a programmable full-scale range.

(2) **ESP32 Microcontroller**: The ESP32 microcontroller is a 32-bit, dual-core processor that operates at speeds up to 240 MHz. It has built-in Wi-Fi and Bluetooth connectivity, as well as a variety of other peripherals, such as GPIOs, UARTs, I2C, SPI, ADC, and DAC. 520 KB of SRAM and 4 MB of flash memory are also included on the ESP32's on-board memory. For the purposes of this project, the ESP32 is responsible for processing the IMU data, inserting timestamps, and transmitting the data to the database via HTTP protocol.

(3) **Battery**: The wearable module is powered by an 850mAh Li-Po battery, providing approximately 3.5 hours of continuous measurements.

(4) **Charging Module**: The adaptation of a powerbank module enables the battery to be charged and the operating voltage to be set to 5V.

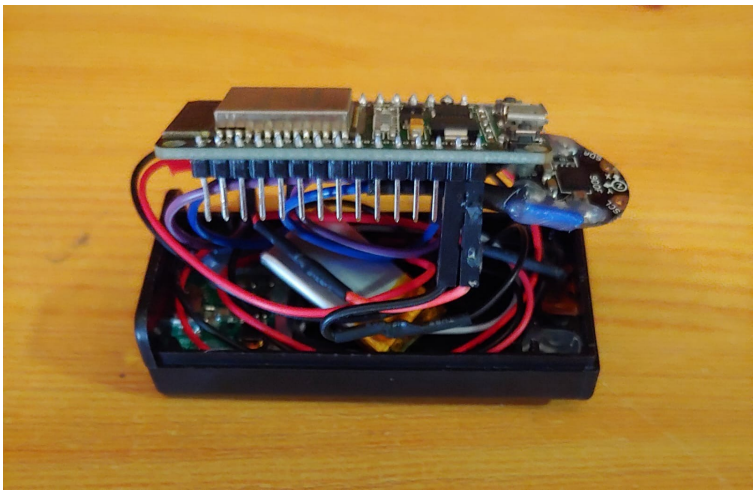


FIGURE 4.7. Wearable Motion Measurement Unit.

The user should use the motion measurement system in his back securing it in place with a velcro tape as Figure 4.8 exemplifies.



(A) (B)

FIGURE 4.8. Wearable Motion Device. (a) Device with velcro tape to facilitate the use. (b) User example using the wearable device.

Figure 4.9 depicts the motion device operation.

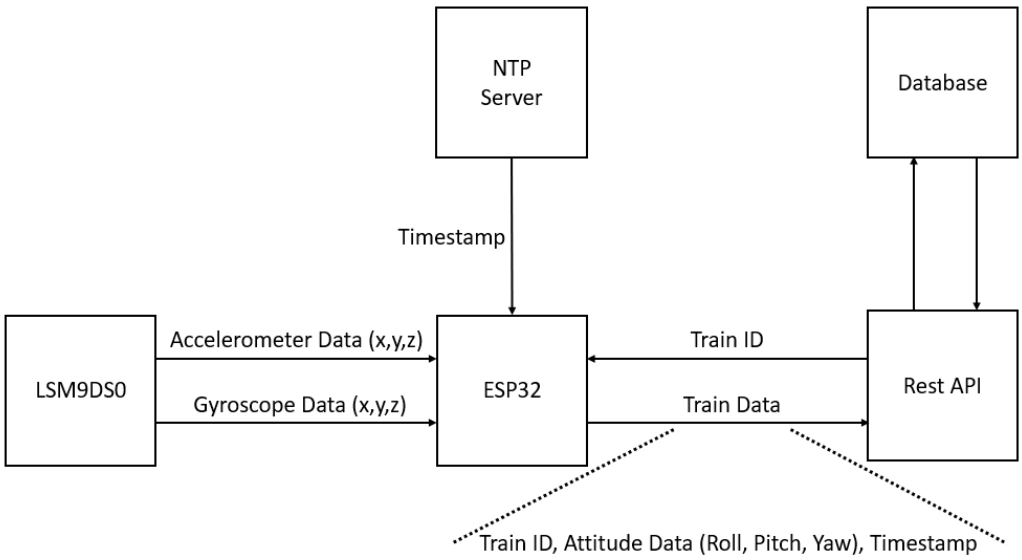


FIGURE 4.9. Motion Device Operation.

Data was acquired for the x, y, and z components of both the accelerometer and gyroscope embedded in the LSM9DS0 sensor, sampled with a periodicity of 10 seconds. The ESP32 microcontroller processed this data to extract the spatial orientation of the user, specifically calculating Roll (ϕ), Pitch (θ), and Yaw (ψ), which correspond to rotations around the front-to-back, side-to-side, and vertical axes, respectively.

A complementary sensor fusion algorithm was implemented to combine the short-term stability of the gyroscope with the long-term drift correction provided by the accelerometer. The gyroscope measurements were integrated over time to estimate angular displacement, following:

$$\begin{aligned} \phi_g(t) &= \phi_g(t - \Delta t) + \omega_x \cdot \Delta t \\ \theta_g(t) &= \theta_g(t - \Delta t) + \omega_y \cdot \Delta t \\ \psi_g(t) &= \psi_g(t - \Delta t) + \omega_z \cdot \Delta t \end{aligned} \tag{4.1}$$

where ω_x, ω_y, and ω_z denote the angular velocity components from the gyroscope.

To correct drift inherent to gyroscopic integration, the accelerometer was used to estimate Roll and Pitch based on the measured gravity vector:

$$\begin{aligned} \phi_a &= \arctan\left(\frac{a_y}{\sqrt{a_x^2 + a_z^2}}\right) \\ \theta_a &= \arctan\left(\frac{-a_x}{\sqrt{a_y^2 + a_z^2}}\right) \end{aligned} \tag{4.2}$$

The final orientation estimates were obtained by blending the gyroscope and accelerometer contributions through a weighted complementary filter:

$$\begin{aligned} \phi &= \alpha\,[\phi_g(t)] + (1 - \alpha)\,[\phi_a] \\ \theta &= \alpha\,[\theta_g(t)] + (1 - \alpha)\,[\theta_a] \end{aligned} \tag{4.3}$$

where α is a filter constant ($0 < \alpha < 1$), typically chosen around 0.98 to favor gyroscope stability while gradually correcting for drift using the accelerometer.

The Yaw angle (ψ) was primarily derived from the integrated gyroscope data, due to the absence of a magnetometer correction in this configuration.

Temporal synchronization was achieved by associating each measurement with a timestamp obtained via an NTP (Network Time Protocol) server. Additionally, a refinement procedure was implemented to achieve millisecond-level resolution, ensuring precise temporal alignment of orientation data with other sensor modalities.

To validate the motion direction estimation, controlled tests were performed in which known rotational movements were executed and the resulting Roll, Pitch, and Yaw trajectories were compared to the expected kinematic profiles, confirming the consistency and responsiveness of the orientation tracking under practical conditions.

4.3.3. Software Description

This section provides a detailed understanding of the software developed for the system, divided into two main parts: the embedded firmware responsible for low-level data acquisition and transmission, and the high-level software architecture that processes, stores, and presents this data to healthcare professionals and patients.

4.3.3.1. ***Firmware Description.*** The firmware was developed in C using the Arduino framework and compiled for deployment on the ESP32 microcontroller. Its primary responsibilities are to acquire sensor data, synchronize time, establish network connectivity, and transmit measurements to the higher-level software components.

- **Sensor acquisition:** The firmware interfaces with the LSM9DS0 inertial measurement unit (IMU) to acquire three-axis accelerometer and gyroscope data. Sampling occurs at a defined interval, with initial filtering and checks to discard anomalous readings that could indicate sensor faults or transient disturbances.
- **Time synchronization:** To ensure precise temporal alignment of the acquired motion data, the ESP32 periodically connects to an NTP (Network Time Protocol) server. This process synchronizes the internal clock to UTC, with additional refinement to achieve millisecond-level resolution. Accurate timestamps are crucial for correlating IMU data with external systems, such as the SensFloor.
- **Network connectivity and data transmission:** The ESP32 establishes a secure Wi-Fi connection to the local network. Once connected, the firmware packages the timestamped sensor data into JSON payloads and transmits them to a RESTful API via HTTP POST requests. To enhance robustness, an automatic reconnection mechanism is implemented, along with a lightweight retry strategy using exponential backoff to handle transient connectivity issues.
- **Resilience and watchdogs:** The firmware includes watchdog timers and periodic health checks to detect potential deadlocks or communication breakdowns. If such issues are identified, the microcontroller automatically resets specific interfaces or reinitializes the system to maintain continuous operation.

This embedded layer ensures that reliable, time-synchronized sensor data is consistently delivered to the high-level software for further processing and analysis.

4.3.3.2. ***High-Level Software Description.*** The high-level software layer is a fundamental component of the system, enabling data processing, evaluation, and execution

of application-specific tasks. This section provides an overview of the software architecture, with particular emphasis on the interaction between sensing, data handling, and user-facing components.

At the user level, healthcare professionals interact with the system through a dedicated web-based application. This interface provides real-time and historical visualization of patient data, supporting monitoring and assessment during rehabilitation sessions. The application presents the users' planar position coordinates (x, y) on a grid-based layout, as well as motion-related information derived from the inertial measurement unit (IMU), including yaw, pitch, and roll. Interactive dashboards allow clinicians to observe movement trajectories, orientation trends over time, and summaries of overall activity patterns, facilitating informed clinical evaluation.

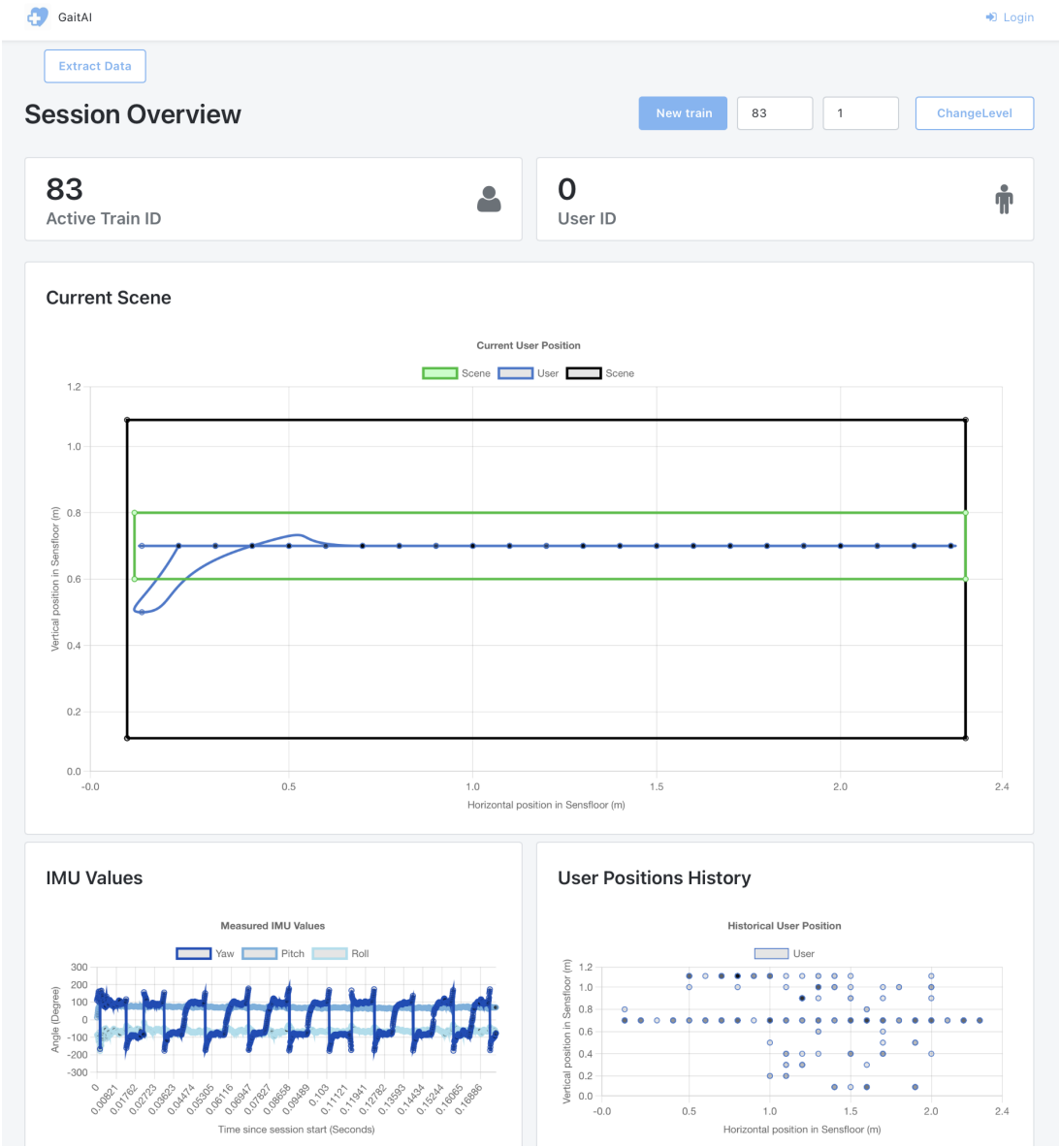


FIGURE 4.10. Physiotherapist application homepage dashboards.

The web application retrieves sensor data stored in a DynamoDB database and updates the visual interface in real-time, as illustrated in Figure 4.10. Historical data are also accessible through interactive charts implemented using the Chart.js library. These charts display the user's position history during individual training sessions, the temporal evolution of IMU orientation angles, and cumulative movement patterns across multiple sessions, providing physiotherapists with intuitive tools to assess adherence and progress.

At the sensing layer, the SensFloor system is connected to a Raspberry Pi 3 microcontroller through the SensFloor Shield, as previously described. The Raspberry Pi uses the SensFloor API, implemented in NodeJS, to collect, filter, and process raw sensor data. A custom script was developed to expose the processed data to the web application.

Prior to transmission, the data are formatted and filtered to prioritize the most relevant information for gait and balance analysis.

To mitigate process-related errors and reduce the impact of false positive detections, an error-handling mechanism was implemented. This mechanism compares consecutive positional data points using a predefined distance threshold based on feasible human movement. When the distance between two points exceeds this threshold—indicating that the displacement is unlikely to have been produced by a human step within the sampling interval—the new data point is discarded, thereby improving data reliability.

This strategy is particularly relevant in rehabilitation contexts where assistive devices such as crutches may be used. Although such devices were not explicitly tested in this study, it is hypothesized that contacts generated by assistive devices would produce sensor activations corresponding to unrealistically distant points. By rejecting these outliers, the system minimizes their potential impact on gait analysis. Overall, this error mitigation approach enhances the robustness of the system and supports its applicability in real-world rehabilitation environments.

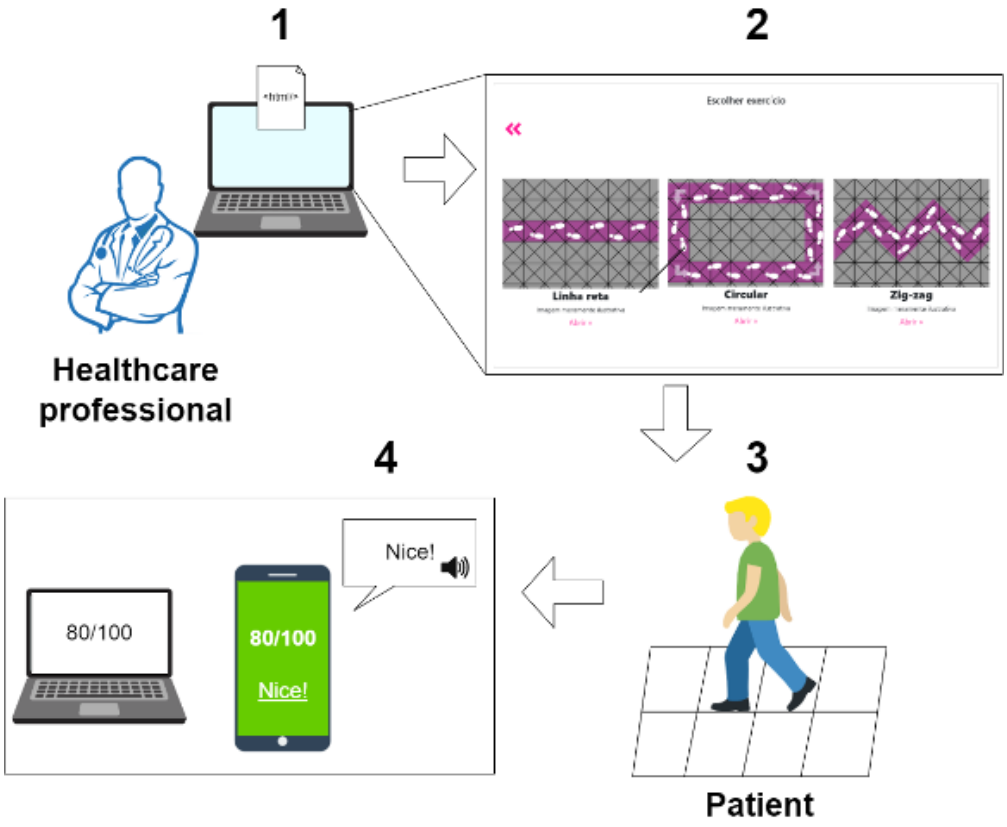


FIGURE 4.11. User application flow.

The use case of the system is demonstrated in Figure 4.11:

(1) The healthcare professional selects the level for the user.

(2) The user receives a notification and visualizes the path and their position in real-time on a monitor or TV.

(3) The user finishes the session and can view their score in the application.

If the patient is registered in the mobile application, data is also stored in a real-time cloud database, providing access to dashboards that allow them to track their progress over time and review scores obtained.

Given that maintaining an organized medical history is a key requirement in eHealth systems, this functionality was incorporated and is illustrated in Figure 4.12.

Using Google's Firebase as a real-time database dedicated to patient and healthcare professional data, the objectives of data sharing and synchronization are achieved. Firebase, being a cloud-hosted NoSQL database, ensures that whenever a CRUD operation (Create, Read, Update, Delete) occurs, all connected devices are updated in real-time — for instance, when a healthcare professional prescribes a new exam, it immediately appears in the patient's mobile application. The patient application itself was developed using Google's Flutter, chosen for its cross-platform capabilities and strong integration with Firebase.

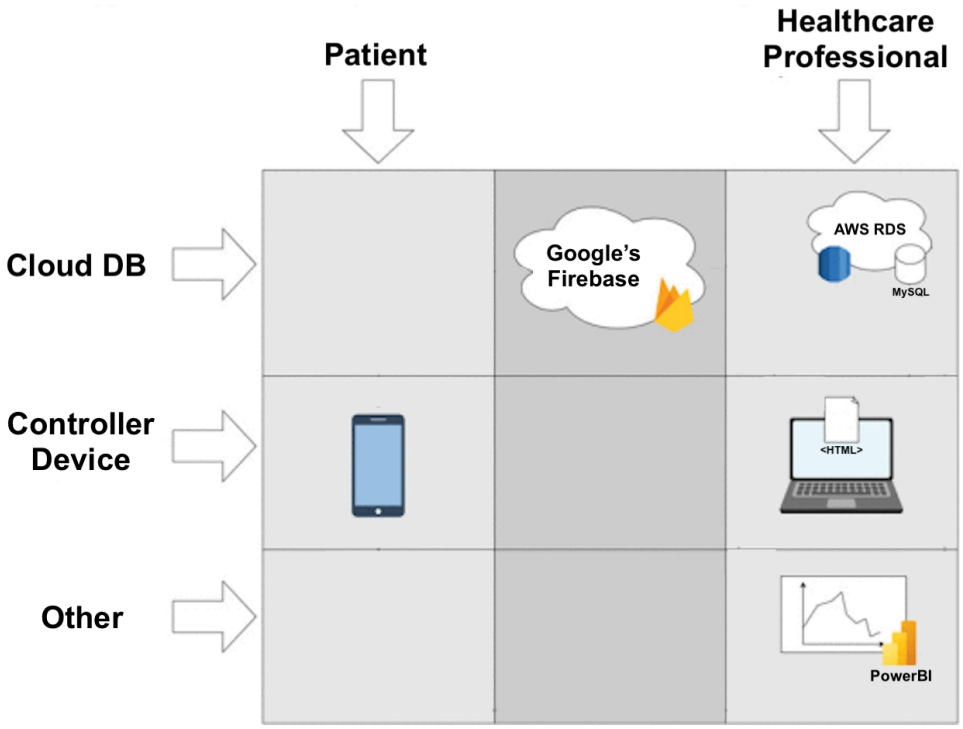


FIGURE 4.12. Application data flow.

According to Figure 4.12:

(1) **Mobile application uploads data to Firebase**: The mobile application enables patients to register and securely upload their data to Firebase Cloud Firestore. This database was selected due to its fully managed, scalable, and real-time capabilities, which are well suited for mobile health applications that require continuous data synchronization across devices. Firestore supports low-latency data access and automatic synchronization, allowing patient information to be updated and retrieved in real-time without the need for complex backend infrastructure management.

    Patient profile data can be updated dynamically, and an optional profile picture is stored using Firebase Storage, which integrates seamlessly with Firestore for handling multimedia content. In addition, patients can record personal health metrics such as weight, height, blood pressure, and glucose levels. The use of Firebase services also provides built-in authentication, role-based access control, and secure communication channels, simplifying compliance with data protection and privacy requirements. Overall, Firebase Firestore offers a robust and flexible backend solution that supports scalability, reliability, and rapid development for the proposed mobile health monitoring system.

(2) **Mobile application retrieves data from Firebase**: On accessing the application, the saved data and profile picture are automatically loaded. Any exams or medications prescribed by healthcare professionals are also displayed via a timeline interface.

(3) **Web application uploads data to Firebase**: Healthcare professionals register in the web application, which saves their data to Cloud Firestore. They can then upload exam or medication files to patients, stored in Firebase Storage and accessible in the patient app. Each file is linked with the prescribing professional's details.

(4) **Web application retrieves data from Firebase**: The web interface lists all registered users and their medical histories, also retrieving health metrics submitted by patients.

Long-term patient data is stored in a MySQL database hosted on AWS RDS for permanent record-keeping, with Firebase acting as a temporary database to support real-time operations. Dashboards are generated and published in a secured workspace, accessible only via authenticated application sessions.

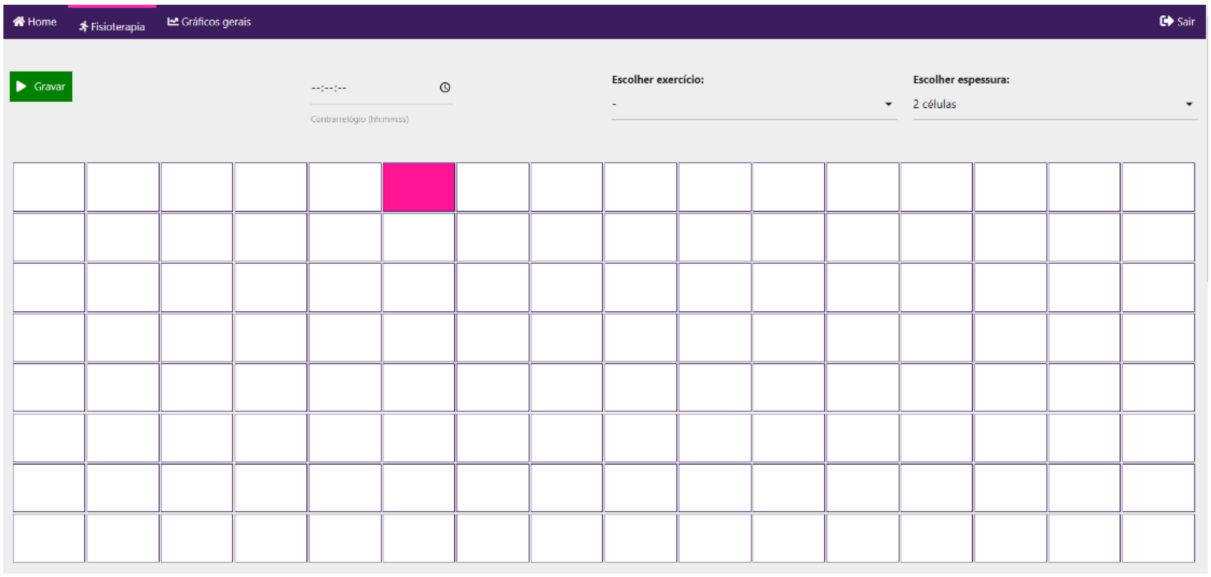


FIGURE 4.13. Users' side application.

Finally, these dashboards are embedded within the web application and can also be accessed by patients who are granted permissions. This allows users to track their progress and see their current location, enabling an augmented reality scenario where they receive immediate feedback if they deviate from the designated path (Figure 4.13).

4.3.4. Machine Learning for Balance and Gait Stability Analysis

In this section, we discuss the machine learning (ML) techniques employed to analyze and process the data collected by the SensFloor and IMU sensors. ML plays a crucial role in extracting clinically relevant insights from the sensor data, enabling the detection of specific patterns and anomalies associated with user stability and locomotion. In our context, anomalies primarily refer to indicators of unbalance, such as irregular gait patterns, abrupt changes in orientation (Roll, Pitch, Yaw) exceeding expected thresholds, or deviations from predefined walking paths. Unbalance is operationally defined by observing either excessive sway, rapid corrective movements, or inconsistent center-of-pressure trajectories relative to normative datasets.

To validate the effectiveness of the proposed models in detecting such events, methods such as cross-validation with labeled datasets, confusion matrix analysis, and comparison with established clinical assessments (e.g., Timed Up and Go or force platform metrics) can be employed. We previously demonstrated an initial version of our system in [**191**]. In this work, we extend that approach by integrating ML models with a wearable IMU to improve the detection accuracy of unbalanced events and enhance the system's applicability to personalized rehabilitation interventions.

For the training and model testing we used Edge Impulse software (Figure 4.14) which provide a user interface to facilitate embedded ML model training. It features Tensorflow [**192**] and Keras [**193**] which are suitable for the demands of this work.

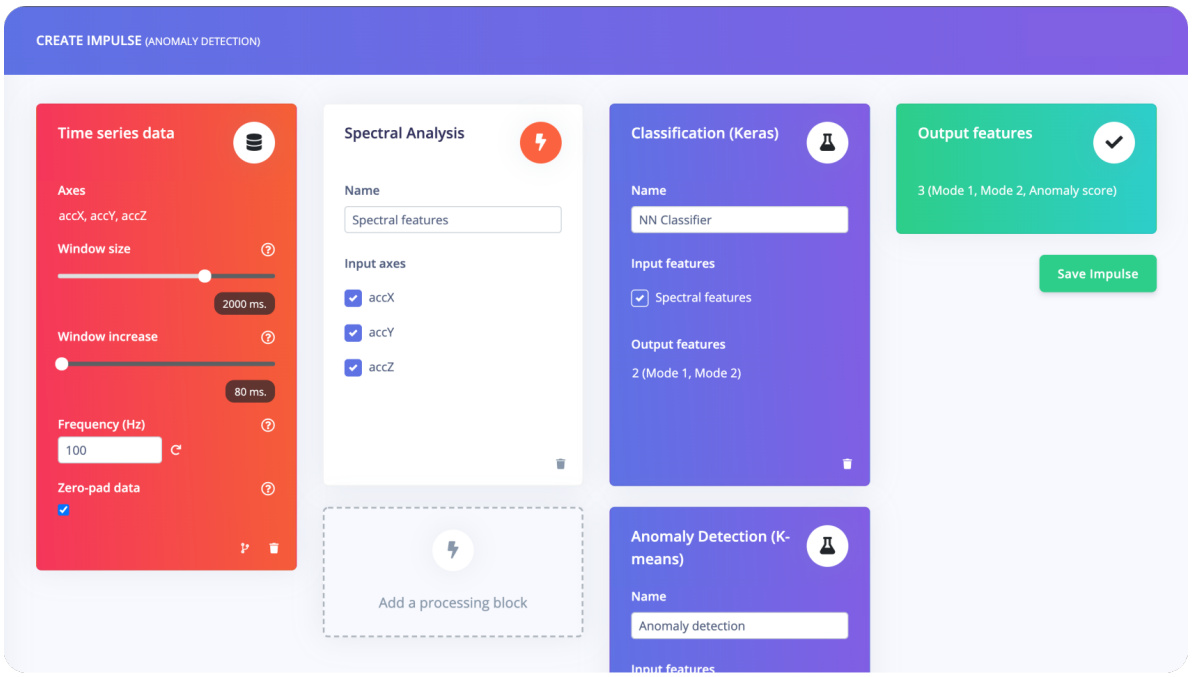


FIGURE 4.14. Edge Impulse Software

4.3.4.1. ***Data Preprocessing.*** Due to the sensing principle of the SensFloor , sometimes is possible to observe false positives about users' current position, therefore and as we had previously delimited a area of the floor we removed some points that were incorrect. For the IMU values we had also remove initial and final seconds of the training to ensure that only movement were actually captured.

TABLE 4.1. Summarised features extracted according to sensing element.

Sensing Unit	**Features extracted**
LSM9DS0	yaw, pitch, roll, average, minimum, maximum, root-mean square and standard deviation
Sensfloor	x, y

4.3.4.2. ***Feature Extraction.*** In the forthcoming findings section, we delve into a detailed exploration of numerous experiments we conducted, employing a variety of data

pre-processing methodologies. In contrast to our previous study [**191**], where we derived key indicators without leveraging ML, in this study we experimented with the range of x and y values, specifically their maximum and minimum values, along with their standard deviations. We found that the utilization of ML techniques, in place of raw values, led to the discovery of certain metrics that yielded superior results.

Table 4.1 presents a summary of the features extracted based on the sensing elements used in the study. In terms of feature extraction from the IMU data, we pre-processed it and implemented a sliding window approach to extract average, minimum, maximum, root-mean square, and standard deviation. As we observed, the use of ML with these extracted features outperformed models that were trained purely on raw values.

The feature extraction method we employed is designed to distill salient features from the preprocessed data, which can accurately illustrate the underlying trends in user behavior and mobility. These features may take the form of statistical measures, frequency-domain features, or time-domain features, all of which are derived from the sensor data. The chosen features are then utilized as input for ML algorithms.

In the context of synthesizing features from different sensors, we've refined the data integration process. Data from the SensFloor smart carpet and the IMU wearable sensor are merged and processed using ML algorithms designed to handle different data types. The algorithms effectively integrate the positional and movement data from the SensFloor with the detailed movement data from the IMU, providing a nuanced and comprehensive overview of the patient's gait and balance. This sophisticated synthesis of data from multiple sensors allows for a more accurate interpretation of the patient's movements, subsequently informing the creation of personalized training plans for more effective rehabilitation.

4.3.4.3. *Model Selection and Training.* In our study, we applied various ML models to the extracted features with the aim of classifying and predicting balance. We considered several models and selected the most suitable one based on the specific problem, data characteristics, and desired performance. During the model training process, we divided the dataset into training and validation sets. The training set was utilized to fine-tune the model's parameters, whereas the validation set served as a means to evaluate the model's performance and mitigate overfitting.

To clarify the determination of classes before the start of the training process, a predefined classification scheme is followed for gait analysis. The system defines three classes to represent different gait patterns:

- Class 1 is associated with an abnormal gait pattern, indicating a deviation from the expected or typical gait. This class represents instances where individuals exhibit significant deviations in their walking pattern, potentially indicating a gait impairment or dysfunction.
- Class 2 is assigned to a less-abnormal gait pattern. It represents instances where individuals demonstrate some deviations from the optimal gait, but to a lesser extent compared to Class 1. This class may include individuals with mild gait abnormalities or those in the early stages of recovery from a gait-related condition.
- Lastly, Class 3 represents the optimal gait pattern. It represents instances where individuals exhibit a normal, healthy gait without significant deviations or abnormalities. This class serves as a reference point to compare against the other classes and provides a benchmark for the ideal gait pattern.

By defining these three classes, the system is able to capture and classify various gait patterns observed in the dataset. This classification scheme allows the system to differentiate between different levels of abnormality and assess the degree of deviation from the optimal gait.

Moreover, the models can be optimized by repeating the training process while adding new and relevant data. However, the frequency at which the training process should be repeated depends on several factors, including the stability of the underlying data and the dynamic nature of the gait patterns being analyzed. In the context of this study, it is recommended to periodically retrain the model to ensure its accuracy and adaptability over time.

The training process should be repeated when there are significant changes in the dataset or when new data becomes available that could potentially enhance the model's performance. For instance, if there are updates to the dataset with a larger and more diverse set of gait patterns, it is beneficial to incorporate this new information into the training process.

Additionally, if there are changes in the target population or if individuals with different characteristics are included in the dataset, retraining the model becomes crucial to capture these variations and improve the model's generalizability.

It is important to strike a balance between the frequency of training and the computational resources required. While regular retraining can ensure the model's accuracy, it can also be resource-intensive. Therefore, it is recommended to assess the stability of the data and the potential impact of any changes before determining the appropriate frequency for retraining. By periodically revisiting the training process, researchers and practitioners can maintain the model's relevance and optimize its performance, allowing it to adapt to new data and provide accurate gait analysis results over time.

4.3.4.4. *Model Evaluation and Optimization.* Once the model is trained, its performance is evaluated using various evaluation metrics such as Accuracy (Acc), Precision (P), Recall (R) and F1-score ($F1$), and their values can be obtained by using the following equations:

$$Acc = \frac{\mathrm{TP} + \mathrm{TN}}{\mathrm{TP} + \mathrm{TN} + \mathrm{FP} + \mathrm{FN}} \tag{4.4}$$

$$P = \frac{\mathrm{TP}}{\mathrm{TP} + \mathrm{FP}} \tag{4.5}$$

$$R = \frac{\mathrm{TP}}{\mathrm{TP} + \mathrm{FN}} \tag{4.6}$$

$$F1 = 2 \times \frac{P \times R}{P + R} \tag{4.7}$$

The Accuracy (Acc) is a commonly used evaluation metric that calculates the proportion of correct predictions (True Positives, TP, and True Negatives, TN) out of the total number of predictions, including False Positives (FP) and False Negatives (FN). Precision (P) measures the fraction of True Positives (TP) out of the sum of True Positives (TP) and False Positives (FP), providing insight into how well the model identifies positive instances among all instances predicted as positive. Recall (R), also known as sensitivity or true positive rate, calculates the fraction of True Positives (TP) out of the sum of True Positives (TP) and False Negatives (FN), indicating the ability of the model to correctly identify positive instances among all actual positive instances. The F1-score is the harmonic mean of P and R, providing a balanced measure that considers both P and R, especially when dealing with imbalanced datasets where one class dominates the other [**194**].

4.3.4.5. *Deployment and Monitoring.* After achieving satisfactory performance, the trained ML model is deployed to analyze the real-time data collected by the hardware components. The model's performance should be continuously monitored and updated as needed to ensure its effectiveness in providing accurate and meaningful insights into user behavior and movements.

In summary, the integration of ML techniques in our system enhances the analysis and interpretation of the data collected by the Sensfloor and IMU. These techniques enable the identification of patterns and anomalies, informing healthcare professionals and supporting personalized interventions for improved patient outcomes.

4.3.5. Results & Discussion

In this section, we present the findings and insights derived from the application of various ML models to the previously presented work [**191**]. The results highlight the effectiveness of the selected models in classifying and predicting user balance. Additionally, we discuss the implications of a new IMU unit sensing system to provide more metrics and features to the systems. Using the developed system, including hardware and software, we defined a straight virtual path with positions the user needs to follow, and coordinate intervals to evaluate if the user stays in the correct path and maintains the balance. In this developed prototype, the virtual path and current user position is displayed in a TV screen for the user to visualize.

4.3.6. Participant Selection

For the evaluation of the system, a total of sixteen volunteers participated in the study. Each volunteer was instructed to follow a line that was marked on the floor. During the test sessions, the participants wore the wearable sensing system, which collected their motion. A total of 10 trials per volunteer were conducted, and all the data captured were stored in a database for further analysis. Specific biometric information for the volunteers is presented in Table 4.2 below. All participants were informed about the experiments and gave their verbal consent. None of the participants reported any mental, cardiac, respiratory, or other disturbances. However due to a failure between the sensing system communications with internet one of the trials were excluded.

TABLE 4.2. Volunteers Specific Biometric Information.

	Male	**Female**	**Total**
Participants	7	9	16
Age Range	21 - 32	18 - 28	18 - 32
Average Range	26	23	25
Standard Deviation of Ages	3.34	3.5	3.77

4.3.7. Experimental Protocol

The experimental protocol for this study included recruiting fourteen users of various ages to participate in the experiments. The participants were informed about the study's objectives and given a thorough explanation of the experimental procedure.

Each participant was asked to try to follow a straight line several times going forward and then turn and repeat.

During the testing phase, the system was used to record several motion parameters such as x and y position according to the Sensfloor and yaw, $pitch$ and $roll$. The data gathered during the testing phase was later used to train and evaluate the ML models.

The experimental protocol was created to ensure the accuracy and reliability of the data collected during the experiments. The data collection process was meticulously monitored to ensure that all relevant parameters were recorded.

4.3.8. Preliminary assessment

Initially the presented system evaluated the user performance following some metrics based on statistics, resulting in two different mathematical relations. The first metric consists in obtaining the total number of measurements during the time the user takes to complete the exercise (N), the number of measurements out of the virtual path's bounds (NO), the real Sensfloor dimensions, in meters (in this case, $MaxX = 4$ and $MaxY = 2$) and the maximum X and Y deviations ($MaxDevX$ and $MaxDevY$). It is also possible to calculate the average X and Y deviations, $AvDevX$ and $AvDevY$, respectively, as follows:

$$Av\,\mathrm{Dev}\,X = \frac{\sum_0^{NO} \mathrm{dev}\,X}{N}; Av\,\mathrm{Dev}\,Y = \frac{\sum_0^{NO} \mathrm{devY}}{N} \quad (1)$$

in which $dev(X/Y)$ represents the array with all deviations. By doing so, the final score formula is achieved, shown in Equation 2.

$$score = \frac{N - NO}{N} \cdot \frac{MaxX - MaxDevX}{MaxX} \cdot \frac{MaxY - MaxDevY}{MaxY} \cdot \frac{MaxX - AvDevX}{MaxX} \cdot \frac{MaxY - AvDevY}{MaxY} \cdot 100 \quad (2)$$

In an ideal scenario, variables NO, $MaxDevX$, $MaxDevY$, $AvDevX$ and $AvDevY$ are equal to zero, corresponding to a perfect score (100%) however, in the worst-case scenario, if $MaxDevX = MaxX$, $MaxDevY = MaxY$, $AvDevX = MaxX$ or $AvDevY = MaxY$, the score is automatically 0%. By analyzing the first term of the equation, if the user spends most of the time outside bounds, the score tends to be lower.

As to the second solution, it makes use of RMSE (Root Mean Square Error), as a way to measure differences between the correct values and the deviations. RSME is calculated as follows:

$$RMSE = \sqrt{\sum_{i=1}^{N} \frac{(y^n{}_i - y_i)^2}{N}} \quad (3)$$

The term

$$y^n{}_i - y_i$$

corresponds to the deviations calculated previously. This gives an estimation of how deviated the measurements are from the ideal. $RMSE = 0$ corresponds to a perfect scenario, where no deviations were made throughout the path. By testing the IoT system, the worst-case scenarios reached to a $RMSE$ of 0.15. These $RMSE$ values can be converted to a percentage, as to generate the final score, using Equation 4.

$$score = \frac{k}{RMSE + k} \cdot 100 \quad (4)$$

It is possible to conclude that if $RMSE = 0$, $score = 100\%$, thus for a bigger the $RMSE$ value, the score is lower. By incrementing / decrementing the parameter k, the score is less/more sensible to the $RMSE$ value, respectively.

Although this technique can provide a metric it is not possible to correctly evaluate gait or balance only based on the users' position. Therefore, we had included in this work one more sensing system capable of monitoring users' lateral motion and thus we can now obtain more parameters but we cannot use this scoring system. With the new parameters

we had implemented ML. From the previous work mentioned in [**191**] we still concluded that some of the metrics referred on this section such as $MaxDevX$, $MaxDevY$, $AvDevX$ and $AvDevY$ were important features when training the ML modules.

4.3.9. ML Application

In this study, we evaluated the performance of three different ANN architectures (MLP, LSTM and GRU) to classify the balance of the users in three different levels. To assess their performance, we measured various performance metrics such as accuracy, loss, and F1-score. Both architectures were trained on a dataset using the same training and validation processes. During training, we monitored the model's accuracy and loss on both training and validation data to prevent overfitting and ensure generalization performance. In addition, we evaluated the models' performance using the F1-score metric, which takes into account both P and R to provide a balanced measure of the model's effectiveness.

The network hyperparameters that were configured for the training process are shown in Table 4.3.

Table 4.3. Network hyperparameters.

Hyperparameter	**Value**
Epochs	100
Optimizer	ADAM
Loss	Sparse Categorical Cross Entropy
Initial LR	0.0001
Batch size	512
Batch Normalization	Yes
Activation Function	ReLU & Softmax

The table presents the network hyperparameters used in the study. These hyperparameters are settings that were manually set before training the neural network to optimize its performance. The hyperparameters include the number of epochs, which was set to 100, indicating that the network was trained for a total of 100 cycles. The optimizer used was the Adaptive Moment Estimation (ADAM), which is a popular optimization algorithm for DL models. The loss function employed was Sparse Categorical Cross Entropy (SCCE), which is suitable for multi-class classification problems.

The selection of the SCCE as the loss function in this study is justified by the categorical nature of the target variable, which has a cardinality of more than two. The use of this loss function allows us to effectively handle multi-class classification tasks and preserve the non-ordinality of the target variable. It also avoids the need for creating dummy variables by directly encoding the target labels [**195**]. This approach is particularly advantageous when dealing with a large number of classes, as it helps to reduce the computational complexity associated with one-hot encoding. Moreover, by using SCCE, we can leverage the inherent structure of the target variable and train the model to make predictions based on the actual class labels, without introducing any artificial ordering of the classes. This is especially important in this case, as we want to preserve the categorical nature of the gait classification problem and avoid any assumptions of an inherent order among the classes.

The initial Learning Rate (LR) was set to 0.0001, which is a small value commonly used to prevent the model from diverging during training. The batch size was set to 512, which indicates that the model was trained on batches of 512 samples at a time. Batch normalization was also used, which is a technique to normalize the input data to the network to prevent overfitting and improve training stability. Overall, these hyperparameters were chosen to optimize the network's performance and balance between underfitting and overfitting.

To capture the complex relationships and patterns in the gait data, the MLP model employs a total of 9 hidden layers. With multiple hidden layers, the model can learn hierarchical representations and abstract features from the input data, potentially improving its performance.

The MLP model's inclusion of various hidden layers allows the network to learn increasingly complex and abstract representations of the input data. This depth may aid the model's ability to capture fine details and intricate patterns that may exist within gait patterns, resulting in improved performance.

It is important to note, however, that the optimal number of layers in a neural network depends on the specific problem and dataset. While deeper models may perform better, there is a trade-off between model complexity and the risk of overfitting. In our case, 9 hidden layers struck a balance between model complexity and generalization capability.

The Rectified Linear Unit (ReLU) activation function has been used for the hidden layers, while the softmax function has been employed for the output layer. The ReLU

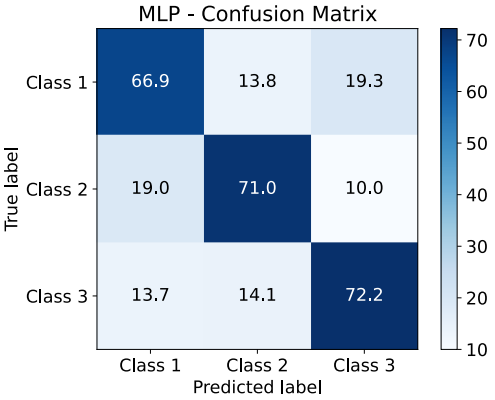
activation function is a popular choice for hidden layers in neural networks. It avoids the vanishing gradient problem and can accelerate the convergence of the learning process.

For the output layer, the softmax activation function was selected. The softmax function is commonly used in multi-class classification problems, such as gait classification, as it normalizes the output scores into probabilities that represent the likelihood of each class. By using the softmax function, we obtain a probability distribution over the different gait classes, enabling us to make confident predictions and assign a class label to each gait pattern.

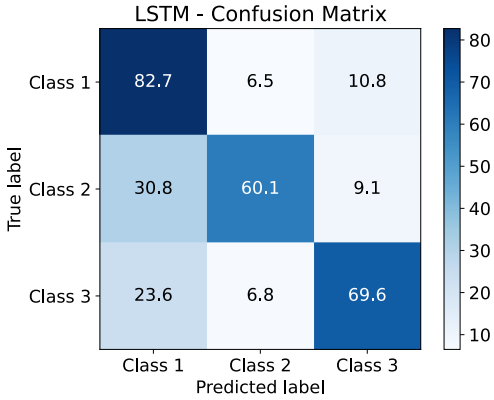
Different activation functions serve different purposes and are suited for different types of problems. In the case of the MLP model for gait classification, the ReLU activation function in the hidden layers allows the model to learn and represent complex features, while the softmax activation function in the output layer provides a probabilistic interpretation of the predictions.

4.3.9.1. ***Performance Evaluation.*** In this section, we present the performance evaluation of the three models: MLP, LSTM, and GRU, which were developed to analyze and classify the given dataset. The models were trained on the same dataset, comprising x, y, *yaw*, *pitch*, and *roll* data. The primary objective of this performance evaluation is to assess the capabilities of each model and compare their effectiveness in terms of accuracy, P, R, and F1-score for each class. By providing a comprehensive analysis of the models' performance, we aim to identify the strengths and weaknesses of each approach and offer insights into their suitability for the given problem domain.

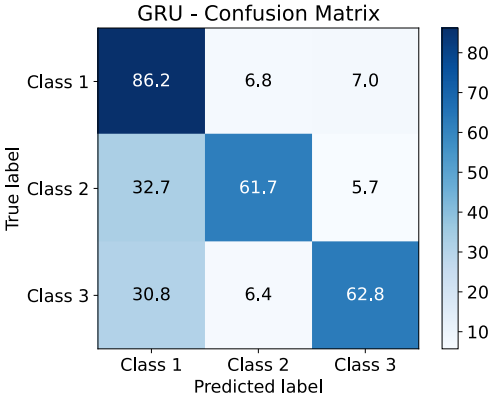
Figure 4.15 depicts the confusion matrices for the three models: MLP, LSTM, and GRU.



(A) Confusion matrix for the MLP network.



(B) Confusion matrix for the LSTM network.



(C) Confusion matrix for the GRU network.

FIGURE 4.15. Confusion matrix of MLP, LSTM and GRU, respectively.

The performance of the three models, MLP, LSTM, and GRU, was evaluated using the confusion matrices shown in Figures 4.15a, 4.15b, and 4.15c. These confusion matrices provide insights into the classification accuracy and misclassification patterns for each class.

Starting with the MLP model (Figure 4.15a), the results indicate that it achieves a relatively high accuracy of 66.9% for Class 1. However, the model encounters difficulties in correctly classifying instances from Classes 2 and 3. It misclassifies 19% of Class 2 instances as Class 1, indicating a certain degree of confusion between these two classes. Similarly, it misclassifies 13.7% of Class 3 instances as Class 1, further highlighting the challenge in distinguishing between these classes.

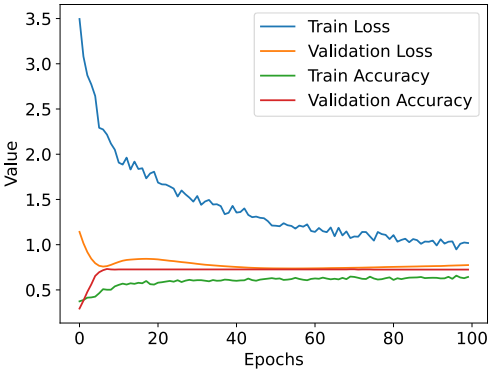
In the case of the LSTM model (Figure 4.15b), some improvements were observed in the classification accuracy for Class 1, which reaches 82.7%. The model shows a better ability to differentiate Class 1 instances from the other classes. However, it still faces challenges in correctly classifying instances from Classes 2 and 3. Specifically, it misclassifies

30.8% of Class 2 instances as Class 1, indicating a significant confusion between these two classes. It also misclassifies 23.6% of Class 3 instances as Class 1, further highlighting the difficulty in distinguishing between these two classes.

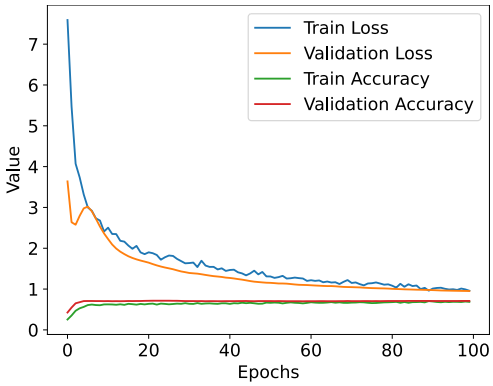
Lastly, the GRU model (Figure 4.15c) demonstrates a higher classification accuracy for Class 1, achieving 86.2%. This indicates its better ability to correctly classify Class 1 instances compared to the other models. However, similar to the previous models, it struggles with differentiating between Classes 2 and 3. It misclassifies 32.7% of Class 2 instances as Class 1, suggesting a considerable overlap between these two classes. Additionally, it misclassifies 30.8% of Class 3 instances as Class 1, further emphasizing the challenge in distinguishing between these classes.

In summary, the evaluation of the three models reveals a higher classification accuracy for Class 1 compared to Classes 2 and 3. The LSTM and GRU models demonstrate improvements in classification performance compared to the MLP model, particularly in terms of accurately classifying Class 1 instances. However, they still face challenges in differentiating between Classes 2 and 3. These misclassifications suggest an inherent difficulty in distinguishing certain patterns or characteristics of the data related to these classes. Further investigation and optimization of the model architectures, training parameters, and potentially incorporating additional features may help enhance the classification performance for all classes.

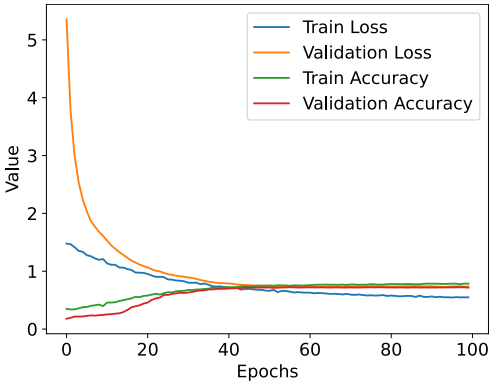
Figure 4.16 shows the training behavior over time on accuracy and loss values.



(A) Training behavior of the MLP network.



(B) Training behavior of the LSTM network.



(C) Training behavior of the GRU network.

FIGURE 4.16. Training parameters over time of accuracy and loss values.

Figure 4.16 presents the training behavior over time for the MLP, LSTM, and GRU models in terms of accuracy and loss. Although all three models converge and achieve comparable performance trends, differences can be observed in their convergence speed and final performance.

The MLP model exhibits slower convergence in loss values when compared to the recurrent models. This behavior is expected, as MLPs lack an explicit mechanism to model temporal dependencies and therefore rely solely on instantaneous feature relationships. As a result, their ability to capture sequential patterns present in gait and balance data is limited.

The LSTM and GRU models display very similar training behavior, characterized by faster convergence and more stable loss evolution. This similarity can be attributed to their recurrent architectures, which are specifically designed to model temporal dependencies through gating mechanisms. These mechanisms allow both models to retain relevant historical information while mitigating vanishing gradient issues, making them well suited for sequence-based sensor data.

TABLE 4.4. Models Performance evaluation.

	Class 1			Class 2			Class 3			
Model	**P**	**R**	**F1**	**P**	**R**	**F1**	**P**	**R**	**F1**	**Acc**
MLP	0.84	0.67	0.75	0.56	0.71	0.62	0.58	0.72	0.64	0.69
LSTM	0.80	0.83	0.81	0.69	0.6	0.64	0.68	0.70	0.69	0.751
GRU	0.78	0.86	0.82	0.69	0.62	0.65	0.75	0.63	0.68	0.757

The summary of the quantitative evaluation metrics for all models is presented Table 4.4. The MLP model achieves the lowest overall accuracy (0.69) and demonstrates unbalanced performance across classes, particularly for Class 2 and Class 3, indicating limited generalization capability. In contrast, both recurrent models outperform the MLP across most metrics.

Between the recurrent architectures, the GRU model achieves the highest overall accuracy (0.757), slightly surpassing the LSTM model (0.751). In addition, the GRU demonstrates a more balanced performance across the three classes, particularly in terms of recall and F1-score for Class 3, which is critical for reliable detection of balance-related patterns. Given its competitive performance, reduced architectural complexity, and lower computational overhead compared to LSTM, the GRU model was selected as the most suitable model for this application.

Overall, these results indicate that recurrent neural networks are better suited for modeling the temporal characteristics of the sensor data, with the GRU offering the best trade-off between accuracy, robustness, and computational efficiency.

4.3.10. Conclusions

Table 4.4 provides a comprehensive performance evaluation of the three models: MLP, LSTM, and GRU. All models were trained on the same dataset, which includes x, y, yaw, *pitch*, and *roll* data. The table displays the precision (P), recall (R), and F1-score for each class.

The MLP model achieved a validation accuracy of 69%. For Class 1, the model showed a P of 0.84 and a R of 0.67, resulting in an F1-score of 0.75. The model performed moderately well in correctly identifying instances from Class 1. However, it exhibited

lower performance in distinguishing instances from Class 2, misclassifying 19% of them as Class 1, and instances from Class 3, misclassifying 13.7% of them as Class 1.

Comparatively, the LSTM model showcased superior performance compared to the MLP model, achieving a validation accuracy of 75.1%. For Class 1, the model demonstrated a P of 0.80, a R of 0.83, and an F1-score of 0.81, indicating a strong ability to correctly identify instances from Class 1. While the model faced challenges in distinguishing between Classes 2 and 3, it showed improved performance compared to the MLP model.

Lastly, the GRU model also demonstrated excellent performance, achieving a validation accuracy of 75.7%. For Class 1, the model exhibited a P of 0.78, a R of 0.86, and an F1-score of 0.82, indicating its proficiency in correctly classifying instances from Class 1. The model faced similar challenges as the LSTM model in distinguishing between Classes 2 and 3 but showcased improved performance compared to the MLP model.

In conclusion, the LSTM and GRU models demonstrated superior performance compared to the MLP model. This improvement can be attributed to the LSTM and GRU architectures' ability to effectively capture temporal dependencies present in the data. The use of the same dataset for all three models ensures a fair comparison, highlighting the strengths of the LSTM and GRU architectures in modeling time series data. These findings validate the significance of incorporating sophisticated recurrent neural network models for accurate and reliable predictions in our task.

The proposed non-intrusive IoT-based smart sensing system, which combines an VR application, IMU data, and ML algorithms, has the potential to significantly enhance physical rehabilitation efficacy. The system's ability to detect and analyze users' gait and physiological health characteristics in real-time provides invaluable insights to physical therapists and patients, allowing them to adapt their gait and posture during rehabilitation exercises.

By incorporating IMU data on the previous work mentioned in [**191**], the system can now capture more detailed information on the user's movements and orientations. This additional data, when combined with ML algorithms, enables the precise classification of user's balance in three levels. As a result, therapists can provide more targeted and personalized interventions to improve patients' gait and overall rehabilitation outcomes.

Furthermore, the system's use of real-time cloud database storage allows for the development of tailored analysis, which can be paired with essential metrics and graphics to

provide a report based on traditional physical rehabilitation reports. Overall, this system has the potential to improve physical therapy by shortening the time required by existing procedures, giving real-time feedback, and enabling a planned and organized approach to monitoring and improving users' health status and gait during rehabilitation exercises.

In the face of growing demand for healthcare services worldwide, innovative technologies like this non-intrusive IoT-based smart sensing system can play a crucial role in optimizing rehabilitation procedures and improving patient outcomes.

Several potential directions for future work can further enhance our system. Firstly, we plan to expand the number of participants in our experiments to validate the system's effectiveness on a larger sample size. Moreover, we intend to address limitations, such as movement artifacts and sensor floor capacitance characteristics, to increase the accuracy of our wearable sensing system. Another possible future approach is to include additional modalities, such as audio or visual feedback, to increase the patient's engagement with the rehabilitation exercises. Lastly, we seek to investigate the remote patient monitoring capabilities of our system, which could significantly increase access to physical therapy for individuals who are unable to attend in-person sessions.

CHAPTER 5

Conclusions and Future Work

This thesis investigated the integration of smart wearable sensing technologies, artificial intelligence, and interactive digital environments for applications in physiological monitoring, sports science, and physical rehabilitation. The research was motivated by the growing need for continuous, personalized, and non-invasive health assessment tools capable of operating outside controlled laboratory or clinical environments. To address this need, the work focused on two complementary research directions: the development of wearable and portable biosensing systems for real-time physiological monitoring, and the use of software-driven environments and machine learning techniques to interpret movement and rehabilitation-related data.

5.1. Conclusions

One of the primary outcomes of this thesis is the demonstration that compact, low-power electrochemical sensing platforms can be effectively designed for wearable operation while maintaining sufficient measurement fidelity for real-world use. Through the development and validation of the PotLink and MultiPot platforms, this work showed that miniaturized potentiostat architectures are capable of acquiring meaningful electrochemical signals and supporting wireless communication, embedded processing, and user interaction. Experimental comparisons with laboratory-grade instrumentation confirmed that, while some limitations exist in terms of resolution and long-term stability, the proposed platforms provide a viable foundation for wearable electrochemical sensing.

Building upon these hardware contributions, the AIDrated system demonstrated the feasibility of non-invasive hydration monitoring through sweat electrolyte analysis. By targeting sodium and potassium concentrations and combining these biochemical measurements with physiological context such as heart rate and heart rate variability, the system moved beyond traditional hydration assessment methods based on indirect or intermittent indicators. Controlled running and cycling experiments showed that relative variations in sweat electrolytes correlate with changes in hydration status and exercise intensity, supporting the relevance of these biomarkers for continuous monitoring.

Artificial intelligence played a central role in transforming raw sensor data into higher-level insights. The successful deployment of machine learning models on a smartwatch platform demonstrated the practicality of Edge AI for real-time physiological assessment without reliance on constant cloud connectivity. The proposed Graph Neural Network–based model proved effective in capturing relationships between multimodal physiological inputs and hydration-related patterns, enabling personalized recommendations that adapt to individual responses. These results directly address the research question concerning the effectiveness of machine learning for real-time feedback, showing that data-driven approaches can operate within the constraints of wearable devices.

In parallel, this thesis addressed rehabilitation-oriented sensing and analysis through the integration of floor-based position tracking, inertial sensing, and clinician-facing software tools. The SensFloor–IMU system provided a richer representation of gait and balance behavior than conventional single-sensor approaches. Machine learning models applied to this data confirmed that temporal architectures such as LSTM and GRU outperform static models, highlighting the importance of sequence modeling for locomotion analysis. The associated software infrastructure, including real-time dashboards and historical data visualization, demonstrated how sensing and analytics can be translated into tools that support clinical decision-making and patient monitoring.

Taken together, the results of this thesis provide partial but meaningful answers to the research questions posed at the outset. The work confirms that wearable smart sensors are feasible and capable of acquiring biologically and biomechanically relevant data, particularly when combined with appropriate signal conditioning and contextual information. It also demonstrates that machine learning techniques can effectively process this data to extract clinically relevant patterns and provide real-time feedback.

However, not all research questions could be fully answered within the scope of this thesis. In particular, questions related to long-term reliability, large-scale clinical validation, and direct comparison with established gold-standard clinical methods remain only partially addressed. While controlled experiments and proof-of-concept deployments provided strong evidence of feasibility, broader validation across diverse populations, environmental conditions, and clinical contexts is required to fully establish accuracy, generalizability, and clinical impact. Similarly, while the proposed systems show clear advantages in terms of continuity, personalization, and accessibility, a comprehensive evaluation

against traditional monitoring and rehabilitation methods would require longitudinal clinical trials beyond the timeframe of this work.

Overall, this thesis establishes a solid conceptual and technical foundation for intelligent health monitoring systems. It demonstrates how wearable biosensing, embedded and mobile computing, artificial intelligence, and interactive software environments can be integrated into cohesive platforms that support both physiological monitoring and rehabilitation assessment.

5.2. Future Work

The limitations identified in this research naturally define several directions for future work. A primary focus should be the long-term robustness and calibration stability of wearable biosensors. Future studies should investigate adaptive calibration strategies, improved sensor materials, and compensation techniques for factors such as sweat rate variability, temperature changes, and sensor drift. Addressing these challenges is essential for answering the research questions related to reliability and long-term feasibility more comprehensively.

Another important direction is large-scale validation. Expanding experimental studies to include larger and more diverse participant cohorts, longer monitoring periods, and a wider range of environmental and exercise conditions will be critical to establish generalizability. In both sports and rehabilitation contexts, future work should include systematic comparisons with gold-standard measurement techniques to quantify accuracy and clinical relevance.

From an artificial intelligence perspective, future research should focus on personalization and adaptability. Inter-individual variability remains a major challenge in physiological and biomechanical monitoring, and approaches such as Federated Learning offer promising solutions for building personalized models while preserving data privacy. These methods could directly address research questions related to personalized monitoring and management that were only partially explored in this thesis.

In the rehabilitation domain, future work should extend the use of virtual and extended reality technologies to enhance patient engagement and therapeutic outcomes. Integrating AR, MR, or VR elements into rehabilitation workflows could enable adaptive feedback, gamification, and more immersive training environments. Clinical studies involving patients with different pathologies and assistive devices are also required to

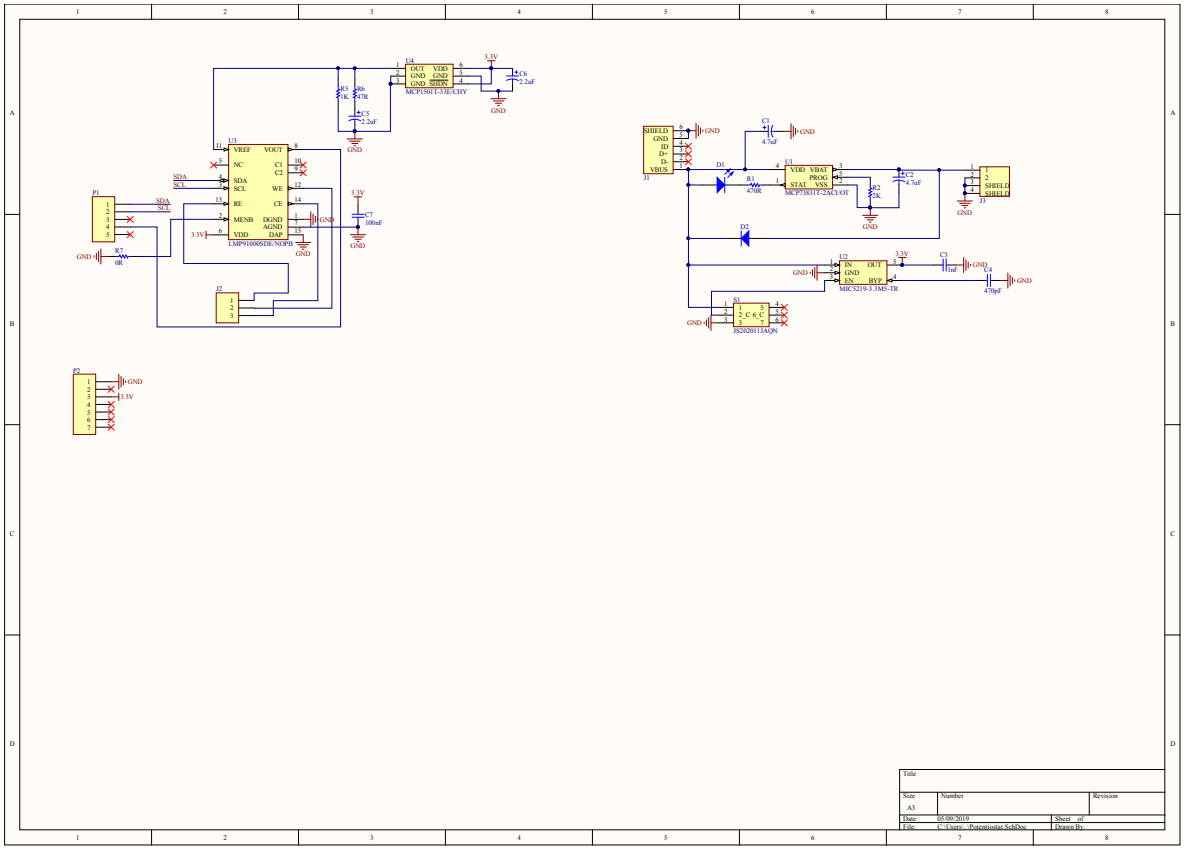
validate the robustness of the sensing and machine learning pipeline under real-world rehabilitation conditions.

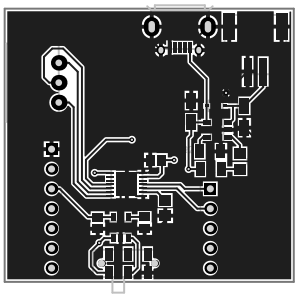
Finally, a long-term vision emerging from this work is the development of a unified closed-loop system that integrates physiological state monitoring and motor performance assessment. By jointly considering biochemical signals, cardiovascular response, and movement quality, future systems could adapt interventions in real-time based on both physiological readiness and functional capability. Such an approach would not only answer remaining research questions but also advance the field toward truly personalized and intelligent health monitoring solutions.

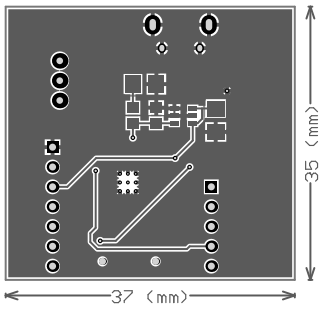
Appendices

APPENDIX A

Potlink Schematic and PCB


U3
OUT VDD
GND GND
GND SHDN
MCP1501T-33E/CHY
3.3V
2.2uF
R5
4.7K
R6
47R
C5
2.2uF
GND
U13
VREF VOUT
NC C1
C2
SDA SDA
SCL SCL
WE
RE CE
MENB DGND
AGND
VDD DAP
LMP91000SDE/NOPB
SDA
SCL
P1
R7
0R
C7
100nF
J2
P2
P-GND
3.3V
SHIELD
GND
ID
D+
D-
VBUS
J1
C1
4.7uF
D1
R1
470R
U1
VDD VBAT
PROG
STAT VSS
MCP73831T-2ACI/OT
R2
2K
C2
4.7uF
J3
SHIELD
SHIELD
D2
U2
IN OUT
GND
EN BYP
MIC5219-3.3M5-TR
C3
1nF
C4
470pF
J1
2_C_6_C
JS2020111AQN
Title
Size
A3
Number
Revision
Date: 05/09/2019
File: C:\Users\...\Potentiostat.SchDoc
Sheet of
Drawn By:

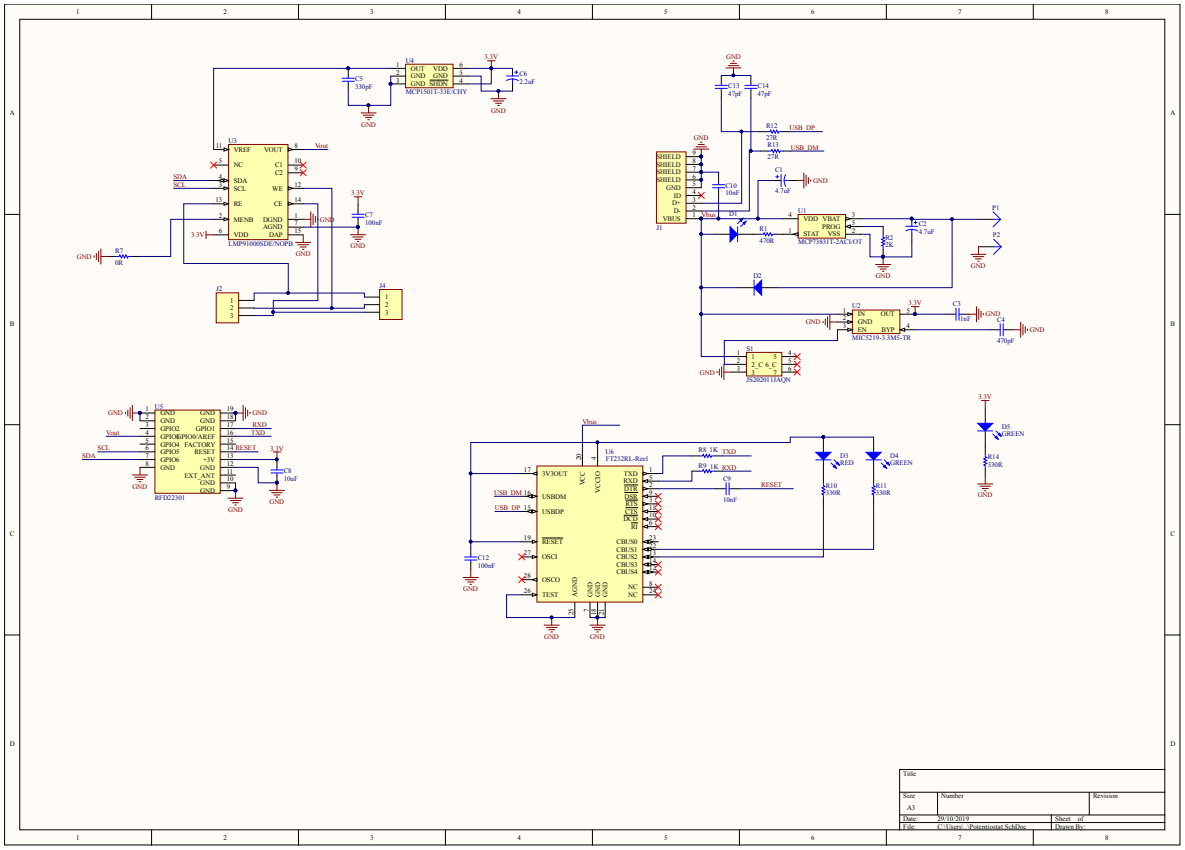


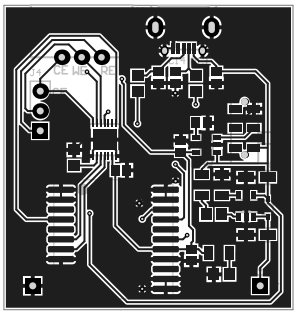

35 (mm)
37 (mm)

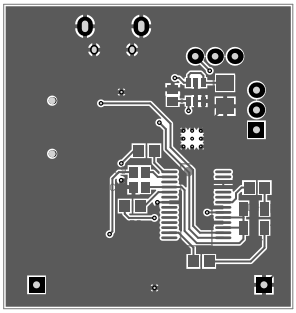
Comment	Description	Designator	Footprint	LibRef	Quantity	Value
Cap Pol1	Polarized Capacitor (Radial)	C1, C2	A	Cap Pol1	2	4.7uF
Cap	Capacitor	C3, C4, C7	C0805	Cap	3	1nF, 470pF, 100nF
Cap Pol1	Polarized Capacitor (Radial)	C5, C6	B	Cap Pol1	2	2.2uF
KP-3216EC (FC:8530025)	Typical INFRARED GaAs LED	D1	C1206	LED0	1	
Diode 1N4148	High Conductance Fast Diode	D2	SOD-323	Diode 1N4148	1	
Micro USB B Receptacle		J1	Micro_USB_B	Micro_USB_B	1	
Header 3	Header, 3-Pin	J2	SPE_Socket	Header 3	1	
S2B-PH-SM4-TB(LF)(SN)		J3	Connector_S2B-PH-SM4-TB(LF)(SN)	Connector_S2B_PH_SM4_TB	1	
Header 5	Header, 5-Pin	P1	HDR1X5	Header 5	1	
Header 7	Header, 7-Pin	P2	HDR1X7	Header 7	1	
Res1	Resistor	R1, R5, R6, R7	6-0805_M	Res1	4	470R, 1K, 47R, 0R
Res1	Resistor	R2	C1206	Res1	1	2K
JS202011JAQN		S1	JS202011JAQN	Switch_JS202011JAQN	1	
MCP73831T-2ACI/OT		U1	SOT-23-5	MCP73831T-2ACI/OT	1	
MIC5219-3.3M5-TR		U2	SOT-23-5	MIC5219-3.3YM5-TR	1	
LMP91000SDE/NOPB		U3	QFN14	LMP91000SDE/NOPB	1	
MCP1501T-33E/CHY		U4	SOT23-6	MCP1501T-33E/CHY	1	

APPENDIX B

NanoPotlink Schematic and PCB


MCP1501T-33E/CHY
LMP91000SDE/NOPB
MCP73831T-2AC1/OT
MIC5219-3.3MS-TR
JS202011JAQN
RFD22301
FT232RL-Reel
Title
Size
A3
Number
Revision
Date: 29/10/2019
File: C:\Users\...\Potentiostat.SchDoc
Sheet of
Drawn By:

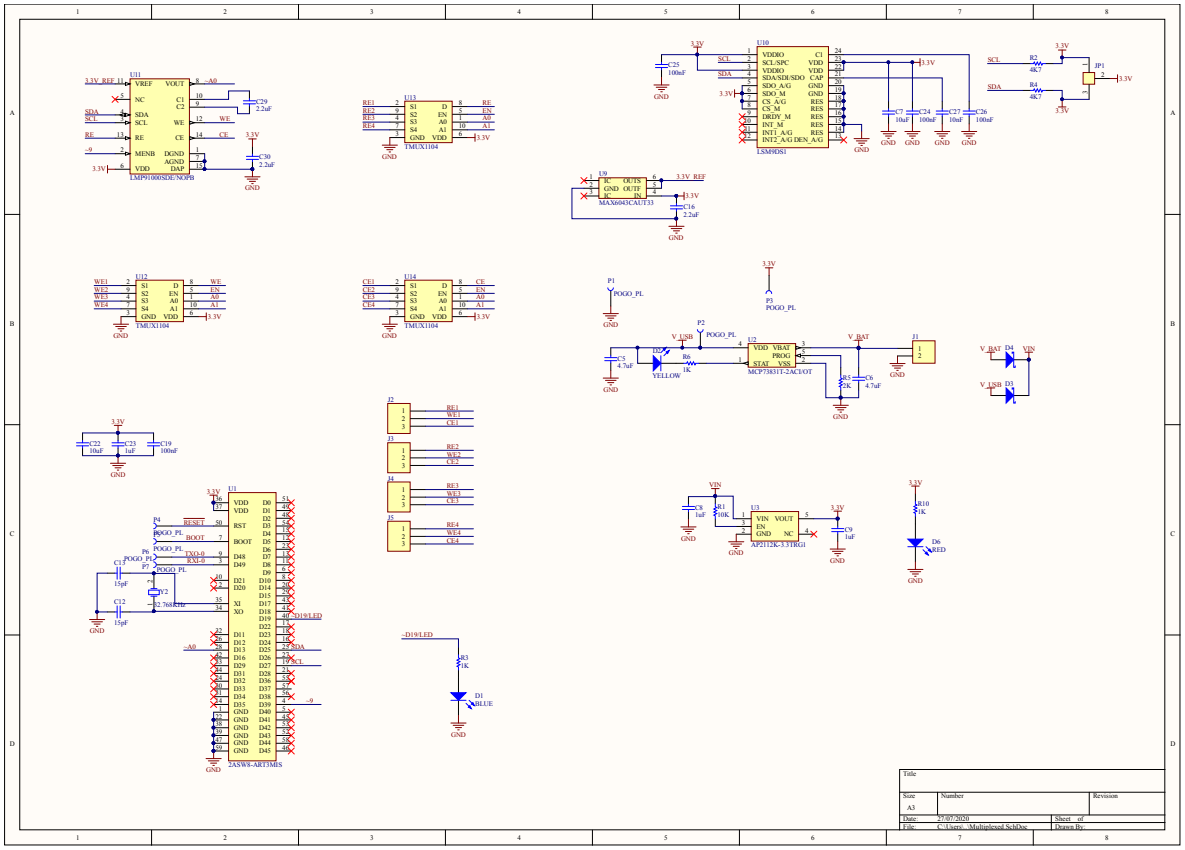


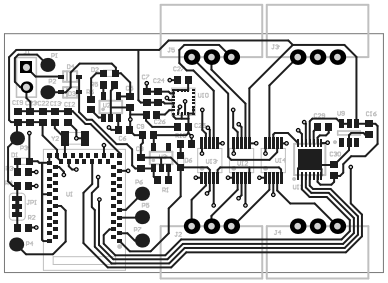


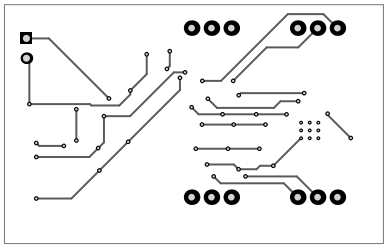
Comment	Description	Designator	Footprint	LibRef	Quantity
Cap Pol1	Polarized Capacitor (Radial)	C1, C2	A	Cap Pol1	2
Cap	Capacitor	C3, C4, C5, C7, C8, C9, C10, C12, C13, C14	C0805	Cap	10
Cap Pol1	Polarized Capacitor (Radial)	C6	B	Cap Pol1	1
KP-3216EC (FC:8530025)	Typical INFRARED GaAs LED	D1	C1206	LED0	1
Diode 1N4148	High Conductance Fast Diode	D2	SOD-323	Diode 1N4148	1
RED	Typical INFRARED GaAs LED	D3	C1206	LED0	1
GREEN	Typical INFRARED GaAs LED	D4, D5	C1206	LED0	2
Micro USB B Receptacle		J1	Micro_USB_B	Micro_USB_B	1
Header 3	Header, 3-Pin	J2	SPE_Socket	Header 3	1
Header 3	Header, 3-Pin	J4	HDR1X3	Header 3	1
Plug	Plug	P1, P2	PIN1	Plug	2
Res1	Resistor	R1, R7, R8, R9, R10, R11, R12, R13, R14	6-0805_M	Res1	9
Res1	Resistor	R2	C1206	Res1	1
JS202011JAQN		S1	JS202011JAQN	Switch_JS202011JAQN	1
MCP73831T-2ACI/OT		U1	SOT-23-5	MCP73831T-2ACI/OT	1
MIC5219-3.3M5-TR		U2	SOT-23-5	MIC5219-3.3YM5-TR	1
LMP91000SDE/NOPB		U3	QFN14	LMP91000SDE/NOPB	1
MCP1501T-33E/CHY		U4	SOT23-6	MCP1501T-33E/CHY	1
RFD22301		U5	RFD22301	RFD22301	1
FT232RL-Reel	USB UART Asynchronou	U6	SSOP-28_N	FT232RL-Reel	1

APPENDIX C

MultiPot platform V1.0 Schematic and PCB


U11
LMP91000SDE/NOPB
U13
TMUX1104
U12
TMUX1104
U14
TMUX1104
U10
LSM9DS1
U9
MAX6643CAUT33
U2
MCP73831T-2ACI/OT
U3
AP2112K-3.3TRG1
U1
LASW8-ART1MIS
J2
J3
J4
J5
P1
P2
P3
P4
P6
P7
D1
BLUE
D2
YELLOW
D5
RED
D6
RED
JP1
Title
Size
A3
Number
Revision
Date: 27/07/2020
File: C:\Users\...\Multiplexed.SchDoc
Sheet of
Drawn By:

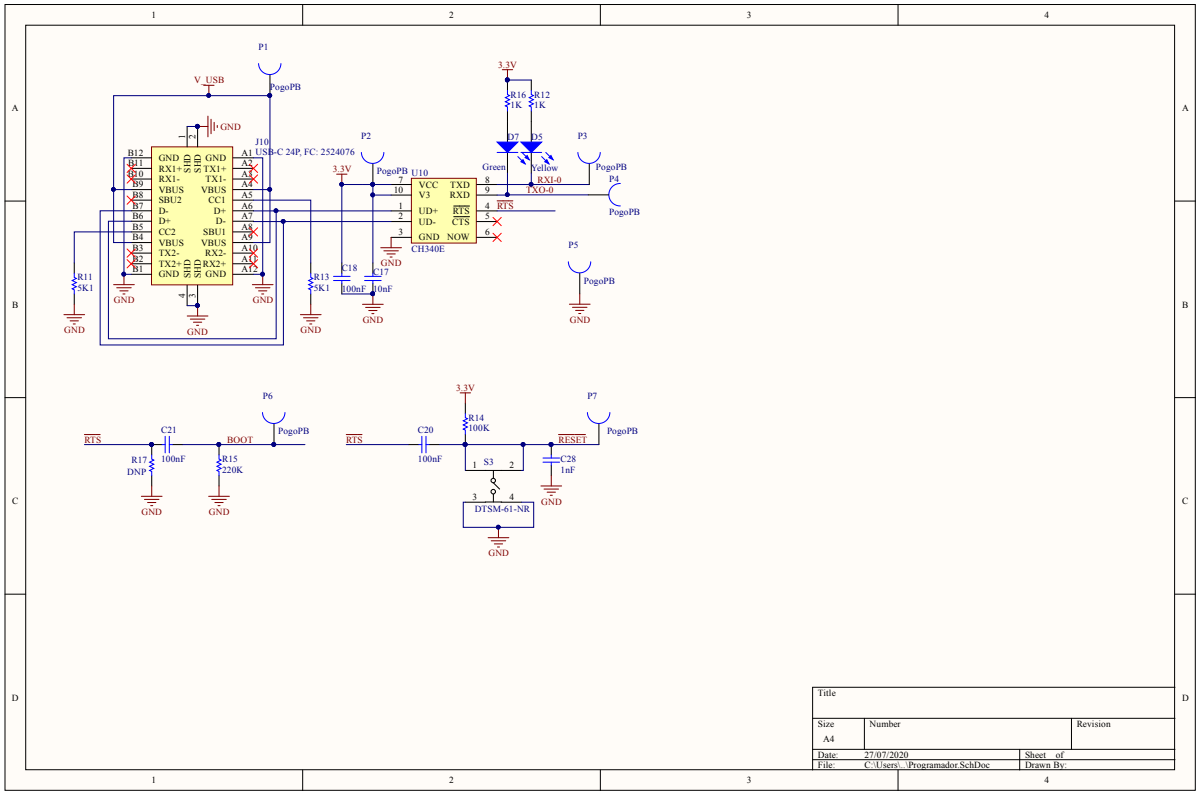


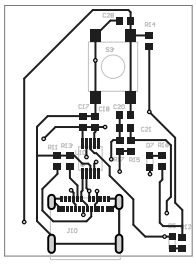


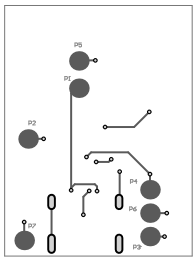
Comment	Description	Designator	Footprint	LibRef	Quantity
Cap	Capacitor	C5, C6, C7, C8, C9, C12, C13, C16, C19, C22, C23, C24, C25, C26, C27, C29, C30	1608[0603]	Cap	17
BLUE	Typical INFRARED GaAs LED	D1	0603 LED	LED0	1
YELLOW	Typical INFRARED GaAs LED	D2	0603 LED	LED0	1
Diode 11DQ03	Schottky Rectifier	D3, D4	SOD-323	Diode 11DQ03	2
RED	Typical INFRARED GaAs LED	D6	0603 LED	LED0	1
Header 2	Header, 2-Pin	J1	HDR1X2	Header 2	1
Header 3	Header, 3-Pin	J2, J3, J4, J5	SPE_Socket	Header 3	4
Jumper-SMT_3_2-NC_TRACE_SILK		JP1	SMT_Jumper_3_2	Jumper_SMT_3_2	1
POGO_PL		P1, P2, P3, P4, P5, P6, P7	POGO PIN LITLE	POGO PIN LITLE	7
Res1	Resistor	R1, R2, R3, R4, R5, R6, R10	1608[0603]	Res1	7
2ASW8-ART3MIS		U1	2ASW8-ART3MIS	2ASW8-ART3MIS	1
MCP73831T-2ACI/OT		U2	SOT-23-5	MCP73831T-2ACI/OT	1
AP2112K-3.3TRG1		U3	SOT-23-5	AP2112K-3.3TRG1	1
MAX6043CAUT33		U9	SOT23-6	MAX6043CAUT33	1
LSM9DS1		U10	LGA-24L	LSM9DS1	1
LMP91000SDE/NOPB		U11	QFN14	LMP91000SDE/NOPB	1
TMUX1104		U12, U13, U14	VSSOP10	TMUX1104	3
32.768KHz	Crystal Oscillator	Y2	CRYSTAL_ABS07AIG	XTAL	1

APPENDIX D

Multipot firmware programmer


P1
V_USB
PogoPB
GND
J10
USB-C 24P, FC: 2524076
B12 GND
B11 RX1+
B10 RX1-
B9 VBUS
B8 SBU2
B7 D-
B6 D+
B5 CC2
B4 VBUS
B3 TX2-
B2 TX2+
B1 GND
SHD
A1 GND
A2 TX1+
A3 TX1-
A4 VBUS
A5 CC1
A6 D+
A7 D-
A8 SBU1
A9 VBUS
A10 RX2-
A11 RX2+
A12 GND
R11 5K1
R13 5K1
C18 100nF
C17 100nF
P2
P3
P4
P5
U10
CH340E
VCC
V3
UD+
UD-
GND
TXD
RXD
RTS
CTS
NOW
3_3V
R16 1K
R12 1K
D7 Green
D5 Yellow
RXI-0
TXO-0
RTS
P6
P7
C21 100nF
R17 DNP
R15 220K
BOOT
C20 100nF
R14 100K
RESET
C28 1nF
S3
DTSM-61-NR
Title
Size A4
Number
Revision
Date: 27/07/2020
File: C:\Users\..\Programador.SchDoc
Sheet of
Drawn By:

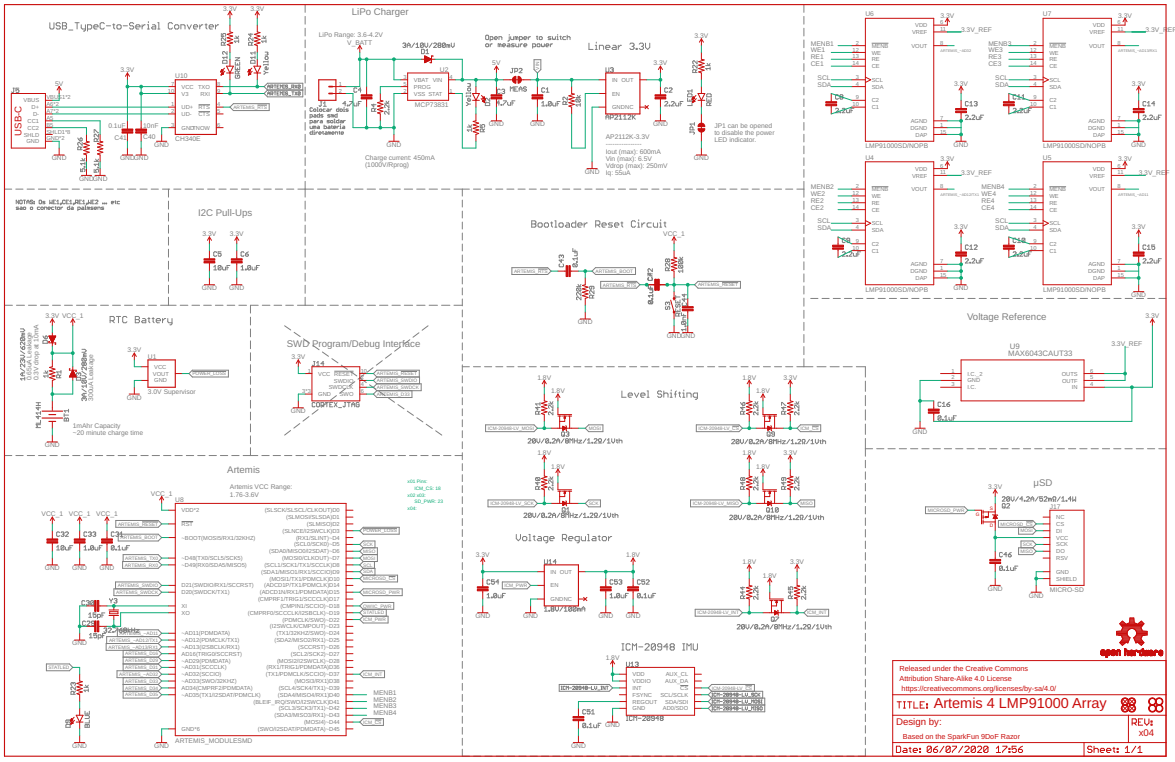



P5
P1
P2
P4
P6
P7
P3

Comment	Description	Designator	Footprint	LibRef	Quantity
Cap	Capacitor	C17, C18, C20, C21, C28	1608[0603]	Cap	5
Yellow	Typical INFRARED GaAs LED	D5	0603 LED	LED0	1
Green	Typical INFRARED GaAs LED	D7	0603 LED	LED0	1
USB-C 24P, FC: 2524076		J10	USB-C-24P	USB-C-24P	1
PogoPB		P1, P2, P3, P4, P5, P6, P7	POGO PIN BIG	POGO PIN BIG	7
Res1	Resistor	R11, R12, R13, R14, R15, R16	1608[0603]	Res1	6
DNP	Resistor	R17	1608[0603]	Res1	1
DTSM-61-NR		S3	Switch_B3FS1000P	SWITCHE_DTSM-61-NR	1
CH340E		U10	MSOP10	CH340E	1

APPENDIX E

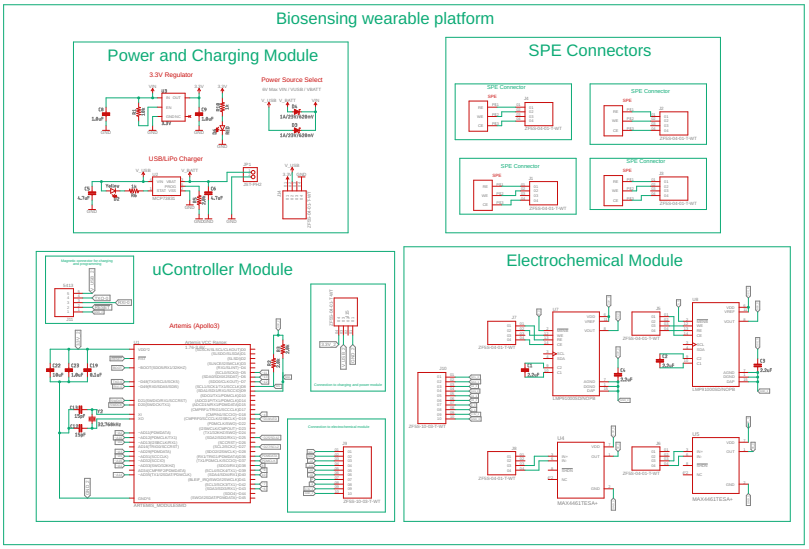
MultiPot platform V2.0 Schematic and PCB



06/07/2020 17:56 f=0.66 /Users/joaomonge/Documents/Projetos/IntelPot/Artemis_4LMP.sch (Sheet: 1/1)

APPENDIX F

AIDrated platform Schematic and PCB



2/10/25 10:45 PM f=0.45 /Users/joaomonge/Downloads/Prototype4_Schematic.pdf (Sheet: 1/1)

References

[1] "Global Strategy on Human Resources for Health: Workforce 2030: Reporting at Seventy-fifth World Health Assembly." [Online]. Available: https://www.who.int/news/item/02-06-2022-global-strategy-on-human-resources-for-health--workforce-2030

[2] M. W. Shrader, C. Church, N. Lennon, T. Shields, J. J. Salazar-Torres, J. J. Howard, and F. Miller, "Well-Being of Ambulatory Adults With Cerebral Palsy: Education, Employment, and Physical Function of a Cohort Who Received Specialized Pediatric Care," *Frontiers in Neurology*, vol. 12, 9 2021. [Online]. Available: https://doi.org/10.3389/fneur.2021.732906https://scite.ai/reports/well-being-of-ambulatory-adults-with-1Z6PODwX

[3] "World Population Prospects - Population Division - United Nations." [Online]. Available: https://population.un.org/wpp/

[4] "The Elderly Population Is Growing Rapidly." [Online]. Available: https://www.pgpf.org/chart-archive/0045_elderly-population-trends

[5] A. Bohr and K. Memarzadeh, "The rise of artificial intelligence in healthcare applications," in *Artificial Intelligence in Healthcare*. Elsevier, 2020, pp. 25–60.

[6] "Artificial intelligence in healthcare — Ideagen." [Online]. Available: https://www.ideagen.com/thought-leadership/blog/the-uk-s-new-approach-to-regulating-artificial-intelligence-in-healthcare

[7] D. R. Kalbande Professor, "Use of Internet of Things (IoT) in Healthcare : A Survey," 2016. [Online]. Available: http://dx.doi.org/10.1145/2909067.2909079

[8] M. Aapro, P. Bossi, A. Dasari, L. Fallowfield, P. Gascón, M. Geller, K. Jordan, J. Kim, K. Martin, and S. Porzig, "Digital health for optimal supportive care in oncology: benefits, limits, and future perspectives," *Supportive Care in Cancer*, vol. 28, no. 10, pp. 4589–4612, 10 2020.

[9] "(PDF) AI-Enhanced Strategies for Information Security: Safeguarding PHI in Government and Healthcare Sectors." [Online]. Available: https://www.researchgate.net/publication/383044025_AI-Enhanced_Strategies_for_Information_Security_Safeguarding_PHI_in_Government_and_Healthcare_Sectors

[10] E. Laurenza, M. Quintano, F. Schiavone, and D. Vrontis, "The effect of digital technologies adoption in healthcare industry: a case based analysis," *Business Process Management Journal*, vol. 24, no. 5, pp. 1124–1144, 8 2018.

[11] R. Natarajan, G. H. Lokesh, F. Flammini, A. Premkumar, V. K. Venkatesan, and S. K. Gupta, "A Novel Framework on Security and Energy Enhancement Based on Internet of Medical Things for Healthcare 5.0," *Infrastructures*, vol. 8, no. 2, 2 2023.

[12] E. Mbunge, B. Muchemwa, e. Jiyane, and J. Batani, "Sensors and healthcare 5.0: transformative shift in virtual care through emerging digital health technologies," *Global Health Journal journal homepage*, vol. 5, pp. 169–177, 2021.

[13] A. Rehman, S. Abbas, M. A. Khan, T. M. Ghazal, K. M. Adnan, and A. Mosavi, "A secure healthcare 5.0 system based on blockchain technology entangled with federated learning technique," *Computers in Biology and Medicine*, vol. 150, 11 2022.

[14] M. Bhavin, S. Tanwar, N. Sharma, S. Tyagi, and N. Kumar, "Blockchain and quantum blind signature-based hybrid scheme for healthcare 5.0 applications," *Journal of Information Security and Applications*, vol. 56, p. 102673, 2 2021.

[15] D. Formica and E. Schena, "Smart Sensors for Healthcare and Medical Applications," *Sensors*, vol. 21, no. 2, p. 543, 1 2021.

[16] P. Garatva, Y. Terhorst, E.-M. Messner, W. Karlen, R. Pryss, and H. Baumeister, "Smart Sensors for Health Research and Improvement." Springer, Cham, 2023, pp. 395–411. [Online]. Available: https://link.springer.com/10.1007/978-3-030-98546-2_23

[17] A. Fleury, M. Sugar, and T. Chau, "E-textiles in Clinical Rehabilitation: A Scoping Review," *Electronics*, vol. 4, no. 1, pp. 173–203, 5 2015. [Online]. Available: http://www.mdpi.com/2079-9292/4/1/173

[18] L. Buechley and M. Eisenberg, "Fabric PCBs, electronic sequins, and socket buttons: techniques for e-textile craft," *Personal and Ubiquitous Computing*, vol. 13, no. 2, pp. 133–150, 5 2009. [Online]. Available: http://link.springer.com/10.1007/s00779-007-0181-0

[19] A. Pantelopoulos and N. G. Bourbakis, "A Survey on Wearable Sensor-Based Systems for Health Monitoring and Prognosis," *IEEE Transactions on Systems, Man, and Cybernetics, Part C (Applications and Reviews)*, vol. 40, no. 1, pp. 1–12, 5 2010. [Online]. Available: http://ieeexplore.ieee.org/document/5306098/

[20] A. Akter, M. M. H. Apu, Y. R. Veeranki, T. N. Baroud, and H. F. Posada-Quintero, "Recent Studies on Smart Textile-Based Wearable Sweat Sensors for Medical Monitoring: A Systematic Review," *Journal of Sensor and Actuator Networks 2024, Vol. 13, Page 40*, vol. 13, no. 4, p. 40, 7 2024. [Online]. Available: https://www.mdpi.com/2224-2708/13/4/40/htmhttps://www.mdpi.com/2224-2708/13/4/40

[21] A. Steinhage and C. Lauterbach, "SensFloor® and NaviFloor®," *International Journal of Intelligent Mechatronics and Robotics*, vol. 3, no. 3, pp. 43–59, 5 2013. [Online]. Available: https://services.igi-global.com/resolvedoi/resolve.aspx?doi=10.4018/ijimr.2013070104

[22] A. H. Abdul Razak, A. Zayegh, R. K. Begg, and Y. Wahab, "Foot Plantar Pressure Measurement System: A Review," *Sensors*, vol. 12, no. 7, pp. 9884–9912, 2012. [Online]. Available: https://www.mdpi.com/1424-8220/12/7/9884

[23] J. Monge, O. Postolache, R. Alexandre, M. d. Fatima Domingues, P. Antunes, and V. Viegas, "Fiber Bragg Gratings Solution for Gait Assessement," in *2020 IEEE International Instrumentation and Measurement Technology Conference (I2MTC)*. IEEE, 5 2020, pp. 1–6. [Online]. Available: https://ieeexplore.ieee.org/document/9128421/

[24] D. Ferreira, R. Oliveira, and O. Postolache, "Physical rehabilitation based on kinect serious games," in *2017 Eleventh International Conference on Sensing Technology (ICST)*. IEEE, 5 2017, pp. 1–6. [Online]. Available: http://ieeexplore.ieee.org/document/8304512/

[25] N. Duarte, O. Postolache, and J. Scharcanski, "KSGphysio-Kinect serious game for physiotherapy," in *2014 International Conference and Exposition on Electrical and Power Engineering (EPE)*, 2014, pp. 606–611.

[26] M. Oudah, A. Al-Naji, and J. Chahl, "Hand gestures for elderly care using a microsoft Kinect," *Nano biomed. eng*, vol. 12, no. 3, pp. 197–204, 2020.

[27] C. Luca, R. Fuior, C. Corciovă, and D. Andri\c{t}oi, "Development of an Interactive Post-stroke Rehabilitation Tool based on Microsoft Kinect," in *2019 E-Health and Bioengineering Conference (EHB)*, 2019, pp. 1–4.

[28] C. M. Tseng, C. L. Lai, D. Erdenetsogt, and Y. F. Chen, "A Microsoft Kinect based virtual rehabilitation system," in *2014 International Symposium on Computer, Consumer and Control*, 2014, pp. 934–937.

[29] "Início Rápido – Configurar o controlo do corpo do Azure Kinect — Microsoft Learn." [Online]. Available: https://learn.microsoft.com/pt-pt/azure/kinect-dk/body-sdk-setup

[30] A. Papa, M. Mital, P. Pisano, and M. Del Giudice, "E-health and wellbeing monitoring using smart healthcare devices: An empirical investigation," *Technological Forecasting and Social Change*, vol. 153, p. 119226, 2020.

[31] "Mobile Sensing - movisens GmbH." [Online]. Available: https://www.movisens.com/en/solutions/mobile-sensing/

[32] D. J. Wile, R. Ranawaya, and Z. H. Kiss, "Smart watch accelerometry for analysis and diagnosis of tremor," *Journal of Neuroscience Methods*, vol. 230, pp. 1–4, 6 2014.

[33] C. Camara, P. Isasi, K. Warwick, V. Ruiz, T. Aziz, J. Stein, and E. Bakštein, "Resting tremor classification and detection in Parkinson's disease patients," *Biomedical Signal Processing and Control*, vol. 16, pp. 88–97, 2015.

[34] A. De, K. P. Bhatia, J. Volkmann, R. Peach, and S. R. Schreglmann, "Machine Learning in Tremor Analysis: Critique and Directions," *Movement Disorders*, vol. 38, no. 5, pp. 717–731, 5 2023.

[35] L. P. Sánchez-Fernández, L. A. Sánchez-Pérez, P. D. Concha-Gómez, and A. Shaout, "Kinetic tremor analysis using wearable sensors and fuzzy inference systems in Parkinson's disease," *Biomedical Signal Processing and Control*, vol. 84, 7 2023.

[36] J. Tran, R. Tran, and J. John R. White, "Smartphone-based glucose monitors and applications in the management of diabetes: an overview of 10 salient "apps" and a novel smartphone-connected blood glucose monitor," *Clinical Diabetes*, vol. 30, no. 4, pp. 173–179, 9 2012. [Online]. Available: https://go.gale.com/ps/i.do?p=HRCA&sw=w&issn=08918929&v=2.1&it=r&id=GALE%7CA307269853&sid=googleScholar&linkaccess=fulltexthttps://go.gale.com/ps/i.do?p=HRCA&sw=w&issn=08918929&v=2.1&it=r&id=GALE%7CA307269853&sid=googleScholar&linkaccess=abs

[37] K. S. Blondon, P. L. Hebert, and J. D. Ralston, "An Exploration of the Potential Reach of Smartphones in Diabetes," *AMIA Annual Symposium Proceedings*, vol. 2014, p. 289, 2014. [Online]. Available: /pmc/articles/PMC4419894//pmc/articles/PMC4419894/?report=abstracthttps://www.ncbi.nlm.nih.gov/pmc/articles/PMC4419894/

[38] A. P. Demidowich, K. Lu, R. Tamler, and Z. Bloomgarden, "An evaluation of diabetes self-management applications for Android smartphones," *http://dx.doi.org/10.1258/jtt.2012.111002*, vol. 18, no. 4, pp. 235–238, 5 2012. [Online]. Available: https://journals.sagepub.com/doi/abs/10.1258/jtt.2012.111002

[39] R. Avram, M. Ramsis, A. D. Cristal, V. Nathan, L. Zhu, J. Kim, J. Kuang, A. Gao, E. Vittinghoff, L. Rohdin-Bibby, S. Yogi, E. Seremet, V. Carp, F. Badilini, M. J. Pletcher, G. M. Marcus, D. Mortara, and J. E. Olgin, "Validation of an algorithm for continuous monitoring of atrial fibrillation using a consumer smartwatch," *Heart Rhythm*, vol. 18, no. 9, pp. 1482–1490, 9 2021.

[40] J. M. Bumgarner, C. T. Lambert, A. A. Hussein, D. J. Cantillon, B. Baranowski, K. Wolski, B. D. Lindsay, O. M. Wazni, and K. G. Tarakji, "Smartwatch Algorithm for Automated Detection of Atrial Fibrillation," *Journal of the American College of Cardiology*, vol. 71, no. 21, pp. 2381–2388, 5 2018.

[41] M. V. Perez, K. W. Mahaffey, H. Hedlin, J. S. Rumsfeld, A. Garcia, T. Ferris, V. Balasubramanian, A. M. Russo, A. Rajmane, L. Cheung, G. Hung, J. Lee, P. Kowey, N. Talati, D. Nag, S. E. Gummidipundi, A. Beatty, M. T. Hills, S. Desai, C. B. Granger, M. Desai, and M. P. Turakhia, "Large-Scale Assessment of a Smartwatch to Identify Atrial Fibrillation," *New England Journal of Medicine*, vol. 381, no. 20, pp. 1909–1917, 11 2019.

[42] T. Inui, H. Kohno, Y. Kawasaki, K. Matsuura, H. Ueda, Y. Tamura, M. Watanabe, Y. Inage, Y. Yakita, Y. Wakabayashi, and G. Matsumiya, "Use of a Smart Watch for Early Detection of Paroxysmal Atrial Fibrillation: Validation Study," *JMIR Cardio*, vol. 4, no. 1, 1 2020.

[43] S. Nazarian, K. Lam, A. Darzi, and H. Ashrafian, "Diagnostic accuracy of smartwatches for the detection of cardiac arrhythmia: Systematic review and meta-analysis," 2021.

[44] A. Schütze, N. Helwig, and T. Schneider, "Sensors 4.0 - Smart sensors and measurement technology enable Industry 4.0," *Journal of Sensors and Sensor Systems*, vol. 7, no. 1, pp. 359–371, 5 2018.

[45] K. Lee, "IEEE 1451: A standard in support of smart transducer networking," *Conference Record - IEEE Instrumentation and Measurement Technology Conference*, vol. 2, pp. 525–528, 2000.

[46] L. M. S. Do Nascimento, L. V. Bonfati, M. L. B. Freitas, J. J. A. Mendes Junior, H. V. Siqueira, and S. L. Stevan, "Sensors and Systems for Physical Rehabilitation and Health Monitoring—A Review," *Sensors 2020, Vol. 20, Page 4063*, vol. 20, no. 15, p. 4063, 7 2020. [Online]. Available: https://www.mdpi.com/1424-8220/20/15/4063/htmhttps://www.mdpi.com/1424-8220/20/15/4063

[47] M. M. Rodgers, G. Alon, V. M. Pai, and R. S. Conroy, "Wearable technologies for active living and rehabilitation: Current research challenges and future opportunities," *https://doi.org/10.1177/2055668319839607*, vol. 6, p. 205566831983960, 4 2019. [Online]. Available: https://journals.sagepub.com/doi/full/10.1177/2055668319839607

[48] C. E. Lang, J. Barth, C. L. Holleran, J. D. Konrad, and M. D. Bland, "Implementation of Wearable Sensing Technology for Movement: Pushing Forward into the Routine Physical Rehabilitation Care Field," *Sensors 2020, Vol. 20, Page 5744*, vol. 20, no. 20, p. 5744, 10 2020. [Online]. Available: https://www.mdpi.com/1424-8220/20/20/5744/htmhttps://www.mdpi.com/1424-8220/20/20/5744

[49] S. Ahn, J. Kim, B. Koo, and Y. Kim, "Evaluation of Inertial Sensor-Based Pre-Impact Fall Detection Algorithms Using Public Dataset," *Sensors 2019, Vol. 19, Page 774*, vol. 19, no. 4, p. 774, 2 2019. [Online]. Available: https://www.mdpi.com/1424-8220/19/4/774/htmhttps://www.mdpi.com/1424-8220/19/4/774

[50] P. Bet, P. C. Castro, and M. A. Ponti, "Fall detection and fall risk assessment in older person using wearable sensors: A systematic review," *International Journal of Medical Informatics*, vol. 130, p. 103946, 10 2019.

[51] M. R. Rahman, M. M. Islam, A. I. Pritom, and Y. Alsaawy, "ASRPH: Application Specific Routing Protocol for Health care," *Computer Networks*, vol. 197, p. 108273, 10 2021.

[52] L. Angelini, W. Hodgkinson, C. Smith, J. M. Dodd, B. Sharrack, C. Mazzà, and D. Paling, "Wearable sensors can reliably quantify gait alterations associated with disability in people with progressive multiple sclerosis in a clinical setting," *Journal of Neurology*, vol. 267, no. 10, pp. 2897–2909, 10 2020. [Online]. Available: https://link.springer.com/article/10.1007/s00415-020-09928-8

[53] F. Khoshmanesh, P. Thurgood, E. Pirogova, S. Nahavandi, and S. Baratchi, "Wearable sensors: At the frontier of personalised health monitoring, smart prosthetics and assistive technologies," *Biosensors and Bioelectronics*, vol. 176, p. 112946, 3 2021.

[54] Z. Bauer, A. Dominguez, E. Cruz, F. Gomez-Donoso, S. Orts-Escolano, and M. Cazorla, "Enhancing perception for the visually impaired with deep learning techniques and low-cost wearable sensors," *Pattern Recognition Letters*, vol. 137, pp. 27–36, 9 2020.

[55] T. G. Stavropoulos, A. Papastergiou, L. Mpaltadoros, S. Nikolopoulos, and I. Kompatsiaris, "IoT Wearable Sensors and Devices in Elderly Care: A Literature Review," *Sensors 2020, Vol. 20, Page 2826*, vol. 20, no. 10, p. 2826, 5 2020. [Online]. Available: https://www.mdpi.com/1424-8220/20/10/2826/htmhttps://www.mdpi.com/1424-8220/20/10/2826

[56] G. Marques, "Ambient Assisted Living and Internet of Things," *https://services.igi-global.com/resolvedoi/resolve.aspx?doi=10.4018/978-1-5225-7332-6.ch005*, pp. 100–115, 1 1. [Online]. Available: https://www.igi-global.com/chapter/ambient-assisted-living-and-internet-of-things/221284www.igi-global.com/chapter/ambient-assisted-living-and-internet-of-things/221284

[57] D. Loza-Matovelle, A. Verdugo, E. Zalama, and J. Gómez-García-Bermejo, "An Architecture for the Integration of Robots and Sensors for the Care of the Elderly in an Ambient Assisted Living Environment," *Robotics 2019, Vol. 8, Page 76*, vol. 8, no. 3, p. 76, 9 2019. [Online]. Available: https://www.mdpi.com/2218-6581/8/3/76/htmhttps://www.mdpi.com/2218-6581/8/3/76

[58] B. Ganesan, T. Gowda, A. Al-Jumaily, K. N. Fong, S. K. Meena, and R. K. Tong, "Ambient assisted living technologies for older adults with cognitive and physical impairments: A review,"

European Review for Medical and Pharmacological Sciences, vol. 23, no. 23, pp. 10 470–10 481, 1 2019. [Online]. Available: https://opus.lib.uts.edu.au/handle/10453/137559

[59] G. Cicirelli, R. Marani, A. Petitti, A. Milella, and T. D'orazio, "Ambient Assisted Living: A Review of Technologies, Methodologies and Future Perspectives for Healthy Aging of Population," *Sensors 2021, Vol. 21, Page 3549*, vol. 21, no. 10, p. 3549, 5 2021. [Online]. Available: https://www.mdpi.com/1424-8220/21/10/3549/htmhttps://www.mdpi.com/1424-8220/21/10/3549

[60] M. Kandil, F. AlAttar, R. Al-Baghdadi, and I. Damaj, "AmIE: An Ambient Intelligent Environment for Blind and Visually Impaired People," *EAI/Springer Innovations in Communication and Computing*, pp. 207–236, 2020. [Online]. Available: https://link.springer.com/chapter/10.1007/978-3-030-16450-8_9

[61] A. Sabil, M. Glos, A. GüNther, C. Schöbel, C. Veauthier, I. Fietze, and T. Penzel, "Comparison of Apnea Detection Using Oronasal Thermal Airflow Sensor, Nasal Pressure Transducer, Respiratory Inductance Plethysmography and Tracheal Sound Sensor," *Journal of Clinical Sleep Medicine*, vol. 15, no. 2, pp. 285–292, 2019. [Online]. Available: https://jcsm.aasm.org/doi/10.5664/jcsm.7634https://jcsm.aasm.org/

[62] P. Jagadev and L. I. Giri, "Non-contact monitoring of human respiration using infrared thermography and machine learning," *Infrared Physics & Technology*, vol. 104, p. 103117, 1 2020.

[63] Z. Li, F. Liu, W. Yang, S. Peng, and J. Zhou, "A Survey of Convolutional Neural Networks: Analysis, Applications, and Prospects," *IEEE Transactions on Neural Networks and Learning Systems*, vol. 33, no. 12, pp. 6999–7019, 5 2022. [Online]. Available: https://ieeexplore.ieee.org/document/9451544/

[64] J. He, S. Li, X. Hou, Y. Zhou, H. Li, M. Cui, T. Guo, X. Wang, J. Mu, W. Geng, and X. Chou, "A non-contact flexible pyroelectric sensor for wireless physiological monitoring system," *Science China Information Sciences*, vol. 65, no. 2, pp. 1–11, 2 2022. [Online]. Available: https://link.springer.com/article/10.1007/s11432-020-3175-6

[65] R. De Fazio, M. Stabile, M. De Vittorio, R. Velázquez, and P. Visconti, "An Overview of Wearable Piezoresistive and Inertial Sensors for Respiration Rate Monitoring," *Electronics 2021, Vol. 10, Page 2178*, vol. 10, no. 17, p. 2178, 9 2021. [Online]. Available: https://www.mdpi.com/2079-9292/10/17/2178/htmhttps://www.mdpi.com/2079-9292/10/17/2178

[66] W. Wang and A. C. den Brinker, "Camera-based respiration monitoring: Motion and PPG-based measurement," *Contactless Vital Signs Monitoring*, pp. 79–97, 1 2022.

[67] G. Schifino, V. Cimolin, M. Pau, M. J. da Cunha, B. Leban, M. Porta, M. Galli, and A. S. Pagnussat, "Functional Electrical Stimulation for Foot Drop in Post-Stroke People: Quantitative Effects on Step-to-Step Symmetry of Gait Using a Wearable Inertial Sensor," *Sensors 2021, Vol. 21, Page 921*, vol. 21, no. 3, p. 921, 1 2021. [Online]. Available: https://www.mdpi.com/1424-8220/21/3/921/htmhttps://www.mdpi.com/1424-8220/21/3/921

[68] S. Díaz, J. B. Stephenson, and M. A. Labrador, "Use of wearable sensor technology in gait, balance, and range of motion analysis," 2020.

[69] A. Zampogna, I. Mileti, E. Palermo, C. Celletti, M. Paoloni, A. Manoni, I. Mazzetta, G. D. Costa, C. Pérez-López, F. Camerota, L. Leocani, J. Cabestany, F. Irrera, and A. Suppa, "Fifteen Years of Wireless Sensors for Balance Assessment in Neurological Disorders," *Sensors 2020, Vol. 20, Page 3247*, vol. 20, no. 11, p. 3247, 6 2020. [Online]. Available: https://www.mdpi.com/1424-8220/20/11/3247/htmhttps://www.mdpi.com/1424-8220/20/11/3247

[70] H. Schmidt, C. Werner, R. Bernhardt, S. Hesse, and J. Krüger, "Gait rehabilitation machines based on programmable footplates," *Journal of NeuroEngineering and Rehabilitation*, vol. 4, no. 1, pp. 1–7, 2 2007. [Online]. Available: https://jneuroengrehab.biomedcentral.com/articles/10.1186/1743-0003-4-2

[71] T. Mikolajczyk, I. Ciobanu, D. I. Badea, A. Iliescu, S. Pizzamiglio, T. Schauer, T. Seel, P. L. Seiciu, D. L. Turner, and M. Berteanu, "Advanced technology for gait rehabilitation: An overview," *https://doi.org/10.1177/1687814018783627*, vol. 10, no. 7, 7 2018. [Online]. Available: https://journals.sagepub.com/doi/full/10.1177/1687814018783627

[72] B. Milosevic, A. Leardini, and E. Farella, "Kinect and wearable inertial sensors for motor rehabilitation programs at home: State of the art and an experimental comparison," *BioMedical Engineering Online*, vol. 19, no. 1, pp. 1–26, 4 2020. [Online]. Available: https://link.springer.com/articles/10.1186/s12938-020-00762-7https://link.springer.com/article/10.1186/s12938-020-00762-7

[73] L. Bavan, K. Surmacz, D. Beard, S. Mellon, and J. Rees, "Adherence monitoring of rehabilitation exercise with inertial sensors: A clinical validation study," *Gait & Posture*, vol. 70, pp. 211–217, 5 2019.

[74] P. Picerno, M. Iosa, C. D'Souza, M. G. Benedetti, S. Paolucci, and G. Morone, "Wearable inertial sensors for human movement analysis: a five-year update," *https://doi.org/10.1080/17434440.2021.1988849*, vol. 18, no. sup1, pp. 79–94, 2021. [Online]. Available: https://www.tandfonline.com/doi/abs/10.1080/17434440.2021.1988849

[75] C. El-Hajj and P. A. Kyriacou, "Deep learning models for cuffless blood pressure monitoring from PPG signals using attention mechanism," *Biomedical Signal Processing and Control*, vol. 65, p. 102301, 3 2021.

[76] V. P. Rachim and W. Y. Chung, "Wearable-band type visible-near infrared optical biosensor for non-invasive blood glucose monitoring," *Sensors and Actuators B: Chemical*, vol. 286, pp. 173–180, 5 2019.

[77] K. Kario, "Management of Hypertension in the Digital Era," *Hypertension*, vol. 76, no. 3, pp. 640–650, 9 2020. [Online]. Available: https://www.ahajournals.org/doi/abs/10.1161/HYPERTENSIONAHA.120.14742

[78] D. Djeldjli, F. Bousefsaf, C. Maaoui, F. Bereksi-Reguig, and A. Pruski, "Remote estimation of pulse wave features related to arterial stiffness and blood pressure using a camera," *Biomedical Signal Processing and Control*, vol. 64, p. 102242, 2 2021.

[79] L. Tang, S. J. Chang, C. J. Chen, and J. T. Liu, "Non-Invasive Blood Glucose Monitoring Technology: A Review," *Sensors 2020, Vol. 20, Page 6925*, vol. 20, no. 23,

p. 6925, 12 2020. [Online]. Available: https://www.mdpi.com/1424-8220/20/23/6925/htmhttps://www.mdpi.com/1424-8220/20/23/6925

[80] T. Battelino, C. M. Alexander, S. A. Amiel, G. Arreaza-Rubin, R. W. Beck, R. M. Bergenstal, B. A. Buckingham, J. Carroll, A. Ceriello, E. Chow, P. Choudhary, K. Close, T. Danne, S. Dutta, R. Gabbay, S. Garg, J. Heverly, I. B. Hirsch, T. Kader, J. Kenney, B. Kovatchev, L. Laffel, D. Maahs, C. Mathieu, D. Mauricio, R. Nimri, R. Nishimura, M. Scharf, S. Del Prato, E. Renard, J. Rosenstock, B. Saboo, K. Ueki, G. E. Umpierrez, S. A. Weinzimer, and M. Phillip, "Continuous glucose monitoring and metrics for clinical trials: an international consensus statement," *The Lancet Diabetes & Endocrinology*, vol. 11, no. 1, pp. 42–57, 1 2023. [Online]. Available: http://www.thelancet.com/article/S2213858722003199/fulltexthttp://www.thelancet.com/article/S2213858722003199/abstracthttps://www.thelancet.com/journals/landia/article/PIIS2213-8587(22)00319-9/abstract

[81] J. R. Sempionatto, J. M. Moon, and J. Wang, "Touch-Based Fingertip Blood-Free Reliable Glucose Monitoring: Personalized Data Processing for Predicting Blood Glucose Concentrations," *ACS Sensors*, vol. 6, no. 5, pp. 1875–1883, 5 2021. [Online]. Available: https://pubs.acs.org/doi/abs/10.1021/acssensors.1c00139

[82] L. M. Laffel, L. G. Kanapka, R. W. Beck, K. Bergamo, M. A. Clements, A. Criego, D. J. Desalvo, R. Goland, K. Hood, D. Liljenquist, L. H. Messer, R. Monzavi, T. J. Mouse, P. Prahalad, J. Sherr, J. H. Simmons, R. P. Wadwa, R. S. Weinstock, S. M. Willi, and K. M. Miller, "Effect of Continuous Glucose Monitoring on Glycemic Control in Adolescents and Young Adults With Type 1 Diabetes: A Randomized Clinical Trial," *JAMA*, vol. 323, no. 23, pp. 2388–2396, 6 2020. [Online]. Available: https://jamanetwork.com/journals/jama/fullarticle/2767160

[83] R. J. Galindo, G. Aleppo, D. C. Klonoff, E. K. Spanakis, S. Agarwal, P. Vellanki, D. E. Olson, G. E. Umpierrez, G. M. Davis, and F. J. Pasquel, "Implementation of Continuous Glucose Monitoring in the Hospital: Emergent Considerations for Remote Glucose Monitoring During the COVID-19 Pandemic," *Journal of Diabetes Science and Technology*, vol. 14, no. 4, pp. 822–832, 7 2020. [Online]. Available: https://journals.sagepub.com/doi/full/10.1177/1932296820932903

[84] Z. Mian, K. L. Hermayer, and A. Jenkins, "Continuous Glucose Monitoring: Review of an Innovation in Diabetes Management," *The American Journal of the Medical Sciences*, vol. 358, no. 5, pp. 332–339, 11 2019.

[85] I. Lee, D. Probst, D. Klonoff, and K. Sode, "Continuous glucose monitoring systems - Current status and future perspectives of the flagship technologies in biosensor research -," *Biosensors and Bioelectronics*, vol. 181, p. 113054, 6 2021.

[86] W. V. Gonzales, A. T. Mobashsher, and A. Abbosh, "The Progress of Glucose Monitoring—A Review of Invasive to Minimally and Non-Invasive Techniques, Devices and Sensors," *Sensors 2019, Vol. 19, Page 800*, vol. 19, no. 4, p. 800, 2 2019. [Online]. Available: https://www.mdpi.com/1424-8220/19/4/800/htmhttps://www.mdpi.com/1424-8220/19/4/800

[87] J. Zhao, Y. Lin, J. Wu, H. Y. Y. Nyein, M. Bariya, L. C. Tai, M. Chao, W. Ji, G. Zhang, Z. Fan, and A. Javey, "A Fully Integrated and Self-Powered Smartwatch for Continuous Sweat

Glucose Monitoring," *ACS Sensors*, vol. 4, no. 7, pp. 1925–1933, 7 2019. [Online]. Available: https://pubs.acs.org/doi/full/10.1021/acssensors.9b00891

[88] "Eccrine Systems raises $5.5M, hopes to make sweat sensing the next big thing in wearables — MobiHealthNews." [Online]. Available: https://www.mobihealthnews.com/content/eccrine-systems-raises-55m-hopes-make-sweat-sensing-next-big-thing-wearables

[89] K. K. Yeung, T. Huang, Y. Hua, K. Zhang, M. M. Yuen, and Z. Gao, "Recent Advances in Electrochemical Sensors for Wearable Sweat Monitoring: A Review," *IEEE Sensors Journal*, vol. 21, no. 13, pp. 14 522–14 539, 7 2021.

[90] H. Zafar, A. Channa, V. Jeoti, and G. M. Stojanović, "Comprehensive Review on Wearable Sweat-Glucose Sensors for Continuous Glucose Monitoring," *Sensors 2022, Vol. 22, Page 638*, vol. 22, no. 2, p. 638, 1 2022. [Online]. Available: https://www.mdpi.com/1424-8220/22/2/638/htmhttps://www.mdpi.com/1424-8220/22/2/638

[91] Y. Lu, K. Jiang, D. Chen, and G. Shen, "Wearable sweat monitoring system with integrated micro-supercapacitors," *Nano Energy*, vol. 58, pp. 624–632, 4 2019.

[92] Y. Gai, E. Wang, M. Liu, L. Xie, Y. Bai, Y. Yang, J. Xue, X. Qu, Y. Xi, L. Li, D. Luo, and Z. Li, "A Self-Powered Wearable Sensor for Continuous Wireless Sweat Monitoring," *Small Methods*, vol. 6, no. 10, p. 2200653, 10 2022. [Online]. Available: https://onlinelibrary.wiley.com/doi/full/10.1002/smtd.202200653https://onlinelibrary.wiley.com/doi/abs/10.1002/smtd.202200653https://onlinelibrary.wiley.com/doi/10.1002/smtd.202200653

[93] L. C. Tai, W. Gao, M. Chao, M. Bariya, Q. P. Ngo, Z. Shahpar, H. Y. Nyein, H. Park, J. Sun, Y. Jung, E. Wu, H. M. Fahad, D. H. Lien, H. Ota, G. Cho, and A. Javey, "Methylxanthine Drug Monitoring with Wearable Sweat Sensors," *Advanced Materials*, vol. 30, no. 23, p. 1707442, 6 2018. [Online]. Available: https://onlinelibrary.wiley.com/doi/full/10.1002/adma.201707442https://onlinelibrary.wiley.com/doi/abs/10.1002/adma.201707442https://onlinelibrary.wiley.com/doi/10.1002/adma.201707442

[94] F. Mazzara, B. Patella, C. D'agostino, M. G. Bruno, S. Carbone, F. Lopresti, G. Aiello, C. Torino, A. Vilasi, A. O'riordan, and R. Inguanta, "Pani-based wearable electrochemical sensor for ph sweat monitoring," *Chemosensors*, vol. 9, no. 7, p. 169, 7 2021. [Online]. Available: https://www.mdpi.com/2227-9040/9/7/169/htmhttps://www.mdpi.com/2227-9040/9/7/169

[95] W. Dang, L. Manjakkal, W. T. Navaraj, L. Lorenzelli, V. Vinciguerra, and R. Dahiya, "Stretchable wireless system for sweat pH monitoring," *Biosensors and Bioelectronics*, vol. 107, pp. 192–202, 6 2018.

[96] L. Gao, G. Zheng, M. Yang, N. Sun, X. Lai, Y. Li, X. Zhao, J. Wu, and W. Zhou, "Screen-Printed Wearable Sweat Sensor for Cost-Effective Assessment of Human Hydration Status through Potassium and Sodium Ion Detection," *Micromachines 2023, Vol. 14, Page 1497*, vol. 14, no. 8, p. 1497, 7 2023. [Online]. Available: https://www.mdpi.com/2072-666X/14/8/1497/htmhttps://www.mdpi.com/2072-666X/14/8/1497

[97] K. M. Stanney and J. V. Cohn, "VIRTUAL ENVIRONMENTS," *Human-Computer Interaction: Design Issues, Solutions, and Applications*, pp. 293–310, 1 2009.

[Online]. Available: https://www.taylorfrancis.com/chapters/edit/10.1201/9781420088861-20/virtual-environments-kay-stanney-joseph-cohn

[98] J. Carmigniani and B. Furht, "Augmented Reality: An Overview," in *Handbook of Augmented Reality*. New York, NY: Springer New York, 2011, pp. 3–46.

[99] M. Speicher, B. D. Hall, and M. Nebeling, "What is Mixed Reality?" in *Proceedings of the 2019 CHI Conference on Human Factors in Computing Systems*. New York, NY, USA: ACM, 5 2019, pp. 1–15.

[100] C. Anthes, R. J. García-Hernández, M. Wiedemann, and D. Kranzlmüller, "State of the art of virtual reality technology," *IEEE Aerospace Conference Proceedings*, vol. 2016-June, 6 2016.

[101] F. Kern, C. Winter, D. Gall, I. Käthner, P. Pauli, and M. E. Latoschik, "Immersive virtual reality and gamification within procedurally generated environments to increase motivation during gait rehabilitation," in *2019 IEEE Conference on Virtual Reality and 3D User Interfaces (VR)*, 2019, pp. 500–509.

[102] Y. Jin, "Augmented reality system with application in physical rehabilitation," Ph.D. dissertation, 2019.

[103] J. Monge and O. Postolache, "Augmented Reality and Smart Sensors for Physical Rehabilitation," in *EPE 2018 - Proceedings of the 2018 10th International Conference and Expositions on Electrical And Power Engineering*, 2018.

[104] T. Paredes, O. Postolache, J. Monge, and P. Girao, "Gait rehabilitation system based on mixed reality," in *2021 Telecoms Conference, ConfTELE 2021*, 2021.

[105] P. M. Emmelkamp and K. Meyerbröker, "Virtual Reality Therapy in Mental Health," *https://doi.org/10.1146/annurev-clinpsy-081219-115923*, vol. 17, pp. 495–519, 5 2021. [Online]. Available: https://www.annualreviews.org/doi/abs/10.1146/annurev-clinpsy-081219-115923

[106] M. Ma and H. Zheng, "No Title," pp. 169–192, 2011. [Online]. Available: http://link.springer.com/10.1007/978-3-642-17824-5_9

[107] R. Alexandre, O. Postolache, and P. S. Girao, "Physical Rehabilitation based on Smart Wearable and Virtual Reality Serious Game," in *2019 IEEE International Instrumentation and Measurement Technology Conference (I2MTC)*. IEEE, 5 2019, pp. 1–6. [Online]. Available: https://ieeexplore.ieee.org/document/8826947/

[108] O. Postolache, J. Monge, R. Alexandre, O. Geman, Y. Jin, and G. Postolache, "Virtual Reality and Augmented Reality Technologies for Smart Physical Rehabilitation," in *Smart Sensors, Measurement and Instrumentation*, 2021, vol. 39, pp. 155–180. [Online]. Available: https://link.springer.com/10.1007/978-3-030-71221-1_8

[109] P. Tamayo-Serrano, S. Garbaya, S. Bouakaz, and P. Blazevic, "A game-based rehabilitation therapy for post-stroke patients: An approach for improving patient motivation and engagement," *IEEE Systems, Man, and Cybernetics Magazine*, vol. 6, no. 4, pp. 54–62, 2020.

[110] B. Zhang, D. Li, Y. Liu, J. Wang, and Q. Xiao, "Virtual reality for limb motor function, balance, gait, cognition and daily function of stroke patients: A systematic review and meta-analysis," *Journal of advanced nursing*, vol. 77, no. 8, pp. 3255–3273, 2021.

[111] Y. Jin, J. Monge, O. Postolache, and W. Niu, "Augmented Reality with Application in Physical Rehabilitation," in *2019 International Conference on Sensing and Instrumentation in IoT Era (ISSI)*. IEEE, 5 2019, pp. 1–6. [Online]. Available: https://ieeexplore.ieee.org/document/9043665/

[112] O. Postolache, L. Teixeira, J. Cordeiro, L. Lima, P. Arriaga, M. Rodrigues, and P. Girão, "Tailored virtual reality for smart physiotherapy," in *2019 11th International Symposium on Advanced Topics in Electrical Engineering (ATEE)*, 2019, pp. 1–6.

[113] R. Alexandre, O. Postolache, and P. S. Girão, "Physical rehabilitation based on smart wearable and virtual reality serious game," in *2019 IEEE international instrumentation and measurement technology conference (I2MTC)*, 2019, pp. 1–6.

[114] M. Gumaa and A. Rehan Youssef, "Is Virtual Reality Effective in Orthopedic Rehabilitation? A Systematic Review and Meta-Analysis," *Physical Therapy*, vol. 99, no. 10, pp. 1304–1325, 5 2019. [Online]. Available: https://academic.oup.com/ptj/article/99/10/1304/5537309

[115] R. N. Madeira, L. Costa, and O. Postolache, "PhysioMate - Pervasive physical rehabilitation based on NUI and gamification," in *2014 International Conference and Exposition on Electrical and Power Engineering (EPE)*. IEEE, 5 2014, pp. 612–616. [Online]. Available: http://ieeexplore.ieee.org/document/6969982/

[116] D. Ferreira, R. Oliveira, and O. Postolache, "Physical rehabilitation based on kinect serious games," in *2017 Eleventh international conference on sensing technology (ICST)*, 2017, pp. 1–6.

[117] J. Monge and O. Postolache, "Augmented Reality and Smart Sensors for Physical Rehabilitation," in *EPE 2018 - Proceedings of the 2018 10th International Conference and Expositions on Electrical And Power Engineering*, 2018.

[118] T. V. Paredes, O. Postolache, J. Monge, and P. S. Girao, "Gait Rehabilitation System based on Mixed Reality," in *2021 Telecoms Conference (ConfTELE)*. IEEE, 5 2021, pp. 1–6. [Online]. Available: https://ieeexplore.ieee.org/document/9435458/

[119] G. Hu, W. Wang, B. Chen, H. Zhi, Yudi Li, Y. Shen, and K. Wang, "Concurrent validity of evaluating knee kinematics using Kinect system during rehabilitation exercise," *Medicine in Novel Technology and Devices*, vol. 11, p. 100068, 9 2021.

[120] M. Wochatz, N. Tilgner, S. Mueller, S. Rabe, S. Eichler, M. John, H. Völler, and F. Mayer, "Reliability and validity of the Kinect V2 for the assessment of lower extremity rehabilitation exercises," *Gait & Posture*, vol. 70, pp. 330–335, 5 2019.

[121] T. B. Xavier-Rocha, L. Carneiro, G. C. Martins, G. d. B. Vilela, R. P. Passos, C. C. B. Pupe, O. J. M. d. Nascimento, D. S. A. Haikal, and R. S. Monteiro, "The Xbox/Kinect use in poststroke rehabilitation settings: a systematic review," *Arquivos de Neuro-Psiquiatria*, vol. 78, no. 7, pp. 361–369, 6 2020. [Online]. Available: https://www.scielo.br/j/anp/a/THT84snJgk8DgRpcrfCdn5z/?lang=en

[122] A. Aguilera-Rubio, I. M. Alguacil-Diego, A. Mallo-López, and A. Cuesta-Gomez, "Use of the Leap Motion Controller® System in the Rehabilitation of the Upper Limb in Stroke. A Systematic Review," *Journal of Stroke and Cerebrovascular Diseases*, vol. 31, no. 1, p. 106174, 1 2022.

[123] M. N. Ogun, R. Kurul, M. F. Yasar, S. A. Turkoglu, S. Avci, and N. Yildiz, "Effect of Leap Motion-based 3D Immersive Virtual Reality Usage on Upper Extremity Function in Ischemic Stroke Patients," *Arquivos de Neuro-Psiquiatria*, vol. 77, no. 10, pp. 681–688, 10 2019. [Online]. Available: https://www.scielo.br/j/anp/a/LX8RSmhypcBFxW6HmJmfpHc/?lang=en

[124] Q. Wang, B. Kang, and P. O. Kristensson, "Supporting Playful Rehabilitation in the Home using Virtual Reality Headsets and Force Feedback Gloves," *Proceedings - 2022 IEEE Conference on Virtual Reality and 3D User Interfaces, VR 2022*, pp. 504–513, 2022.

[125] Y. Tokuyama, R. P. Rajapakse, S. Yamabe, K. Konno, and Y. P. Hung, "A kinect-based augmented reality game for lower limb exercise," *Proceedings - 2019 International Conference on Cyberworlds, CW 2019*, pp. 399–402, 10 2019.

[126] P.-H. Chien and Y.-C. Lin, "GESTURE-BASED HEAD-MOUNTED AUGMENTED REALITY GAME DEVELOPMENT USING LEAP MOTION AND USABILITY EVALUATION," 2021.

[127] M. Alnajjar, A. Abutabikh, A. Issa, M. Debeljak, and I. Cikajlo, "Development of 3D exergame for upper limbs rehabilitation using leap motion controller and unity," *Proceedings - 2020 International Conference on Assistive and Rehabilitation Technologies, iCareTech 2020*, pp. 24–29, 8 2020.

[128] A. Boschmann, D. Neuhaus, S. Vogt, C. Kaltschmidt, M. Platzner, and S. Dosen, "Immersive augmented reality system for the training of pattern classification control with a myoelectric prosthesis," *Journal of NeuroEngineering and Rehabilitation*, vol. 18, no. 1, pp. 1–15, 12 2021. [Online]. Available: https://jneuroengrehab.biomedcentral.com/articles/10.1186/s12984-021-00822-6

[129] O. Ozioko and R. Dahiya, "Smart Tactile Gloves for Haptic Interaction, Communication, and Rehabilitation," *Advanced Intelligent Systems*, vol. 4, no. 2, p. 2100091, 2 2022. [Online]. Available: https://onlinelibrary.wiley.com/doi/full/10.1002/aisy.202100091https://onlinelibrary.wiley.com/doi/abs/10.1002/aisy.202100091https://onlinelibrary.wiley.com/doi/10.1002/aisy.202100091

[130] M. Franzo', S. Pascucci, M. Serrao, F. Marinozzi, and F. Bini, "Exergaming in mixed reality for the rehabilitation of ataxic patients," *2022 IEEE International Symposium on Medical Measurements and Applications, MeMeA 2022 - Conference Proceedings*, 2022.

[131] F. Ababsa, J. He, and J. R. Chardonnet, "Combining hololens and leap-motion for free hand-based 3d interaction in mr environments," *Lecture Notes in Computer Science (including subseries Lecture Notes in Artificial Intelligence and Lecture Notes in Bioinformatics)*, vol. 12242 LNCS, pp. 315–327, 2020. [Online]. Available: https://link.springer.com/chapter/10.1007/978-3-030-58465-8_24

[132] R. Spain, S. K. Bailey, B. Goldberg, R. Sail, K. Carmody, C. Ficke, A. Bayro, H. Jeong, J. Kim, W. H. Yeo, R. Figueroa-Jacinto, Z. Pugh, C. Mayhorn, A. Gluck, L. S. Beadle, and A. Bond, "Me and My VE 2022: Human Factors Applications Using Virtual Reality, Mixed Reality, and Virtual Environments," *https://doi.org/10.1177/1071181322661001*, vol. 66, no. 1, pp. 2188–2192, 10 2022. [Online]. Available: https://journals.sagepub.com/doi/abs/10.1177/1071181322661001

[133] T. Maeda, S. Yoshida, T. Murakami, K. Matsuda, T. Tanikawa, and H. Sakai, "Fingeret: A Wearable Fingerpad-Free Haptic Device for Mixed Reality," *Proceedings* -

SUI 2022: ACM Conference on Spatial User Interaction, 12 2022. [Online]. Available: https://dl.acm.org/doi/10.1145/3565970.3567703

[134] J. M. Fulvio, M. Ji, and B. Rokers, "Variations in visual sensitivity predict motion sickness in virtual reality," *Entertainment Computing*, vol. 38, p. 100423, 5 2021.

[135] J. R. Lackner, "Motion sickness: More than nausea and vomiting," *Experimental Brain Research*, vol. 232, no. 8, pp. 2493–2510, 2014.

[136] M. Treisman, "Motion sickness: An evolutionary hypothesis," *Science*, vol. 197, no. 4302, pp. 493–495, 1977.

[137] J. T. Reason, "Motion sickness adaptation: A neural mismatch model," *Journal of the Royal Society of Medicine*, vol. 71, no. 11, pp. 819–829, 1978.

[138] B. Keshavarz, H. Hecht, and L. Zschutschke, "Intra-visual conflict in visually induced motion sickness," *Displays*, vol. 32, no. 4, pp. 181–188, 10 2011.

[139] A. C. Paillard, G. Quarck, F. Paolino, P. Denise, M. Paolino, J. F. Golding, and V. Ghulyan-Bedikian, "Motion sickness susceptibility in healthy subjects and vestibular patients: Effects of gender, age and trait-anxiety," *Journal of Vestibular Research: Equilibrium and Orientation*, vol. 23, no. 4-5, pp. 203–210, 2013.

[140] S. Tayal, K. Rajagopal, and V. Mahajan, "Virtual Reality based Metaverse of Gamification," *Proceedings - 6th International Conference on Computing Methodologies and Communication, ICCMC 2022*, pp. 1597–1604, 2022.

[141] M. Hassan, F. M. Awan, A. Naz, E. J. deAndrés Galiana, O. Alvarez, A. Cernea, L. Fernández-Brillet, J. L. Fernández-Martínez, and A. Kloczkowski, "Innovations in Genomics and Big Data Analytics for Personalized Medicine and Health Care: A Review," *International Journal of Molecular Sciences*, vol. 23, no. 9, p. 4645, 4 2022.

[142] M. Attaran, "Blockchain technology in healthcare: Challenges and opportunities," *International Journal of Healthcare Management*, vol. 15, no. 1, pp. 70–83, 1 2022.

[143] O. Boric-Lubecke, X. Gao, E. Yavari, M. Baboli, A. Singh, and V. M. Lubecke, "E-healthcare: Remote monitoring, privacy, and security," *IEEE MTT-S International Microwave Symposium Digest*, 2014.

[144] M. Elhoseny, G. Ramírez-González, O. M. Abu-Elnasr, S. A. Shawkat, N. Arunkumar, and A. Farouk, "Secure Medical Data Transmission Model for IoT-Based Healthcare Systems," *IEEE Access*, vol. 6, pp. 20 596–20 608, 2018.

[145] F. Ordóñez and D. Roggen, "Deep Convolutional and LSTM Recurrent Neural Networks for Multimodal Wearable Activity Recognition," *Sensors*, vol. 16, no. 1, p. 115, 2 2016. [Online]. Available: http://www.mdpi.com/1424-8220/16/1/115

[146] R. Igual, C. Medrano, and I. Plaza, "Challenges, issues and trends in fall detection systems," 2013.

[147] F. Cavallo, M. Aquilano, and M. Arvati, "An Ambient Assisted Living Approach in Designing Domiciliary Services Combined With Innovative Technologies for Patients With Alzheimer's Disease," *American Journal of Alzheimer's Disease & Other Dementiasr*, vol. 30, no. 1, pp. 69–77, 5 2015. [Online]. Available: http://journals.sagepub.com/doi/10.1177/1533317514539724

[148] R. L. Bashshur, J. D. Howell, E. A. Krupinski, K. M. Harms, N. Bashshur, and C. R. Doarn, "The Empirical Foundations of Telemedicine Interventions in Primary Care," *Telemedicine and e-Health*, vol. 22, no. 5, pp. 342–375, 5 2016. [Online]. Available: https://www.liebertpub.com/doi/10.1089/tmj.2016.0045

[149] R. H. A Alsagheer, A. F. H Alharan, and A. S. A Al-Haboobi, "International Journal of Computer Science and Mobile Computing Popular Decision Tree Algorithms of Data Mining Techniques: A Review," *International Journal of Computer Science and Mobile Computing*, vol. 6, no. 6, pp. 133–142, 2017. [Online]. Available: www.ijcsmc.com

[150] M. Belgiu and L. Drăgu, "Random forest in remote sensing: A review of applications and future directions," *ISPRS Journal of Photogrammetry and Remote Sensing*, vol. 114, pp. 24–31, 4 2016. [Online]. Available: https://www.sciencedirect.com/science/article/abs/pii/S0924271616000265

[151] D. M. Abdullah and A. M. Abdulazeez, "Machine Learning Applications based on SVM Classification A Review," *Qubahan Academic Journal*, vol. 1, no. 2, pp. 81–90, 4 2021. [Online]. Available: https://journal.qubahan.com/index.php/qaj/article/view/50

[152] K. Taunk, S. De, S. Verma, and A. Swetapadma, "A brief review of nearest neighbor algorithm for learning and classification," *2019 International Conference on Intelligent Computing and Control Systems, ICCS 2019*, pp. 1255–1260, 5 2019. [Online]. Available: https://ieeexplore.ieee.org/abstract/document/9065747

[153] D. E. Rumelhart, G. E. Hinton, and R. J. Williams, "Learning representations by back-propagating errors," *nature*, vol. 323, no. 6088, pp. 533–536, 1986.

[154] A. Sherstinsky, "Fundamentals of Recurrent Neural Network (RNN) and Long Short-Term Memory (LSTM) network," *Physica D: Nonlinear Phenomena*, vol. 404, p. 132306, 5 2020. [Online]. Available: https://linkinghub.elsevier.com/retrieve/pii/S0167278919305974

[155] S. Grossberg, "Recurrent neural networks," *Scholarpedia*, vol. 8, no. 2, p. 1888, 2013. [Online]. Available: http://www.scholarpedia.org/article/Recurrent_neural_networks

[156] B. A. Pearlmutter, "Learning State Space Trajectories in Recurrent Neural Networks," *Neural Computation*, vol. 1, no. 2, pp. 263–269, 5 1989. [Online]. Available: https://direct.mit.edu/neco/article/1/2/263-269/5477

[157] Wikimedia Commons, "File:Recurrent neural network unfold.svg - Wikimedia Commons," 2017. [Online]. Available: https://commons.wikimedia.org/wiki/File:Recurrent_neural_network_unfold.svg

[158] F. Ordóñez and D. Roggen, "Deep Convolutional and LSTM Recurrent Neural Networks for Multimodal Wearable Activity Recognition," *Sensors*, vol. 16, no. 1, p. 115, 5 2016. [Online]. Available: http://www.mdpi.com/1424-8220/16/1/115

[159] G. Van Houdt, C. Mosquera, and G. Nápoles, "A review on the long short-term memory model," *Artificial Intelligence Review*, vol. 53, no. 8, pp. 5929–5955, 5 2020. [Online]. Available: https://link.springer.com/10.1007/s10462-020-09838-1

[160] K. Cho, B. van Merrienboer, C. Gulcehre, D. Bahdanau, F. Bougares, H. Schwenk, and Y. Bengio, "Learning Phrase Representations using RNN Encoder–Decoder for Statistical Machine

Translation," in *Proceedings of the 2014 Conference on Empirical Methods in Natural Language Processing (EMNLP)*. Stroudsburg, PA, USA: Association for Computational Linguistics, 5 2014, pp. 1724–1734. [Online]. Available: http://aclweb.org/anthology/D14-1179

[161] Wikimedia Commons, "File:Gated Recurrent Unit.svg - Wikimedia Commons," 2017. [Online]. Available: https://commons.wikimedia.org/wiki/File:Gated_Recurrent_Unit.svg

[162] A. Shewalkar, D. Nyavanandi, and S. A. Ludwig, "Performance Evaluation of Deep Neural Networks Applied to Speech Recognition: RNN, LSTM and GRU," *Journal of Artificial Intelligence and Soft Computing Research*, vol. 9, no. 4, pp. 235–245, 5 2019. [Online]. Available: https://www.sciendo.com/article/10.2478/jaiscr-2019-0006

[163] H. Arora and R. Sinha, "Multi-Modal Graph Neural Networks for Physiological Signal Analysis," *4th International Conference on Sentiment Analysis and Deep Learning, ICSADL 2025 - Proceedings*, pp. 1202–1208, 2025. [Online]. Available: https://ieeexplore.ieee.org/abstract/document/10933022

[164] B. Khemani, S. Patil, K. Kotecha, and S. Tanwar, "A review of graph neural networks: concepts, architectures, techniques, challenges, datasets, applications, and future directions," *Journal of Big Data 2024 11:1*, vol. 11, no. 1, pp. 18–, 1 2024. [Online]. Available: https://link.springer.com/article/10.1186/s40537-023-00876-4

[165] T. R. Murgod, P. S. Reddy, S. Gaddam, S. M. Sundaram, and C. Anitha, "A Survey on Graph Neural Networks and its Applications in Various Domains," *SN Computer Science 2024 6:1*, vol. 6, no. 1, pp. 26–, 12 2024. [Online]. Available: https://link.springer.com/article/10.1007/s42979-024-03543-4

[166] L. Meng, "Tailoring Conducting Polymer Interface for Sensing and Biosensing," vol. 2094, 10 2020. [Online]. Available: https://urn.kb.se/resolve?urn=urn:nbn:se:liu:diva-169499

[167] A. Sun, A. G. Venkatesh, and D. A. Hall, "A Multi-Technique Reconfigurable Electrochemical Biosensor: Enabling Personal Health Monitoring in Mobile Devices," *IEEE Transactions on Biomedical Circuits and Systems*, vol. 10, no. 5, pp. 945–954, 10 2016.

[168] "Performing Cyclic Voltammetry — Tektronix." [Online]. Available: https://www.tek.com/en/blog/performing-cyclic-voltammetry

[169] R. Ghaffari, A. J. Aranyosi, S. P. Lee, J. B. Model, and L. B. Baker, "The Gx Sweat Patch for personalized hydration management," *Nature Reviews Bioengineering 2023 1:1*, vol. 1, no. 1, pp. 5–7, 1 2023. [Online]. Available: https://www.nature.com/articles/s44222-022-00005-5

[170] A. Ainla, M. P. Mousavi, M. N. Tsaloglou, J. Redston, J. G. Bell, M. T. Fernández-Abedul, and G. M. Whitesides, "Open-Source Potentiostat for Wireless Electrochemical Detection with Smartphones," *Analytical Chemistry*, vol. 90, no. 10, pp. 6240–6246, 5 2018. [Online]. Available: https://pubs.acs.org/doi/full/10.1021/acs.analchem.8b00850

[171] Bio-, "EC-Lab-Application Note #04 2005 The mystery of potentiostat stability explained." [Online]. Available: www.biologic.net

[172] O. S. Hoilett, J. F. Walker, B. M. Balash, N. J. Jaras, S. Boppana, and J. C. Linnes, "KickStat: A Coin-Sized Potentiostat for High-Resolution Electrochemical Analysis,"

Sensors 2020, Vol. 20, Page 2407, vol. 20, no. 8, p. 2407, 4 2020. [Online]. Available: https://www.mdpi.com/1424-8220/20/8/2407/htmhttps://www.mdpi.com/1424-8220/20/8/2407

[173] J. Mahato, C. R. Raj, and K. Biswas, "Low-Noise Potentiostat Circuit for Electrochemical Detection of Heavy Metals or Metalloids," *IEEE Transactions on Instrumentation and Measurement*, vol. 71, 2022.

[174] "Electrochemical Methods: Fundamentals and Applications - Allen J. Bard, Larry R. Faulkner, Henry S. White - Google Books." [Online]. Available: https://books.google.pt/books?hl=en&lr=&id=4ShuEAAAQBAJ&oi=fnd&pg=PR21&dq=BardFaulkner+cyclic+voltammetry&ots=SJFqAYVEqF&sig=qVRgMl3AAzzwpKeh_k1x0eyVLag&redir_esc=y#v=onepage&q=BardFaulkner%20cyclic%20voltammetry&f=false

[175] C. Mercer, R. Bennett, P. Conghaile, J. F. Rusling, and D. Leech, "Glucose biosensor based on open-source wireless microfluidic potentiostat," *Sensors and Actuators B: Chemical*, vol. 290, pp. 616–624, 7 2019.

[176] H. Zafar, A. Channa, V. Jeoti, and G. M. Stojanović, "Comprehensive Review on Wearable Sweat-Glucose Sensors for Continuous Glucose Monitoring," *Sensors 2022, Vol. 22, Page 638*, vol. 22, no. 2, p. 638, 1 2022. [Online]. Available: https://www.mdpi.com/1424-8220/22/2/638/htmhttps://www.mdpi.com/1424-8220/22/2/638

[177] E. P. Achterberg, "Laboratory techniques in electroanalytical chemistry," *TrAC Trends in Analytical Chemistry*, vol. 15, no. 10, 1996.

[178] E. Severeyn, J. Velasquez, G. Perpinan, H. Herrera, M. Pacheco, and S. Wong, "Heart rate variability analysis during a dehydration protocol on athletes," *2016 21st Symposium on Signal Processing, Images and Artificial Vision, STSIVA 2016*, 11 2016.

[179] R. M. Morgan, M. J. Patterson, and M. A. Nimmo, "Acute effects of dehydration on sweat composition in men during prolonged exercise in the heat," *Acta Physiologica Scandinavica*, vol. 182, no. 1, pp. 37–43, 9 2004. [Online]. Available: https://onlinelibrary.wiley.com/doi/full/10.1111/j.1365-201X.2004.01305.xhttps://onlinelibrary.wiley.com/doi/abs/10.1111/j.1365-201X.2004.01305.xhttps://onlinelibrary.wiley.com/doi/10.1111/j.1365-201X.2004.01305.x

[180] F. Ftaiti, L. Grélot, J. M. Coudreuse, and C. Nicol, "Combined effect of heat stress, dehydration and exercise on neuromuscular function in humans," *European Journal of Applied Physiology*, vol. 84, no. 1-2, pp. 87–94, 2001. [Online]. Available: https://link.springer.com/article/10.1007/s004210000339

[181] P. Pham, L. T. Nguyen, W. Pedrycz, and B. Vo, "Deep learning, graph-based text representation and classification: a survey, perspectives and challenges," *Artificial Intelligence Review*, vol. 56, no. 6, pp. 4893–4927, 6 2023. [Online]. Available: https://www.researchgate.net/publication/364319099_Deep_learning_graph-based_text_representation_and_classification_a_survey_perspectives_and_challenges

[182] "Beginning Machine Learning in iOS: CoreML Framework - Mohit Thakkar - Google Livros." [Online]. Available: https://books.google.pt/books?hl=pt-PT&lr=&id=wBaJDwAAQBAJ&

oi=fnd&pg=PP5&dq=CoreMl&ots=l1CXy28cQK&sig=sMEqe6s6q4765lVpIhQLlXOXROw&redir_esc=y#v=onepage&q=CoreMl&f=false

[183] M. J. Vinolo Gil, G. Gonzalez-Medina, D. Lucena-Anton, V. Perez-Cabezas, M. D. C. Ruiz-Molinero, and R. Martín-Valero, "Augmented Reality in Physical Therapy: Systematic Review and Meta-analysis," *JMIR Serious Games*, vol. 9, no. 4, p. e30985, 5 2021. [Online]. Available: https://games.jmir.org/2021/4/e30985

[184] A. Shumway-Cook and M. H. Woollacott, *Motor Control: Translating Research Into Clinical Practice - Anne Shumway-Cook, Marjorie H. Woollacott - Google Books*, 3rd ed., 2007.

[185] M. Ni, K. Mooney, L. Richards, A. Balachandran, M. Sun, K. Harriell, M. Potiaumpai, and J. F. Signorile, "Comparative Impacts of Tai Chi, Balance Training, and a Specially-Designed Yoga Program on Balance in Older Fallers," *Archives of Physical Medicine and Rehabilitation*, vol. 95, no. 9, pp. 1620–1628, 9 2014. [Online]. Available: https://www.sciencedirect.com/science/article/pii/S0003999314003426

[186] M. Mancini and F. B. Horak, "The relevance of clinical balance assessment tools to differentiate balance deficits," *European journal of physical and rehabilitation medicine*, vol. 46, no. 2, p. 239, 6 2010. [Online]. Available: https://pmc.ncbi.nlm.nih.gov/articles/PMC3033730/

[187] R. Llorens, M. A. Fuentes, A. Borrego, J. Latorre, M. Alcañiz, C. Colomer, and E. Noé, "Effectiveness of a combined transcranial direct current stimulation and virtual reality-based intervention on upper limb function in chronic individuals post-stroke with persistent severe hemiparesis: a randomized controlled trial," *Journal of NeuroEngineering and Rehabilitation*, vol. 18, no. 1, pp. 1–13, 12 2021. [Online]. Available: https://link.springer.com/articles/10.1186/s12984-021-00896-2https://link.springer.com/article/10.1186/s12984-021-00896-2

[188] "sensfloor — FUTURE-SHAPE — KP®." [Online]. Available: https://conceptsandprojects.com/en/2020/07/28/sensfloor-future-shape-en/

[189] "SensFloor®: a smart floor to detect falls -." [Online]. Available: https://www.silvereco.org/en/sensfloor-a-smart-floor-to-detect-falls/

[190] C. Lauterbach, A. Steinhage, and A. Techmer, "Large-area wireless sensor system based on smart textiles," in *International Multi-Conference on Systems, Sygnals & Devices*. IEEE, 5 2012, pp. 1–2. [Online]. Available: http://ieeexplore.ieee.org/document/6198101/

[191] J. Santos, O. Postolache, and D. Mendes, "Ambient Assisted Living using Non-intrusive Smart Sensing and IoT for Gait Rehabilitation," in *2022 IEEE International Conference on Metrology for Extended Reality, Artificial Intelligence and Neural Engineering (MetroXRAINE)*, 2022, pp. 489–494.

[192] K. Fricklas, "Nishant Shukla," 2018.

[193] J. Moolayil, "Learn Keras for Deep Neural Networks: A Fast-Track Approach to Modern Deep Learning with Python," *Learn Keras for Deep Neural Networks: A Fast-Track Approach to Modern Deep Learning with Python*, pp. 1–182, 1 2018.

[194] G. S. Handelman, H. K. Kok, R. V. Chandra, A. H. Razavi, S. Huang, M. Brooks, M. J. Lee, and H. Asadi, "Peering into the black box of artificial intelligence: evaluation metrics of machine learning methods," *American Journal of Roentgenology*, vol. 212, no. 1, pp. 38–43, 2019.

[195] L. Deng and D. Yu, "Deep learning: Methods and applications," *Foundations and Trends in Signal Processing*, vol. 7, no. 3-4, pp. 197–387, 2013.